Aus dem Veterinärwissenschaftlichen Departement
der Tierärztlichen Fakultät
der Ludwig-Maximilians-Universität München

Arbeit angefertigt unter der Leitung von
Univ.-Prof. Dr. Eckhard Wolf

Genotypic and phenotypic characterization of *INS*^{C94Y} transgenic pigs – a novel large animal model for permanent neonatal diabetes mellitus

Inaugural-Dissertation
zur Erlangung der tiermedizinischen Doktorwürde
der Tierärztlichen Fakultät
der Ludwig-Maximilians-Universität München

von

Christina Franziska Maria Braun-Reichhart

aus Regensburg

München 2013

Gedruckt mit der Genehmigung der Tierärztlichen Fakultät

der Ludwig-Maximilians-Universität München

Dekan:	Univ.-Prof. Dr. Joachim Braun
Referent:	Univ.-Prof. Dr. Eckhard Wolf
Korreferent:	Prof. Dr. Herbert Kaltner
	Univ.-Prof. Dr. Katrin Hartmann
	Priv.-Doz. Dr. Nadja Herbach
	Univ.-Prof. Dr. Dušan Palić

Tag der Promotion: 20. Juli 2013

Für meine Eltern und meine Patenfamilie

During the preparation of this thesis the following paper has been published:

Renner, S., **Braun-Reichhart, C.**, Blutke, A., Herbach, N., Emrich, D., Streckel, E., Wunsch, A., Kessler, B., Kurome, M., Baehr, A., Klymiuk, N., Krebs, S., Puk, O., Nagashima, H., Graw, J., Blum, H., Wanke, R., and Wolf, E. (2012). Permanent Neonatal Diabetes in INS^{C94Y} Transgenic Pigs. *Diabetes*. 2012, December 28. (published online ahead of print).

Parts of this study were presented at the following congresses:

Swine in Biomedical Research Conference, Chicago, Illinois, 2011, July 17-19

XXIV Congress of the Transplantation Society (TTS), Berlin, Germany, 2012, July 15-19

48th meeting of the European Association for the Study of Diabetes (EASD), Berlin, Germany, 2012, October 1-5

TABLE OF CONTENTS

INDEX OF ABBREVIATIONS

ABCC8	ATP-binding cassette, sub-family C, member 8
ADA	American Diabetes Association
APAF1	apoptotic peptidase activating factor 1
AP	alkaline phophatase
APS	ammonium persulfate
ASK1	apoptosis signal-regulating kinase 1
ATF4	activating transcription factor 4
ATF6α/β	activating transcription factor 6 α and β
ATP	adenosine triphosphate
Bcl-2	B-cell CLL/lymphoma 2
BiP	binding Ig protein
BMI	body mass index
BSA	bovine serum albumin
BW	body weight
bZIP	basic domain/leucin zipper
cAMP	cyclic adenosine monophosphate
CASP12	caspase 12
CD	cluster of differentiation
cDNA	complementary DNA
C/EBP	CCAAT/enhancer binding protein
CHOP	C/EBP homologous protein
COP	coat protein complex
CpG	cytosine-phosphate-guanine

cpm	counts per minute
CV	coefficient of variance
Cyt-c	cytochrome *c*
DAB	3,3´diaminobenzidine tetrahydrochloride
dATP	deoxyadenosine triphosphate
dCTP	deoxycytidine triphosphate
DEPC	diethylpyrocarbonate
dGTP	Desoxyguanosine triphosphate
DKA	diabetic ketoacidosis
DNase	desoxyribonuclease
DTT	1,4-dithiothreitol
EDTA	ethylenediaminetetraacetic acid
EGTA	ethyleneglycol-bis-(2-aminoethyl-) tetra-acetic acid
EIF2AK3	eukaryotic translation initiation factor 2 α kinase 3
ELISA	enzyme-linked immunosorbent assay
ENU	*N*-ethyl-*N*-nitrosourea
ER	endoplasmic reticulum
ERAD	ER-associated degradation
ERSE	ER stress response element
ET	embryo transfer
FoxP3	forkhead box P3
GAD 65	glutamic acid decarboxylase 65
GADD153	growth arrest and DNA damage protein 153
GBM	glomerular basement membrane
GCK	glucokinase

GDP	guanine diphosphate
GFP	green fluorescent protein
$GIPR^{dn}$	dominant-negative glucose-dependent insulinotropic polypeptide receptor
GLIS3	GLIS family zinc finger 3 transcription factor
GLP-1	incretin hormone glucagon-like peptide-1
GLS	Golgi localization sequence
GLUT	glucose transporter 2
G-protein	guanine nucleotide binding protein
GTP	guanine triphosphate
H.E.	hematoxylin and eosin
HEMA	2-hydroxyethyl methacrylate
HLA	human leukocyte antigen
HNF	hepatocyte nuclear factor
HOMA-B	homeostasis model assessment of baseline insulin secretion
HOMA-IR	HOMA of insulin resistance
HP	horseradish peroxidase
HYAMI	hydatidiform mole associated and imprinted gene
IA-2 (IA-2β)	insulinoma antigen 2 (2β)
IAA	insulin autoantibody
IAPP	islet amyloid polypeptide
ICA	islet cell antibody
ICG	interstitial glucose concentration
ICSI	intracytoplasmic sperm injection

IPEX	immune dysregulation, polyendocrinopathy, enteropathy, X-linked syndrome
INS	insulin gene
INSR	insulin receptor gene
IPF1	insulin promoter factor 1
IRE1α	inositol requiring ER-to nucleus signal kinase 1 α
I.U.	international unit
IUGR	intrauterine growth retardation
IVGTT	intravenous glucose tolerance test
JNK	c-Jun N-terminal kinase
K_{ATP}	ATP-dependent potassium channel
kb	kilobase
KCNJ11	potassium inwardly-rectifying channel, subfamily J, member 11
Kir6.2	potassium channel inwardly-rectifing subfamily J, member 11
MAPK	mitogen-activated protein kinase
Met-RNA	translation initiator methionyl tRNA
MHC	major histocompatibility complex
MMA	methyl methacrylate
MODY	maturity-onset diabetes of the young
mRNA	messenger RNA
NEUROD1	neuronal differentiation factor 1
NF-κB	NF-κB
NDDG	National Diabetes Data Group of the USA
p.a.	pro analysis
PACAP-1	pituitary adenylate cyclase polypeptide 1

PARP	poly (ADP-ribose) polymerase
PAS	periodic acid Schiff staining
PASM	periodic acid silver methenamine staining
PBS	phosphate buffered saline
PCR	polymerase chain reaction
PDI	protein disulfide isomerase
PDX1	pancreatic and duodenal homeobox protein 1
PeIF2α	phosphorylated eukaryotic initiation factor-2α
PERK	RNA-dependent protein kinase-like endoplasmic reticulum eIF2α kinase
RIA	radioimmunoassay
Rip	regulated intramembrane proteolysis
PLAGL1	pleiomorphic adenoma-like protein 1
PMSF	phenylmethylsulfanylfluoride
PNDM	permanent neonatal diabetes mellitus
RNase	ribonuclease
RT	room temperature
RT-PCR	reverse transcription PCR
SCNT	somatic cell nuclear transfer
SDS	sodium dodecyl sulphate
SDS-PAGE	SDS polyacrylamide gel electrophoesis
SRP	signal recognition particle
SST	somatostatin
STZ	streptozotocin
SUR1	sulfonylurea receptor 1

TAE	tris-acetate-EDTA
TBE	Tris-boric acid-EDTA
TEM	transmission electron microscopy
Temed	tetraethylethylenediamine
TNDM	transient neonatal diabetes mellitus
TRAF2	tumor necrosis factor type 2 receptor associated protein
Tris	Tris-(hydroxymethyl)-aminomethan
UDP	uridine 5'-diphosphate
UGGT	UDP-glucose:glycoprotein glucosyl transferase
uORF	upstream open reading frame
UPD	uniparental paternal disomy
UPRE	unfolded protein response element
UPR	unfolded protein response
VTC	vesicular-tubular clusters
XBP1	bZIP protein X-box binding protein 1
ZnT8	zinc transporter 8

I. INTRODUCTION

Diabetes mellitus has emerged into a steadily increasing health problem of global extent and a considerable cause of early death nowadays (Roglic and Unwin, 2010; Scully, 2012; Shaw et al., 2010). The predicted future dimension of the global diabetic epidemic is alarming. A tremendous increase in the prevalence of diabetes mellitus from currently 346 million to over 400 million affected people worldwide by the year 2030 was extrapolated (Scully, 2012; Shaw et al., 2010). In consideration of the growing burden of diabetes mellitus, research efforts are imperative to provide a basis for the development of preventive and therapeutic strategies (Wild et al., 2004; Zimmet et al., 2001). Diabetic rodent models have traditionally been used in this field and contributed decisively to the clarification of important disease mechanisms and pathomorphological consequences (Aigner et al., 2008). However, the pig is becoming firmly established as biomedical model for translational diabetes research due to its enhanced comparability to human conditions (Aigner et al., 2010; Bahr and Wolf, 2012; Douglas, 1972; Lunney, 2007). To date insulin-deficient diabetes mellitus in the pig has been experimentally induced by either total pancreatectomy or by cytotoxic β-cell destruction through diabetogenic agents such as streptozotocin. Both methods have substantial drawbacks (Dufrane et al., 2006; Stump et al., 1988; Wilson et al., 1986). Therefore the establishment of genetically engineered diabetic pig models represents an opportunity to overcome disadvantages of existing methods to induce diabetes.

The aim of the present study was the generation as well as the genotypic and phenotypic characterization of the first genetically engineered porcine animal model of permanent neonatal diabetes mellitus, corresponding to the human INS^{C96Y} mutation and the *Ins2* mutation of the Akita mouse model. Hemizygous INS^{C94Y} transgenic pigs develop a severe diabetic phenotype based upon expression of a mutated *INS* gene (INS^{C94Y}), leading to a clinically relevant disturbance of pancreatic β-cells. In this thesis, the underlying disease mechanisms, clinical features and pathomorphological properties of hemizygous INS^{C94Y} transgenic pigs were investigated.

II. REVIEW OF THE LITERATURE

1. Diabetes mellitus

1.1. Definition and description of diabetes mellitus

The term diabetes mellitus encompasses a heterogeneous group of metabolic disorders characterized by steadily increasing blood glucose levels, polydipsia, polyuria, weight loss as well as diabetic ketoacidosis (DKA) and nonketotic hyperosmolar syndrome in life-threatening consequence of metabolic decompensation (Expert Committee on the Diagnosis and Classification of Diabetes Mellitus,2003; ADA, 2013; Kuzuya et al., 2002; Yared and Chiasson, 2003). These characteristic symptoms and a variety of severe long-term complications of sustained diabetes mellitus such as cardiovascular diseases, diabetic retinopathy, diabetic nephropathy and diabetic neuropathy leading to substantial organ failure and supposed to be a major cause of death with diabetes, predispose diabetes mellitus towards a general health problem nowadays (ADA, 2013; Wild et al., 2004). The pathogenesis of hyperglycemia in diabetes is due to insulin deficiency resulting from inadequate insulin secretion or insufficient tissue response to insulin (ADA, 2013). A large range of pathogenic processes diversifies the etiology of this disease, which is therefore not completely elucidated.

1.2. Classification criteria of diabetes mellitus

The first organization, who went about establishing a systematic classification for diabetes mellitus, was the National Diabetes Data Group of the USA (NDDG) and the second World Health Organization Expert Committee on Diabetes Mellitus in 1979 and in 1985 respectively (Expert Committee on the Diagnosis and Classification of Diabetes Mellitus, 2003). Since the introduction of this first classification scheme in 1980, the classification for diabetes mellitus was constantly revised and current knowledge was included (Alberti and Zimmet, 1998; Harris, 1988). These days, the generally accepted classification criteria based on etiologic and pathogenic aspects were first established by an Expert Committee of the American Diabetes Association (ADA) in 1997 and is annually published after revision by the ADA (Gavin, 1998). According to the definitions

of the ADA, diabetes mellitus in humans is subdivided into four etiopathogenic groups. The majority of diabetic patients are assigned to type 1 and type 2 diabetes mellitus, which accounts for 5 to 10% and 90 to 95% respectively of those with diabetes and mainly contributes to diabetes mellitus emerging as epidemic (ADA, 2013). The third group is outlined as other specific types of diabetes and summarizes a group of monogenetic disorders accompanied by mutations in genes encoding for several transcription factors (*HNF1A, HNF4A, HNF1B, IPF1/PDX1, NEUROD1*) and for the glucokinase (*GCK*) (Froguel et al., 1992; Horikawa et al., 1997; Stoffers et al., 1997a; Yamagata et al., 1996a; Yamagata et al., 1996b). These genetic defects result in a disturbed β-cell function and are referred to as maturity-onset diabetes of the young 1-6 (MODY1-6) according to the respective gene involved (ADA, 2013; Vaxillaire and Froguel, 2006). Recently, the clinical variants transient neonatal diabetes mellitus (*e.g. ZAC/HYAMI* imprinting defect on chromosome 6q24) and permanent neonatal diabetes mellitus (*e.g. KCNJ11*) were included in this category (ADA, 2013; Aguilar-Bryan and Bryan, 2008; Hutchison et al., 1962; Polak and Cave, 2007; Shield, 2000). Additionally the third group combines abnormalities of insulin action resulting from genetic disturbance of the insulin receptor function in consequence of mutations in the insulin receptor gene (*INSR*) and mainly presents within a pediatric syndrome (ADA, 2013). Furthermore affections of the exocrine pancreas including recurrent pancreatitis, traumata and neoplasia as well as hormone-related diabetogenic metabolic status of certain endocrinopathies and several infectious diseases can be causative for diabetes mellitus and are likewise categorized in the third group (ADA, 2013). As approximately 7% of pregnant women are diagnosed with diabetes mellitus or diminished glucose tolerance with first onset during pregnancy and associated with adverse effects on fetuses, a fourth systematic group was defined, called gestational diabetes mellitus (Metzger et al., 2007).

1.2.1. Diabetes mellitus – a major public health problem

Diabetes mellitus has evolved into a steadily increasing socioeconomic health problem of global extent and a considerable cause of early death nowadays (Roglic and Unwin, 2010; Shaw et al., 2010). According to extrapolations, the demographic change, urbanization attended by changing lifestyles and the overall growing world population will provoke an explosive increase of the prevalence of

diabetes mellitus worldwide by the year 2030 (Ramachandran et al., 1999; Wild et al., 2004). A tremendous increase from currently 346 million to 439 million affected people suffering from diabetes mellitus worldwide is expected by the year 2030 (Scully, 2012; Shaw et al., 2010). This represents an increase of 20% in the Western civilization and an increase of 68% in developing and newly industrialized countries, with the main focus on India, China, Indonesia, Bangladesh and Brazil for instances. The greatest absolute increase is extrapolated for India and China (Shaw et al., 2010; Wild et al., 2004). In addition these calculations are based on the assumption that the effects of other risk factors including general public adiposity will remain constant and that a large number of people are undiagnosed with diabetes mellitus (Flores-Le Roux et al., 2011; Gray et al., 2004; Ishihara et al., 2006). Therefore, the estimates of the extent of the global diabetic epidemic are anticipated to be even exceeded by the year 2030 (Wild et al., 2004). An enormous economic burden for the healthcare systems is unavoidable. Due to the chronic character of the disease and the severe complications a doubling of the costs is expected by the year 2034 (Huang et al., 2009). Moreover, expenses caused by economic exposure through premature morbidity and disability should not be neglected. The total expenditures just spent for medical care of diabetes patients and financial losses sustained by reduced national economic productivity in the USA will increase from $ 174 billion determined in 2007 to $ 336 billion due to the increased population of diabetics by the year 2034 (ADA, 2008; Huang et al., 2009; Tao et al., 2010). In consideration of the serious global and societal implications of the growing burden of diabetes mellitus, internationally concerted research efforts are imperative to clarify the etiology and pathogenesis of the various forms of diabetes mellitus in order to create the basis for comprehensive new prevention strategies and the development of new diagnostic and treatment methods (Wild et al., 2004; Zimmet et al., 2001).

1.2.1.1. Type 2 diabetes mellitus – a heterogeneous disease

Indeed, the epidemic of diabetes mellitus is chiefly represented through type 2 diabetics (Zimmet et al., 2001). Strong genetic predisposition for glucose intolerance and obesity caused by an unhealthy hypercaloric diet and physical inactivity are risk factors for the dysregulation of glycemic control and at last clinically overt diabetes mellitus (ADA, 2013; Leahy, 2005). In the early latency phase, a dynamic interaction between insulin secretion and insulin resistance is

crucial to maintain normal glucose tolerance. Therefore the prediabetic phase remains unnoticed for years (ADA, 2013; DeFronzo, 2004). Nevertheless the increased risk of developing severe diabetes-associated long-term vascular complications persists (ADA, 2013). The insulin resistant organism reacts to chronically elevated blood glucose levels with increased insulin secretion and insulin synthesis as positive adaptive response (DeFronzo, 2004; Kahn, 2003). The increased insulin supply leads to a reduction of the density of peripheral insulin receptors present on the cell surface of all insulin target tissues. Thus the peripheral insulin resistance of the target cells results in a relative insulin deficiency vice versa (ADA, 2013; DeFronzo, 2004; Leahy, 2005). Certainly, obesity itself or an increased proportion of abdominal fat tissue contributes to insulin resistance even in non-diabetic subjects on a large scale (Bogardus et al., 1985; Ludvik et al., 1995). The exhaustion of these compensatory mechanisms consequently results in an increased apoptosis rate of pancreatic β-cells with a progressive reduction of pancreatic β-cell mass through exposure to high blood glucose levels. Consecutive hypoinsulinemia leads to clinical manifestation of diabetes mellitus, reaching reduction of functional β-cell mass by 60% (Butler et al., 2003). Moreover pancreatic islet amyloidosis triggering β-cell apoptosis are supposed to contribute to the development of insulin resistance and impaired insulin secretion in type 2 diabetes patients (Butler et al., 2003; DeFronzo, 2004).

1.2.1.2. Type 1 diabetes mellitus – glycemic dysregulation through autoimmunity

Type 1 A diabetes mellitus is a chronic autoimmune disease (Imagawa et al., 2000). Cellular autoimmune-mediated inflammatory processes in the endocrine pancreas and the consecutive destruction of pancreatic islet mass by CD4+ and CD8+ cytotoxic T cells and macrophages lead to an insufficient endogenous insulin secretion and thereby to an absolute insulin deficiency (ADA, 2013; Gillespie, 2006). At diagnosis of pathognomonic symptoms, 70 to 80% of functional β-cell mass has been destroyed (Cnop et al., 2005). Autoantibodies, consistently present in type 1 diabetics, show specific binding affinity to islet cells (ICA), to insulin (IAA), to glutamic acid decarboxylase (GAD 65), to zinc transporter 8 (ZnT8) and to protein tyrosine phosphatases IA-2 and IA-2β, both transmembrane proteins expressed in human pancreatic islets. The detection of any of these autoantibodies in otherwise healthy individuals is highly predictive in

even diagnosing those with increased risk (Gillespie, 2006; Kukreja and Maclaren, 1999; Lan et al., 1996; Lu et al., 1996; Merger et al., 2012; Notkins et al., 1996). Moreover the progression to insulin dependency is also related to genetic predisposition associated with 20 chromosomal regions including contribution of the major histocompatibility complex region (MHC) on chromosome 6p21, namely the human leukocyte antigen (HLA) risk alleles (DQ, DR) (ADA, 2013; Cudworth and Woodrow, 1975; Kukreja and Maclaren, 1999; Merger et al., 2012; Pociot and McDermott, 2002). Unfortunately an additional susceptibility to other autoimmune endocrine diseases including Hashimoto´s thyroiditis, Addison disease, vitiligo and myasthenia gravis for instances can be diagnosed as a corollary of diabetes mellitus in these patients (ADA, 2013; Merger et al., 2012). Gestational infections, hemolytic diseases of the newborn (erythroplastosis fetalis), viral infections (*e.g.* Coxsackie B virus, human rotavirus, cytomegalovirus, measles virus) and some dietary proteins of milk and wheat are supposed to contribute to β-cell autoimmunity by generation of monoclonal autoantibodies through molecular mimicry to cell components of the host (Bach, 1994; Kukreja and Maclaren, 1999; Larsson et al., 2004). Evidence for autoimmunity and risk HLA haplotypes are not mandatory for 10% of the patients newly diagnosed with type 1 diabetes mellitus and the etiology remains idiopathic (type 1 B) (ADA, 2013; Imagawa et al., 2000). Type 1 diabetes mellitus is likely to be diagnosed between childhood and puberty with a second peak in the fifth decade of life due to preservation of sufficient residual β-cell function for years and therefore fairly resembling characteristics of type 2 diabetes mellitus (ADA, 2013; Karjalainen et al., 1989; Merger et al., 2012). In early childhood diabetic ketoacidosis (DKA) is commonly the first clinical manifestation of previously undiagnosed diabetes mellitus and young patients are hospitalized with distinctive symptoms in an altered state of consciousness (Expert Comittee on the Diagnosis and Classification of Diabetes mellitus, 2003; ADA, 2013; Merger et al., 2012).

1.2.2. Diabetes mellitus – a rare monogenetic disorder

In rare cases of juvenile-onset diabetes mellitus classic autoimmunity related to type 1 diabetes is not the underlying pathogenesis, but rather monogenetic diseases (Edghill et al., 2008; Shield et al., 1997). In general, monogenetic diabetes is subdivided into maturity-onset diabetes of the young (MODY) and

neonatal diabetes (Edghill et al., 2008; Malecki and Mlynarski, 2008; Molven et al., 2008). MODY subjects are normally diagnosed under the age of 25 years revealing progressive β-cell dysfunction with primarily disturbed glucose-stimulated insulin secretion and autosomal dominant inheritance of the genetic defects intimately connected with multigenerational pedigree (ADA, 2013; Edghill et al., 2008; Fajans et al., 2001; Vaxillaire and Froguel, 2006; Velho and Froguel, 1998; Yamagata et al., 1996a). Severe β-cell dysfunction accompanied by insulin deficiency causing severe hyperglycemia requiring supplementary insulin and ketoacidosis within six months of age, highly-associated with heredity, are pathognomonic characteristics of neonatal diabetes mellitus and a monogenic origin of the disease should be implicitly evidenced (Edghill et al., 2006; Polak and Cave, 2007; Shield et al., 1997; von Muhlendahl and Herkenhoff, 1995). Although monogenicity is very rare with diabetes mellitus, precise elucidation of the genetic defect is essential for accurate prognosis and an optimized treatment regimen for previously unspecified diabetics possibly through gene-based therapies in the future (Hattersley, 2005; Malecki and Mlynarski, 2008; Pearson et al., 2003; Slingerland, 2006; Stoy et al., 2007). Furthermore the well-known pattern of inheritance offers the possibility to identify further carriers of specific mutations in MODY-associated genes in pedigrees at risk through genetic screening for augmented prediabetic therapeutic intervention (Fajans et al., 2001).

1.2.2.1. Maturity-onset diabetes of the young (MODY)

Mutations in six susceptibility alleles on different chromosomes have been unveiled so far as a cause of maturity-onset diabetes of the young (MODY) (ADA, 2013; Froguel and Velho, 1999; Hansen et al., 2002; Vaxillaire and Froguel, 2006). Comprising 2% to 5% of rarely obese patients previously diagnosed with type 2 diabetes, MODY is the most common form of monogenetic diabetes mellitus, especially by reason of the very prevalence of 15% to 20% of MODY subjects with abnormalities in unknown genes and the high feasibility of further monogenetic forms of type 2 diabetes to be identified soon (Edghill et al., 2008; Frayling et al., 2003; Hansen et al., 2002; Vaxillaire and Froguel, 2006). Since the discovery of heterozygous monogenetic mutations in the glucokinase locus (*GCK*) on chromosome 7p as a cause of deficient glucose-stimulated insulin release of pancreatic β-cells as well as imbalance of hepatic glycogen storage and gluconeogenesis through defective glycolytic enzyme glucokinase in 1992, more

than 130 distinct monogenetic mutations have been identified in the *GCK* related to MODY 2 (Fajans et al., 2001; Froguel et al., 1992; Glaser et al., 1998; Matschinsky et al., 1998; Velho et al., 1996). Clinical MODY criteria are also linked to monogenetic defects of transcription factors predominantly expressed in pancreatic β-cells (Fajans et al., 2001). Hepatocyte nuclear factor 1α (*HNF1A*, MODY 3), HNF 4 α (*HNF4A*, MODY 1), insulin promoter factor 1 (*IPF1/PDX1*, MODY 4), HNF 1β (*HNF1B*, MODY 5) and neurogenic differentiation factor 1 (*NEUROD1*, MODY 6) are nuclear proteins mediating glucose metabolism and prenatal pancreas development through specific transcriptional modulation of genes encoding insulin (*INS*), somatostatin (*SST*), glucokinase (*GCK*), islet amyloid polypeptide (*IAPP*) as well as the glucose transporter 2 (*GLUT-2*) but also collaborating in the regulation of hepatic gene expression (Fajans et al., 2001; Froguel and Velho, 1999; Horikawa et al., 1997; Jonsson et al., 1994; Ladias et al., 1992; Malecki et al., 1999; Stoffel and Duncan, 1997; Stoffers et al., 1997a; Yamagata et al., 1996a; Yamagata et al., 1996b). MODY 2 and MODY 3, diagnosed in one third of MODY patients and therefore estimated to be the most common subtypes of monogenetic diabetes among adults and the other very rare MODY-associated mutations are linked to clinical heterogeneity of the severity of hyperglycemia and time point of the onset of conspicuous symptoms (ADA, 2013; Edghill et al., 2008; Fajans et al., 2001; Froguel and Velho, 1999; Vaxillaire and Froguel, 2006).

1.2.2.2. Neonatal diabetes mellitus (NDM)

Neonatal diabetes, also referred to as congenital diabetes mellitus is divided into two clinical variants - transient neonatal diabetes mellitus (TNDM) and permanent neonatal diabetes mellitus (PNDM) - according to whether insulin dependency goes into complete remission or remains throughout life (Aguilar-Bryan and Bryan, 2008; Hutchison et al., 1962; Polak and Cave, 2007; Shield, 2000). With an estimated incidence rate of 1:300000 to 1: 500000 live newborns, diabetes mellitus is diagnosed on very rare occasions within the neonatal period (Aguilar-Bryan and Bryan, 2008; Polak and Cave, 2007; Shield et al., 1997). Clinical features such as intrauterine growth retardation (IUGR) attributed to the absence of insulin *in utero* as fetal growth factor, life-threatening hyperglycemia with ketoacidosis and emaciation are hardly implementable for accurate discrimination between TNDM and PNDM. Diagnosis at the molecular level becomes obligatory

(Cave et al., 2000; Hutchison et al., 1962; Polak and Cave, 2007; Shield et al., 1997; von Muhlendahl and Herkenhoff, 1995). In general infants born with TNDM recover completely from their severe symptoms and become independent of insulin medication most likely within one year but are susceptible to relapse into a non-autoimmune related diabetic state requiring permanent medical care usually around adolescence. Thus preventive checkups at close intervals are advised (Fosel, 1995; Gentz and Cornblath, 1969; Gottschalk et al., 1992; Polak and Cave, 2007; Shield et al., 1997; Vanelli et al., 1994). Disturbed glucose tolerance and type 2 diabetes mellitus after 20 years of complete remission occur to some extent but also permanent remission throughout life was observed (Temple et al., 1996; von Muhlendahl and Herkenhoff, 1995). Both TNDM and PNDM are each related to numerous specific genetic mutations, which can be identified in almost 60 to 90% of the cases (Aguilar-Bryan and Bryan, 2008; Edghill et al., 2010; Hamilton-Shield, 2007; Shield, 2000). The genetic basis of insulin secretory failure present in PNDM is based upon a more heterogeneous genetic background and diabetes mellitus either arises as solitary disease or constitutes as an epiphenomenon of a multisystem pediatric syndrome including neonatal diabetes mellitus (Edghill et al., 2004; Polak et al., 2008; Stoy et al., 2007). Predominantly heterozygous activating mutations in the *KCNJ11* gene encoding the pore-forming inwardly rectifying protein subunit (Kir6.2) and less frequent in the *ABCC8* gene responsible for sulfonylurea receptor (SUR1) expression of the ATP-sensitive potassium channel (K_{ATP}) localized within the membranes of pancreatic β-cells lead to PNDM due to disturbance of transmembrane depolarization and failure of insulin exocytosis through absent fusion of the insulin secretory granules with the membrane (Babenko et al., 2006; Edghill et al., 2004; Gloyn et al., 2004; Polak and Cave, 2007). Accounting for 80% of subjects diagnosed with *KCNJ11* mutations, the mutation arose spontaneously (Gloyn et al., 2004; Stoy et al., 2007). Furthermore offspring of parents carrying a heterozygous mutant *GCK* both, are prone to homozygosity and permanent neonatal diabetes mellitus resulting from lack of glycolytic activity (Fajans et al., 2001; Njolstad et al., 2001; Stoy et al., 2007). Moreover homozygous patients with an autosomal recessive point mutation in the human insulin promoter factor 1 gene (*IPF1/PDX1*) within codon 63 display severe diabetic symptoms with additional impairment of the exocrine function of the pancreas resulting from pancreas aplasia (Polak and Cave, 2007; Stoffers et al.,

1997b). Mutations in the forkhead box P3 gene (*FOXP3*) transcriptionally regulating immune homeostasis through regulatory T cells was found as leading cause of the autosomal recessive human immune dysregulation, polyendocrinopathy, enteropathy, X-linked syndrome (IPEX), which combines permanent diabetes mellitus and failure of many organ systems resulting from inflammatory infiltration with autoreactive immune cells (Bennett et al., 2001; Wildin et al., 2002; Zhang and Zhao, 2007). The Wolcott-Rallison syndrome is another severe autosomal recessive pediatric syndrome linked to mutations of the gene encoding the eukaryotic translation initiation factor 2 α kinase 3 (*EIF2AK3*) mapped to chromosome 2p12 (Delepine et al., 2000). In addition to progressive diabetes mellitus, disturbed regulation of protein synthesis with consecutive increased stress on the endoplasmic reticulum leads to a variety of fatal concomitant symptoms including spondylo-epiphyseal dysplasia, hepatomegaly, renal failure and mental retardation (Polak and Cave, 2007; Wolcott and Rallison, 1972). Another rare congenital syndromic disorder characterized by pancreas and cerebellar hypoplasia is caused by mutant pancreas specific transcription factor 1α (PTF1A) being expressed in pancreatic β-cells as well as in the cerebellum (Sellick et al., 2004). Mutations in the GLIS family zinc finger 3 transcription factor gene (*GLIS3*) have recently been identified as a cause of permanent neonatal diabetes mellitus accompanied by hypothyroidism and deformity of the face amongst others (Hamilton-Shield, 2007; Senee et al., 2006). Paternally inherited anomalies of an imprinted region on chromosome 6q24 including paternal uniparental disomy (UPD 6), paternal partial duplication as well as incomplete or absent methylation, which each result in overexpression of critical paternally expressed alleles due to imprinting malfunction, are frequently leading cause of the diabetic phenotype in transient diabetic neonates (Cave et al., 2000; Gardner et al., 2000; Polak et al., 2008; Shield, 2000; von Muhlendahl and Herkenhoff, 1995). Genes encoding zinc finger protein pleiomorphic adenoma-like protein 1 *(PLAGL1)*, antiproliverative transcription factor of the cell cycle, pituitary adenylate cyclase polypeptide (*PACAP1*) involved in insulin secretion, and the imprinted *HYMAI* gene (hydatidiform mole associated and imprinted gene) are supposed as suitable candidate genes due to their location on chromosome 6 (Arima et al., 2001; Arima et al., 2000; Spengler et al., 1997). Mutations in the *KCNJ11* and the *ABCC8* genes, encoding the critical protein subunits Kir6.2 and SUR1 of the K_{ATP}-channels of pancreatic β-cells have also

been demonstrated as a rare cause of TNDM (Babenko et al., 2006; Flanagan et al., 2007; Gloyn et al., 2005; Polak et al., 2008).

1.2.2.3. Insulin gene mutations

Recently screening studies with linkage analyzes of families with PNDM substantiated reasonable suspicion that the insulin gene (*INS*) on chromosome 11p15 might be a candidate gene involved in the pathogenesis of subjects diagnosed with permanent neonatal diabetes of unknown genetic background but unrelated to autoimmunity (Edghill et al., 2008; Stoy et al., 2007; Stoy et al., 2010). To date, 20 heterozygous missense mutations in the human *INS* gene have been identified as common cause of insulin-deficient, permanent diabetes mellitus diagnosed predominantly in the neonatal period but definitely within one year of life and therefore referred to as mutant *INS* gene-induced diabetes of youth (MIDY) (Colombo et al., 2008; Edghill et al., 2008; Liu et al., 2010; Stoy et al., 2007). Classified by a nomenclature according to their position in the polypeptide chain of the mature insulin molecule and under specification of the amino acid residues being affected, identified dominant-acting heterozygous *INS* mutations were located at following codons: A24D at the signal peptide, H29D, L30P/V, G32S/R, L35P, L39_Y40delinsH, C43G, G47V and F48C located at the B-chain, R89C at the enzymatic cleavage site between C-peptide and the A-chain, as well as G90C, C95Y, C96Y/S, S101C, Y103C and Y108C/X situated in the A-chain of the preproinsulin molecule could be identified and are highly preserved throughout species (Colombo et al., 2008; Edghill et al., 2008; Stoy et al., 2010). Accounting for 56% of all *INS* mutations detected in permanent diabetic probands so far, A24D, G32S/R, F48C, R89C and C96Y/S were supposed to be the most common (Stoy et al., 2010). Diagnosed at the median age of nine to eleven weeks, neonatal patients suffer from severe hyperglycemia with menacing plasma glucose levels of 681 mg/dl accompanied by ketoacidosis, mostly undetectable C-peptide levels reflecting complete insulin deficiency and barely residual β-cell function. Drastically reduced birth weights showing tendency towards cachexia are regularly observed (Edghill et al., 2008; Stoy et al., 2007; Stoy et al., 2010). Glycemia in all investigated subjects was controlled with exogenous insulin medication in usually full replacement dosage of 0.5 units per kg per day leastwise (Edghill et al., 2008). Thus, symptoms of PNDM due to heterozygous mutations in the *INS* gene are hardly capable of being differentiated from those of

KCNJ11 and *ABCC8* mutations previously described (Stoy et al., 2007). Moreover in the vast majority of subjects carrying mutant *INS* heterozygosity so far, the mutation arose *de novo*, except for around 20% of probands born to affected parents showing autosomal dominant inheritance in origin (Colombo et al., 2008; Edghill et al., 2008; Stoy et al., 2010). By the way of an exception, mutations at codon A23S/T, R6C/H, G32S, L30M, R46Q and R55C at the enzymatic cleavage site between B-chain and C-peptide as well as R89C were identified to be also rare cause of idiopathic childhood-onset type 1 B diabetes mellitus, maturity-onset diabetes of the young (MODY) and unusually early type 2 diabetes mellitus associated with generally mild diabetic phenotypes, even though the estimated incidence was less than 2% (Bonfanti et al., 2009; Edghill et al., 2008; Molven et al., 2008; Polak et al., 2008; Rubio-Cabezas et al., 2009; Stoy et al., 2010). Beyond severe permanent diabetes mellitus due to dominantly acting *INS* mutations, recessive *INS* mutations in the homozygous state affecting essential regulatory nucleotide sequences for proinsulin biosynthesis are potent enough to result in permanent neonatal diabetes mellitus, non-autoimmune type 1 B diabetes mellitus and by the way of an exception in transient neonatal diabetes mellitus (Stoy et al., 2010). Due to the recessive inheritance pattern, neonates born to asymptomatic heterozygous carriers and especially subjects of consanguineous pedigrees are at increased risk of homozygosity and clinical manifestation of diabetic symptoms (Garin et al., 2010). Pathogenicity is based on recessively acting mutations occurring to transcription factor binding sites of the *INS* gene promoter region (c.366_-343del, c.-218A>C, c.331C>G/A, c.332C>G), to the translation initiation site c.3G>A/T, to the polyadenylation signal of the 3´untranslated region (3´UTR) (c.*59A>G) as well as resulting in a nonsense mutation c.184C>T (p.Q62X) and a complete multiexon deletion (M1_Q62del) affecting translation initiation site M1I (Garin et al., 2010; Hay and Docherty, 2006; Matsuoka et al., 2003; Naya et al., 1995; Wicksteed et al., 2007). Another subgroup of autosomal dominant inherited mutations in the *INS* gene was detected earlier to contribute on rare occasions to familial syndromes of hyperproinsulinemia as well as hyperinsulinemia by point mutations followed by amino acid substitution and have already been known for years as classical insulinopathies (Liu et al., 2010; Steiner et al., 1990; Stoy et al., 2010). The earlier described missense *INS* mutations V93L at position 3 of the A-chain, F48S and F49L at position 24 and 25 of the B-chain respectively are located at critical

recognition regions for insulin receptor binding and thereby influence the biological activity of the mutant insulin molecules (Haneda et al., 1983; Kwok et al., 1983; Nanjo et al., 1986; Tager et al., 1979). Hyperinsulinemia in these patients results from reduced receptor-mediated endocytosis through diminished receptor binding affinity of structurally abnormal insulin molecules (Steiner et al., 1990; Stoy et al., 2010). Additionally point mutations at codon H34D at position 10 of the B-chain as well as R89H/L/P at the endoproteolytic cleavage site between C-peptide and A-chain of the proinsulin polypeptide chain impair physiological processing to mature insulin and promote marked hyperproinsulinemia by releasing unprocessed or partially cleaved proinsulin intermediates into the circulation (Carroll et al., 1988; Chan et al., 1987; Collinet et al., 1998; Warren-Perry et al., 1997; Yano et al., 1992). In contrast to the disease pattern of the recently reported heterozygous and homozygous *INS* mutations, patients displaying familial hyperinsulinemia or hyperproinsulinemia mainly remain asymptomatic or reveal a certain degree of glucose intolerance and mild diabetic symptoms driven by insulin resistance with increasing age but barely overt diabetes mellitus (Oohashi et al., 1993; Steiner et al., 1990; Stoy et al., 2007). Hence, *INS* mutations were disregarded as potent pathogenic factors contributing to severe β-cell failure a long time (Stoy et al., 2010).

2. Pathophysiological consequences of insulin gene mutations

2.1. Insulin biosynthesis and posttranslational modification in the endoplasmic reticulum in the context of insulin gene mutations

Throughout vertebrate species the amino acid sequence of insulin is fairly well preserved and was first completely enlightened by Frederick Sanger in 1951 with bovine insulin followed by Nicol and colleagues in 1960 sequencing the human insulin (Mayer et al., 2007; Nicol and Smith, 1960; Sanger, 1959; Stoy et al., 2010). The insulin gene (*INS*) located at chromosome 11p15 is the encoding region for a cytosolic single-chain precursor molecule preproinsulin comprising the signal peptide of 24 amino acid residues, the B-chain consistent of 30 amino acid residues, the C-peptide flanked on both sides by dibasic cleavage sites and the A-chain of 21 amino acid residues in length (Liu et al., 2010; Stoy et al., 2010; Weiss, 2009). Efficiency of initiation and elongation of insulin mRNA towards

the nascent preproinsulin polypeptide is predominantly adjusted consistent with blood glucose levels (Welsh et al., 1986). Signal recognition particle-mediated transfer (SRP) through the cytosol of pancreatic β-cells and co-translational delivery into the lumen of the endoplasmic reticulum (ER) are enabled by the sequence of the signal peptide mediating required interactions (Liu et al., 2010). Following translocation into the ER and cleavage of the signal peptide, folding and posttranslational modification including formation of highly conserved disulfide bonds connecting B7-A7, B19-A20 and A6-A11 cysteine residues of the resulting proinsulin monomer is achieved successively with the objective of achieving biological activity linked to the three-dimensional structure of the mature insulin molecule (Mayer et al., 2007; Stoy et al., 2010). Subsequent processing of the prohormone including sorting into immature secretory granules, hexamer formation and endoproteolytic cleavage of the C-peptide via a des-31, 32 split proinsulin intermediate is completed transitioning through the Golgi compartment (Halban, 1994; Liu et al., 2010). Finally, the mature hormone is densely packed as Zn^{2+}-hexameric assembly through hydrogen-bonding in mature secretory granules of pancreatic β-cells until being secreted as monomers into the portal circulation (Huang and Arvan, 1994). X-ray crystallography has shown that the mature insulin molecule is a globular protein constituted of three α-helical domains facilitating disulfide bonding by approximating appropriate amino acid residues (Baker et al., 1988; Liu et al., 2010). The A-chain forms two α-helices including amino acid residues A3 to A8 as well as A 13 to A19 adjoining antiparallel to each other and enabling C95(A6) - C100(A7) and C31(B7) – C96(A7) alignment (Baker et al., 1988; Derewenda et al., 1989; Hua et al., 2002; Liu et al., 2010). The B-chain is composed of a N-terminal chain, a central α-helix by the amino acid residues 9 to 19 contributing to the acquisition of the C43(B19) - C109(A20) linking as well as two β-turns spanning residues B7 to B10 and B20 to B23 respectively (Baker et al., 1988; Hu et al., 1993; Nakagawa et al., 2006). The steric arrangement of the U-shaped double helix of the A-chain and the helical segment of the B-chain surrounds a hydrophobic core keeping non-polar amino residues inwardly (Baker et al., 1988; Mayer et al., 2007). Indeed, the highly preserved structural topology of the mature insulin, which consists ultimately of two polypeptide chains connected through disulfide bonds, hydrogen bonds as well as several hydrophobic and numerous non-covalent interactions showing strict homology in their localization within the molecule throughout

species, is most likely of particular importance for physiological competence of the hormone such as receptor binding affinity and structural stability (Hua et al., 2006a; Mayer et al., 2007; Zoete and Meuwly, 2006). Therefore, heterozygous mutations of the *INS* gene causing steric rearrangement of the insulin molecule give rise to a profound failure of hormone biosynthesis and action (Liu et al., 2010; Mayer et al., 2007).

2.2. Structural and functional consequences of insulin gene mutations

Heterozygous missense mutations in the *INS* gene disturbing insulin biosynthesis by shifting the amino acid sequence of the insulin precursor molecule have recently been reported as a new monogenetic cause of permanent neonatal diabetes mellitus through activation of the unfolded protein response and ultimately endoplasmic reticulum stress-induced β-cell apoptosis (Colombo et al., 2008; Edghill et al., 2008; Garin et al., 2010; Stoy et al., 2007). The majority of the dominant-acting mutations either directly affect integrity of the three highly conserved disulfide bonds (C31(B7)–C96(A7), C43(B19)-C109(A20), C95(A6)-C100(A11)) occurring in coding regions for cysteine residues involved in proinsulin disulfide pairing (C43G, C95Y, C96Y/S) or indirectly, occurring in critical regions for thermodynamic stability in the vicinity of such disulfide bonds (H29D, L30P/V, G32S/R, G47V, Y108X) (Colombo et al., 2008; Edghill et al., 2008; Liu et al., 2010; Mayer et al., 2007; Stoy et al., 2007). The side chain of the histidine imidazole ring at B5 is indispensably entangled in A7–B7 alignment during biosynthesis and therefore substitution of the histidine residue at B5 for aspartic acid (H29D) hampers the kinetic folding process in the ER (Hua et al., 2006a; Liu et al., 2010). Additionally H29 substitution directly affects steric configuration of the mature insulin protein and prevents aggregation towards a compact dimer by destabilizing the A7–B7 disulfide bridge, which is completely exposed on the surface of the molecule predominantly stabilized by the histidine residue at position B5 and thereby influences the conformation of neighboring structures (Baker et al., 1988; Hua et al., 2006a). The mutation L30P/V leads to augmented hydrophobicity and to altered orientation of the N-terminal domain of the B-chain provoking negative steric impact on A7 – B7 disulfide conjunction and on receptor recognition domains of the A-chain. Reduced receptor binding potency and folding capability were found to arise as a consequence (Blundell et al., 1972; Mayer et al., 2007; Nakagawa and Tager, 1991). A characteristic feature

of hexameric insulin is the capability of transitioning between the T and the R confirmation mainly directed by the glycine residue at position 8 of the B-chain exhibiting a positive dihedral angle or an anhedral angle. The stereospecific conformational change facilitates stability through disulfide pairing and folding of the immature molecule adopting the T-state confirmation but enhancing biological activity and receptor binding potency in the R-state (Nakagawa et al., 2005). The mutation G32S/R substituting the glycine residue at position B8 for L-serine or L-arginine necessitates an axially symmetric rotation of the N-terminal domain of the B-chain, imitating R-like confirmation, which in consequence impairs folding by impeding A7–B7 disulfide linking (Hua et al., 2006c; Stoy et al., 2007). The G47V mutation at position B23 results in L-amino acid substitution and thereby affects A20–B19 disulfide bond and additional folding steps by perturbation of the specific A20–B19-related folding nucleus (Hua et al., 2006b; Nakagawa et al., 2006; Stoy et al., 2007). Replacing the tyrosine residue at position A19 with a variable amino acid residue (Y108X) introduces a premature stop codon within the insulin mRNA neighboring the C43(B19)-C109(A20) disulfide bond. Therefore Y108X mutation directly inhibits translation of cysteine (C109) at position A20 as well as asparagine at position A21 of the N-terminal domain of the A-chain and the resultant preproinsulin cDNA completely lacks the utmost important disulfide bond C43(B19)-C109(A20) (Colombo et al., 2008). Furthermore several mutations in the *INS* gene introduce additional unpaired cysteine residues (F48C, R89C, G90C, S101C, Y103C, Y108C) increasing the risk of mispairing in critical regions of proteolytic cleavage sites at the A-chain-C-peptide junction and especially in the contiguity to the C43(B19)-C109(A20) disulfide bond (Stoy et al., 2007). Additionally critical mutations were found at the N-terminal site of the signal peptide (R6C/H) or at the C-terminal cleavage site of the signal peptide (A24D), which are assumed to have adverse effects either on translocation of nascent preproinsulin into the lumen of the ER mainly through alterations of electrical properties or on cleavage of the signal peptide affecting the subsequent protein folding pathway in the ER (Park et al., 2010; Stoy et al., 2007; von Heijne, 1988). As previously described, the mutual steric alignment of the A-chain and the B-chain is predominantly perpetuated by hydrophobic interactions of several non-polar amino acids (L102(A13), L105(A16), L30(B6), L35(B11), L39(B15), V42(B18), Y108(A19)) constituting a hydrophobic core (Mayer et al., 2007; Zoete and Meuwly, 2006). Presumably,

mutations around these critical residues, such as L35P (B11) and the in-frame substitution L39_Y40delinsH (B15, B16) are highly conducive to serious conformational changes of the entire proinsulin monomer especially through hydrophobic interaction with neighboring water molecules and therefore to impairment of thermodynamic stability, imperative for the subsequent protein folding process (Colombo et al., 2008; Schroder and Kaufman, 2005; Zoete and Meuwly, 2006). Moreover insulin receptor recognition-site of the mature insulin molecule is equably composed of the invariant amino acid residues G90(A1), Q94(A5), Y108(A19), N110(A21), V36(B12),Y40(B16), G47(B23), F48(B24) as well as F49(B25) conveying high affinity binding energy to the receptor. Besides steric impact on secondary structure of the immature protein, mutant alleles encoding these amino acids consequently abate biological activity of the resultant insulin hormone defined by efficient receptor binding acquirement (Mayer et al., 2007; Mirmira et al., 1991; Mirmira and Tager, 1989). By way of derogation, rarely observed mutations at codon A23S/T, L68M, and G84R are supposed to be barely pathogenic, as they are either capable to escape entrapment within the ER and effectively reach the Golgi compartment or as they are located at CpG hotspots for mutations in mammalians and thus are not conserved throughout species (Edghill et al., 2008; Park et al., 2010; Stoy et al., 2010). Furthermore mutant proinsulin variants are assumed to additionally affect biosynthesis and secretion of the synchronously expressed wild-type proinsulin in a dominant-negative pattern by constituting covalent intermolecular protein complexes recruiting wild-type proinsulin molecules through highly reactive cysteine residues and hydrophobic interactions (Hodish et al., 2010; Liu et al., 2007; Park et al., 2010; Weiss, 2009). Hence, additionally retained wild-type insulin contributes to already insufficient insulin supply and acuminates ER-stress culminating in β-cell death (Hodish et al., 2010). Indeed, the diabetic phenotype in subjects genotyped with heterozygous *INS* mutations are based upon perturbation of proinsulin biosynthesis and assembly (Stoy et al., 2007; Weiss, 2009). In general mutant proinsulin shows an increased propensity to incorrect folding and steric rearrangement definitely failing the quality inspection in the endoplasmic reticulum (ER) and is therefore trapped within the ER (Ellgaard and Helenius, 2003; Park et al., 2010; Rajan et al., 2010; Stoy et al., 2007). Altered side chain properties of the substituted amino acid residues, incorrect disulfide pairing with resultant reactive unpaired cysteine residues and accumulation of unfolded

immature proteins presumably through defective communication of the mutant proinsulin polypeptide with the folding machinery of the ER, initiate an unfolded protein response pathway (UPR) ultimately triggering β-cell apoptosis accompanied by absolute insulin deficiency (Colombo et al., 2008; Liu et al., 2007; Noiva, 1999; Stoy et al., 2010; Wedemeyer et al., 2000; Weiss, 2009).

2.3. The endoplasmic reticulum stress – critical role in the pathogenesis of diabetes mellitus

2.3.1. Physiology of the endoplasmic reticulum – complex interaction of concomitant cellular factors

The endoplasmic reticulum is a highly specialized and prolific organelle of eukaryotic cells featuring a suitable oxidative environment for the posttranslational modification of newly synthesized proteins and is therefore pivotal for the cells to survive (Araki et al., 2003; Ma and Hendershot, 2002; Scheuner and Kaufman, 2008; Sundar Rajan et al., 2007). Almost all secretory proteins are initially delivered to the endoplasmic reticulum for further modification followed by the release to target sites (Eizirik et al., 2008; Ghaemmaghami et al., 2003; Schroder and Kaufman, 2005). Nascent polypeptides are recruited into ribosome-nascent-chain-signal-recognition-particle complexes mediating translocation into the luminal space of the endoplasmic reticulum through the Sec61p protein channel (Adesnik et al., 1976; Connolly and Gilmore, 1989; Neuhof et al., 1998; Walter and Johnson, 1994; Wilkinson et al., 1997). The ER harbors complex folding machinery composed of a diversity of molecular chaperones, several protein foldases as well as lectins imperative to accomplish numerous posttranslational modifications to the immature proteins. N-linked glycosylation and formation of disulfide bonds were identified to be the most common biosynthetic functions of the ER (Freedman, 1989; Gething and Sambrook, 1992; Schroder and Kaufman, 2005; Sundar Rajan et al., 2007; Walsh and Jefferis, 2006). The protein disulfide isomerase (PDI), catalyzing dithiol oxidation of protein substrates through a high intrinsic reduction potential of cysteine pairs in their active site, is the essential contributor of disulfide formation (Freedman, 1989; Gething and Sambrook, 1992; Kemmink et al., 1997; Sundar Rajan et al., 2007). Furthermore the oxidative redox state of the luminal compartment of the endoplasmic reticulum is mainly perpetuated by the electron

acceptor glutathione (GSH↔GSSG) buffering thiol-disulfide exchange reactions (Hwang et al., 1992). In either case, proteins, undergone ER-associated posttranslational modification and assumed to be folded properly, are not targeted to subsequent compartments *a priori* but have to pass through an quality control program (Ellgaard et al., 1999; Sayeed and Ng, 2005; Schroder and Kaufman, 2005). A variety of molecular mechanisms function as effective monitoring system for correct folding of immature polypeptides by stabilizing misfolded protein intermediates, preventing aggregation, and retaining them in the ER (Ellgaard et al., 1999; Marquardt and Helenius, 1992). Unfolded polypeptides are characterized by completely or fractionally exposed hydrophobic regions or unpaired cysteine residues, normally kept safe within the core of a mature protein and are therefore certainly identified (Parodi, 2000; Schroder and Kaufman, 2005). The adenosine triphosphate (ATP)-dependent chaperone BiP, highly expressed in pancreatic β-cells, binds folding intermediates energized by ATP hydrolysis through a *N*-terminal ATPase (Araki et al., 2003; Flynn et al., 1989). The calnexin-calreticulin cycle, also referred to as glucose trimming, is a dynamic process of glycosylation linked to increased substrate binding affinity of calnexin-calreticulin and deglycosylation adherent with substrate release from the lectin anchor. This process is alternately regulated by the uridine 5'-diphosphate (UDP)-glucose:glycoprotein glucosyl transferase (UGGT) and the α(1,3) glucosidase II (Ellgaard et al., 1999; Sousa et al., 1992). Improperly processed glycoproteins are efficiently retrieved via their hydrophobic properties and withdrawn by UGGT through another round of reglycosylation. Thus, the inchoate protein is retained within the endoplasmic reticulum and subjected to further folding cycles exerting for complete folding and steric conformation (Ellgaard et al., 1999; Parodi, 2000; Sousa and Parodi, 1995; Sousa et al., 1992). Furthermore, the protein disulfide isomerase (PDI) features an additional substrate-binding domain functioning as a molecular chaperone (Kemmink et al., 1997; Noiva, 1999; Ren et al., 1998; Wang, 1998). Following a stringent quality control, properly folded proteins are targeted for final modifications and sorting to the Golgi apparatus mediated by a vesicular transport system, known as ER-Golgi intermediate compartment or vesicular-tubular clusters (VTC) (Lee et al., 2004). *De facto* transport is mediated through COPII- and COPI-coated vesicles (Gorelick and Shugrue, 2001). Pancreatic β-cells are exceedingly addicted to a highly developed and undisturbed ER function due to their highly effective insulin biosynthesis (Araki et al., 2003;

Van Lommel et al., 2006). Vice versa, perturbations of the complex operational sequences of protein biosynthesis within the ER of pancreatic β-cells are often devastating (Eizirik et al., 2008; Liu et al., 2007; Sundar Rajan et al., 2007). Hence, mutations such as heterozygous mutations in the *INS* gene, affecting their own physiological protein folding process and provoking aggregation of unfolded polypeptides, have the ability to exert chronic stress on the ER and at last apoptotic cell death (Eizirik et al., 2008; Harding and Ron, 2002).

2.3.2. The unfolded protein response (UPR) of the endoplasmic reticulum – distinct pathway in answer to ER stress

Endoplasmic reticulum stress describes per definition a cellular state, which occurs when the functional demand on the ER overburdens the folding capacity of the ER resulting in the accumulation of incorrectly folded or unfolded proteins in the luminal space of the endoplasmic reticulum (Harding and Ron, 2002; Sundar Rajan et al., 2007; Yamamoto et al., 2004). The unfolded protein response (UPR) is a positive adaptive signaling pathway of the endoplasmic reticulum adapting the folding capacity and efficiency to variable requirements in order to overcome a certain level of ER stress (Bernales et al., 2006; Eizirik et al., 2008; Rutkowski and Kaufman, 2004). Thus the accumulation of unfolded proteins prompts a complex signaling pathway largely resulting in the transcriptional enhancement of molecular chaperones and folding enzymes to prevent aggregation, adjustment of new protein synthesis on the transcriptional level to prevent advancing accumulation of client polypeptides and augmented ER-associated degradation (ERAD) by the ubiquitin-proteasome pathway following retro-translocation to the cytosol to discard irreversibly unfolded proteins (Araki et al., 2003; Eizirik et al., 2008; Patil and Walter, 2001; Sundar Rajan et al., 2007).

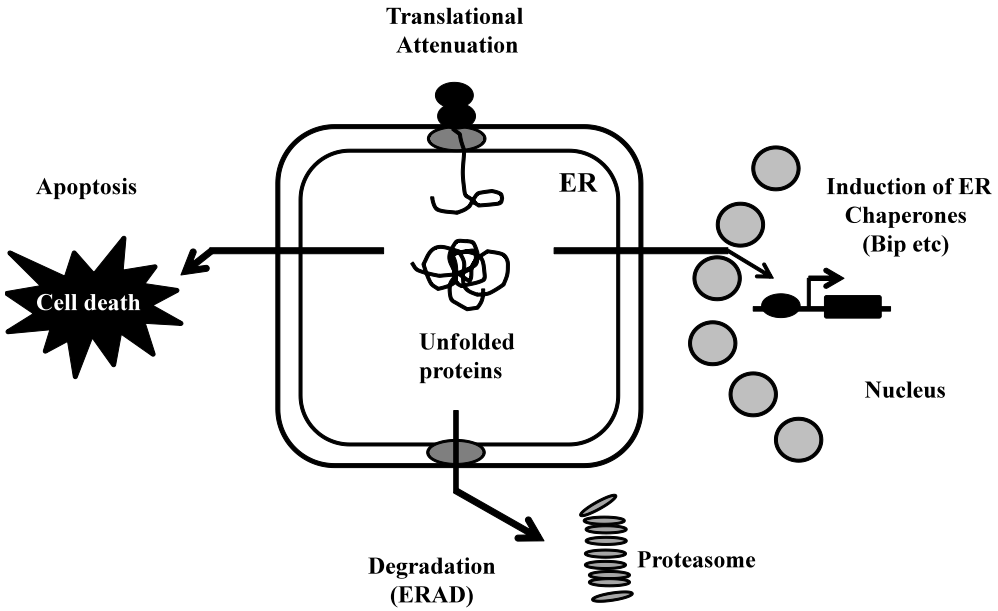

Figure 1: The unfolded protein response (UPR) pathway

The UPR initializes broadly based strategies to overcome ER stress and to preserve cellular integrity (Araki et al., 2003); with kind permission from the Society of Experimental Biology and Medicine.

2.3.2.1. Signal transduction of the unfolded protein response – ambitious interdisciplinary efforts to preserve cellular integrity

The inositol requiring ER-to nucleus signal kinase 1 α (IRE1α), RNA-dependent protein kinase-like endoplasmic reticulum eIF2α kinase (PERK) and activating transcription factor 6 α and β (ATF6α/β) are stress-regulated transcription factors triggering signal transduction from the ER to the nucleus as proximal components of the UPR in eukaryotic cells (Bertolotti et al., 2000; Harding et al., 1999; Haze et al., 2001; Rutkowski and Kaufman, 2004; Scheuner and Kaufman, 2008; Shi et al., 1998; Tirasophon et al., 1998; Wu et al., 2007; Yoshida et al., 1998). IRE1α, PERK and ATF6 are maintained in the inactive state through complex formation with the molecular chaperone BiP bound to their luminal domains (Bertolotti et al., 2000; Ron, 2002; Shen et al., 2002). PERK is a type I transmembrane protein kinase, which possesses an oligomerized and trans-autophosphorylated luminal domain in its active state increasing protein-kinase activity of the cytoplasmic domain (Bertolotti et al., 2000; Harding et al., 1999; Liu et al., 2000; Taylor et al., 1996). Activated PERK phosphorylates the highly conserved serine residue 51

located in the α-subunit of the guanine nucleotide binding protein (G-protein) eukaryotic initiation factor-2α (eIF2α), diminishing protein synthesis through disturbed translation initiation (Harding et al., 1999; Samuel, 1993; Shi et al., 1998; Vachon et al., 1990). Phosphorylated eIF2α (PeIF2α) is unable to interconnect with the translation initiator methionyl tRNA (Met-RNA), imperative for guanine triphosphate (GTP)-dependent binding to the 40S ribosomal subunit and translation initiation of most client mRNAs (de Haro et al., 1996; Harding et al., 2000; Pain, 1996; Samuel, 1993). PeIF2α reveals augmented affinity for guanine diphosphate (GDP) and is therefore sequestered in the inactive conformation (Clemens, 1994; de Haro et al., 1996; Pain, 1996). Beyond the attenuation of mRNA translation, PERK is additionally involved in the transcriptional regulation of the UPR through translational up-regulation of the activating transcription factor 4 (ATF4) by PeIF2α mediating selective translation of two upstream open reading frames (uORF) in the 5'untranslated region of ATF4 mRNA (Harding et al., 2000; Hinnebusch, 1997; Lu et al., 2004; Pain, 1996; Sundar Rajan et al., 2007; Vattem and Wek, 2004). Moreover ATF4 is an important activator of the proapoptotic transcription factor C/EBP homologous protein (CHOP) mRNA expression and therefore involved in apoptosis initiation (2.3.2.2) (Harding et al., 2000; Liu and Kaufman, 2003; Oyadomari and Mori, 2004). The highly preserved type I transmembrane protein kinase IRE1α is also activated by oligomerization and autophosphorylation in almost the same manner as stated for PERK activation displaying vast homology in their stress-sensing luminal domains (Bertolotti et al., 2000; Liu et al., 2000; Liu et al., 2002; Tirasophon et al., 2000). Activated IRE1α elicits distinct endoribonuclease activity in the cytoplasmic carboxy-terminal domain and participates in downstream signaling by splicing an intron of 26 nucleotides in length from the basic domain/leucin zipper (bZIP) protein X-box binding protein 1 (*XBP1*) mRNA (Calfon et al., 2002; Tirasophon et al., 1998; Yoshida et al., 2001a). Spliced XBP1 (XBP1s) is characterized by a translational frame shift through selective translation of overlapping open reading frames (ORFs) resulting in the exchange of the C-terminal domain for a bZIP containing domain enhancing transcriptional activity (Lee et al., 2003; Yoshida et al., 2001a). Microarray analysis identified XBP1s to most likely target ERAD components after translocation to the nucleus (Lee et al., 2003). Moreover IRE1α is supposed to directly enable mRNA degradation by hampering translocation through alterations

in the target message of client mRNAs by endonucleolytic cleavage (Hollien et al., 2009; Hollien and Weissman, 2006; Lipson et al., 2008). In addition, IRE1α is instrumental upon others in initiating stress-induced apoptosis through activation of the mitogen-activated protein kinase (MAPK) c-Jun N-terminal kinase (JNK) and nuclear factor κB (NF-κB) (2.3.2.2.) (Davis, 1999; Hu et al., 2006; Urano et al., 2000). The bZIP transcription factors ATF6α and ATF6β are type II transmembrane glycoproteins and function as the third stress sensing institution of the UPR in mammalian cells (Eizirik et al., 2008; Haze et al., 1999; Nadanaka et al., 2007). The only difference between ATF6α and ATF6β appears to be, that they are encoded by different genes, the *ATF6* gene on chromosome 1 and the G13 (cAMP response element-binding protein-related protein) gene (*ATF6B*) localized on chromosome 6 (Haze et al., 2001; Yoshida et al., 2001b). ATF6 (α/β) is compound of a cytosolic N-terminal bZIP-portion, a luminal domain containing three highly conserved *N*-linked glycosylation sites modulating interaction with the calnexin-calreticulin cycle as well as two Golgi localization sequences (GLS1, GLS2) mediating stable attachment to the molecular chaperone BiP and trafficking of the activated cytosolic domain of ATF6 to the Golgi compartment (Haze et al., 1999; Hong et al., 2004; Schroder and Kaufman, 2005; Shen et al., 2002; Shen et al., 2005). ER stress entails ATF6 activation through regulated intramembrane proteolysis (Rip) (Brown et al., 2000; Ye et al., 2000). Following divestiture of the BiP-ATF6 complex in response to ER stress, monomeric ATF6 is released towards the Golgi compartment through vesicular transport and targeted by exposed GLS2 (Chen et al., 2002; Nadanaka et al., 2007; Nadanaka et al., 2004; Shen et al., 2002). Golgi-resident site-1 (S1P) and site-2 (S2P) proteases cleave ATF6 and an activated transcription factor composed of the cytosolic bZIP portion achieves the competence to enter the nucleus and exert influence on the expression of UPR-related target genes in order to optimize the folding capacity of the ER (Haze et al., 1999; Melville et al., 1999; Okada et al., 2002; Wu et al., 2007; Yamamoto et al., 2007; Ye et al., 2000; Yoshida et al., 1998). Furthermore activated ATF6 interferes with the IRE1-XPB1 pathway through heterodimerization with XPB1 and is thereby synergistically conducive to the transcriptional regulation of ERAD mediators (Lee et al., 2003; Yamamoto et al., 2007; Yoshida et al., 2003). In addition, the ATF6 pathway and the previously described ATF4 pathway converge in the transcriptional activation of the *CHOP* promoter resulting in enhanced expression of the *CHOP* gene commencing

growth arrest and apoptosis (Ma et al., 2002; Yoshida et al., 2000; Zinszner et al., 1998). UPR-related transcription factors deploy their transcriptional activity through direct DNA binding sites in the promoter regions of their target genes (Haze et al., 1999; Kokame et al., 2001; Roy and Lee, 1999; Yoshida et al., 1998). In mammals, a *cis*-acting tripartite consensus sequence 5'CCAAT-9 nucleotides-CCACG'3, which is in part reiterated as structural identic CCAAT motif throughout the whole promoter sequence, has been identified as crucial for stress-induced transcriptional up-regulation of genes coping with endoplasmic reticulum stress and was therefore referred to as ER stress response element (ERSE) (Roy and Lee, 1999; Yoshida et al., 1998). Another *cis*-acting ER stress response element sequence (ERSE-II) ATTGG-N-CCACG was solely found in the promoter region of the homocysteine-induced endoplasmic reticulum protein (Herp), an ER-stress induced integral membrane protein of unknown function to date (Kokame et al., 2000; Kokame et al., 2001; Yamamoto et al., 2004). Enhancer activity for ERSE II was stated for ATF6 just as for XBP1 binding to the CCACG motif (Kokame et al., 2001; Yamamoto et al., 2004). The third regulatory *cis*-acting element involved in ER stress-associated induction of UPR-related genes is the mammalian unfolded protein response element (UPRE) characterized by the palindromic sequence TGACGTGG/A mediating induction of ERAD components through prevailing XBP1 binding (Wang et al., 2000; Yamamoto et al., 2007; Yamamoto et al., 2004; Yoshida et al., 2001a). ATF6 attain binding affinity to UPRE merely by heterodimerization with XBP1 displaying even higher binding affinity than XBP1 homodimer reclusively (Yamamoto et al., 2007; Yoshida et al., 2001a).

2.3.2.2. Stress-induced apoptosis triggers tissue dysfunction - β-cell apoptosis causes insulin deficiency in permanent neonatal diabetes

Under conditions of sustained and insuperable endoplasmic reticulum stress to all appearances, programmed apoptotic cell death is instituted predominantly through inducible proapoptotic activity of UPR-associated regulators PERK, ATF6 and IRE1α mediating downstream signaling aimed at preservation of the integrity of the organism (Eizirik et al., 2008; Harding and Ron, 2002; Rao et al., 2004; Sundar Rajan et al., 2007; Szegezdi et al., 2006; van der Kallen et al., 2009). Unfortunately progressive cell demise undermines physiological tissue function and ultimately contributes to various diseases (Kaufman, 2002; Kim et al., 2008;

van der Kallen et al., 2009). Although the complex cross linking of ER stress-induced apoptotic signaling is barely elucidated, three apoptotic pathways are defined: The upregulation of the proapoptotic transcription factor CHOP, the activation of the mitogen-activated protein kinases (MAPK) JNK and apoptosis signal-regulating kinase 1 (ASK1) as well as the bipartite activation of caspase 12 (CASP12) (Fornace et al., 1988; Nakagawa and Yuan, 2000; Nishitoh et al., 1998; Urano et al., 2000; Yoneda et al., 2001; Zinszner et al., 1998).

The activating phosphorylation of the mitogen-activated protein kinase (MAPK) c-Jun N-terminal kinase (JNK) is based on activated IRE1α recruiting the adaptor molecule tumor necrosis factor type 2 receptor associated protein (TRAF2) to form a heterodimeric complex with ASK1 on the outer membrane of the ER (Nishitoh et al., 2002; Nishitoh et al., 1998; Urano et al., 2000). JNK initiates apoptosis through activating or inhibitory phosphorylation of serine (Ser) or threonine (Thr) residues of a proline (Pro)-rich consensus sequence (Pro-X-Ser/Thr-Pro) in the polypeptide sequence of effector subjects. The proto-oncogenes c-Jun and c-Myc, tumor suppressor p53 as well as mitochondrial-derived transcription factors of Bcl2 related proteins (Bcl2, Bcl-x_L, Bad, Bim_{EL}, Bax, Bmf) are activated in consequence of ER-related proapoptotic stimuli (Besnard et al., 2011; Bogoyevitch and Kobe, 2006; Davis, 2000; Germain et al., 2006; Kaufman, 2002; Lei et al., 2002; Leppa and Bohmann, 1999; Noguchi et al., 1999; Rogatsky et al., 1998; Schreiber et al., 1999; Scorrano et al., 2003; Yamamoto et al., 1999; Yang et al., 2007). Furthermore recruitment of TRAF2 by IRE1α leads to the separation of procaspase-12 (pCASP12), which is sequestered in the inactive state in a stable complex with TRAF2 on the cytosolic surface of the endoplasmic reticulum until its activation solely through ER affecting insults (Kaufman, 2002; Nakagawa et al., 2000; Yoneda et al., 2001). Activating cleavage and dimerization of pCASP12 enables transmission of apoptotic signals from the ER to the cytoplasm and initiation of a cytosolic caspase-9-dependent signal cascade, which ultimately triggers ER stress-induced apoptosis through caspase 3 activation (Morishima et al., 2002; Rao et al., 2001; Yoneda et al., 2001). Beyond caspase-8 activated by death receptor-mediated signaling, JNK was identified to facilitate mitochondrial cytochrome *c* (Cyt-c) release upon ER stress tightly linked to the apoptotic peptidase activating factor 1 (APAF1)-dependent activation of caspase-9, which in turn mediates apoptosis initiation by

caspase-3 activation (Davis, 1999; Gross et al., 1999; Jimbo et al., 2003; Tournier et al., 2000; Zou et al., 1999). Furthermore overexpression of the proapoptotic transcription factor CHOP is tightly linked to the initiation of apoptosis in response to chronic ER stress (Oyadomari and Mori, 2004; Zinszner et al., 1998). As a member of the CCAAT/enhancer binding protein family (C/EBP), CHOP, also designated as growth arrest- and DNA damage-inducible gene 153 (GADD 153), features a C-terminal basic leucine zipper (bZIP) domain mediating binding to consensus sequences of target genes (Maytin et al., 2001; Oyadomari and Mori, 2004; Ramji and Foka, 2002; Ron and Habener, 1992). *CHOP* transcription is mainly regulated through ATF6 and ATF4 pathway converging in the transcriptional activation of the *CHOP* promoter by binding to a functional ERSE element in the promoter sequence of the *CHOP* gene (Ma et al., 2002; Shen et al., 2002; Yoshida et al., 2000; Zinszner et al., 1998). ER stress-associated *CHOP* activation leads to the initialization of several proapoptotic strategies including downregulation of the anti-apoptotic factor B-cell CLL/lymphoma 2 (Bcl-2), interactions with mitochondria-derived apoptotic signaling and alteration of the cellular redox-state by gluthatione depletion, the main buffer system of the endoplasmic reticulum and imperative for antioxidative defense as well as undisturbed ER function (McCullough et al., 2001; Oyadomari and Mori, 2004). For instances, high-level expression of mutant insulin mRNA as a result of heterozygous mutations in the insulin gene (*INS*) and the consequent interminable accumulation of misfolded proinsulin polypeptides in the endoplasmic reticulum ultimately triggers apoptosis of perturbed β-cells following exhausting of compensatory abilities of the UPR by chronic ER stress. Progressive β-cell demise gradually culminates in insulin deficiency and full-blown clinical diabetes mellitus (Eizirik et al., 2008; Harding and Ron, 2002; Hodish et al., 2010; van der Kallen et al., 2009).

3. Animal models for translational diabetes research

Translational medicine means by definition the interface between basic research and clinical application (Wehling, 2008). Animal models, which are reasonably predictive of humans in terms of safety and efficacy of new therapeutic strategies are of particular relevance in this field (Kirk, 2003). Animal models are useful for investigations on the etiology and pathogenesis of various human diseases and on the feasibility of new effective therapeutic concepts (Kirk, 2003). The increasing

supply of a diverse spectrum of new technologies for the genetic engineering of animal models provides the opportunity to create a diversity of tailored animal models for specific questions of translational research and thus complies the requirements on the refinement of animal experiments (Aigner et al., 2010; Kues and Niemann, 2004; Melo et al., 2007; Prather et al., 2003; Rees and Alcolado, 2005). In particular, diabetes research necessitates suitable animal models for investigations on the genetics and pathogenesis of this complex disease as well as on the accruement of its associated complications to directly draw benefits for human counterparts (Rees and Alcolado, 2005).

3.1. Mutations in the insulin gene and diabetes mellitus in rodent models

Diabetic rodent models have traditionally been used for molecular genetic analyzes of accountable genes, description of related phenotypic characteristics as well as for studying the underlying disease mechanisms and the pathomorphologial consequences of hyperglycemia (Aigner et al., 2008). Hyperglycemic mouse lines expressing mutant *Ins2* gene are derived either from spontaneous mutations or from chemical mutagenesis within the *N*-ethyl-*N*-nitrosourea (ENU) mouse mutagenesis project paving the way for the establishment of mutant mouse lines through selective phenotype-driven breeding, which in turn facilitates genotypic analyzes through the identification of the chromosomal regions by linkage analyzes followed by analyzes of candidate genes (forward genetics) (Aigner et al., 2008; Herbach et al., 2007; Yoshioka et al., 1997). Mutagenic effect of the alkylating ENU is deployed at high frequency on premeiotic spermatogonial stem cells of male mice after intraperitoneal application, inflicting random point mutations on their genome (Aigner et al., 2008; Justice et al., 1999; Russell et al., 1979).

3.1.1. The Munich *Ins2*^{C95S} mutant mouse – diabetic mouse line derived from the Munich ENU mouse mutagenesis project

The diabetic Munich *Ins2*^{C95S} mutant mouse is derived from the Munich ENU mouse mutagenesis project based on the genetic background of the inbred strain C3HeB/FeJ (C3H) (Aigner et al., 2008; Herbach et al., 2007). Genome-wide linkage analyzes and candidate sequencing identified a T→A transversion at nucleotide position 1903 in exon 3 of the *Ins2* gene to underlie the diabetic

phenotype in these mice. The distinct mutation was inherited in an autosomal dominant manner and results in an amino acid exchange from cysteine to serine at position 95 (C95S) of the preproinsulin polypeptide and the disruption of the C95(A6)-C100(A11) intrachain disulfide bond, disturbing preproinsulin biosynthesis and assembly (Herbach et al., 2007; Stoy et al., 2007; Weiss, 2009).

Heterozygous Munich *Ins2*^{C95S} mutant mice remained normoglycemic until the age of almost four weeks and showed unaltered fasted and postprandial serum insulin levels compared to corresponding age- and sex-matched wild-type mice. However serum insulin levels 10 minutes after oral glucose challenge were already significantly reduced in comparison to controls, indicating disturbed glucose-stimulated insulin secretion of β-cells in heterozygous *Ins2*^{C95S} mutant mice. This is underlined by significantly reduced homeostasis model assessment of baseline insulin secretion (HOMA-B) indices in heterozygous *Ins2*^{C95S} mutants compared to sex-matched wild-type mice, suggesting disturbed steady-state β-cell function (Herbach et al., 2007; Matthews et al., 1985). Fasting blood glucose levels of male heterozygous Munich *Ins2*^{C95S} mutant mice increased further over time and reached almost 400 mg/dl, whereas female mutants preserved a mild hyperglycemia and marginally disturbed glucose tolerance. Furthermore heterozygous male *Ins2*^{C95S} mutants exhibited growth retardation compared to corresponding females at the age of 3 months (Herbach et al., 2007). Studies conducted on ovariecomized heterozygous Munich *Ins2*^{C95S} mutant mice have shown that the gender dimorphism observed in these mice is mainly based upon protective effects of estrogen in females (Schuster, 2011). Furthermore significantly increased HOMA of insulin resistance (HOMA-IR) indices and delayed response to exogenous insulin injection in male heterozygous *Ins2*^{C95S} mutant mice compared to wild-type controls were suggestive of a certain degree of insulin resistance (Herbach et al., 2007). Qualitative-histological and quantitative-stereological analyzes on immunohistochemically stained sections of pancreatic tissue detected a largely altered composition of the pancreatic islets with a progressive reduction of the total β-cell volume in male hetereozygous *Ins*^{C95S} mutant mice accountable for the seriously disturbed glycemic control in these mice (Herbach et al., 2007). On the electron microscopic level, pancreatic β-cells of heterozygous Munich *Ins2*^{C95S} mutant mice were correspondingly almost devoid of insulin secretory granules and the ER appeared enlarged, whereas

alterations in female mutants were present but less pronounced (Herbach et al., 2007; Kautz, 2011). Kidney weights of heterozygous male *Ins2*^{C95S} mutant mice were significantly increased, displaying an early sign for diabetic kidney disease (Kautz, 2011; Mahimainathan et al., 2006). Diabetes-associated pathological alterations of the kidney have not been investigated in the Munich *Ins2*^{C95S} mouse model so far (Kautz, 2011).

Homozygous *Ins2*^{C95S} mutant mice revealed a fulminant early-onset hyperglycaemic phenotype with significantly elevated blood glucose levels of almost 400 mg/dl and significantly reduced body weights compared to wild-type mice irrespective of the gender. Life expectancy of both genders was lower compared to sex-matched heterozygous *Ins2*^{C95S} mutant mice and wild-type control mice (Herbach et al., 2007).

3.1.2. The Akita mouse model expressing *Ins2*^{C96Y} mutant gene

The Akita mouse model is a stable diabetic mouse line based on the genetic background C57BL/6 (B6) and originally derived from a spontaneous mutation in the *Ins2* gene (Yoshioka et al., 1997). A G→A transition at nucleotide position 1907 in exon 3 of the *Ins2* gene on chromosome 7 was identified as diabetogenic locus in these mice. This missense mutation is inherited in an autosomal-dominant manner and precludes formation of the C96(A7)-C31(B7) intermolecular disulfide bond by substitution of the cysteine residue at position 96 to tyrosine (C96Y) (Wang et al., 1999). The Akita *Ins2*^{C96Y} mutation entails conformational rearrangement of the nascent preproinsulin 2 polypeptide with detrimental influence on the insulin secretory pathway as previously described (Stoy et al., 2007; Wang et al., 1999; Weiss, 2009).

As observed in heterozygous Munich *Ins2*^{C95S} mutant mice, severe diabetic symptoms in heterozygous Akita *Ins2*^{C96Y} mutant mice were recognised from the age of four weeks and showed likewise a distinct gender dimorphism (Herbach et al., 2007; Yoshioka et al., 1997). Male heterozygous Akita *Ins2*^{C96Y} mutant mice revealed significantly increased randomly fed blood glucose levels of 280 mg/dl at four weeks of age progressing steadily up to over 500 mg/dl at the age of nine weeks, demonstrating the highly diabetogenic impact of one mutated *Ins2* allele in spite of the presence of one wild-type *Ins2* and two wild-type *Ins1* alleles in rodents (Wang et al., 1999; Yoshioka et al., 1997). Attendant randomly fed

immunoreactive plasma insulin levels of male heterozygous Akita *Ins2*^{C96Y} mutant mice were reduced by 60% compared to age- and sex-matched wild-type controls and by 22% compared to age-matched female mutants. In addition hyperglycaemic male heterozygous Akita *Ins2*^{C96Y} mutant mice developed a peripheral insulin resistance (Hong et al., 2007). Furthermore impaired growth was observed in male heterozygous Akita *Ins2*^{C96Y} mutant mice in comparison to female mutants and non-affected wild-type mice. The diabetic phenotype in male mutants was ultimately severe enough to halve their life expectancy compared to female mutants and sex-matched wild-type mice (Yoshioka et al., 1997). Insulin staining on pancreatic sections of male and female heterozygous Akita *Ins2*^{C96Y} mutant mice and sex-matched non-affected control mice of four to 30 weeks of age revealed a time-dependent progressive loss of functional β-cells. The volume fraction of insulin-positive cells in the islets was diminished by approximately 90% in proportion to an unaltered relative area of islets in the endocrine pancreas of male heterozygous Akita *Ins2*^{C96Y} mutant mice compared to age- and sex-related control mice at the age of 30 weeks (Yoshioka et al., 1997). Moreover autoimmune components, diagnostic for type 1 diabetes mellitus were not detected in the pancreas of sex-matched heterozygous mutant mice at any time point investigated (Yoshioka et al., 1997). Electron microscopy of pancreatic β-cells of sex-matched heterozygous Akita *Ins2*^{C96Y} mutant mice revealed remarkable enlargement of the rough endoplasmic reticulum characterized by vacuole-like appearance and progressive degranulation from the earliest time point investigated. Swollen mitochondria were regularly observed (Izumi et al., 2003; Kayo and Koizumi, 1998; Wang et al., 1999; Zuber et al., 2004). In fact, accumulated proinsulin 2 was identified in the lumen of the ER by immunogold-labeling of pancreatic β-cells and electron microscopic morphometry revealed a significantly reduced average volume and volume density of secretory granules in pancreatic β-cells of Akita mutant mice compared to wild-type mice (Wang et al., 1999; Zuber et al., 2004).

As described for homozygous Munich *Ins2*^{C95S} mutant mice, the hyperglycaemic phenotype was much more pronounced in homozygous Akita *Ins2*^{C96Y} indicating dose-dependent impact of *Ins2*^{C96Y} expression in the homozygous state (Kayo and Koizumi, 1998).

The Akita *Ins2*^{C96Y} mouse model reflects clinical features of humans with PNDM due to a mutation in the *INS* gene and contributed substantially to the understanding of molecular mechanisms underlying β-cell failure in PNDM (Kayo and Koizumi, 1998).

3.2. Large animal models and diabetes mellitus

Although a large number of mouse models for diabetes research has been already established and rodents still represent the predominant species in biomedical research (Animal Welfare Report of the German Government, 2012), large animal models have been proven to bridge the gap between mouse models and human patients (Larsen and Rolin, 2004; Srinivasan and Ramarao, 2007; Swindle, 2008). Although rodent models seem to better suit biomedical research due to their well-defined genetic background bearing vast analogy to humans, their high availability, the possibility of experimental standardization and not least because of the lower cost expenditure, investigations based on non-rodent models are urgently required with regard to enhanced comparability to human conditions (Bogue, 2003; Clee and Attie, 2007; Lunney, 2007; Mouse Genome Sequencing et al., 2002; Srinivasan and Ramarao, 2007). In particular the pig turned out to be an attractive model organism for human physiology and pathophysiology in many respects (Douglas, 1972; Lunney, 2007). Furthermore early sexual maturity, favorable short generation time, and the possibility of multiple offspring are conditions precedent to rapid establishment of a representative cohort of pigs to address specific questions of translational research (Aigner et al., 2010; Vajta et al., 2007).

3.2.1. Importance of porcine animal models for translational diabetes research

In general important similarities between humans and pigs in terms of anatomy and physiology of the gastrointestinal tract, morphology of the pancreas as well as structure and pharmacokinetics of insulin underline the importance of the pig as excellent biomedical model for translational diabetes research (Larsen and Rolin, 2004; Larsen et al., 2003b). Moreover body weight and size of the pig, considerably mimicking the human conditions, enable application of standard diagnostic and surgical techniques of human medicine for research purposes on the pig. Vice versa new diagnostic methods, already experimentally validated in

pigs, can be directly implemented in humans (Lunney, 2007; Matsunari and Nagashima, 2009; Roberts et al., 2009). Despite some anatomical differences of the efferent pancreatic duct system, the porcine pancreas is akin to the human pancreas in size, shape, in situ position and blood supply of the endocrine and exocrine parts of the organ (Murakami et al., 1997). In both species, endocrine cells are predominantly clustered in the islets of Langerhans or as single scattered isolated cells including small cell clusters in the exocrine part of the pancreas, emphasizing a less defined islet architecture than rodents (Cabrera et al., 2006; Jay et al., 1999; Kim et al., 2009; Steiner et al., 2010; Wieczorek et al., 1998). β-cells represent the most abundant endocrine cell type of the porcine pancreas by 80% volume fraction at last and thus resembling the β-cell content of humans (Cabrera et al., 2006; Jay et al., 1999; Larsen et al., 2003b; Veriter et al., 2012). The distribution of the different endocrine cell types is almost comparable in both species (Cabrera et al., 2006; Jay et al., 1999; Steiner et al., 2010; Wieczorek et al., 1998). The structure and size of pancreatic islets of adult individuals is comparable throughout all species, ranging between 90 and 200 µm in diameter (Murakami et al., 1997) but is very similar in humans and pigs (Kim et al., 2009). However, adult pigs are preferred for experimental islet isolation and as feasible donor species for experimental islet xenotransplantation due to a more distinct reticular capsule separating endocrine and exocrine parts of the pancreas and thus resembling those of humans (Brandhorst et al., 1995; Jay et al., 1999; van Deijnen et al., 1992; Wieczorek et al., 1998). The human insulin amino acid sequence differs from that of the porcine insulin by only one amino acid at position 30 of the B-chain and has been effectively used for treating humans suffering from diabetes for decades (Bromberg and LeRoith, 2006; Sonnenberg and Berger, 1983). The human and porcine amino acid sequence of the incretin hormone glucose-dependent insulinotropic polypeptide (GIP) agree except for two amino acid substitutions at positions 18 (His → Arg) and 34 (Asn → Ser), and the sequence of the incretin hormone glucagon-like peptide-1 (GLP-1) is even completely conserved in both species (Moody et al., 1984; Orskov, 1992). Throughout almost all mammalian species, the islet amyloid polypeptide (IAPP) is predominantly synthesized in pancreatic β-cells and stored in the halo region of their secretory granules, co-localised and co-secreted with hexameric insulin (Johnson et al., 1988; Lukinius et al., 1996; O'Brien et al., 1993; Westermark et al., 2011). The process of islet amyloid polypeptide expression is observed early

during ontogeny in immature, pluripotent endocrine stem cells of the fetal pancreas and thus IAPP immunoreactivity is detectable from gestational week 13 in humans for instance (In 't Veld et al., 1992; Lukinius et al., 1996). By the way of an exception in humans and in the pig likewise, IAPP storage is not only confined to β-cell granules but also found in the immediate vicinity of α-cell granules and randomly throughout δ-cells, even if less pronounced (Lukinius et al., 1996). In contrast to humans, the porcine IAPP is unsusceptible to amyloid fibrillogenesis (Betsholtz et al., 1989). Cytotoxic amyloid deposits derived from human IAPP are found in pancreatic islets of 90% of diabetic subjects and therefore contribute to β-cell failure and consequently to the progression of diabetic symptoms in humans (Butler et al., 2003; Clark et al., 1996; Turner et al., 1988; Westermark et al., 2011). The propensity to form amyloid deposits due to β-pleated sheet confirmation of human IAPP is related to the amyloidogenic sequence in the portion of molecule spanning amino acid residues at position 20 to 29 of IAPP, bearing less homology to the corresponding region of porcine IAPP molecules (Betsholtz et al., 1989; Clark et al., 1996; Potter et al., 2010; Westermark et al., 2011). Not exclusively human IAPP is highly fibrillogenic, but also domestic cats and cynomolgus macaques (*M. fascicularis*) feature an almost identical amyloidogenic region of IAPP related to the ability of amyloid plaque formation and therefore contributing to spontaneous diabetes mellitus similar to human age-associated type 2 diabetes mellitus (Hoenig et al., 2000; O'Brien et al., 1996). In pigs just as much as in humans, β-cell mass clearly correlates with β-cell function and therefore with undisturbed metabolic control respectively. A decrease in β-cell mass by 50% was found to be sufficient for deficient insulin secretion accompanied by disturbed glucose tolerance and tentative hyperglycemia in pigs as well as in humans (Butler et al., 2003; Kendall et al., 1990; Kjems et al., 2001; Kloppel et al., 1985; Renner et al., 2010). In contrast, rodents compensate for a reduction of functional β-cell mass by 80% through substantial capability of β-cell proliferation. The regulation of β-cell mass is therefore much more dynamic in comparison to humans and pigs, where β-cell replication does not seem to be an important strategy to prevent hyperglycemia (Bonner-Weir, 2000; Bonner-Weir et al., 1983; Butler et al., 2003; Finegood et al., 1995; Renner et al., 2010; Tyrberg et al., 2001). The instant, extensive postmortal autolysis of pancreatic tissue restricts the availability of human tissue

for pathological examinations and thus the ascertainment of representative studies about islet morphology and dynamics of β-cell mass with diabetes (Butler et al., 2003). In the pig, a decline of blood glucose levels related to abrosia is concomitant with diverse adaptation mechanisms, including an increase of free fatty acids (FFA) and glycerol by force of enhanced oxidation of body fat, adaptive hepatic gluconeogenesis and formation of ketone bodies, almost identical to human metabolism (Larsen and Rolin, 2004). The plasma glucose and insulin levels rise steadily with increasing age, assumedly due to incremental peripheral insulin resistance and reduced beta-cell function, whereas glucose tolerance declines with age individually influenced by the general health status and the body mass index (BMI) (Broughton and Taylor, 1991; Larsen et al., 2001; Matthews et al., 1985; Rosenthal et al., 1982). Generally, physiological blood glucose levels of both species range between 70 and 115 mg/dl and are therefore comparable in domestic pigs and humans, whereas the Göttingen minipig displays significantly lower plasma glucose levels questioning the conformance to human criteria (Canavan et al., 1997; Eriksson et al., 1989; Fritsche et al., 2000; Kraft W., 2005; Larsen et al., 2001; Weyer et al., 1999). Hence, the domestic pig represents an excellent model for human glucose metabolism and constitutes an available source of pancreatic tissue suitably conserved at euthanasia (Lunney, 2007). The accomplishment of physiological tests, including glucose tolerance tests followed by quantitative stereological evaluation of the β-cell mass post mortem in a representative porcine disease model thus impart knowledge of islet morphology, the relation between β-cell function and β-cell mass and enable new possibilities for the development of new diagnostic approaches for humans (Larsen et al., 2003a). Despite anatomical differences in the gastrointestinal tract, there are a variety of functional compatibilities between pigs and humans regarding the physiology of digestion. For instance, the time required for intestinal transit and the efficiency of digestion correspond most closely to that of humans (Miller and Ullrey, 1987). As humans, the pig is truly omnivorous and balanced nutrition is particularly combined with dietary quality in contrast to ruminants, where fermentation of nutrients through symbiotic microorganisms is crucial (Huge et al., 1995). By reason of connatural constitution of the skin and the subcutaneous tissue, including scarce body hair, thickness of dermis and epidermis, transdermal permeability as well as dimension, distribution and accessibility of peripheral veins, the pig was found to be closely comparable to humans in this regard.

Evaluation of pharmacokinetics and pharmacodynamics after subcutaneous injection of drugs in the pig model is advisable (Benech-Kieffer et al., 2000; Meyer, 1996; Qvist et al., 2000). Moreover, there are decisive equivalents in the biotransformation of drugs through a similar cytochrome p450 oxidase concentration in the liver. Even though there are some differences compared to humans, the pig represents a considerable model for preclinical pharmacology (Monshouwer and Witkamp, 2000).

3.2.2. Induction of insulin-deficient diabetes mellitus in the pig model

3.2.2.1. Chemical and surgical induction of insulin deficiency in the pig model

Clinically apparent diabetes mellitus caused by an absolute insulin deficiency in the pig model has been experimentally induced as yet by either total pancreatectomy or by β-cell destruction through cytotoxic action of chemical agents such as streptozotocin and alloxan (Dufrane et al., 2006; Renner et al., 2012; Stump et al., 1988; Wilson et al., 1986). Satisfactory results including constant severe hyperglycemia and impaired intravenous glucose tolerance were achieved first at resection of the pancreas by 80% involving both, other endocrine cell types and exocrine parts of the pancreas (Chaib et al., 2011; Lohr et al., 1989; Stump et al., 1988). Thus, total pancreatectomy is an disputable invasive method exerting intended detrimental influence on pancreatic β-cells but also attended with unrequested serious dyspepsia requiring irrepealable replacement of pancreas-derived digestive enzymes and dysfunction of endocrine pancreas-related signaling pathways at large, barely imitating human diabetics (Stump et al., 1988; Wilson et al., 1986). The diabetogenic agent streptozotocin (STZ) (2-deoxy-2(3-(methyl-3-nitrosoureido)-D-glucopyranose) constitutes a cytotoxic glucosamine analogue forcing the way in pancreatic β-cells through selective glucose transporter 2 (GLUT2) affinity (Herr et al., 1967; Schnedl et al., 1994; Tjalve et al., 1976). In succession, STZ specifically alkylates DNA and provokes strand breaks, which in turn induce tivation of the poly (ADP-ribose) polymerase (PARP) to restore DNA integrity. The thereby immense ATP demand leads to a negative cellular energy balance and ultimately provokes β-cell necrosis promoting consecutive insulin deficiency (Bennett and Pegg, 1981; Lenzen, 2008; Uchigata et al., 1982; Yamamoto et al., 1981a, b). The glucomimetic agent

alloxan (2, 4, 5, 6-tetraoxypyrimidine) displays likewise a substrate of the GLUT2 transporter of pancreatic β-cells (Gorus et al., 1982; Lenzen, 2008). The bipartite diabetogenic effect of alloxan impinges pancreatic β-cell function upon disturbance of the glucose-mediated insulin release by inhibiting glucokinase activity and inflicts damage on pancreatic DNA by generation of reactive oxygen species through redox cycling reactions and thereby inducing same fatal cellular responses as stated previously for STZ (Lenzen, 2008; Lenzen et al., 1988; Lenzen et al., 1987; Malaisse, 1982; Tiedge et al., 2000; Yamamoto et al., 1981b). However, the effects of STZ and alloxan on the pig model are unsatisfactory variable due to low physiological expression levels of the GLUT2 transporter (Dufrane et al., 2006). Therefore the establishment and characterization of clinically relevant genetically engineered pig models constitute a major improvement (Aigner et al., 2010).

3.2.2.2. Permanent neonatal diabetes mellitus in transgenic pigs expressing a dominant-negative hepatocyte nuclear factor 1 alpha (HNF-1α) – diabetes induction by genetic modification of the porcine genome

Nine autosomal dominant mutations in the hepatocyte nuclear factor 1α (*HNF1A*) gene located on chromosome 12q, referred to as *MODY3* locus, have recently been reported to be responsible for genetic defects in insulin secretion and thus for derailed glucose homeostasis and onset of clinically manifest type 2 diabetes mellitus before 25 years of age (Byrne et al., 1996; Fajans et al., 1994; Vaxillaire et al., 1995; Vaxillaire et al., 1997; Yamagata et al., 1996b). Although there are diverse promising approaches, the pathomechanism of this progressive disease is still poorly understood since the identification of transcription factor HNF 1α by Yamamata et al. (Yamagata et al., 1996b). To clarify the underlying reason for human *HNF1A* mutant gene implicating β-cell dysfunction and disturbed insulin secretion in humans, Umeyama et al. generated a transgenic porcine model expressing a dominant-negative transcription factor HNF 1-α (Umeyama et al., 2009). An expression vector consisting of the 2.3 kb cDNA sequence with the insertion of a cytosine into a poly C tract in exon 4, identified as most common frameshift mutation HNF1αP291fsinsC (Kaisaki et al., 1997), under the transcriptional control of the porcine insulin promoter flanked by chicken β-globin insulators (Watanabe et al., 2007) was introduced into porcine *in-vitro* matured oocytes using a combined method of intracytoplasmic sperm injection (ICSI) with

somatic cell nuclear transfer (SCNT) (Kurome et al., 2006). Fibroblasts, recovered from a transgenic male cell clone carrying ten copies of the transgene, served as nuclear donor cells for another SCNT. A total of 22 live piglets were born, however only five of them survived the postnatal period and only 2 piglets grew older than two months, respectively. Piglets exhibited a persistent diabetic phenotype with non-fasting blood glucose levels over 200 mg/dl and a disturbed oral glucose tolerance due to immunohistochemically detectable pathological alterations of the pancreatic islet structure and insufficient insulin content of the pancreatic β-cells. Despite efforts to limit expression of mutant HNF-1α to the pancreas by utilization of the porcine insulin promoter, ectopic expression was observed. On this account, altered biochemical parameters were suggestive of hepatic dysfunction and could be histologically confirmed, whereas histologically stained kidney tissue showed abnormal morphogenesis without any clinical effects. In conclusion, a longer survival time is essential to properly characterize an animal model and make it practically useful as a model of human diseases for translational research. Therefore further studies are required to improve the survival rate of dominant-negative mutant HNF-1α transgenic pigs and on exclusive pancreas expression of the transgene (Umeyama et al., 2009).

III. ANIMALS, MATERIALS AND METHODS

1. Animals

All animals investigated in this study were hemizygous male and female transgenic pigs expressing a mutant porcine *INS* gene (*INS*^{C94Y}) as well as non-transgenic littermates. Animals were housed under controlled conditions in single pens or in age-matched groups. Stables were planar-fixed and interspersed with straw. Animals were fed a standard commercial diet (Table 1) once daily and had free access to water. Pigs were trained carefully prior to all experiments as well as for insulin therapy. All animal experiments were approved by the responsible animal welfare authority (Regierung von Oberbayern, Munich, AZ 55.2-1-54-2531-26-06 and AZ 55.2-1-54-2532-68-11).

Table 1: Diet composition

	Deuka primo care (piglets 6.5 kg up to 40 kg)	**Deuka porfina U** (growing and adult pigs)
MJ ME/kg	14.0	12.6
Crude protein%	17.0	16.5
Lysine%	1.4	0.9
Methionine%	0.42	0.27
Crude fat%	4.3	3.0
Crude ash%	4,6	5.5
Crude fiber	4.0	6.0
Calcium%	0.65	0.85
Phosphorus%	0.55	0.55
Sodium%	0.25	0.2

ME: metabolizable energy

2. Materials

2.1. Apparatuses

Accu-jet® pro pipette controller	Brand, Wertheim
Agarose gel electrophoresis chamber	WG-Biotech, Ebersberg
Agarose gel electrophoresis chamber	OWL Inc., USA
AU 400 autoanalyzer	Olympus, Hamburg
AxioCam scanning camera	Carl Zeiss AG, Oberkochen

Beckmann DU-640 spectrophotome	Beckman Coulter GmbH, Krefeld
Benchtop 96 tube working rack	Stratagene, La Jolla, USA
Branson sonifier cell disrupter B15	Branson Ultrasonic Corporation, USA
DryEase® Mini-Gel drying base and frame	Life Technologies™ GmbH, Darmstadt
Electrophoresis Power Supply EPS 500/400	GE Healthcare GmbH, Munich
EM 10 transmission electron microscope	Carl Zeiss AG, Oberkochen
Gel documentation system	Bio Rad, Munich
Gel documentation system	Intas, Göttingen
Glass cuvette with glass rack insert	VWR International GmbH, Darmstadt
Guardian® REAL-Time System	Medtronic GmbH, Meerbusch
Hellma®cuvette suprasil	Hellma GmbH, Müllheim
HM 315 microtome	Microm, Walldorf
Homogeniser ART-Micra D-8	ART, Müllheim
Hybridisation oven	H.Saur, Reutlingen
Illumina Genome Analyzer IIx	Illumina Inc., San Diego, USA
Incubator	Memmert, Schwabach
LB 2111 γ-counter	Berthold, Bad Wildbach
Mettler PM 6000	Mettler-Toledo, Gießen
Microprocessor pH meter	WTW, Weilheim
Microwave	Siemens, Munich
Mini Proteom® 3 Cell Assembly	Bio Rad, Munich
MS1 minishaker	IKA, Staufen
Multipipette® plus	Eppendorf, Hamburg
Object micrometer	Carl Zeiss AG, Oberkochen
Optimax X-Ray Film Processor 1170-1-0000	PROTEC, Oberstenfeld
NanoDrop ND-1000 spectrophotometer	NanoDrop Technologies, Wilmington, USA
Pipettes (1000 µl, 200 µl, 20 µl, 10 µl, 2 µl)	Gilson Inc, USA
Power Pac 300 gel electrophoresis unit	BioRad, Munich

Precision® Xceed™ Glucometer	Abbott, Wiesbaden
Reichert-Jung TM60 milling maschine	Leica Microsystems GmbH, Wetzlar
Reichert-Jung Ultracut E microtome	Leica Microsystems GmbH, Wetzlar
RH Basic heating plate with magnetic stirrer	IKA, Staufen
Shandon Citadel tissue processor 1000	Thermo Fisher Scientific, GmbH, Schwerte
Stemi SV11 stereomicroscope	Carl Zeiss AG, Oberkochen
Severin 900 microwave	Severin, Sundern
Staining box according to Schifferdecker	Carl Roth GmbH & Co. KG, Karlsruhe
Sterilising oven	Heraeus, Munich
Sunrise™ microplate reader for ELISA	Tecan, Austria
Thermomixer 5436	Eppendorf, Hamburg
Trans Blot® SD Semi-Dry Transfer cell	BioRad, Munich
Varioklav 400 autoclave	H+P Labortechnik, Oberschleißheim
WB 6 water bath	Firmengruppe Preiss-Daimler,
X-ray cassette Siemens Titan (18 x 24 cm)	Rego, Augsburg

Centrifuges:

Biofuge pico	Heraeus, Munich
Megafuge 1.0 R	Heraeus, Munich
Rotanta 96	Hettich, Tuttlingen
Eppendorf centrifuge 5810R	Eppendorf, Hamburg
Eppendorf centrifuge 5430R	Eppendorf, Hamburg

Thermocycler:

Biometra Uno Thermoblock	Biometra,Göttingen
Biometra T Professional	Biometra, Göttingen
Mastercycler® gradient	Eppendorf, Hamburg

Scales:

Analytical balance	Sartorius, Göttingen
Chyo Petit Balance MK-2000B	YMC Co, Japan
Chyo IL-200	YMC Co, Japan
Chyo MJ-3000	YMC Co, Japan
Kern EOB 15K5	Kern und Sohn GmbH, Barlingen-Frommern

2.2. Consumables

Amersham™ Hyperfilm™ ECL High Performance chemiluminescense film	GE Healthcare limited, Munich
BD Micro-Fine Ultra™ pen needles (0.33 x 12.7 mm 29 G)	Becton Dickinson GmbH, Heidelberg
Blood lancets	Henry Schein® Vet GmbH, Hamburg
Cavafix® Certo® central venous catheter	B. Braun, Melsungen
Cellstar® cell culture plates (12 well)	Greiner Bio-One GmbH, Solingen
Cover slips for histology	Greiner Bio-One GmbH, Solingen
Cover slips for histology	VWR International GmbH, Darmstadt
Cover slips	Carl Menzel GmbH, Braunschweig
Culture tubes with caps (12 ml, 6ml)	Carl Roth GmbH & Co. KG, Karlsru
Culture tubes with caps (12 ml, 6 ml)	Carl Roth GmbH & Co. KG, Karlsruhe
Disposable plastic pipettes	Falcon®, Becton Dickinson, Heidelberg
Disposal polypropylene bags	Sarstedt AG+Co Nürnbrecht
DryEase® Mini cellophane	Life Technologies™ GmbH, Darmstadt
1000 eco Lab pipette tips (200 µl, 1000 µl)	neoLAB Migge Laborbedarf-Vertriebs, GmbH, Heidelberg
Extra Thick Blot Paper, Protean®II xi size, pre-cut	Bio Rad, Munich
Freestyle Precision Xtra™ Plus blood glucose stripes	Abbott, Wiesbaden
Gelatine epon embedding capsules	Plano, Germany
Gel blotting paper (Whatman paper)	Schleicher&Schüll, Dassel

Hybond-N+ nylon membrane	GE Healthcare, Munich
Hypodermic needles (18 G/ 20 G)	Henry Schein®Vet GmbH, Hamburg
Immobilon®-P nitrocellulose transfer membranes	Millipore™, Billerica, USA
Latex Powder-Free sempercare premiumgloves	Satra Technology Center, Nordhamshire, UK
Microscope slides Star Frost®	Engelbrecht, Edermünde
Monovette® blood collection system (Serum, EDTA)	Sarstedt, Nümbrecht
Multi Guiard Barrier Tips (10 µl, 20 µl, 200 µl, 1000 µl)	Sorenson™ Bioscience Inc., Utah, USA
OP-Cover (60 x 90 cm)	A. Albrecht, Aulendorf
Pipette tips (20 µl)	Treff Lab, Degersheim, Switzerland
Parafilm®M	American Can Company, Greenwich,USA
PCR reaction tubes (0.2 ml)	Braun, Wertheim
Perfusor® cable (50 cm)	B. Braun, Melsungen
Quali-PCR tubes (0.2 ml) and cap-strips	G. Kisker Biotech GbR, Steinfurt
Rotilabo® weighing bowls (20 ml, 330 ml)	Carl Roth GmbH & Co. KG, Karlsruhe
Safe-Lock 1.5 ml Eppendorf Tubes®	Eppendorf, Hamburg
Saran Barrier Food wrap	Dow, USA
Sempercare® nitrile gloves	Satra Technology Center, Nordh
Sephadex G-50 columns	GE Healthcare limited, Munich
Single-use syringes (2,5 ml, 10 ml, 20 ml)	Henry Schein®Vet GmbH, Hamburg
Skin adhesive spray	A. Albrecht, Aulendorf
Sterican® cannulas (18 G, 20 G)	B. Braun, Melsungen
Super RX Fuji medical x-ray film	FujiFilm Corp., Japan
Tissue culture dishes (60 x 15 mm)	Sarstedt, Nümbrecht
Uni-Link embedding cassettes	Engelbrecht, Edermünde
Vasco® OP Protect gloves	B. Braun, Melsungen
Vascocan® indwelling venous catheters and stylets	B. Braun, Melsungen
Vicryl (2-0) suture material	Ethicon, Norderstedt

3-way-Stopcock	Fresenius Kabi, Bad Homburg

2.3. Chemicals

All chemicals were used in p.a. quality unless noted otherwise.

Acrylamide (30%)/ Bis solution	Bio Rad, Munich
Agarose UltraPure™ Electrophoresis grade	Invitrogen™, Karlsruhe
Ammonium persulfate (APS)	Bio Rad, Munich
Acetic acid (glacial acetic acid)	Rotipuran®, Carl Roth GmbH & Co KG, Karlsruhe
Benzoylperoxide	Merck KGaA, Darmstadt
Boric acid (H_3BO_3)	Carl Roth GmbH & Co KG, Karlsruhe
Bromophenolblue	Merck KGaA, Darmstadt
Complete Protease inhibitor cocktail tablets	Roche Diagnostics Deutschland, GmbH, Mannheim
Coomassie® Brilliant Blue R250 (0.05%)	Sigma-Aldrich Chemie GmbH, Steinheim
Coomassie® Brilliant Blue G250	Sigma-Aldrich Chemie GmbH, Steinheim
3,3´Diaminobenzidine tetrahydrochloride (DAB)	KemEnTec, Copenhagen, Denmark
5,5´Diethylbarbituric acid sodium salt	Merck KGaA, Darmstadt
Diethylpyrocarbonate (DEPC)	Sigma-Aldrich Chemie GmbH, Steinheim
1,4-Dithiothreitol (DTT)	Biomol Feinchemikalien GmbH, Hamburg
1.4-Dithiothreitol (DTT, 0.1 M)	Invitrogen™, Karlsruhe
2-Dodecenyl succinic acid anhydride	SERVA Electrophoresis, Heidelberg
Ethanol	Merck KGaA, Darmstadt
Ethidiumbromide (1mg/ml)	Merck KGaA, Darmstadt
Ethylenediaminetetraacetic acid (EDTA, Titriplex®III)	Merck KGaA, Darmstadt
Ethyleneglycol-bis-(2-aminoethyl-)	Carl Roth GmbH & Co. KG,

tetra-acetic acid (EGTA)	Karlsruhe
Ethylene glycol monobutyl ether	Merck KGaA, Darmstadt
Ethylmercury thiosalicylic acid sodium salt	SERVA Electrophoresis, Heidelberg
Formaldehyde solution (37%)	Sigma-Aldrich Chemie GmbH, Steinheim
Glucose solution (50%)	B. Braun, Melsungen
Glutaraldehyde	Merck KGaA, Darmstadt
Glycerol Rotipuran®	Carl Roth GmbH & Co. KG, Karlsruhe
Glycidyl ether 100	Serva Electrophoresis, Heidelberg
Glycine	Carl Roth GmbH & Co. KG, Karlsruhe
Hydrochloric acid (2 M)	neoLAB Migge Laborbedarf-Vertriebs GmbH, Heidelberg
Hydrochloric acid (25%) (Prolabo®)	VWR International GmbH, Darmstadt
Hydrogen peroxide (35%)	neoLAB Migge Laborbedarf-Vertriebs GmbH, Heidelberg
2-Hydroxyethyl methacrylate (HEMA)	Sigma-Aldrich Chemie GmbH, Steinheim
Lead nitrate solution (1 M) ($Pb(NO_3)_2$	Merck KGaA, Darmstadt
Magnesium chloride	Sigma-Aldrich Chemie GmbH, Steinheim
Magnesium chloride (25 mM)	Qiagen GmbH, Hilden
Mayer`s Hemalum solution	Applichem GmbH, Darmstadt
2-Mercaptoethanol	Sigma-Aldrich Chemie GmbH, Steinheim
Methanol (Ensure®)	Merck KGaA, Darmstadt
Methyl methacrylate (MMA)	Sigma-Aldrich Chemie GmbH, Steinheim
Methyl nadic anhydride	SERVA Electrophoresis GmbH, Heidelberg
Nonylphenyl polyethylene glycol (Nonidet® P-40)	Fluka Chemie, Buchs, Schweiz
Osmium tetroxide (OsO_4)	chemPUR®, Karlsruhe
Paraformaldehyde	Merck KGaA, Darmstadt
Phenylmethylsulfanylfluoride	Sigma-Aldrich Chemie GmbH, Steinheim

(PMSF)	
Polyethylene glycol 400	Merck KGaA, Darmstadt
Phosphoric acid (H_3PO_4) (Emprove®)	Merck KGaA, Darmstadt
Ponceau S	Sigma-Aldrich Chemie GmbH, Steinheim
Potassium chloride	Merck KGaA, Darmstadt
Potassium dihydrogen phosphate (KH_2PO_4)	neoLAB Migge Laborbedarf-Vertriebs GmbH, Heidelberg
Potassiumhydrogenphosphate	Merck KGaA, Darmstadt
Potassium hydroxide pellets	Merck KGaA, Darmstadt
2-Propanol	Merck KGaA, Darmstadt
RPMI 1640 cell culture medium	Biochrom AG, Berlin
D(+) saccharose	neoLAB Migge Laborbedarf-Vertriebs GmbH, Heidelberg
Saccharose	Merck KGaA, Darmstadt
Safranin O	Chroma Technology GmbH, Olching
Silver nitrate ($AgNO_3$)	Applichem GmbH, Darmstadt
Sodium acetate ($C_2H_3NaO_2$)	Merck KGaA, Darmstadt
Sodium carbonate (Suprapur®)	Merck KGaA, Darmstadt
Sodium chloride (Ensure®)	Merck KGaA, Darmstadt
Sodium citrate solution (1 M)	Merck KGaA, Darmstadt
Sodiumdodecylsulfate (SDS)	Serva Electrophoresis, Heidelberg
Sodium hydroxide (NaOH)	VWR International GmbH, Darmstadt
Sodium hydroxide solution (2 M)	VWR International GmbH, Darmstadt
Sodium-orthovanadate (Na_3VO_4)	Sigma-Aldrich Chemie GmbH, Steinheim
Sodium phosphate dibasic dehydrate (Na_2HPO_4 x 2 H_2O)	neoLAB Migge Laborbedarf-Vertriebs GmbH, Heidelberg
2-Sodium tetraborate (Borax)	Merck KGaA, Darmstadt
Sodium thiosulfate-pentahydrate ($Na_2S_2O_3$ x 5 H_2O)	Merck KGaA, Darmstadt
Tetraethylethylenediamine (Temed)	Carl Roth GmbH & Co. KG, Karlsruhe
2, 4, 6-tris-(dimethylaminomethyl) phenol	Serva Electrophoresis GmbH, Heidelberg

Tris-(hydroxymethyl)-aminomethane (Tris)	Carl Roth GmbH & Co. KG, Karlsruhe
Tween®20	Sigma-Aldrich Chemie GmbH, Steinheim
Uranyl acetate	Merck KGaA, Darmstadt
w/v nonfat dry milk (blotting grade)	Carl Roth GmbH & Co. KG, Karlsruhe
Xylene	Applichem GmbH, Darmstadt

2.4. Antibodies, drugs, enzymes, oligonucleotides, standards

2.4.1. Antibodies

2.4.1.1. Primary antibodies

Monoclonal mouse anti-human actin, clone C4	Millipore™, Billerica, USA
Monoclonal rabbit anti-human phospho-eIF2α XP™	Cell Signaling Technology®, New England Biolabs GmbH, Frankfurt am Main
Polyclonal rabbit anti-human BiP	Cell Signaling Technology®, New England Biolabs GmbH, Frankfurt am Main
Polyclonal rabbit anti-mouse GADD153	Santa Cruz Biotechnology®, Heidelberg
Polyclonal guinea pig anti-porcine insulin	Dako cytomation, Hamburg
Polyclonal rabbit anti-human glucagon	Dako cytomation, Hamburg
Polyclonal rabbit anti-bovine pancreatic polypeptide	Dunn Labortechnik GmbH, Asbach
Polyclonal rabbit anti-human somatostatin	Dako cytomation, Hamburg

2.4.1.2. Secondary antibodies

AP-conjugated goat anti-guinea pig IgG	Southern Biotech, Birmingham, USA
HRP-conjugated goat anti-rabbit IgG	Cell Signaling Technology®, New England Biolabs GmbH, Frankfurt am Main

HRP-conjugated goat anti-rabbit IgG	Dako cytomation, Hamburg
HRP-conjugated goat anti-mouse IgG	Dianova GmbH, Hamburg

2.4.2. Drugs

Altrenogest (Regumate®)	Serumwerke Bernburg, Bernburg
Azaperon (Stresnil®)	Janssen Pharmaceutica, Beerse, Belgium
Cefquinom (Cobactan®)	Intervet, Unterschleißheim
Choriongonadotropine (hCG) (Ovogest®)	Intervet, Unterschleißheim
Embutramid, Mebezonium, Tetracain (T61®)	Intervet, Unterschleißheim
Heparin-Sodium (25.000 IE/5ml)	B. Braun, Melsungen
Insulin aspart (NovoRapid® Penfill®, 100 units/ml)	Novo Nordisk Pharmaceuticals, Bagsvaerd, Denmark
Insulin glargine (Lantus® Solostar® Pen, 100 units/ml)	Sanofi-Aventis Deutschland GmbH, Frankfurt
PMSG (Intergonan®)	Intervet, Unterschleißheim
Sodium chloride solution (0.9%) ad us. vet.	B. Braun, Melsungen
Ketamine hydrochloride (Ursotamin®)	Serumwerke Bernburg, Bernburg
Metamizol-Sodium (Vetalgin®)	Intervet, Unterschleißheim
Meloxicam (Metacam®)	Boehringer Ingelheim, Ingelheim
Xylazine (Xylazin 2%)	WDT, Garbsen

2.4.3. Enzymes

*Bam*H1 and recommended buffer	MBI Fermentas, St. Leon Roth
DNA Polymerase I (*E.coli*) (DNaseI)	Invitrogen™, Karlsruhe
Herculase®II and buffer (10 x)	Agilent, Böblingen
Klenow fragment exo$^-$ (5 U/µl) and buffer (10 x)	MBI Fermentas, St. Leon Roth
Proteinase K (20 mg/ml)	Roche Diagnostics Deutschland GmbH, Mannheim
RNaseOUT™ (Recombinant Ribonuclease Inhibitor) (40 U/µl)	Invitrogen™, Karlsruhe
SuperScript™ II Reverse Transcriptase (200 U/µl)	Invitrogen™, Karlsruhe

Taq DNA Polymerase (5 U/ml)	Agrobiogen, Hilgertshausen

2.4.4. Oligonucleotides

All oligonucleotides were designed manually and manufactured by Thermo Fisher Scientific, USA.

ACTB (sense)	5′ TGGACTTCGAGCAGAGATGG 3′
ACTB (antisense)	5′ CACCGTGTTGGCGTAGAGG 3′
Insulin (sense)	5‘ CGGGAGGCGGAGAACCCTCA 3‘
Insulin (antisense)	5‘ CCCTCAGGGGCGGCCTAGTT 3‘
neoPf (sense)	5′ CAGCTGTGCTCGACGTTGTC 3′
neoSr (antisense)	5′ GAGTCAACTAGTCCTCAGAAGAACTCGTCAAG 3`

2.4.5. Protein standards

Bovine serum albumin (BSA) Fraction V	Carl Roth GmbH & Co. KG, Karlsruhe

2.5. Buffers, media and solutions

Unless indicated otherwise, water, deionized in a Millipore device (EASYpure® II, pure Aqua, Schnaitsee) and termed as aqua bidest., was used as solvent. Buffers, media and solutions were stored at room temperature (RT) unless indicated otherwise.

2.5.1. Buffers and solutions for electron microscopy

2.5.1.1. Soerensen´s phosphate buffer

192 ml	Solution A
808 ml	Solution B

2.5.1.1.1. Solution A

4.5 g	KH_2PO_4
ad 500 ml	Aqua bidest.

2.5.1.1.2. Solution B

11.9 g	Na_2HPO_4 x 2 H_2O
ad 1000 ml	Aqua bidest.

2.5.1.2. Soerensen´s washing solution

6.8 g	D(+) Saccharose
100 ml	Soerensen´s phosphate buffer
1%	Merthiolate solution

2.5.1.2.1. Merthiolate solution

1%	Ethylmercury thiosalicylic acid sodium salt

2.5.1.3. Fixation solution for Epon embedding

0.5 g	D(+) Saccharose
0.1 M	HCl
2 ml	Veronal-acetate buffer
5 ml	2% Osmium tetroxide

2.5.1.3.1. Veronal-acetate buffer

1.5 g	5,5´Diethylbarbituric acid sodium salt
1 g	Sodium acetate
ad 50 ml	Aqua bidest.

adjusted to pH 10.3

2.5.1.4. Glycidyl ether embedding mixture

70 ml	Solution A
130 ml	Solution B
3 ml	2,4,6- Tris-(dimethylaminomethyl) phenol

2.5.1.4.1. Solution A

62 ml	Glycidyl ether100
100 ml	2-Dodecenyl succinic acid anhydride

2.5.1.4.2. Solution B

100 ml	Glycidyl ether100
89 ml	Methyl nadic anhydride

2.5.1.5. Azur II-methyleneblue/Toluidine blue staining solution

1 g	2-Sodiumtetraborate (Borax)
1 g	Toluidine blue/Azur II-methyleneblue
ad 100 ml	Aqua bidest.

Borax was dissolved in aqua bidest. Azur II-methyleneblue/Toluidine blue was added to the solution and subsequently the solution was stirred on a magnetic stirrer for two hours. Solution needs to be filtered prior to use.

2.5.1.6. Safranin O staining solution

1 g	2-Sodiumtetraborate (Borax)
1 g	Safranin O
40 g	Saccharose
ad 100 ml	Aqua bidest.

First borax was dissolved in aqua bidest. After addition of Safranin O and saccharose, the solution was stirred for approximately two hours. The next day, solution was completed by adding some drops of formaldehyde (37%) followed by filtration.

2.5.1.7. Uranyl acetate contrasting solution

1 g	Uranyl acetate
ad 50 ml	Aqua bidest.

Solution was carefully pivoted and filtered prior to use.

2.5.1.8. Lead acetate contrasting solution

6 ml	Sodium citrate
4 ml	Lead nitrate solution (1 M)
8 ml	NaOH (1 M)
ad 50 ml	Aqua bidest.

Sodium citrate was gently stirred in aqua bidest. Lead nitrate solution was added dropwise causing precipitation. Application of NaOH cleared the solution immediately. Filtration was required prior to use.

2.5.1.9. Solution A for plastic embedding

338 mg	Benzoylperoxide
20 ml	Methyl methacrylate
60 ml	2-Hydroxyethyl methacrylate
16 ml	Ethylene glycol monobutyl ether
2 ml	Polyethylene glycol 400

2.5.2. Buffers and solutions for molecular biological procedures

2.5.2.1. DEPC water (0.1% (v/v))

1 ml DEPC was dissolved in 1000 ml aqua bidest. overnight at room temperature while stirring. Afterwards the solution was autoclaved three times to inactivate DEPC and stored at -20°C.

2.5.2.2. DNase I buffer

10 mM	Tris
10 mM	$MgCl_2$

adjusted to pH 7.4 and stored at -20°C.

2.5.2.3. dNTPs

dATP, dCTP, dGTP and dTTP were mixed with aqua bidest. in a final concentration 2 mM or 10 mM respectively, aliquoted and stored at -20°C.

2.5.2.4. Proteinase-K-solution

20 mg	Proteinase K
1 ml	Aqua bidest.

aliquoted and stored at -20°C.

2.5.2.5. Buffers for agarose gel electrophoresis

2.5.2.5.1. TAE buffer (50x)

542 g	Tris
57.1 ml	Glacial acetic acid
100 ml	EDTA 0.5 M (pH 8.0)
ad 1000 ml	Aqua bidest.

Buffer was diluted to single concentration with aqua bidest. prior to use.

2.5.2.5.2. TBE buffer (10x)

108 g	Tris
55 g	Boric acid
40 ml	EDTA 0.5 M (pH 8.0)
ad 1000 ml	Aqua bidest.

Concentrated stock buffer was autoclaved and diluted to single concentration prior to use.

2.5.3. Buffers and solutions for protein extraction and polyacrylamide gel electrophoresis

2.5.3.1. Bradford reagent

0.01%	Coomassie G-250
5%	Ethanol
10%	H_3PO_4
ad 500 ml	Aqua bidest.

Solution was well mixed, filtered and stored protected from light.

2.5.3.2. 5 x Laemmli

65.5 ml	1 M Tris pH 6.8
100 ml	Glycerol (100%)
2 ml	0.5 M EDTA pH 8
20 g	SDS
0.1%	Bromophenol blue
ad 200 ml	Aqua bidest

2.5.3.3. PBS buffer (10x)

136 mM	NaCl
8.1 mM	Na_2HPO_4
2.7 mM	KCl
1.5 mM	KH_2PO_4

adjusted to pH 7.4

After filtration, buffer was autoclaved and diluted to single concentration with aqua bidest. for use.

2.5.3.4. Ponceau S solution

0.2 g	Ponceau
3 ml	Glacial acetic acid
ad 100 ml	Aqua bidest.

2.5.3.5. SDS running buffer (10x)

30.3 g	Tris
144 g	Glycine
10 g	SDS
ad 1000 ml	Aqua bidest.

Buffer was stored at 4°C and diluted with aqua bidest. to single concentration right before use.

2.5.3.6. Stock solutions for protein extraction buffer

2.5.3.6.1. Complete Protease inhibitor solution (25x)

One tablet was dissolved in 2 ml aqua bidest. to prepare a 25x stock solution, aliquoted, stored at -20°C and used within 12 weeks according to manufacturer´s instructions.

2.5.3.6.2. 1 M DTT

1 M DTT

dissolved in aqua bidest., aliquoted and stored at -20°C.

2.5.3.6.3. 300 mM EDTA

300 mM EDTA

adjusted to pH 8.0, autoclaved and stored at room temperature.

2.5.3.6.4. 300 mM EGTA

300 mM EGTA

adjusted to pH 8.0, autoclaved and stored at room temperature.

2.5.3.6.5. 2,5 M NaCl/ 261 mM Tris/ HCl pH 7.6

2.5 M NaCl

261 mM Tris

adjusted to pH 7.6, autoclaved and stored at room temperature.

2.5.3.6.6. 200 mM Na_3VO_4

200 mM Na_3VO_4

dissolved in aqua bidest. on a magnetic stirrer and adjusted to pH 10 until solution turns yellow. Solution was boiled for approximately 10 minutes until it cleared again and cooled down on ice. Solution was repeatedly adjusted to pH 10, boiled, and cooled down on ice until it remained clear and of stable pH 10. Aliquots of 1 ml were stored at -20°C. Prior to use, solution was thawed by boiling for 10 minutes on a heating block to dissolve crystals.

2.5.3.6.7. 100 mM PMSF

100 mM	PMSF

dissolved in isopropanol, aliquoted and stored at -20°C.

2.5.3.6.8. Protein extraction buffer working solution

100 µl	2,5 M NaCl/261 mM Tris HCl pH 7.6
5 µl	Nonidet® P-40
10 µl	300 mM EDTA
10 µl	300 mM EGTA
10 µl	100 mM PMSF
10 µl	200 mM Na_3VO_4
1 µl	1 M DTT
40 µl	Complete 25x
814 µl	Aqua bidest.

2.5.4. Buffers and solutions for Southern blot analysis

2.5.4.1. Southern blot church buffer

1%	BSA
1 mM	EDTA pH 8.0
500 mM	Sodium phosphate buffer pH 7.2
7%	SDS

2.5.4.2. 1 M Sodium-phosphate buffer pH 7.2

4 ml	H_3PO_4 (85%)
89 g	Na_2HPO_4 x 2 H_2O
ad 1000 ml	Aqua bidest.

2.5.4.3. Southern blot high-stringency buffer

1 mM	EDTA pH 8.0
40 mM	Sodium phosphate buffer pH 7.2
1%	SDS

2.5.4.4. Southern blot low-stringency buffer

0.5%	BSA
1 mM	EDTA pH 8.0
40 mM	Sodium phosphate buffer pH 7.2
5%	SDS

2.5.4.5. Southern blot neutralisation buffer

0.5 M	Tris
1.5 M	NaCl

adjusted to pH 7.5

2.5.4.6. Southern blot SSC (20x)

0.3 M	Sodium citrate
3 M	NaCl

2.5.4.7. Southern blot strand break solution

0.5 M	NaOH
1.5 M	NaCl

2.5.5. Buffers and solutions for tissue preparation and immunhistochemical procedures

2.5.5.1. DAB solution

One tablet DAB was dissolved in 10 ml aqua bidest, filtered, aliquoted and stored at -20°C protected from light. Prior to use 1 µl H_2O_2 per 1 ml DAB solution was added.

2.5.5.2. Paraformaldehyde solution (4%)

4%	paraformaldehyde
ad 1000 ml	PBS buffer (1x)

Solution was heated to 55°C in a water bath, repeatedly interrupted by vigorous stirring on a magnetic stirrer. A few drops of 2 M NaOH were added to clear the solution. After cooling down to room temperature the solution was adjusted to pH 7.4, filtered and stored at 4°C.

2.5.5.3. TBS buffer for immunohistochemistry (10x)

90 g	NaCl
60.5 g	Tris
ad 1000 ml	Aqua bidest.

adjusted to pH 7.6.

Concentrated stock buffer was autoclaved and diluted to single concentration with aqua bidest. right before use.

2.5.5.4. 100 mM Tris/HCl pH 8.5

100 mM	Tris

adjusted to pH 8.5. Exact adjustment to pH 8.5 is crucial for desirable staining intensity.

2.5.6. Buffers and solutions for Western blot analyzes

2.5.6.1. Elution buffer

62.5 mM	Tris/HCl pH 6.7
2%	SDS
100 mM	2-Mercaptoethanol

2.5.6.2. TBS-T-BSA

0.1%	TBS-T
5%	BSA

2.5.6.3. TBS –T (0.1%)

100 ml	10 x TBS buffer for Western blot
1 ml	Tween® 20
ad 1000 ml	Aqua bidest.

2.5.6.4. TBS-T-w/v nonfat dry milk

0.1%	TBS-T
5%	w/v nonfat dry milk

2.5.6.5. Transfer buffer (10x)

58 g	Tris
29 g	Glycine
3.7 g	SDS
ad 1000 ml	Aqua bidest.

Buffer was stored at 4°C. Prior to further processing concentrated buffer was diluted to single concentration with aqua bidest. and 20% methanol was added.

2.5.6.6. Tris-buffered saline (TBS) buffer for Western blot (10x)

80 g	NaCl
30 g	Tris
ad 1000 ml	Aqua bidest.
adjusted to pH 7.4	

Buffer was autoclaved, stored at room temperature and diluted to single concentration with aqua bidest. prior to use.

2.5.7. Solutions for non-colloidal Coomassie staining of polyacrylamide gels

2.5.7.1. Coomassie solution (Non-colloidal)

0.5 g	Coomassie® Brilliant Blue R250 (0.05%)
50%	Methanol
10%	Glacial acetic acid
ad 1000 ml	Aqua bidest.

2.5.7.2. Destaining solution

7%	Glacial acetic acid

2.5.8. Solutions for silver staining of polyacrylamide gels

2.5.8.1. Fixation solution

500 ml	Ethanol
120 ml	Glacial acetic acid
500 µl	Formaldehyde (37%)
ad 1000 ml	Aqua bidest.

2.5.8.2. Pretreating solution

50 mg	$Na_2S_2O_3$ x 5 H_2O
50 ml	Aqua bidest.

2.5.8.3. Impregnation solution

50 mg	$AgNO_3$
35 µl	Formaldehyde (37%)
50 ml	Aqua bidest.

2.5.8.4. Development solution

1.5 g	Na_2CO_3
0.1 mg	$Na_2S_2O_3$ x 5 H_2O
50 µl	Formaldehyde (37%)
50 ml	Aqua bidest.

2.5.8.5. Stop solution

0.1 M	EDTA pH 8.0

2.5.8.6. Drying solution

30%	Methanol
10%	Glycerol

diluted in aqua bidest.

2.6. Kits

Glucagon Radioimmunoassay (RIA) Kit	Millipore™, Billerica , USA
Nexttec™ Genomic DNA Isolation Kit	Nexttec GmbH, Leverkusen
Porcine Insulin Radioimmunoassay (RIA) Kit	Millipore™, Billerica, USA
QiaexII™ Gel Extraction Kit	Qiagen GmbH, Hilden
RNeasy® Mini total RNA isolation Kit	Qiagen GmbH, Hilden
Vector Red® Alkaline Phosphatase Substrate Kit	Vector Laboratories, Inc., Burlingame, USA
Taq DNA Polymerase Kit	Qiagen GmbH, Hilden
Wizard genomic DNA purification Kit®	Promega, Wisconsin, USA

2.7. Other reagents

α-[^{32}P]-dCTP	Perkin-Elmer, Netherlands
Amersham™ ECL™ Western Blotting Detection Reagent	GE Healthcare , Munich
Developing and fixing solution	Agfa-Gevaert N.V., Mortsel, Belgium
Bode Sterilium® hand sanitizer	Bode Chemie, Hamburg
6 x DNA loading dye	MBI Fermentas, St. Leon Roth
dNTPs (dATP, dCTP, dGTP, dTTP) (100 mM)	MBI Fermentas, St. Leon Roth
Exendine-4	Sigma Aldrich Chemie GmbH, Steinheim
5 x First-Strand Buffer for cDNA synthesis	Invitrogen™, Karlsruhe
Goat serum	MP Biomedicals, Illkirch, France
Histokitt	Glaswarenfabrik Karl Hecht GmbH, Sondheim/Rhön
Porcine serum	MP Biomedicals, Illkirch, France
Lifosan® soft wash lotion	B. Braun, Melsungen
Q-solution	Qiagen GmbH, Hilden
Random Primer Hexamers (600 µg/ml)	Invitrogen™, Karlsruhe
Random Primers (3 µg/µl)	Invitrogen™, Karlsruhe

RNase-free water	Affymetrix Inc., USA
Vet-Sept® solution (10%)	A. Albrecht, Aulendorf

2.8. DNA molecular weight markers and protein molecular weight markers

Gene Ruler™ (1kb DNA Ladder)	MBI Fermentas, St. Leon Roth
Lambda DNA/EcoRI + *Hind*III-Marker	MBI Fermentas, St. Leon Roth
PageRuler™ Prestained Protein Ladder	Thermo Fisher Scientific, Schwerte
pUC Mix Marker 8	MBI Fermentas, St. Leon Roth
Unstained Protein Molecular Weight Marker	Thermo Fisher Scientific, Schwerte

2.9. Software

GraphPad Prism® version 5.02	GraphPad Software Inc., La Jolla, USA
IMAGEQUANT® image processing software (version 5.2)	MolecularDynamics Inc., Sunnyvale, California, USA
Magellan™ data analysis software	Tecan, Austria
Medtronic CareLink Pro software, version 3.2A	Medtronic GmbH Diabetes, Meerbusch
Olympus Visiomorph™image analysis	Visiopharm, Hoersholm, Denmark
SAS (version 8.2)	SAS Institut Inc., USA
SPSS (version 21.0)	IBM, New York, USA
Videoplan® image analysis system	Carl Zeiss AG, Oberkochen

3. Methods

3.1. Generation of *INS*^{C94Y} transgenic pigs

INS^{C94Y} transgenic pigs were generated by additive gene transfer and somatic cell nuclear transfer (SCNT). The expression construct consisting of a 2.1 kb fragment of the porcine insulin promoter for β-cell-specific expression, a 1.0 kb coding region of the porcine insulin gene sequence including the G→A transition at nucleotide position 340 leading to an amino acid exchange from Cysteine to Tyrosine at amino acid position 94 and a neomycine resistance cassette flanked by two loxP sites was kindly provided by Dr. Heinrich Flaswinkel, LMU Munich. Primary porcine fetal fibroblasts were cultered, nucleofected with the *INS*^{C94Y} expression construct and selected in principle as previously described (Klymiuk et al., 2012). Stable transfected cell clones were used for SCNT using *in vitro* matured oocytes according to the method of Kurome et al. (2006). Reconstructed embryos were laparoscopically transferred into estrus synchronized recipient gilts in accordance to Besenfelder et al. (1997). Operational procedure is in principle illustrated in Figure 2. Cell culture experiments have been performed by Dr. Annegret Wünsch, Institute of Molecular Animal Breeding and Biotechnology, LMU Munich. SCNT and embryo transfer (ET) have been carried out by Dr. Mayuko Kurome and Dr. Barbara Kessler, Institute of Molecular Animal Breeding and Biotechnology, LMU Munich.

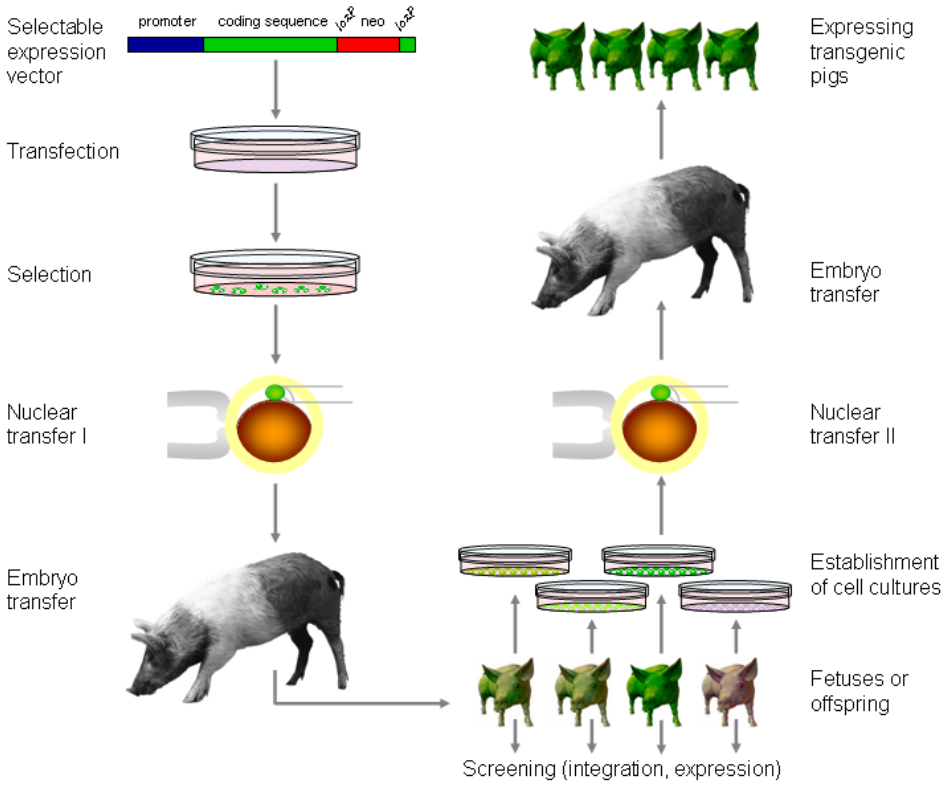

Figure 2: Schematic illustration of effective *INS*^{C94Y} transgenesis in the pig by somatic cell nuclear transfer

The graphic illustrates the generation of *INS*^{C94Y} transgenic pigs by additive gene transfer followed by SCNT. The *INS*^{C94Y} expression vector was nucleofected into porcine fetal fibroblasts and transgenic clones were selected according to the neomycine resistance cassette. Pools of stable transfected cell clones were used for SCNT and ET procuring *INS*^{C94Y} founder animals for potential re-cloning or establishment of transgenic lines (Aigner et al., 2010); with kind permission from *Springer Science and Business Media*.

3.2. Identification of *INS*^{C94Y} transgenic pigs

Genotyping of founder animals and offspring was achieved by specific PCR on tissue samples of newborn piglets. Furthermore Southern blot analysis was carried out on genomic DNA of founder boars and transgenic offspring to visualize transgene integration pattern and to determinate numbers of integration sites.

3.2.1. Polymerase chain reaction (PCR)

3.2.1.1. DNA isolation from ear punches

Ear punches were obtained from newborn piglets and stored at -20°C until further processing. For isolation of genomic DNA the Nexttec™ Genomic DNA Isolation Kit (Nexttec GmbH, Leverkusen) was used according to manufacturer´s instructions. All steps were carried out at room temperature unless indicated otherwise. For tissue digestion, samples were transferred into 1.5 ml reaction tubes and incubated in lysis buffer at 60°C overnight. For proper lysis and high DNA yield 3 µl DTT were additionally added to each sample. For DNA purification, 120 µl of the lysate were transferred to Nexttec™ clean columns the next day, incubated for three minutes and centrifugated at 700 x g for one minute. The eluate containing the purified DNA was immediately used for genotyping PCR or stored at 4°C until further processing.

3.2.1.2. PCR conditions

Genotyping was performed using primers specific for the neomycin resistance cassette as follows:

neoPf (sense): 5´- CAGCTGTGCTCGACGTTGTC-3´
neoSr (antisense): 5´- GAGTCAACTAGTCCTCAGAAGAACTCGTCAAG-3`

The ubiquitously expressed house-keeping gene *ACTB* was additionally amplified to control genomic DNA integrity.

The following *ACTB* specific primers were used:

ACTB (sense): 5´-TGGACTTCGAGCAGAGATGG-3´
ACTB (antisense): 5´-CACCGTGTTGGCGTAGAGG-3´

PCR components were mixed on ice to a total volume of 20 µl or 25 µl respectively in 0.2 ml reaction tubes as follows:

Table 2: Reaction batch for neoPf/neoSr PCR

neoPf/neoSr	
10 x PCR buffer (Qiagen)	2.5 µl
$MgCl_2$ (15 mM) (Qiagen)	2.5 µl
dNTPs (2 mM)	2.5 µl
Sense primer (10 µM)	0.4 µl
Antisense primer (10 µM)	0.4 µl
Taq polymerase (5 U/ µl)	0.2 µl
Aqua bidest.	15.5 µl
DNA template	1 µl
Total volume	**25 µl**

Table 3: Reaction batch for the amplification of *ACTB*

ACTB sense/antisense	
10 x PCR buffer (Qiagen)	2 µl
$MgCl_2$ (25 mM) (Qiagen)	1.25 µl
Q-solution (Qiagen)	4 µl
dNTPs (2 mM)	2 µl
Sense primer (10 µM)	0.4 µl
Antisense primer (10 µM)	0.4 µl
Taq polymerase (5 U/ µl)	0.2 µl
Aqua bidest.	8.75 µl
DNA template	1 µl
Total volume	**20 µl**

PCR conditions are listed below:

Table 4: Protocol neoPf/neoSr PCR

neoPf/neoSr			
Denaturation	95°C	4 min.	
Denaturation	95°C	30sec	**35 x**
Annealing	62°C	30 sec	
Elongation	72°C	45 sec	
Final Elongation	72°C	10 min	

Table 5: Protocol *ACTB* PCR

ACTB sense/antisense			
Denaturation	95°C	4 min.	
Denaturation	95°C	30 sec	**35 x**
Annealing	62°C	30 sec	
Elongation	72°C	45 sec	
Final Elongation	72°C	10 min	

For termination of the reaction, thermocycler cooled down to 4°C. PCR samples were stored at 4°C for contemporary processing or frozen at -20°C. Genomic DNA from a previously genotyped transgenic pig served as positive control and aqua bidest. was used as non-template control.

3.2.1.3. Agarose gel electrophoresis

After completion of PCR amplification, DNA fragments were separated according to their length via agarose gel electrophoresis. 1× TAE buffer was heated with 2% agarose in a microwave until agarose was completely melted. Ethidium bromide (0.5 µg/ml) was added and the gel was poured to set in a gel electrophoresis chamber attached with a comb. After gel polymerization the electrophoresis chamber was filled with 1x TAE running buffer and the comb was immediately removed. 6 x DNA loading dye was added to the DNA samples and samples as well as a Gene Ruler^{TM} 1 kb DNA molecular weight standard were loaded into the gel slots. DNA fragments were visualized when irradiated in UV-light and fragment size was analyzed in relation to the molecular weight standard. A digital picture was taken to document the results.

3.2.2. Southern Blot

3.2.2.1. Isolation and restiction digest of genomic DNA

For Southern blot analysis genomic DNA was isolated from ear punches of respective transgenic founder boars and transgenic offspring in accordance with the protocol indicated in chapter 3.3.1.

Digestion of genomic DNA was accomplished by an overnight incubation at 37°C with the restriction enzyme BamH1 in 1.5 ml reaction tubes in a total volume of 60 µl as follows:

15 µg	genomic DNA
4 µl	*Bam*H1 restriction enzyme
ad 60 µl	Aqua bidest.

The next day, after application of a 6 x DNA loading dye to each sample, DNA fragments were separated by electrophoresis on a polymerized 1% TAE agarose gel matrix according to their size. Agarose gel preparation and electrophoresis was performed as described in chapter 3.2.1.3. A Gene Ruler^{TM} 1 kb DNA Ladder served as DNA molecular weight standard.

3.2.2.2. Transfer of restriction enzyme digested DNA

Following electrophoresis, the gel, containing restriction enzyme digested DNA was pivoted in 0.3M hydrochloric acid for approximately 45 minutes until color changeover of the bromophenol blue bands to yellow. After washing twice with aqua bidest., the gel was incubated in strand break solution for around 45 minutes until color of the bands turned back to blue. Pretreatment for transfer was achieved by immersion of the gel in neutralisation buffer for 20 minutes, followed by another washing step and incubation in 5x SSC for 20 minutes. Subsequently assayed DNA was transferred to a positive loaded Hybond-N+ Nylon membrane in a semi-dry manner by capillary transfer. The standard assembly of a Southern blot containing the gel upside-down on cling film, Hybond-N+ Nylon membrane, two layers of Whatman paper and multiple layers of absorbent papers was arranged. Finally weight was applied and transfer was carried out for 24 hours. Cross-linking of transferred DNA to the membrane was accomplished by UV-light irradiation at a dose of 120 J/cm^2 and membrane was stored at room temperature.

3.2.2.3. Establishment and radioactive labeling of the probe

For the detection of the integrated transgene, a probe specific for the neomycin resistance cassette of the *INS*^{C94Y} expression vector was created. Probes were amplified by PCR using transgene-specific primers as mentioned below:

neoPf (sense): 5´- CAGCTGTGCTCGACGTTGTC-3´

neoSr (antisense): 5´- GAGTCAACTAGTCCTCAGAAGAACTCGTCAAG-3`

Plasmid DNA containing the *INS*^{C94Y} construct served as template. PCR was carried out considering details given in chapter 3.2.1.2. The PCR product was loaded onto a 1% TAE agarose gel and separated as described in chapter 3.2.1.3. Band was excised with a scalpel blade and DNA was eluated from the gel using QiaexII Gel Extraction kit (Qiagen) according to manufacturer's instructions. Concentration of extracted DNA was estimated by comparison with a Lambda DNA/EcoRI + *Hind*III- molecular weight marker. The probes were radioactively labeled with α-[^{32}P]-dCTP (Perkin-Emer, Netherlands), integrated using Klenow fragment of Polymerase I (Klenow exo$^-$) as polymerase, and reagents as follows:

50-100 ng	extracted DNA probe
7 µl	10 x Klenow buffer
10 µl	Random Primer (3 µg/µl)
ad 50 µl	Aqua bidest.

Probe DNA was subsequently denatured at 97°C for 10 minutes. Diluents were chilled on ice for 2 minutes and 20 µl hybridisation mix were added to each sample and incubated for one hour at 37°C.

Hybridisation master mix:

3 µl	C-Mix (0.33 M of each dATP, dCTP, dGTP, dTTP)
5 µl	α-[^{32}P]-dCTP (3000 Ci/mmol)
1 µl	Klenow exo$^-$
ad 20 µl	Aqua bidest.

Centrifugation through Sephadex G-50 columns separated unincorporated nucleotides. Adequate amount of purified probes were denatured at 97°C for five minutes a second time and stored on ice.

3.2.2.4. Hybridisation and signal detection

Previously, blotted Hybond-N+ Nylon membranes were moistened with 5 x SSC and prehybridized in 30 ml Southern blot church buffer for one hour at 58°C in a hybridisation oven. Subsequently labeled probes were diluted in Southern blot church buffer and probes were allowed to hybridize to the nylon membranes overnight at 58°C under permanent rotation in the hybridisation oven. The next day, membranes were washed twice with low-stringency buffer at room temperature and twice with high-stringency buffer at 58°C.

For signal detection, blots were exposed to X-ray films in an X-ray cassette for at least 24 hours at -80°C. X-ray films were developed in developing and fixing solutions in accordance with manufacturer's protocol and subsequently analyzed.

3.3. Expression analysis of the *INS*^{C94Y} transgene by reverse transcription PCR (RT-PCR) and next generation sequencing technology

Expression of the *INS*^{C94Y} transgene on RNA level was analyzed in porcine pancreatic tissue of all seven *INS*^{C94Y} transgenic founder boars and representatives of the *INS*^{C94Y} transgenic F1-offspring of diabetic founder boar 9747.

Genomic DNA of an *INS*^{C94Y} transgenic pig was additionally used as template for the PCR reaction to differentiate between genomic DNA and cDNA by amplification with intron-spanning primers.

To verify complete DNaseI digest, minus RT reactions of all samples were performed additionally by replacing SuperScript™ II Reverse Transcriptase with RNase-free water and processed accordingly.

3.3.1. Isolation of genomic DNA from ear punches

For DNA isolation, tissue was obtained from ear punches. Tissue was stored at -80°C until further processing. Isolation of genomic DNA was carried out using the Wizard genomic DNA purification Kit® (Promega) according to the manufacturer's instructions. For tissue digestion, ear punches (3-5 mm) were transferred into separate 1.5 ml reaction tubes and incubated on a thermomixer at 55°C overnight, gently shaking in lysis buffer as follows:

Mastermix:

120 µl	0.5 M EDTA pH8.0
500 µl	Nuclei lysis solution
17.5 µl	Proteinase K

The next day, undigestible components were separated by centrifugation (14.000 x g, 20°C) and supernatant was decanted into new 1.5 ml reaction tubes. For RNA clean-up, RNase-A was added, mixed accurately and incubated for 15 to 30 minutes at 37°C. After cooling down to room temperature, protein precipitation was achieved by addition of 200 µl protein precipitaton solution followed by a centrifugation step (13.000-16.000 x g, 4 minutes). Supernatant was transferred into 1.5 ml reaction tubes, containing 600 µl isopropanol and mixed carefully by inverting the tubes. Two minutes of centrifugation at 13.000 x g yielded a DNA pellet and the supernatant was discarded. The DNA pellet was washed twice in 70% ethanol, vortexed briefly and then centrifuged for two minutes at 13000 x g. Resulting supernatant was discarded reiterately. The DNA pellet was subsequently air-dried and resuspended in 50–100 µl DNA rehydration solution, gently shaking on a thermomixer at 65°C for 60 minutes. Until further usage the samples were stored at 4°C.

The genomic DNA concentration was determined by measuring optic density at wavelengths of 260 nm and 280 nm using NanoDrop ND-1000 spectrophotometer (NanoDrop Technologies) and finally adjusted to 100 ng/µl for PCR use.

3.3.2. Isolation of total RNA from porcine pancreatic tissue

Total RNA was extracted from pancreatic tissue using RNeasy® Mini total RNA isolation Kit (Qiagen) according to manufacturer´s instructions. In brief, 30-50 mg of frozen pancreatic tissue were transferred into sterile 6 ml culture tubes and homogenized for one minute with 600 µl of the recommended buffer using an ART-Micra D-8 tissue-homogenizer (23.500 rpm). Immediately afterwards, lysate was pipetted into a new 1.5 ml reaction tube followed by a centrifugation step (3 minutes, 14.000 rpm, 4°C). Supernatant was decanted into another sterile 1.5 ml reaction tube, diluted 1:1 with ethanol (70%) and dilution was gently mixed by pipetting. After certain purification and centrifugation steps through

clean-up columns in corresponding buffers according to the manufacturer's protocol, total RNA was eluted in 50 µl RNase-free water.

3.3.3. Quantification of total RNA and evaluation of RNA quality

Quantification of total RNA was implemented using a NanoDrop ND-1000 spectrophotometer (NanoDrop Technologies) at a wavelength of 260 and 280 nm respectively. Total RNA quality was evaluated by visualization of 18 S and 28 S ribosomal bands using agarose gel electrophoresis. Therefore, a 1% TBE-agarose gel was prepared as described in chapter 3.2.1.3. Additionally ethidium bromide was both added to the 1% TBE-agarose solution (1 µl/50 ml) and the 1 x TBE running buffer (9 µl/l). A total of 500 ng RNA per sample was diluted to at least equal volumes with DEPC water, 6 x DNA loading dye was applied and samples were transferred into the gel slots.

3.3.4. DNaseI digest and reverse transcription

To prevent DNA contamination, eluted RNA samples were digested with DNaseI. Therefore 800 ng of total RNA were incubated with 20 U of DNaseI for 30 minutes at 37°C on a thermomixer, diluted to an equal volume of 20 µl.

800 ng	Total RNA
2 µl	DNaseI reaction buffer
2 µl	DNaseI (10 U/µl)
ad 20 µl	RNase-free water

Inactivation of the enzyme was achieved by incubation at 75°C for ten minutes followed by cooling down on ice for several minutes and centrifugation.

10 µl DNaseI digested RNA were used for reverse transcription with the SuperScript™ II Reverse Transcriptase (Invitrogen) using random hexamer primers in a total volume of 20 µl as follows:

10 µl	DNaseI digested RNA
1µl	Random Hexamers Primers (600 µg/ml)
1 µl	dNTPs (10 mM)

Reagents were incubated at 65°C on a thermomixer for 5 minutes, chilled on ice for two minutes and spun down briefly.

4 µl	5 x first-strand buffer
2 µl	DTT (100 mM)
1 µl	RNaseOUT

Previously mentioned components were added followed by gentle mixing and an incubation step for 2 minutes at 25°C.

Next, 1 µl of SuperScript™ II Reverse Transcriptase was added to each sample followed by an incubation step for 10 minutes at 25°C. Then, the temperature was raised to 50°C for enzyme activation and samples were incubated for another 50 minutes. To inactivate the enzyme, samples were incubated at 70°C for 15 minutes thereafter. Obtained cDNA was chilled on ice, spun down and stored at -20°C until further processing.

3.3.5. PCR

cDNA was amplified by applying insulin-specific primers:

Insulin (sense):	5´-CGGGAGGCGGAGAACCCTCA-3‘
Insulin (antisense):	5‘-CCCTCAGGGGCGGCCTAGTT-3‘

1 µl of the cDNA served as template for PCR using the following protocol:

Table 6: Reaction batch for amplification of *INS* cDNAs

Insulin sense/antisense	
10 x PCR buffer (Qiagen)	2 µl
$MgCl_2$ (25 mM) (Qiagen)	1.25 µl
Q-solution (Qiagen)	4 µl
dNTPs (2 mM)	2 µl
Sense primer (10 µM)	0.4 µl
Antisense primer (10 µM)	0.4 µl
Taq polymerase (5 U/ µl)	0.2 µl
Aqua bidest.	8.75 µl
cDNA template	1 µl
Total volume	**20 µl**

Table 7: PCR protocol

Denaturation	95°C	4 min.	
Denaturation	95°C	30sec	**35 x**
Annealing	62°C	30 sec	
Elongation	72°C	45 sec	
Final Elongation	72°C	10 min	

Additionally cDNA integrity was verified by amplification of *ACTB* using the same cDNA templates. PCR reaction batch and conditions are described in Table 3 and Table 5. Agarose gel electrophoresis was performed as described in chapter 3.2.1.3.

3.3.6. Next generation sequencing

The ratio of mutant INS^{C94Y} and wild-type *INS* transcripts was determined by next generation sequencing of RT-PCR amplicons (Genome Analyzer IIx, Illumina; >10,000 reads per sample). Previously prepared RT-PCR products were A-tailed and ligated to barcoded adapters using the NEBnext DNA Library Prep Master Mix Set (New England Biolabs, Ipswich, USA). Sequencing-ready amplicons were purified with Agencourt Ampure XP magnetic beads and quantified on a Bioanalyzer DNA1000 chip (Agilent, Santa Clara, USA). Amplicons were sequenced in an 80 bp single read run on an Illumina Genome Analyzer GAIIx. Reads containing either the wild-type or the mutant codon 94 were counted for

each sample. Next generation sequencing analysis was performed by Dr. Stefan Krebs, Laboratory of Functional Genome Analysis, Gene Center, LMU Munich.

3.4. Physiological characterization of *INS*^{C94Y} transgenic pigs

3.4.1. Blood glucose levels and body weight gain

To evaluate the impact of *INS*^{C94Y} transgene expression on glucose homeostasis, random blood glucose levels were determined at short intervals, starting prior to first colostrum ingestion up to the age of weaning. After weaning fasting blood glucose levels (18-hour fasting period) were analyzed regularly in at last 4-week intervals. Therefore a drop of blood was taken from a superficial ear vein with a small lancet and instantly examined using a FreeStyle Precision® Xceed™ Glucometer with Precision Xtra™ Plus blood glucose test stripes (Abbott).

In addition body weight gain was recorded on a regular basis using a mobile animal scale.

In both cases, non-transgenic female and male littermates served as wild-type controls.

3.4.2. Determination of insulin levels by radioimmunoassay (RIA)

Fasting plasma insulin levels of two different age groups were investigated, 8-day-old and 4.5-month-old male and female *INS*^{C94Y} transgenic pigs and littermate controls. Blood samples were collected in EDTA monovettes and immediately stored on ice. After centrifugation (15 minutes, 1500 x g, 4°C), plasma was carefully separated and stored at -80°C until assayed. Fasting plasma insulin levels were determined in duplicates using a porcine insulin RIA kit (Millipore™) according to manufacturer´s instructions. A fixed concentration of ^{125}I-labeled insulin was used as labeled tracer antigen. Unlabeled insulin of the plasma samples and ^{125}I-labeled insulin compete for a constant number of binding sites on the anti-porcine insulin antibody (use of a constant dilution). Consequently, the amount of tracer antigen decreases, if the concentration of unlabeled antigen increases. Following separation of antibody-bound from free tracer, the antibody-bound fraction was counted in a γ-counter. Samples of unknown concentration were analyzed by comparison with a previously determined standard curve. Merely duplicates with a coefficient of variance (CV) less than 10% were taken into account.

3.4.3. Determination of glucagon levels by radioimmunoassay (RIA)

Basal plasma glucagon levels were measured in *INS*^{C94Y} transgenic pigs and non-transgenic littermates at the age of 8 days and at the age of 4.5 months. Blood samples were collected and processed as described in 3.4.2. Glucagon levels were determined using a commercially available glucagon radioimmunoassay (RIA) kit according to the manufacturer's protocol (in principle procedure described in 3.4.2.). ^{125}I-labeled glucagon was utilized as a tracer antigen.

3.4.4. Homeostasis model assessment of β-cell function (HOMA - B) and insulin resistance (HOMA - IR)

The parameters homeostasis model assessment of β-cell function (HOMA - B) and insulin resistance (HOMA - IR) were calculated in 4.5-month-old *INS*^{C94Y} transgenic pigs and non-transgenic littermates according to Matthews et al. (1985).

HOMA - IR= FSI (µU/ml) * FBG (mmol/l) / 22.5

HOMA - B (%) = 20*FSI / (FBG - 3.5)

FSI: Fasting serum insulin (µU/ml)

FBG: Fasting blood glucose (mmol/l)

3.4.5. Insulin therapy of *INS*^{C94Y} transgenic pigs

To guarantee a healthy adolescence and to preserve fertility, *INS*^{C94Y} transgenic pigs were started on insulin therapy at the age of approximately 4.5 months. A combination of long-acting Lantus® insulin (Sanofi) and short-acting NovoRapid® insulin (NovoNordisk) was administered subcutaneously once daily using a commercial insulin pen with appropriate BD Micro-Fine Ultra™ pen needles (Becton Dickinson GmbH). In total, a dosage of 0.5 -1 I.U. per kg body weight was applied. Blood glucose concentration was determined once to twice daily using a Precision® Xceed™ Glucometer with appropriate Precision Xtra™ Plus blood glucose test stripes (Abbott) as described in chapter 3.4.1.

3.4.6. Continuous blood glucose monitoring

In order to evaluate glucose control under insulin treatment continuous glucose monitoring was performed using the Guardian® REAL-Time System (Medtronic). The Guardian® REAL-Time System measures glucose levels within the intracellular fluid. An insulin-treated *INS*^{C94Y} transgenic pig and an untreated control animal were profiled over a period of 42 hours. For this purpose, a sensor was placed subcutaneously behind the ear under general anesthesia (detailed description of general anesthesia regimen in chapter 3.4.7.1) measuring interstitial glucose levels every 10 seconds (Figure 3). A transmitter connected to the glucose sensor transferred all data electronically to an external computer. The mean glucose concentration was calculated by the computer every five minutes and displayed on the monitor. Capillary blood glucose levels were determined up to five times per day using the Precision® Xceed™ glucometer to calibrate the device. Data analysis was carried out using the Medtronic CareLink Pro software (version 3.2A).

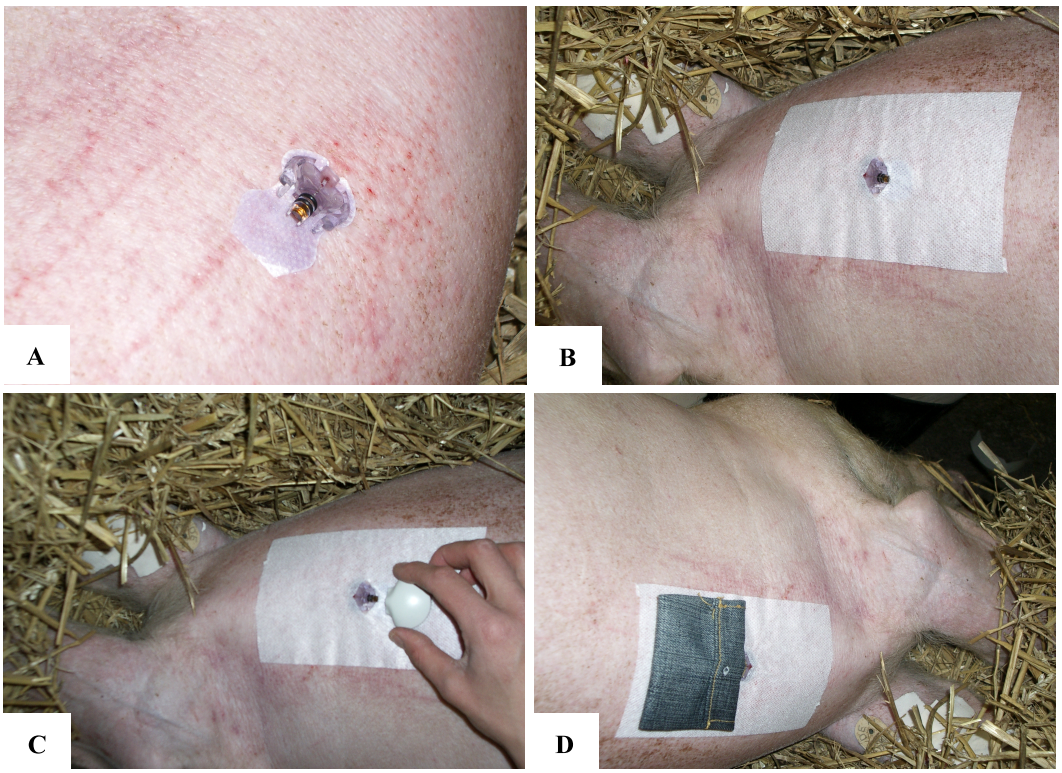

Figure 3: Placement of a continuous glucose monitoring system in a pig

For achieving a continuous glucose monitoring profile of an insulin-treated *INS*^{C94Y} transgenic pig and an untreated control animal a sensor was inserted subcutaneously near the ear **(A/B)** and connected to a transmitter **(C/D)** for electronical data transmission.

3.4.7. Analyzes of glucose metabolism by glucose tolerance tests

Intravenous glucose tolerance tests were performed in normoglycemic transgenic founder boars at the age of seven months to investigate potential early abnormalities in glucose tolerance and insulin secretion indicating prediabetic status.

3.4.7.1. Surgical insertion of central venous catheters

To allow reiterated blood sampling for acccomplishment of glucose tolerance tests, pigs received two central venous catheters, which were both surgically inserted into the external jugular vein. In general, the surgery was performed aseptically under general anaesthesia and pigs were treated peri-and postsurgically with analgesics. In addition antibiotics were administered postsurgically to prevent infections. Pigs were anaesthetised by intramuscular injection of ketamine

hydrochloride (2 ml/10 kg BW) and azaperone (0.5 ml/10 kg BW). To maintain anaesthesia, ketamine hydrochloride (2 ml/10 kg BW) and xylazine (0.5 ml/ 10 kg BW) was injected intravenously through a catheter in the ear vein as needed. Peri- and post-surgical analgesia was achieved by intravenous injection of metamizol (1 ml/10kg BW) and an intramuscular application of meloxicam (2 ml/100 kg BW). Pigs were positioned in dorsal recumbency. After cleansing and disinfection of the jugular grove, an incision of approximately five centimetres length was made to allow vein exposure. Holding sutures were placed, adjacent tissue was carefully removed from the vein and a venotomy was made followed by insertion of the catheters. A proximal and a distal ligature prevented blood reflux and fixed the catheter in the required position. The incision was immediately sutured in two layers. Catheters were externally fixated with a suture to the skin, covered by sterile gauze and adhesive tape was placed like a neck brace. On withers height catheters were coiled in a pouch to allow easy access. To avoid obstruction by coagulation, catheters were flushed once daily with 250 I.U. heparin/ml 0.9% isotonic NaCl solution. Previously to the glucose tolerance test, undisturbed general condition of the pigs was ensured.

3.4.7.2. Intravenous glucose tolerance test (IVGTT)

IVGTT was performed in pigs placed in single pens, freely moving and fasted 18-hours overnight. The pigs were injected a concentrated 50% glucose solution (0.5 g/kg BW) followed by 20 ml 0.9% isotonic NaCl solution.

Blood samples were taken at -10, 0, 1, 3, 5, 7, 10, 15, 20, 30, 40, 50, 60 and 90 minutes relative to intravenous glucose load and the catheter was flushed with 3 ml of a 0.9% isotonic NaCl solution after each blood sampling. Blood samples were processed as described in 3.4.2. Plasma glucose levels were determined using an AU 400 autoanalyzer (Olympus) while insulin levels were measured in duplicates using a porcine insulin RIA kit (Millipore) as described in chapter 3.4.2. The area under the glucose/insulin curve was determined using GraphPad Prism software (version 5.02).

3.5. Morphological characterization of *INS*^{C94Y} transgenic pigs

3.5.1. Necropsy

INS^{C94Y} transgenic and non-transgenic pigs of defined age were subjected to routine necropsy. Therefore pigs were anaesthetised with ketamine hydrochloride (2 ml/10 kg BW) and azaperon (0.5 ml/10 kg BW) in their accustomed surroundings followed by vein catheter insertion and euthanization by an intravenous injection of T61 (1 ml/10 kg BW). Then, organs were subjected to macroscopic evaluation and desired tissue samples were harvested.

3.5.2. Pancreas preparation for quantitative-stereological analyzes

To avoid autolysis, the pancreas was immediately processed. Following explantation of the whole organ, surrounding tissue was carefully removed and the pancreas was weighed. In 4.5-month-old animals the pancreas was cut at the intersection between splenic and connective lobe and placed lengthwise on the table (Figure 4). The pancreas was cut into 0.5 cm thick slices. Slices were tilted to their left side and fixed in 4% neutral buffered formalin overnight. The next day, slices to be analyzed, were selected by systematic random sampling. Therefore slices were covered by a 1 cm^2 point-counting grid and the total number of points hitting pancreatic tissue was counted and divided by the number 20 as total sample number. For simplification, the above-mentioned quotient is called Y in the following. Starting at a random number (X) between one and Y, pieces with a volume of 0.5 cm^3 were collected at the sites X, X+Y, X+2*Y, X+3*Y,…, X+20*Y. Selected samples were placed in an embedding cassette right cut surface downwards and routinely processed for paraffin histology. Following paraffin embedding, half of the pancreatic samples were cut into approximately 4 µm thick sections with a HM 315 microtome (Microm), mounted on 3-aminopropyltriethoxysilane-treated glass slides for immunohistochemistry and dried at 37°C in an incubator overnight.

Due to their smaller size, pancreata of 8-day-old piglets were not subjected to systematic random sampling, but rather fixed in total in 4% neutral buffered formalin overnight, cut longitudinally into 0.3 cm^3 thick slices the next day and routinely processed for paraffin embedding.

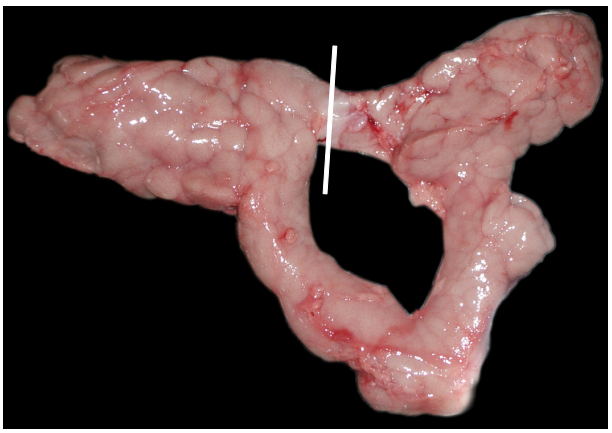

Figure 4: Preparation of the pancreas for quantitative-stereological analyzes

The pancreas of 4.5-month-old *INS*^{C94Y} transgenic pigs and non-transgenic littermates was separated between splenic and connective lobe. White bar indicates the separation site; (picture kindly provided by Dr. Simone Renner).

3.5.3. Immunhistochemical stainings of pancreatic tissue

For quantitative stereological analyzes, different immunohistochemical stainings were performed. In 4.5-month-old *INS*^{C94Y} transgenic pigs (3 male, 4 females) and non-transgenic controls (1 male, 6 female) a double immunohistochemical staining to visualize β-cells and non-β-cells as well as a single staining to detect α-cells was carried out. Pancreatic tissue sections of transgenic and non-transgenic 8-day-old piglets (n=4 per group) were used for a single staining detecting insulin containing β-cells.

For detection of insulin containing cells, the indirect alkaline phophatase method (AP) was implemented, whereas glucagon, somatostatin and pancreatic polypeptide containing cells were immunostained utilizing the indirect immunoperoxidase technique. Sections were deparaffinized for 20 minutes in xylene, rehydrated in a descending alcohol series and washed in distilled water. Endogenous peroxidase activity was blocked by incubation in 1% hydrogen peroxide solution for 15 minutes. Following a washing step in TBS buffer (pH 7.4) for 10 minutes, sections were subjected to incubation with non-immune goat serum for 30 minutes to reduce non-specific binding. Subsequently, slides were incubated for one hour at room temperature with the respective primary antibody diluted to the desired concentration in TBS buffer (pH 7.4), washed again in TBS buffer (pH 7.4) for 10 minutes and incubated with the corresponding

secondary antibody containing 5% porcine serum, likewise diluted in TBS buffer (pH 7.4). After a further washing step in TBS buffer (pH 7.4), immunoreactivity was visualized with a suitable chromogen protected from light. Last, slices were counterstained in Mayer´s hemalum solution, washed in distilled water and dehydrated in an ascending alcohol series, followed by clearing in xylene and mounting using histokitt. For staining of non-β-cells, all three primary antibodies were mixed and sections were simultaneously immunostained.

For details on antibodies and chromogens see Table 8.

Table 8: Immunhistochemical procedures

Antigen	Primary antibody	Dilution	Secondary antibody	Dilution	Chromogen
Insulin	Guinea pig anti-porcine insulin, polyclonal	**1:1000**	Goat anti-guinea pig IgG, AP-conjugated	**1:100**	**Vector® Red**
Glucagon	Rabbit anti-human glucagon, polyclonal	**1:300**	Goat anti-rabbit IgG, HRP-conjugated	**1:100**	**DAB**
Pancreatic polypeptide	Rabbit anti-human somatostatin, polyclonal	**1:100**	Goat anti-rabbit IgG, HRP-conjugated	**1:100**	**DAB**
Somatostatin	Rabbit anti-bovine pancreatic polypeptide, polyclonal	**1:50**	Goat anti-rabbit IgG, HRP-conjugated	**1:100**	**DAB**

3.5.4. Quantitative stereological analyzes of the pancreas

Stereometrical procedure was carried out using an Olympus Visiomorph^{TM} image analysis system (Visiopharm, Hoersholm, Denmark) coupled to a light microscope (BX41, Olympus). That way, images were displayed via a colour video camera (DP72, Olympus) on a monitor in the desired magnifications. Planimetric evaluation of α-, β- and non-β-cell (α-, δ-, pp-cells) areas as well as islet profiles and the cross-sectional area of pancreatic tissue was manually determined on immunhistochemically stained pancreatic sections by circling their cut surfaces with a cursor using the stereology software newCAST (Visiopharm, Hoersholm, Denmark). The area of β-cells in 8-day-old animals was determined in a semi-automated fashion using the software visiomorph (Visiopharm, Hoersholm, Denmark). All photographs were taken under equal conditions. To assess the relative proportions, scale bars were designed by photographing an object micrometer (Zeiss, Oberkochen) at the same magnification. As conventional histological tissue procession provokes shrinkage of the organ, the volume of the pancreas ($V_{(Pan)}$) before embedding was calculated by the quotient of the pancreas weight and the specific weight of the porcine pancreas (1.07 g/cm^3) determined by the submersion method (Scherle, 1970). Volume fractions of target cells in reference compartments were computed values. The volume density of the islets in the pancreas ($Vv_{(Islet/Pan)}$) was calculated by dividing the total islet area ($A_{(Islet)}$) by the total pancreas area ($A_{(Pan)}$). The product of $Vv_{(Islet/Pan)}$ and $V_{(Pan)}$ yielded the total volume of islets in the pancreas ($V_{(Islet,Pan)}$). The volume densities of α- and β-cells in the islet ($Vv_{(\alpha\text{-cells/Islet});}$ $Vv_{(\beta\text{-cells/Islet})}$) or in the pancreas ($Vv_{(\alpha\text{-cells/Pan});}$ $Vv_{(\beta\text{-cells/Pan})}$) respectively as well as their total volumes in their reference compartments ($V_{(\alpha\text{-cell,Islet})}$; $V_{(\alpha\text{-cell,Pan})}$; $V_{(\beta\text{-cell,Islet});}$ $V_{(\beta\text{-cell,Pan})}$) were calculated accordingly. The volume density and the total volume of β-cells in the pancreas refer to β-cells in the islet and isolated β-cells in the pancreas. Isolated β-cells were evaluated separately and their volume fractions were likewise calculated.

3.5.5. Transmission electron microscopy (TEM)

In order to investigate ultrastructural morphology of pancreatic β-cells, pancreata of 8-day-old and 4.5-month-old transgenic and non-transgenic pigs (n=3 per group) were subjected to electron microscopy. Pancreas samples of approximately 1 mm^3 were obtained by systematic random sampling during routine necropsy. Samples were fixed by immersion in 6.25% glutaraldehyde in Soerensen's phosphate buffer (pH 7.4) for 24 hours. After fixation, samples were washed in Soerensen´s washing solution at least three times until complete removal of glutaraldehyde. Subsequently, tissue was fixed in 1% osmium tetroxide fixation solution for two hours at 4°C, followed by another washing step in Soerensen's washing solution. Subsequently pancreas samples were routinely processed for epon embedding containing dehydration in an ascending acetone series, incubation in a solution with equal amounts of acetone (100%) and glycidylic ether 100 (Epon) for one hour at room temperature followed by incubation in undiluted glycidylic ether 100 twice for 30 minutes and final embedding in glycidylic ether-embedding mixture in gelatine capsules. Polymerization was achieved by incubation at 60°C for 48 hours. Epon blocks were trimmed using a TM60 milling machine (Leica) and semi-thin sections (0.5 μm) were prepared using a Reichert-Jung Ultracut E microtome (Leica). In order to visualize the distribution of the pancreatic islets within the semi-thin sections, sections were at first stained with toluidine blue staining solution for 15 seconds at 55°C on a heating plate, rinsed with aqua bidest. and dried. Subsequently sections were incubated in Safranin O staining solution for another 15 seconds, rinsed with aqua bidest., dried and finally covered with coverslips using histofluid mounting medium. Following identification of the islets under a microscope and marking their positions, ultra-thin sections (70-80 nm) were sliced just at these localizations, also using Reichert-Jung Ultracut E microtome. Finally, sections were mounted on copper rings and contrasted with uranyl acetate and lead citrate according to the method of Reynolds (1963). Electron microscopy was performed using an EM 10 transmission electron microscope (Zeiss).

Electron microscopical evaluation of the endocrine pancreas was carried out in Cooperation with the Institute of Veterinary Pathology at the Center for Clinical Veterinary Medicine, LMU Munich, Prof. Dr. Walter Hermanns.

3.5.6. Physiological, morphological and quantitative-stereological evaluation of the kidneys

Morphology of the kidneys as well as the kidney function of *INS*^{C94Y} trangenic pigs (3 males and 4 females) and their corresponding non-transgenic littermate controls (1 male and 6 females) were investigated at 4.5 months of age. Additionally kidney samples of 1-year-old cloned diabetic *INS*^{C94Y} transgenic pigs, kindly provided by Minitube of America, Inc., were examined histologically. Furthermore urine samples of these animals were assayed for evidence of albuminuria as an initial diabetes-induced functional disorder of the kidney. The oldest stage investigated for diabetic kidney disease likewise was the diabetic *INS*^{C94Y} transgenic founder boar at the age of approximately three years. One age-matched, non-transgenic boar served as wild-type control for urine analyzes. Histopathological evaluation of diabetic secondary lesions in the kidneys of *INS*^{C94Y} transgenic pigs was performed in cooperation with Dr. Andreas Blutke, Institute of Veterinary Pathology at the Center for Clinical Veterinary Medicine, LMU Munich, Research Group of Prof. Dr. Rüdiger Wanke.

3.5.6.1. Sodium dodecyl sulfate polyacrylamide gel electrophoresis (SDS-PAGE) analysis of urine samples

Urine samples of respective pigs were either collected after spontaneous emiction or obtained by cystocentesis under general anesthesia as described in chapter 3.4.7.1. Urine samples were mixed well by vortexing, aliquoted and immediately frozen at -80°C until assayed. In advance urine samples were profiled by an AU 400 autoanalyzer (Olympus) and especially creatinine levels were determined. Urine samples were standarized by dilution to a constant creatinine concentration of 1500 µmol/l with aqua bidest. and stored on ice for contemporary processing. Urine protein fractions were separated by electrophoresis on a polymerized gel matrix according to their molecular weight. 12% SDS polyacrylamide separating gel was prepared as indicated in Table 9, poured into the intercept of two glass plates clamped in a Mini Protean® 3 Cell Assembly chamber (BioRad), immediately overlayed with aqua bidest. and allowed to polymerize for one hour at room temperature.

Table 9: Composition of SDS polyacrylamide separating gel (12%, for 4 gels)

Aqua bidest.	6.7 ml
1.5 M Tris pH 6.8	5.0 ml
30 % Acrylamide/Bis solution	8.0 ml
10 % SDS	200 µl
Temed	10 µl
10 % APS	10 µl

Following complete polymerization, aqua bidest. was carefully drained and a 5% stacking SDS polyacrylamide gel (Table 10) was casted instead. Subsequently a 10-well or 15-well comp respectively was inserted into the fluid stacking gel.

Table 10: Composition of SDS polyacrylamide stacking gel (5%, for 4 gels)

Aqua bidest.	7 ml
0.5 M Tris pH 6.8	1.25 ml
30 % Acrylamide/Bis solution	1.5 ml
10 % SDS	100 µl
Temed	5 µl
10 % APS	100 µl

While the stacking gel was polymerizing for at least 45 minutes, previously diluted samples were prepared. One-fifth volume fraction of 5 x Laemmli buffer and 5% 2-mercaptoethanol was added to 1 µl of the urine sample resulting in a final concentration of 25 µl. Before sample application, the urine samples were denatured at 95°C for five minutes on a heating block, chilled on ice for two minutes and finally the lid condensate was briefly centrifuged. A bovine serum albumin standard was prepared with a concentration of 100 µg/ml and 0.6 µg/25 µl were assayed accordingly. The comb was removed carefully and the gel was placed into an electrophoresis cell of the Mini Protean® 3 Cell Assembly. 1 x SDS running buffer was filled to the top of the inner cell and up to one third of the outer cell. Urine samples, the bovine albumin standard and additionally a PageRuler™ Prestained Protein Ladder as well as an unstained protein molecular weight marker (Thermo Fisher Scientific) were loaded into the slots. Electrophoresis was run at 100 V for approximately 15 minutes until chromogen

reached the SDS polyacrylamide separating gel and prestained protein ladder begun to separate. Subsequently electric voltage was raised to 160 V and electrophoresis ran for another 60 minutes until leakage of the chromogen. Finally the gel was removed from the glass frame and subjected to non-colloidal Coomassie staining and silver staining as described in chapter 3.5.6.2. and in chapter 3.5.6.3. For detection of albuminuria, gel bands of approximately 66 kDa corresponding to the molecular weight of bovine serum albumine standard (66.5 kDa) were compared with age-matched non-transgenic control pigs.

3.5.6.2. Non-colloidal Coomassie staining of SDS polyacrylamide gels

For Coomassie staining the gel was at first pivoted in aqua bidest. for two minutes. Then, aqua bidest. was carefully drained and gels were incubated in Coomassie staining solution at 4°C overnight pitching on a tumbling shaker. To prevent evaporation, staining bowl was wrapped in cellophane. The next day, gels were destained, while pivoting in destaining solution for as long as required but at last until gel background has cleared. Destaining solution was replaced whenever necessary. Gels were scanned for documentation and dried for long-term storage. Initially gels were incubated in drying solution for one hour. The DryEase® Mini-Gel drying base and frame (Life Technologies™ GmbH) was used for drying polyacrylmide gels. Previously two cellophane sheets were moistened in drying solution and the stained gel was placed between these two sheets without blisters. Finally the DryEase® Mini-Gel drying base and frame were aligned and closed with plastic clamps. Gels were dried standing upright on a benchtop for approximately 2 days.

3.5.6.3. Silver staining of SDS polyacrylamide gels

In general all steps were performed at room temperature. The SDS polyacrylamide gel was incubated in fixation solution followed by thrice 20 minutes in 50% ethanol on a tumbling shaker. Pretreatment was achieved by incubation in sodium thiosulfate solution for one minute before being rinsed with aqua bidest. for 3 x 20 seconds. Afterwards gel was impregnated for 20 minutes and washed in aqua bidest. twice for 20 seconds. Development in developmental solution under visual control until bands appear was arbitrative. The gel was rinsed again in aqua bidest. for 20 minutes and the reaction was stopped with 0.1 M EDTA pH 8.0. After being washed for further three times two minutes in

aqua bidest., gel was dried and analyzed as described before (3.5.6.2).

3.5.6.4. Tissue preparation for histology and transmission electron microscopy of the kidneys

For histopathological investigation, the left kidney was explanted immediately after euthanasia (3.5.1) and instantly fixed by orthograde vascular perfusion using 4% phosphate buffered formaldehyde solution of 37°C for 15 minutes (Figure 5). After perfusion, the kidney was decapsulated and fixed by immersion in 4% phosphate buffered formaldehyde solution for 24 hours. After dabbing the fixed kidney with a paper towel the organ weight was determined. The perfused kidney was then cut perpendicular to the longitudinal axis. In a systematic random sampling according to Nyengaard (1999), six samples from the renal cortex were selected, carefully resected with a scalpel blade and subjected to either plastic or epon embedding (LIT). Relative kidney weights were calculated from the cumulative weight of both kidneys as percent of body weight.

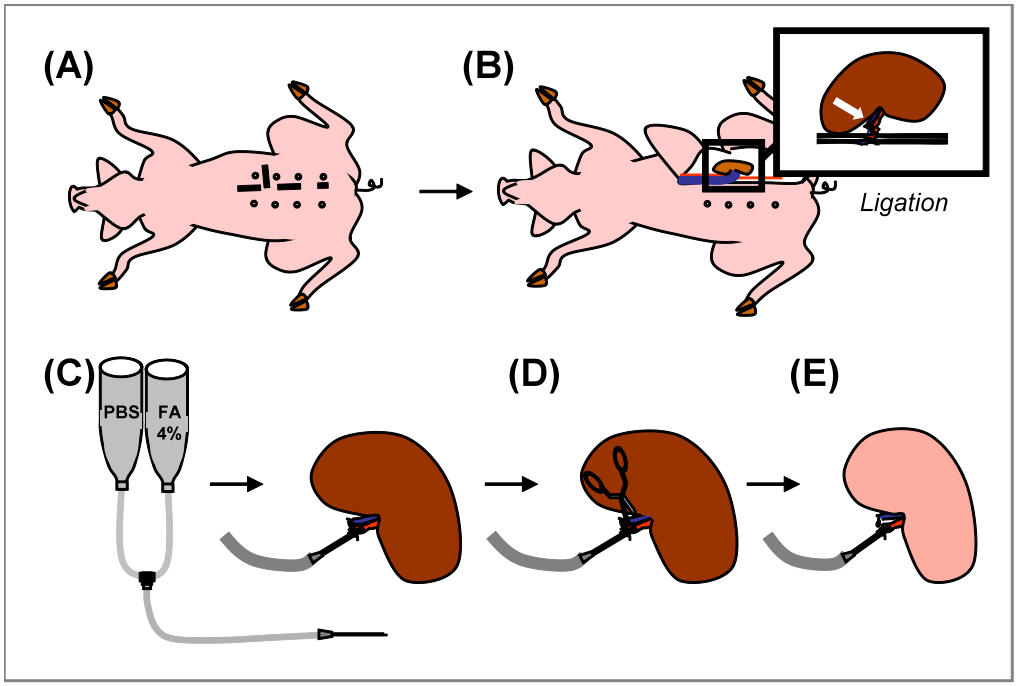

Figure 5: Schematic illustration of orthograde vascular kidney perfusion in the pig

For orthograde vascular kidney perfusion the pig was positioned in dorsal recumbency and the abdomen was opened through a median transection as indicated by the dashed line **(A)**; renal artery and vein were ligated and kidney was immediately removed **(B)**; isolated kidney was perfused using 4% phosphate buffered formaldehyde solution of 37°C for 15 minutes via an arterial access **(C)**, while outflow of the perfusate was ensured through the equilateral vein **(D)**; the change in color of the organ surface to pale yellow was an indicator for sufficient perfusion **(E)**; (illustration kindly provided by Dr. Andreas Blutke).

3.5.6.4.1. Plastic histology of kidney samples

For plastic embedding, renal tissue was left immersed in 4% paraformaldehyde overnight and routinely processed using a Shandon Citadel tissue processor 1000 (Thermo Fisher Scientific). Tissue embedding in glycolmethacrylate and methyl-methacrylate (GMA/MMA) was performed as previously described (Hermanns et al., 1981). Initially paraformaldehyde fixed slices were transferred into embedding capsules and fixed by rubber-sponge kit. Incubation in 2-hydroxymethylmethacrylate-methyl methacrylate solution at 4°C on a tumbling shaker for 18 hours was followed by incubation in plastic embedding solution for

four hours at 4°C. Finally kidney slices were embedded in plastic cups using 60 µl dimethylanilin as initiator of polymerization. Complete polymerization was accomplished by water quenching at 4°C. Sections of approximately 1.5 µm thickness were prepared utilizing a HM 360 rotary microtome (Microm), dried on a heating plate and stored at 64°C overnight prior to further staining procedure. Afterwards a hematoxylin and eosin staining (HE), a periodic acid Schiff staining (PAS) and a periodic acid silver methenamine staining (PASM) was performed on tissue samples as indicated per particular in **Table 11** and in Table 12.

Table 11: Protocol for HE staining

Reagents	Incubation time
Mayer‘s Hemalum solution	20 min.
Running tap water	10 min.
1 % HCL-ethyl alcohol	10 sec.
Running tap water	10 min.
Heating plate	5 min.
Eosin-Phloxin	20 min.
Aqua bidest.	2 x 2 min.
Heating plate	5 min.
Xylene	2 min.

Table 12: Protocol for PAS staining

Reagents	Incubation time
Periodic acid	15 min.
Aqua bidest.	3 x 3 sec.
Schiffs reagent	30-60 min.
Running tap water	30 min.
Desiccation	
Mayer‘s Hemalum	35 min.
Running tap water	10 min.
1 % HCL-ethyl alcohol	1 sec.
Running tap water	10 min.
Desiccation	

Finally sections were covered with coverslips using Histofluid® mounting medium.

3.5.6.4.2. Determination of the mean glomerular volume

The mean glomerular volume was quantitatively stereologically determined in plastic embedded renal tissue from seven 4.5-month-old *INS*^{C94Y} transgenic pigs (3 male, 4 female) and seven age matched non-transgenic controls (3 male, 4 female), using an Olympus Visiomorph^{TM} image analysis system (Visiopharm, Hoersholm, Denmark). Technical details are per particulars given in 3.5.4. The mean glomerular volume was estimated from planimetric measurements of the mean glomerular profile areas as described previously (El-Aouni et al., 2006; Herbach et al., 2009; Weibel and Gomez, 1962). 144 ± 8 glomerular profiles per animal (range: 135–155) were systematically sampled and their contours were circled using the cursor of the analysis system as described in chapter 3.5.4. The mean glomerular volume was calculated as follows:

Equation 1 (Hirose et al., 1982; Wanke, 1996):

$$\mathbf{V_{(glom)(s)} = ß/k * a_{(glom)}^{1.5}}$$

$V_{(glom)(s)}$: stereologically estimated mean glomerular volume

ß: shape coefficient

k: size coefficient

a (glom): arithmetic mean of areas of glomerular profiles

The shape- and the size coefficients were taken from Wanke (1996). The results were corrected for embedding shrinkage by considering a shrinkage correction factor for plastic embedded porcine renal tissue in accordance with Wanke (1996) using the following equation:

Equation 2 (Wanke, 1996):

$$\mathbf{V_{(glom)} = V_{(glom)(s)}/f_s^3}$$

$V_{(glom)}$: stereologically estimated mean glomerular volume

f_s: linear tissue shrinkage correction factor for porcine kidney tissue embedded in GMA/MMA

Additionally the mean glomerular volume to body weight (BW) ratio ($V_{(glom)}$/BW (mm^3/kg)x 10^{-3}) was calculated.

3.5.6.4.3. Transmission electron microscopy of renal samples and determination of the true harmonic mean thickness (Th) of the glomerular basement membrane (GBM)

For the determination of the true harmonic mean thickness of the glomerular basement membrane (ThGBM), cubes of approximately 1 mm^3 of cortical kidney tissue obtained from three female *INS*^{C94Y} transgenic pigs and three female non-transgenic control pigs of 4.5 months of age were fixed by immersion in 6.25% glutaraldehyde in Soerensen´s phosphate buffer (pH 7.4) for 24 hours and routinely assayed for epon embedding (chapter 3.5.5). To localize patent glomerula within Epon embedded cortical kidney tissue, Toluidine blue/Safranin blue-stained semi-thin sections (0.5 µm) were evaluated. Ultra-thin sections (70 nm) were prepared and contrasted with uranyl-acetate and lead citrate considering the standard protocol as described in chapter 3.5.5. Transmission electronical micrographs of peripheral glomerular capillary loops were taken in a systematic pattern (five to six glomerular cross section profiles) at a final magnification of 8.000 fold according to Herbach et al. (2009). Photographs of standard cross-grating replicas at same magnifications served for calibration. The glomerular basement membrane (GBM) thickness was determined by the orthogonal intercept method (Dische, 1992; Hirose et al., 1982; Jensen et al., 1979; Ramage et al., 2002). Micrographs in the respective magnification were covered by a transparent 2.5 x 2.5 cm counting grid. A transparent logarithmic ruler according to the description of Ramage et al. (2002) was surveyed for measuring latitude of the glomerular basement membrane (GBM) by determination of the shortest distance from the endothelial cytoplasmic membrane to the outer lining of the lamina rara externa underneath the cytoplasmic membrane of the epithelial foot processes. An average number of 348 ± 67 intercepts per animal were measured (number of observations). The apparent harmonic mean thickness of the GBM and the true harmonic mean thickness of the GBM are calculated values:

Apparent mean thickness [*mm*] (I_h):

$$I_h = \sum N° / \sum (\text{Midpoints} * N°)$$

N°: Number of observations

Harmonic mean thickness [*nm*] (T_h):

$$T_h = 8/3\pi * 10^6 / M * I_h$$

8/3π: correction factor for potential oblique sectioning

M: Final print magnification

3.5.7. Preparation of the eye lenses for the documentation of diabetic cataract

Entire lenses were immediately removed from remaining ocular tissue of dissected whole eye globes. Isolated lenses were stored in 0.2 M PBS buffer pH 7.4 and evaluated with a Stemi SV11 stereomicroscope (Zeiss, Oberkochen) at 0.6 x zoom. Images were acquired by means of an AxioCam scanning camera (Zeiss, Oberkochen). Preparation of the eye lenses was performed in cooperation with Dr. Oliver Puk, Helmholtz Center Munich-German Research Center for Environmental Health, Institute of Developmental Genetics, Neuherberg, Research group of Prof. Dr. Jochen Graw.

3.5.8. Preparation of the nerves, histological procedure and single fiber teasing

Histopathological evaluation of nervous tissue of *INS*^{C94Y} transgenic pigs was performed in cooperation with Dr. Daniela Emrich, Institute of Veterinary Pathology at the Center for Clinical Veterinary Medicine, LMU Munich, Research group of Prof. Dr. Kaspar Matiasek. Morphology of nervous tissue of *INS*^{C94Y} transgenic pigs and age-matched non-transgenic littermates was investigated at 4.5 months of age. The oldest stage investigated for diabetes-associated nerve injury was the diabetic *INS*^{C94Y} transgenic founder boar at the age of approximately three years. One age-matched, non-transgenic boar served as wild-type control. A biopsy of the tibial nerve fascicle was obtained from its

origin at the fibular nerve during routine necropsy and immediately immersed in 2.5% glutaraldehyde in Soerensen´s phosphate buffer (pH 7.4) for 1 hours and routinely assayed for epon embedding (chapter 3.5.5.). Epon blocks were trimmed using a TM60 milling machine (Leica) and semi-thin sections (0.5 μm) were prepared using a Reichert-Jung Ultracut E microtome (Leica). Semi-thin sections were stained with azur II-methyleneblue-safranin. Sections were at first stained with azur II-methyleneblue staining solutions for 25 seconds at 55°C on a heating plate, rinsed with aqua bidest. and dried. Subsequently sections were incubated in Safranin O staining solution for another 15 seconds, rinsed with aqua bidest., dried and finally covered with coverslips using histofluid mounting medium.

In addition, single tibial nerve fascicles of about 1 cm length were subjected to single fiber teasing as previously described (Wieczorek, 2002). Nerve biopsies were likewise immersed in 2.5% glutaraldehyde in Soerensen´s phosphate buffer (pH 7.4) for 1 hours and subsequently fixed in 2% osmium tetroxide fixation solution for two hours at 4°C. Following a washing step in Soerensen's phosphate buffer stowed with saccharose (0.2 mol/l), fascicles were incubated in glycerol-anhydrous over night and single fiber teasing was performed. Teased fibers were placed on microscope slides, finally covered with coverslips and microscopically evaluated.

3.6. Western blot analysis of isolated pancreatic islets

In order to confirm quantitative-stereological analyzes and electron microscopy of pancreatic β-cells of *INS*^{C94Y} transgenic and non-transgenic pigs of particular age groups, pancreatic islets of one transgenic and one non-transgenic neonatal piglet at 8 days of age were isolated and subjected to Western blot analysis with regard to the abundance of the endoplasmic reticulum stress markers GADD 153/CHOP-10 (Growth arrest and DNA damage 153/ C/EBP-homologous protein 10), PeIF2α (phosphorylated eukaryotic translation initiation factor 2α) and BiP/Grp78 (Binding Ig protein / Glucose regulated protein 78).

3.6.1. Isolation of neonatal porcine islets of Langerhans

Isolation of porcine neonatal pancreatic islets was carried out by Dr. Lelia Wolf-van Bürck, Diabetes Zentrum, Medizinische Klinik Campus Innenstadt, LMU Munich, Research Group of Prof. Dr. Jochen Seißler.

After explantation of pancreata derived from 8-day-old *INS*^{C94Y} transgenic piglets and age-matched non-transgenic littermates (n=3 per group), neonatal islet-like cell clusters were isolated according to Korbutt et al. (1996). Following the isolation process, isolated islet cell clusters (ICC) were cultured in RPMI stowed with 2% human serum albumin, 1% antibiotic-antimycotic, 10 mmol/l nicotinamide as well as 20 nmol/l exendine-4 for 6 days at 37°C. Afterwards, islet-like cell clusters were hand-picked under a stereomicroscope, transferred into a 1.5 ml reaction tube (500 ICCs per sample) and stored at -80°C. Prior to further use, islet cell clusters were suspended in 50 µl protein extraction buffer working solution followed by sonication (7 strokes/1 second) using a Branson sonifier cell disrupter B15 (Branson Ultrasonic Corporation, USA). In order to destroy cell membrane integrity islet sonicates were frozen at -80°C for at least overnight. The next day, sonicated islet samples were carefully thawed on ice followed by a centrifugation step (5 minutes, 5.000 rpm, 4°C). Supernatant was carefully separated, immediately assayed or stored at -20°C.

3.6.2. Determination of islet protein content

To determine the protein content of sonicated islet samples the Bradford method was applied. Previously, a protein standard was prepared referring to the current Bradford reagent by dissolving bovine serum albumin (BSA) in aqua bidest. to a concentration of 5 mg/ml and a spectrophotometrically determined extinction of 0.33 at a wavelength of 595 nm. From the initial solution, standard concentrations of 100, 87.5, 75, 62.2, 50, 37.5, 25, 12.5, 0 (blank) µg/ml were produced in a final volume of 100 µl each, and 1000 µl Bradford reagent were added respectively. Extinction was measured at a wavelength of 595 nm using a Beckmann DU-640 spectrophotometer (Beckman Coulter GmbH). The standard curve was created from extinction values as x-axis and protein concentrations in µg/ml as y-values. Then, islet samples to be analyzed were diluted 1:100 and 1:50 in aqua bidest., absorbance was measured spectrophotometrically at a wavelength of 595 nm and protein concentration of islet lysates was determined using previously established standard curve.

3.6.3. Sodium dodecyl sulfate polyacrylamide gel electrophoresis (SDS-PAGE) and Western blot analysis of isolated islets

Islet sonicates were at first separated by electrophoresis on a 12% SDS polyacrylamide gel as described in 3.5.6.1. Previously, islet samples were diluted with protein extraction buffer working solution, 5 x Laemmli buffer and 5% 2-mercaptoethanol to a final protein concentration of 15 µg/25 µl total sample volume. Denaturation was achieved at 95° C for five minutes on a heating block, chilling on ice for two minutes and final centrifugation of the lid condensate. A PageRuler™ Prestained Protein Ladder and an unstained protein molecular weight marker (Thermo Fisher Scientific) served as protein molecular weight markers.

3.6.4. Western blot analysis

After completion of electrophoresis, the proteins were transferred from SDS-polyacrylamide gel to a protein-binding Immobilon®-P nitrocellulose transfer membrane by means of electrophoresis using a Trans Blot® SD Semi-Dry Transfer cell (BioRad). Previously nitrocellulose transfer membranes were activated by pivoting in 100% methanol for ten minutes followed by immersion in 1 x transfer buffer for 30 minutes on a tumbling shaker. SDS-gel was placed on the moistened nitrocellulose transfer membrane between two layers of extra thick absorbent paper, soaked with 1 x transfer buffer. Proteins were transferred to the membrane with 1 mA/cm^2 (15 V) for one hour. To confirm blotting success, membranes were reversibly stained with Ponceau S solution and washed twice in aqua bidest. until background has cleared. Subsequently membranes were left drying for approximately 30 minutes and were refrigerated at 4°C.

3.6.5. Western immunoblot analyzes

Detection of specific proteins was achieved by immunoblot analyzes via antigen-antibody coupling. Washing and incubation procedures were accomplished under consequent agitation of the membranes in a hybridisation oven at room temperature unless indicated otherwise. The membrane was activated by pivoting in 5 ml 100% methanol and washed afterwards three times for five minutes in an adjustable volume of TBS-T (0.1%). To avoid non-specific binding of respective antibodies, membrane was blocked in 5% TBS-T-w/v nonfat dry milk for one hour. Following another washing step in TBS-T (0.1%) (1 x 15minutes, 2 x 5 minutes), primary antibody was diluted to appropriate

concentration in appropriate buffer and incubated at 4°C overnight. The next day, membrane was washed repeatedly (1 x 15 minutes, 2 x 5 minutes) and subsequently incubated with the corresponding horseradish peroxidase-conjugated secondary antibody in suitable concentration for one hour. After washing thrice in TBS-T (0.1%) as described above, immunoreactivity was detected using Hyperfilm™ ECL chemiluminescense film and ECL™ detection reagent (Amersham™, GE Healthcare Limited) according to manufacturer´s instructions in a darkroom. After suitable exposition time, immunereactivity was visualized using an Optimax X-ray Film processor 1170-1-0000 (PROTEC, Oberstenfeld). After signal detection, ECL™ detection reagent was removed completely by washing in TBS-T (0.1%) and either stripped for further processing or meanwhile stored at 4°C. β-actin was used as loading control. Primary and secondary antibodies with appropriate concentrations and dilution buffers are listed in Table 13. Optical density was determined using the ImageJ 1.410 image processing software and was divided by the optical density of β-actin.

3.6.6. Stripping of the membrane

To reuse the membrane for additional immunoblots, linked antibodies were eluted. Therefore, membranes were incubated in 25 ml elution buffer for 30 minutes at 70°C, while agitating in a hybridisation oven. Subsequently membranes were washed twice in aqua bidest. at room temperature and additionally twice in TBS-T (0.1%). Finally membranes were transferred into a new 50 ml tube and subjected to further antibody incubation.

3.7. Statistics

All data are presented as means ± standard error of means (SEM) or means ± standard deviations (SD) as indicated. Longitudinal data of blood glucose levels and body weight gain were statistically evaluated by analysis of variance (PROC MIXED; SAS 8.2), taking the fixed effects of group (transgenic vs. control) and age as well as random effects of the individual animal into account. For other parameters the two-tailed, unpaired Mann-Whitney-U test in combination with an exact test procedure (SPSS 21.0) or two-tailed, unpaired Student's t-test was used unless indicated otherwise. *P* values less than 0.05 were considered significant.

Table 13: Reagents for Western immunoblot analyzes

Antigen	Primary antibody	Concentrations/Buffers	Secondary antibody	Concentrations/Buffers
GADD153	Rabbit anti-mouse full-length GADD153, polyclonal	**1:500** in 5% TBS-T-w/v nonfat dry milk	Goat anti-rabbit IgG, HRP-linked	**1:2000** in 5% TBS-T-w/v nonfat dry milk
PeIF2α	Rabbit anti-human eIF2α, monoclonal	**1:1000** in 5% TBS-T-w/v nonfat dry milk	Goat anti-rabbit IgG, HRP-linked	**1:2000** in 5% TBS-T-w/v nonfat dry milk
BiP	Rabbit anti-human BiP, polyclonal	**1:1000** in 5% TBS-T-BSA	Goat anti-rabbit IgG, HRP-linked	**1:2000** in 5% TBS-T-w/v nonfat dry milk
β-Actin	Mouse anti-actin, clone C monoclonal	**1:5000** in 5% TBS-T-w/v nonfat dry milk	Goat anti-mouse IgG, HRP-linked	**1:5000** in 5% TBS-T-w/v nonfat dry milk

IV. RESULTS

1. Generation of *INS*^{C94Y} transgenic pigs

Transgenic founder pigs displaying *INS*^{C94Y} transgene expression were established using somatic cell nuclear transfer according to Kurome et al. (2006). The *INS*^{C94Y} construct was constituted of the 2.1 kb sequence of the porcine insulin gene promoter for β-cell-specific expression and the 1.0 kb coding region of the porcine insulin gene (*INS*) including a G→A tranversion at nucleotide position 340. A loxP-flanked neomycin resistance cassette (neo^{R}) was linked for positive selection of transgenic clones (Figure 6 A). This targeted mutation results in an exchange from cysteine to tyrosine (Cys → Tyr) at position 94 of the porcine proinsulin polypeptide (Figure 6 B) and therefore interferes with the insulin secretory pathway (Stoy et al., 2007).

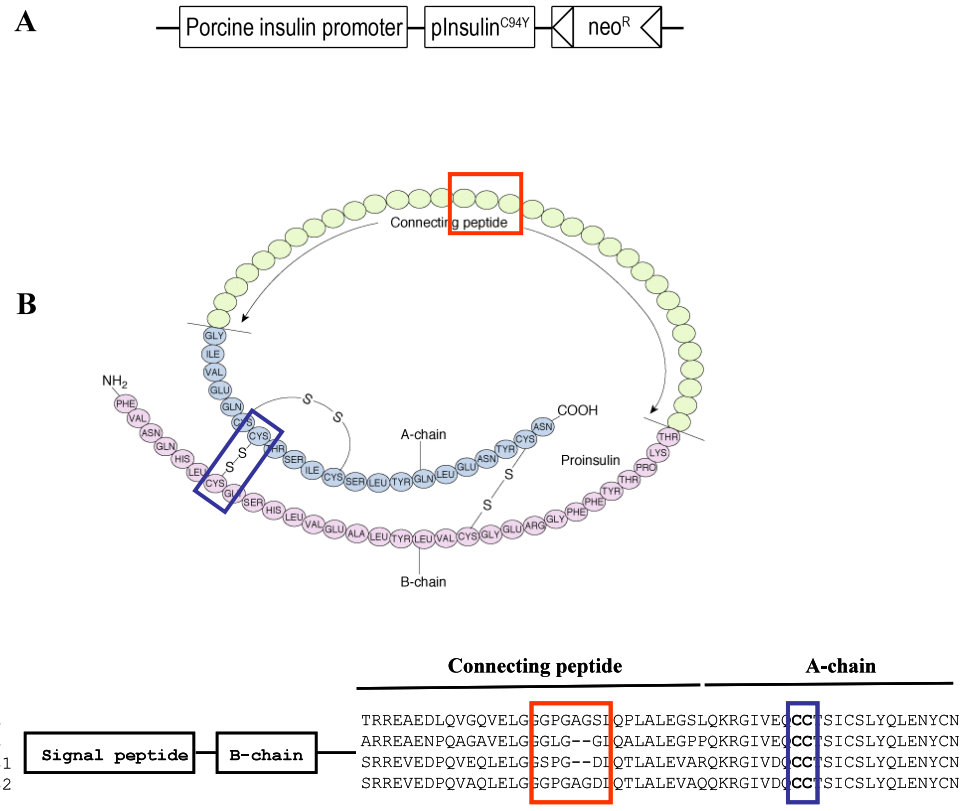

Figure 6: *INS*^{C94Y} construct and alignment of porcine insulin polypeptide

Schematic illustration of the *INS*^{C94Y} genetic construct carrying a fragment of the porcine insulin gene (pInsulin^{C94Y}) under the control of the porcine insulin gene

promoter and a neomycin resistance cassette (neo^R) for positive selection (published in Renner et al. 2012) **(A)**. Amino acid sequence of the human proinsulin molecule with targeted INS^{C96Y} mutation and consequent amino acid shift (Cys→Tyr) indicated in blue. The corresponding porcine *INS* mutation is located at position 94 of the proinsulin polypeptide due to the gap of two amino acid residues in the C-peptide sequence (indicated in red) **(B)**; comparative *INS* alignment was gathered and modified from (http://www.ncbi.nlm.nih.gov/protein (AAA59179.1, AAL69550.1, AAI45869, AAI45555.1).

A total of 562 embryos derived from INS^{C94Y} nucleofected cell clones were transferred laparoscopically to five cycle synchronized recipient gilts. Two pregnancies went to term and provided seven male piglets. Genotyping PCR on genomic DNA isolated from ear punches determined seven transgenic founder animals. Detailed outcomes of cloning are summarized in Table 14.

Table 14: Results of nuclear transfer experiments using INS^{C94Y} transfected nuclear donor cells

Recipients	N° of transferred embryos	N° of successful embryos	Pregnancy	Result
Sow 1	83		-	
Sow 2	90		-	
Sow 3	152	152	+	Abortion
Sow 4	146	146	+	4 piglets (#9725-9728)
Sow 5	91	91	+	3 piglets (#9745-9747)
Total	**562**	**237**	**2**	
Efficiency	**~1.3 %**	**~3%**		

Founder boar 9747 exhibited growth retardation as well as elevated fasting blood glucose levels at the age of 85 days, further increasing over time and was therefore chosen as suitable founder animal for INS^{C94Y} breeding (Figure 7). The other six founders remained normoglycemic within the observation period of seven months (Figure 7). Non-diabetic INS^{C94Y} transgenic founder boars 9727,

9728, 9745 and 9746 exhibited undisturbed intravenous glucose tolerance (IVGT) at the age of seven months, indicated by adequate insulin release compared to intravenous glucose application and commensurate decline of blood glucose levels (Figure 8 A/B). Founder boars 9725 and 9726 showed a delayed and reduced glucose-stimulated insulin secretion and lowering of blood glucose levels was consequently decelerated in comparison with two age-matched non-transgenic control pigs (Figure 8 A/B).

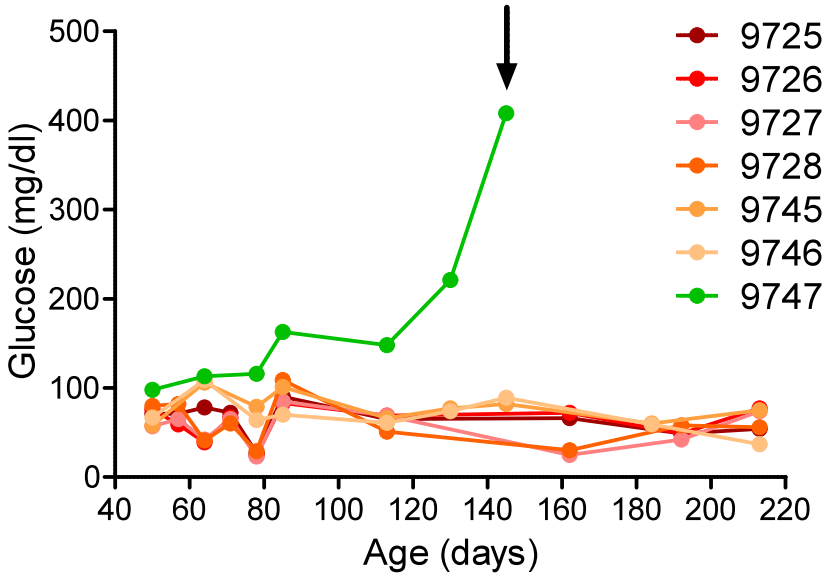

Figure 7: Fasting blood glucose concentrations of *INS*^{C94Y} transgenic founder boars

Transgenic founder boar 9747 exhibited hyperglycemia at the age of 85 days, whereas blood glucose levels of the other six founder boars remained within the reference range (70-115 mg/dl depending on the lab); Start of the insulin therapy is indicated with the black arrow; published by Renner et al. (2012); "Copyright 2012 American Diabetes Association From Diabetes®, Vol. 61, 2012 Reprinted with permission from the *American Diabetes Association*."

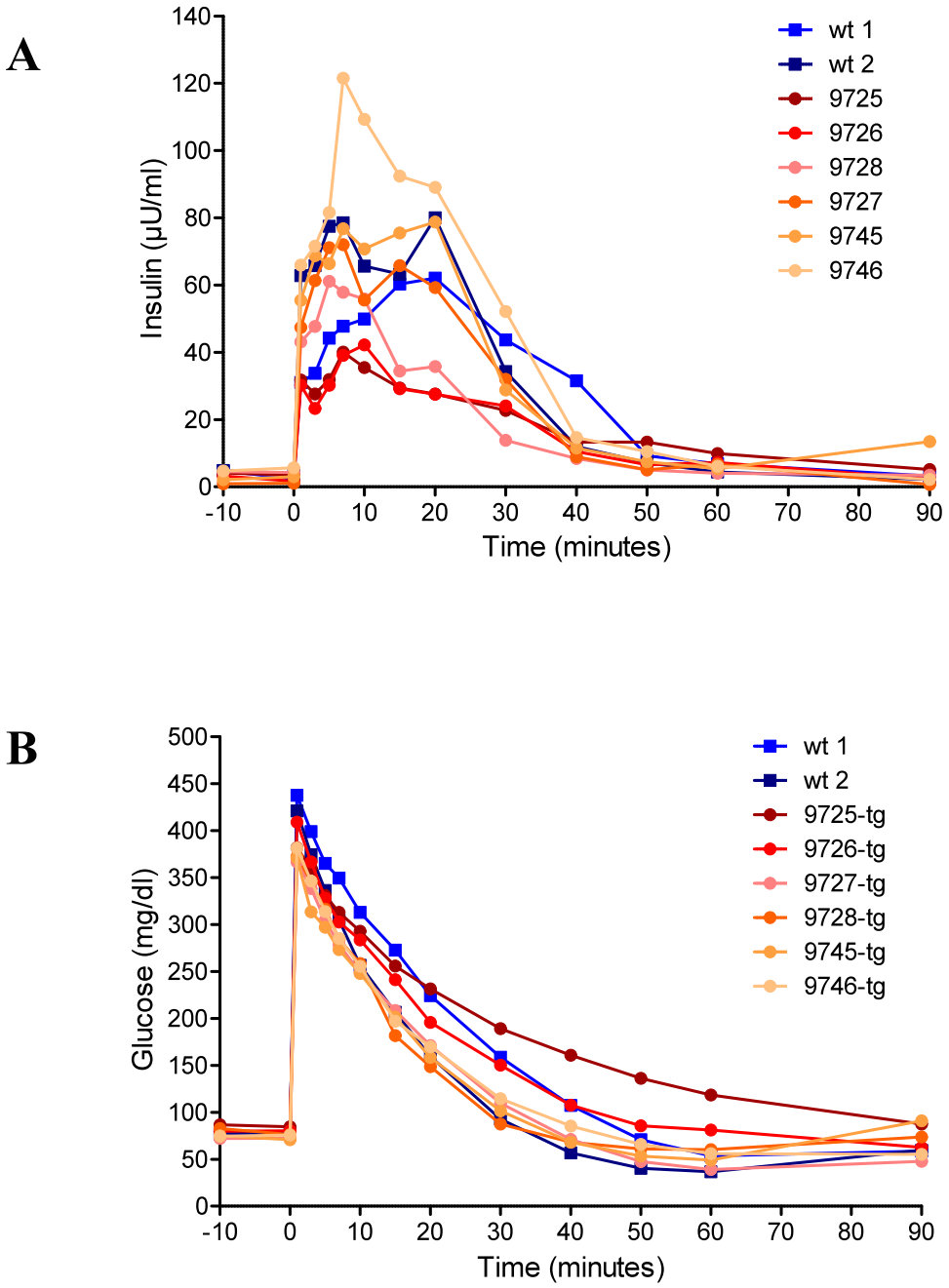

Figure 8: Intravenous glucose tolerance of *INS*^{C94Y} transgenic founder boars

IVGT of non-diabetic *INS*^{C94Y} transgenic founders (tg) 9727, 9728, 9745 and 9746 was unaltered in an intravenous glucose tolerance test at 7 months of age. Non-diabetic *INS*^{C94Y} transgenic founders (tg) 9725 and 9726 showed moderately impaired IVGT compared to age-matched wild-type control pigs (wt); **(A)** plasma insulin levels**; (B)** plasma glucose levels.

To test germ-line transmission of the *INS*^{C94Y} construct, the diabetic founder boar 9747 was mated to non-transgenic German Landrace-Swabian-Hall crossbred sows. He transmitted the *INS*^{C94Y} transgene to half of the offspring adhering to mendelian rules of inheritance. A transgenic line was established by conventional breeding. The efforts of *INS*^{C94Y} transgenic pig breeding are in detail listed below:

Table 15: Inheritance of the *INS*^{C94Y} transgene

			Offspring				
Generation	Transgenic sire	ID number of offspring	m (wt)	m (tg)	f (wt)	f (tg)	Total (tg) [%]
F1	#9747 (F0)	#9899 - 9907	0	2	4	3	55.56
F1	#9747 (F0)	#9914 - 9921	1	3	2	2	62.5
F2	#9914 (F1)	#1112 - 1119	3	2	1	3	55.56
F2	#9914 (F1)	#1334 - 1343	2	4	2	2	60
F2	#9914 (F1)	#1602 - 1611	1	2	4	3	50

2. Genotyping of *INS*^{C94Y} transgenic pigs by PCR and Southern blot analyzes

The *INS*^{C94Y} transgenic offspring were identified by transgene-specific PCR on genomic DNA isolated from ear punches of neonatal piglets. A band of 500 bp could be detected, if the *INS*^{C94Y} transgene has been integrated into the genome, while non-transgenic littermate control pigs did not show any signal (Figure 9 A). Additionally a 330 bp fragment was amplified using *ACTB* specific primers and served as control for DNA integrity (Figure 9 B).

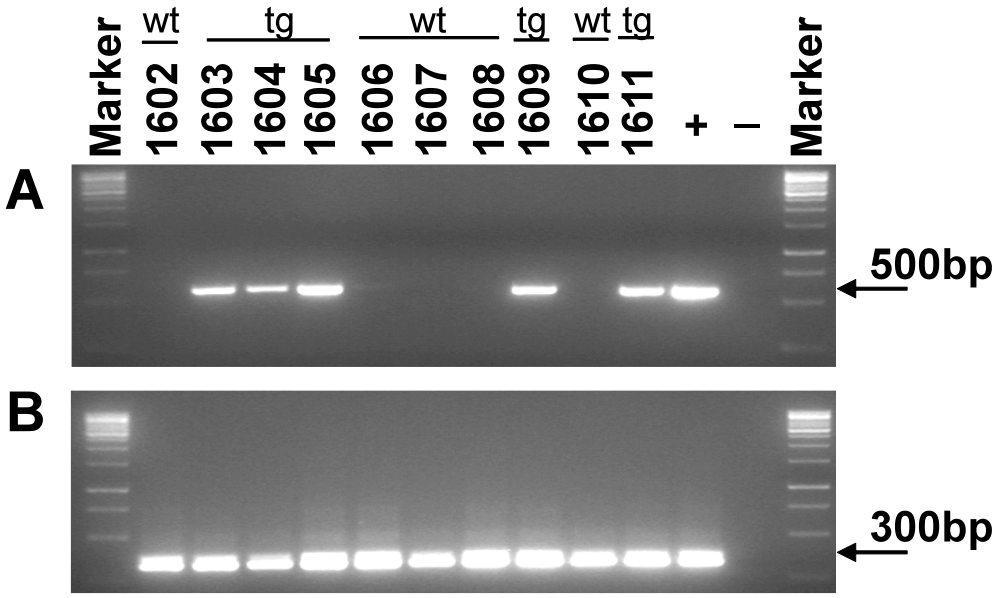

Figure 9: Identification of *INS*^{C94Y} transgenic pigs and non-transgenic littermates by PCR analysis

(A) Transgene-specific PCR to detect the neomycin resistance cassette (neo^{R}) linked to the *INS*^{C94Y} expression vector; **(B)** *ACTB* specific PCR to control genomic DNA integrity; **(A/B)** wt: non-transgenic littermates; tg: *INS*^{C94Y} transgenic pigs; Marker: Gene Ruler^{TM} 1kb DNA ladder with visible marker-bands indicating the size of double-stranded DNA of 10.000 to 250 bp from top to bottom; +: genomic DNA of a previously genotyped *INS*^{C94Y} transgenic pig as positive control; -: aqua bidest. as non-template control.

To visualize transgene integration pattern and to determine numbers of integration sites in the genome, Southern blot analysis was conducted on *Bam*H1 digested genomic DNA using a transgene-specific α-[^{32}P]-dCTP labeled probe specific for the neomycin resistance cassette. All seven *INS*^{C94Y} transgenic founder boars revealed a single integration site of the *INS*^{C94Y} transgene with different pattern of transgene integration. *INS*^{C94Y} transgenic offspring of the diabetic founder 9747 showed an identical trangene integration pattern without segregation, confirming germ line transmission of the transgene and constituting a single integration site in the genome (Figure 10).

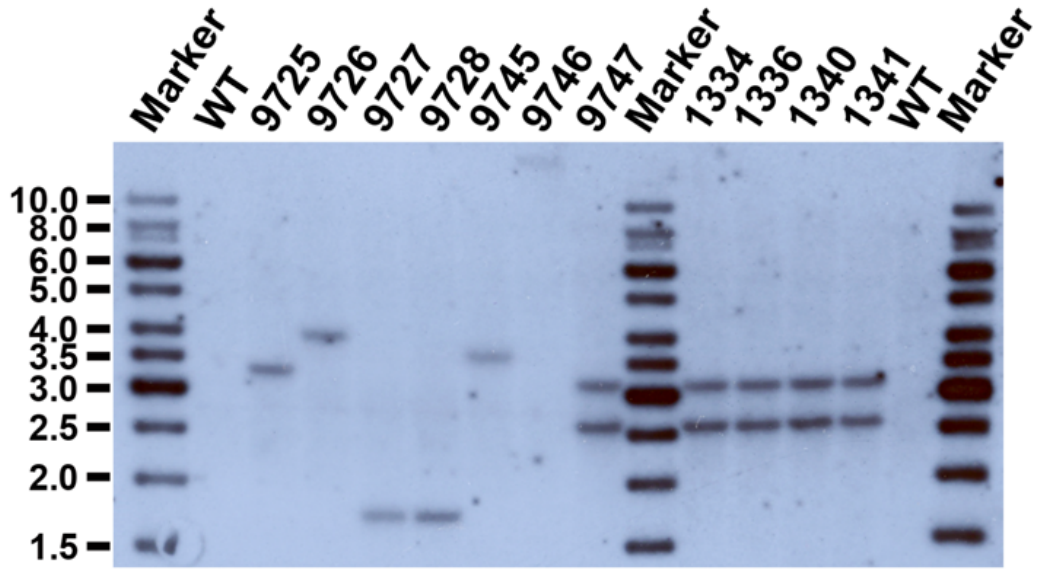

Figure 10: Southern blot analysis of *INS*^{C94Y} transgenic founder boars and *INS*^{C94Y} transgenic offspring (F2-generation)

Southern blot analysis of *Bam*H1 digested genomic DNA derived from *INS*^{C94Y} transgenic founder boars (9725, 9726, 9727, 9728, 9745, 9746, 9747) and *INS*^{C94Y} transgenic offspring of the diabetic founder 9747 (1334, 1336, 1340, 1341) argues for a single integration site for each founder. Transgenic offspring of founder 9747 do not show segregation of transgene copies confirming a single integration site; WT: non-transgenic control pig; Marker: Gene Ruler^{TM} 1kb DNA ladder with visible marker-bands indicating the size of double-stranded DNA of 10.000 to 250 bp from top to bottom; Data provided by Dr. Andrea Bähr, Institute of Molecular Animal Breeding and Biotechnology, LMU Munich; published by Renner et al. (2012); "Copyright 2012 American Diabetes Association From

Diabetes®, Vol. 61, 2012 Reprinted with permission from the *American Diabetes Association*."

3. Expression analysis of the *INS*^{C94Y} transgene in the pancreas

To demonstrate expression of the *INS*^{C94Y} transgene, total RNA was extracted from pancreatic tissue of *INS*^{C94Y} transgenic founder boars as well as of three *INS*^{C94Y} transgenic F1-offspring of founder boar 9747 and separated by agarose gel electrophoresis. Discrete 28S and 18S ribosomal bands in the absence of considerable RNA degradation argued for adequate RNA quality (Figure 11 A). RNA samples were reverse transcribed and cDNA was assayed by PCR using insulin-specific primers. Additionally *ACTB* specific PCR was achieved using the same templates to verify cDNA integrity. Separation by agarose gel electrophoresis revealed sharp bands of 192 bp (Insulin) or 231 bp (ACTB) respectively with identical intensity. Minus RT reactions obtained no signals demonstrating complete DNaseI digest of total RNA (Figure 11 B). The ratio of mutant *INS*^{C94Y} and endogenous *INS* cDNA amplicons was determined by next generation sequencing. The ratio of *INS*^{C94Y} to endogenous *INS* transcripts in pancreas samples of the diabetic *INS*^{C94Y} transgenic founder boar 9747 was 0.75 and at least five-fold higher than in the six normoglycemic transgenic founder boars (0.06 ± 0.02; n=6). *INS*^{C94Y} transgenic F1-offspring exhibited a similar *INS*^{C94Y}: *INS* ratio compared with their diabetic sire (0.78 ± 0.05; n=3) indicating dose-dependent diabetogenic impact of *INS*^{C94Y} expression.

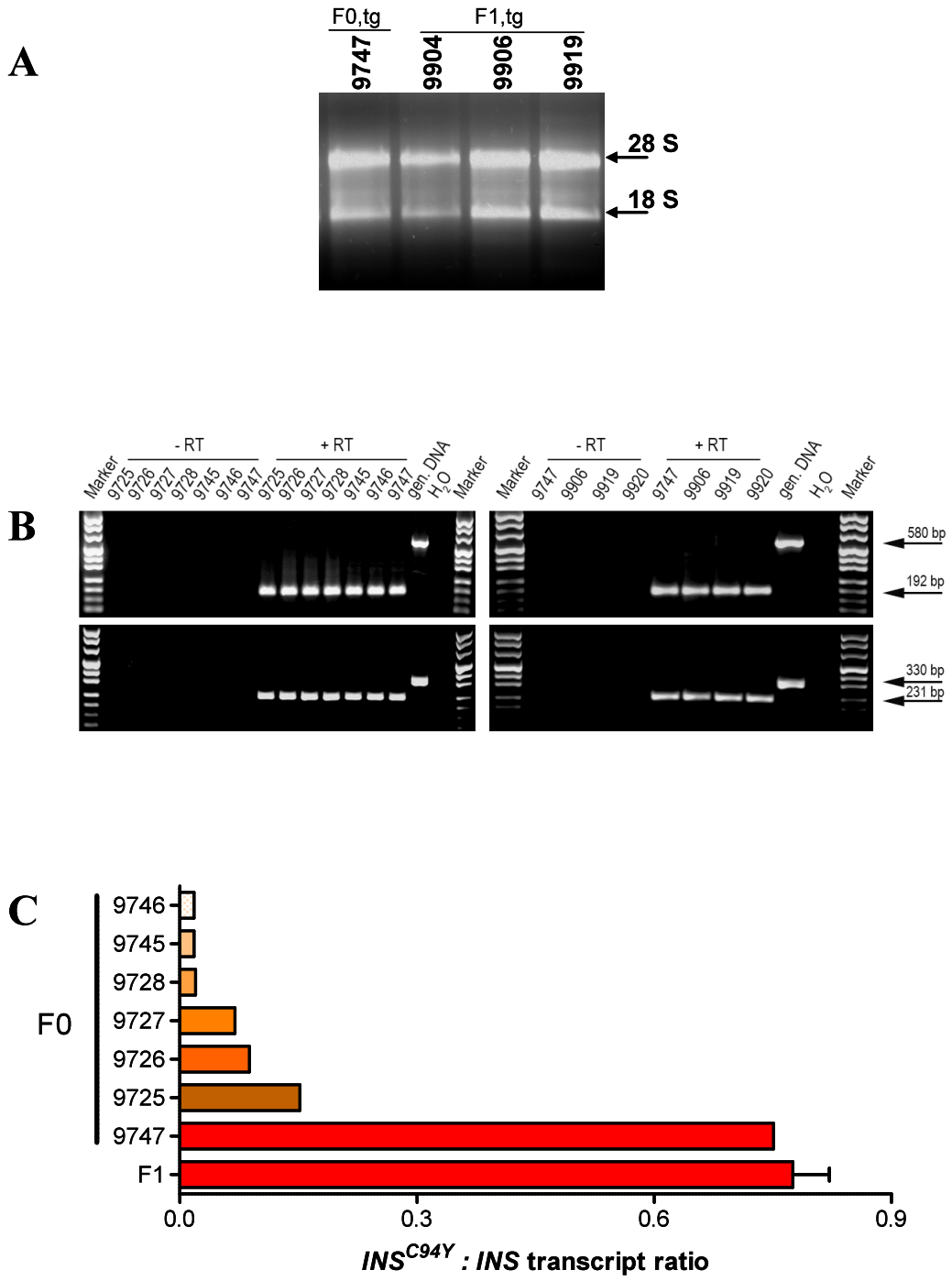

Figure 11: Expression analysis on RNA level from pancreatic tissue of *INS*^{C94Y} transgenic founder boars and transgenic F1-offspring

(A) Total RNA of pancreatic tissue of *INS*^{C94Y} transgenic founder boar (9747) and transgenic F1-offspring (n=3; 9904, 9906, 9919), separated by agarose gel electrophoresis, revealed adaequate RNA quality indicated by defined 28S and discrete 18S ribosomal RNA bands being half as bright as the 28S ribosomal band; tg: *INS*^{C94Y} transgenic pigs; wt: non-transgenic littermate control pigs. **(B)** Insulin and *ACTB* specific PCR of pancreatic tissue of *INS*^{C94Y} transgenic founder

boars (left panel) and diabetic founder 9747 and his offspring (right panel); M: pUC Mix molecular weight marker with visible marker-bands indicating the size of double-stranded DNA of 1118 to 110 bp from top to bottom; gDNA: genomic DNA; H_2O: aqua bidest. as non-template control; -RT: minus RT; +RT: plus RT; (published in Renner et al. 2012; "Copyright 2012 American Diabetes Association From Diabetes®, Vol. 61, 2012 Reprinted with permission from the *American Diabetes Association*."). **(C)** The ratio of mutant INS^{C94Y} to endogenous *INS* transcripts was determined by next generation sequencing of cDNA amplicons derived from RT-PCR. INS^{C94Y} transgenic founder 9747 and his diabetic offspring (F1) exhibited similar INS^{C94Y} expression levels but at least five-fold higher expression compared to normoglycemic founder boars (9725, 9726, 9727, 9728, 9745 and 9746). Data indicated as means ± SEM; published in parts by Renner et al. (2012); "Copyright 2012 American Diabetes Association From Diabetes®, Vol. 61, 2012 Reprinted with permission from the *American Diabetes Association*."

4. Physiological characteristics of *INS*^{C94Y} transgenic pigs

4.1. Body weight gain

Body weight of *INS*^{C94Y} transgenic pigs and non-transgenic littermate control pigs was determined on a regular basis starting at birth to evaluate the impact of *INS*^{C94Y} expression on weight gain. *INS*^{C94Y} transgenic pigs grew comparably to non-transgenic littermates up to 8 weeks of age but then exhibited decelerated growth rates (Figure 12 A) resulting in a 41% reduced body weight at the age of 4.5 months (Figure 12 B).

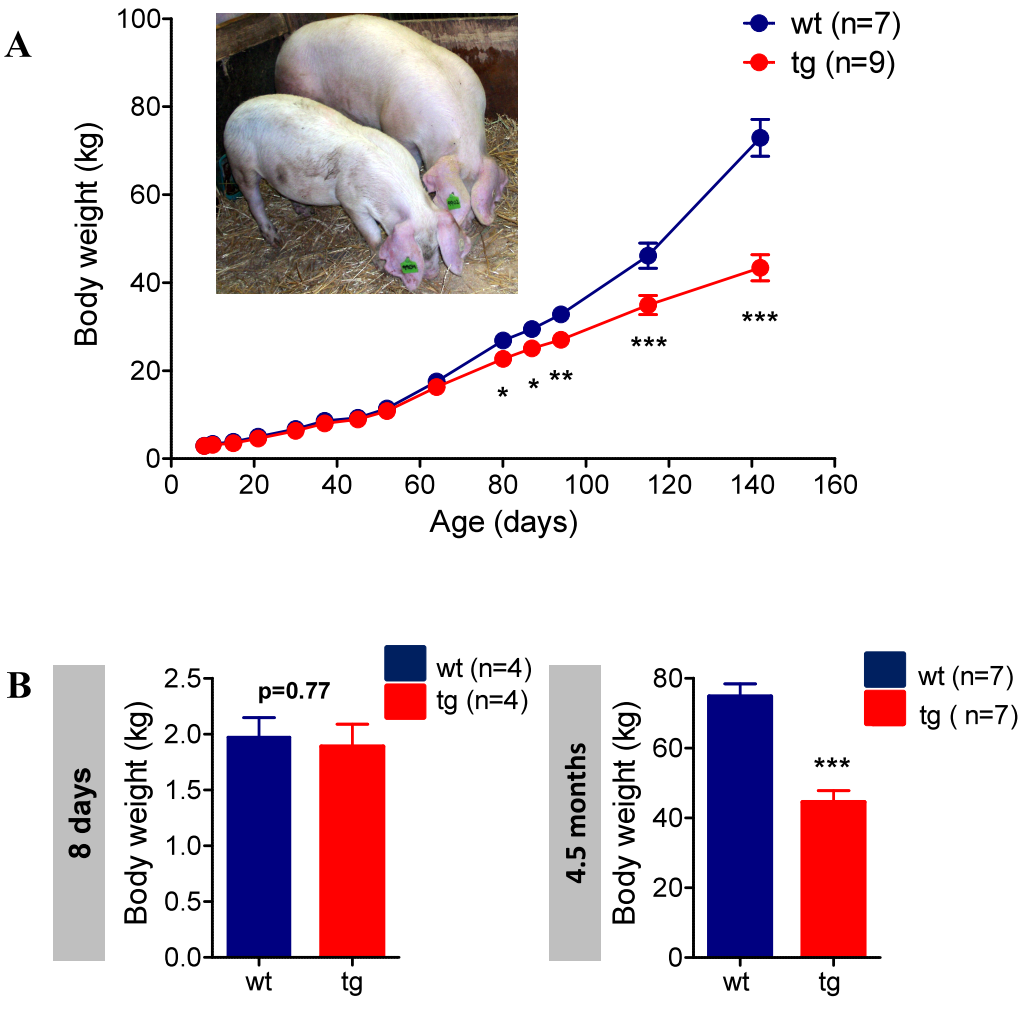

Figure 12: Growth retardation in *INS*^{C94Y} transgenic pigs

(A) Body weight gain of *INS*^{C94Y} transgenic pigs (tg) was significantly reduced compared to littermate controls (wt) within the observation period of 142 days. **(B)** Body weight was unaltered at the age of 8 days (left panel) but was

significantly reduced by 41% in 4.5-month-old *INS*^{C94Y} transgenic pigs compared to non-transgenic littermates (right panel). Data indicated as means ± SEM; *: p<0.05; **: p<0.01; ***: p<0.001 vs. controls; n: number of animals investigated; published in parts by Renner et al. (2012); "Copyright 2012 American Diabetes Association From Diabetes®, Vol. 61, 2012 Reprinted with permission from the *American Diabetes Association*."

4.2. Blood glucose control and insulin secretion

4.2.1. Blood glucose concentration

In order to clarify effects of *INS*^{C94Y} transgene expression on glucose homeostasis, random blood glucose levels were determined at short intervals. After weaning fasting blood glucose levels were measured regularly up to the age of 142 days. Transgenic F1- and F2-offspring exhibited significantly elevated random blood glucose levels within 24 hours after birth compared to wild-type littermates (193.8 ± 11.9 vs. 146 ± 9 mg/dl; p<0.05). Fasting blood glucose levels were increasingly higher in *INS*^{C94Y} transgenic pigs compared to non-transgenic littermates, reaching 415 ± 28 versus 84 ± 9 mg/dl (p<0.001) at 115 days of age (Figure 13).

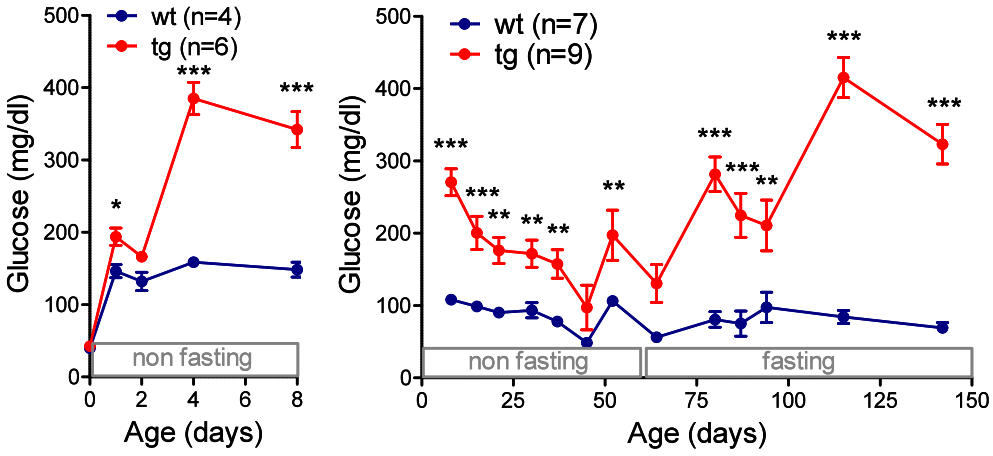

Figure 13: Blood glucose control in *INS*^{C94Y} transgenic and wild-type pigs

INS^{C94Y} transgenic pigs (tg) developed significantly elevated random blood glucose levels within 24 hours after birth in comparison to non-transgenic

littermate controls (wt) (left graph). Fasting blood glucose concentrations were significantly elevated compared to wild-type control pigs throughout the observation period. Data indicated as means ± SEM; *: $p<0.05$; **: $p<0.01$; ***: $p<0.001$ vs. controls; n: number of animals investigated; published by Renner et al. (2012); "Copyright 2012 American Diabetes Association From Diabetes®, Vol. 61, 2012 Reprinted with permission from the *American Diabetes Association*."

4.2.2. Continuous blood glucose monitoring

To preserve an undisturbed general state of health for long-time survival of *INS*^{C94Y} transgenic pigs, an insulin treatment regimen was established starting at the age of 4.5 months. A combination of long-acting insulin (Lantus®) and short-acting insulin (NovoRapid®) was administered subcutaneously once daily in a dosage of 0.5 – 1 unit per kg body weight appropriate to respective blood glucose concentrations. Diabetic *INS*^{C94Y} transgenic pigs were rescued from growth retardation and matured almost normally. Diabetes-associated fertility disorder was prevented over a considerable period. For the ease of verifying successful insulin regimen, glucose control of an insulin-treated *INS*^{C94Y} transgenic pig was evaluated continuously using the Guardian® REAL-Time continuous glucose monitoring device and was compared to an untreated age-matched control pig. Interstitial glucose concentrations were profiled over a period of 42 hours and an average blood glucose concentration of 123.2 ± 41.9 mg/dl (SD) was determined in the insulin-treated pig versus 92 ± 11.9 mg/dl (SD) in the control pig. The amplitude spectrum of interstitial glucose levels of the insulin-treated *INS*^{C94Y} transgenic pig ranged between 40 and 198 mg/dl (Figure 14 A) and was thus more heterogenous than in the control pig (98 to 114 mg/dl) (Figure 14 B), but nevertheless within a fairly controlled range.

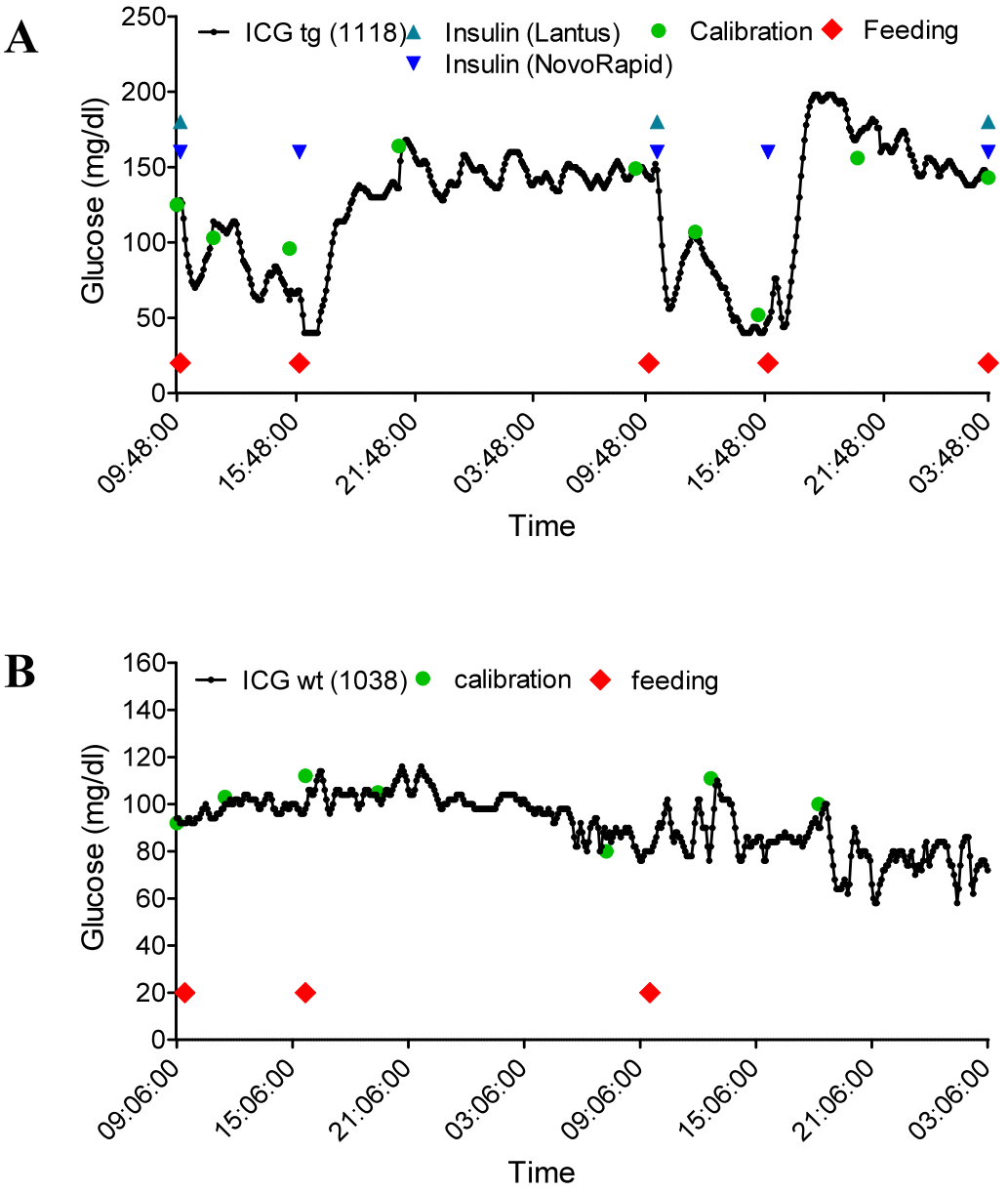

Figure 14: Continuous 42-hour glucose monitoring profile of an *INS*^{C94Y} transgenic pig under insulin treatment and an untreated wild-type littermate

Interstitial glucose levels of an insulin-treated *INS*^{C94Y} transgenic pig (tg) **(A)** and a non-transgenic age-matched control pig (wt) **(B)** were evaluated over 42 hours to control the insulin treatment protocol. The *INS*^{C94Y} transgenic pig was treated with a combination of long-acting (Lantus®) and short-acting (NovoRapid®) insulin injected subcutaneously at a dose of 0.5 to 1 unit/kg BW; ICG: interstitial glucose concentration; modified according to Renner et al. (2012); "Copyright 2012 American Diabetes Association From Diabetes®, Vol. 61, 2012 Reprinted with permission from the *American Diabetes Association*."

4.2.3. Insulin levels

Additionally, plasma insulin levels were determined in 8-day-old as well as in 4.5-month-old *INS*^{C94Y} transgenic pigs (tg) and their non-transgenic littermates (wt) by a commercial radioimmunoassay. Despite early significant hyperglycemia (Figure 13) basal plasma insulin levels of randomly fed 8-day-old *INS*^{C94Y} transgenic pigs (n=6) were only slightly reduced (7 ± 1 vs. 10 ± 4 µU/ml; n=4; p=0.76) compared to non-transgenic littermates (n=4) (Figure 15). In contrast, 4.5-month-old *INS*^{C94Y} transgenic pigs (n=6) revealed significantly reduced fasting plasma insulin levels (2 ± 0.42 vs. 5.1 ± 0.77 µU/ml; p<0.01) compared to non-transgenic littermate control pigs (n=6) (Figure 15).

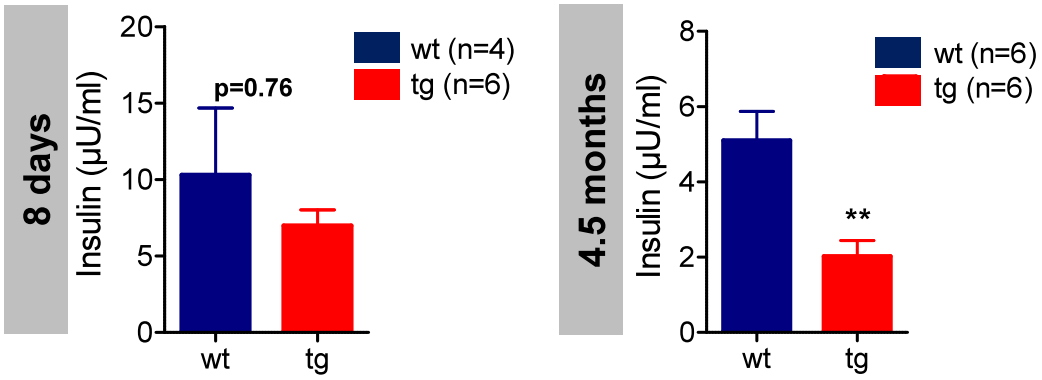

Figure 15: Basal and fasting insulin levels of 8-day-old and 4.5-month-old *INS*^{C94Y} transgenic and age-matched wild-type littermates

Basal plasma insulin levels of 8-day-old *INS*^{C94Y} transgenic pigs (tg) were nearly unaltered in comparison to wild-type littermates (wt) (left panel), while 4.5-month-old *INS*^{C94Y} transgenic pigs (tg) revealed significantly reduced fasting plasma insulin levels compared to non-transgenic littermates (wt) (right panel). Data indicated as means ± SEM; **: p<0.01 vs. control; n: number of animals investigated; published by Renner et al. (2012); "Copyright 2012 American Diabetes Association From Diabetes®, Vol. 61, 2012 Reprinted with permission from the *American Diabetes Association*."

4.2.4. Homeostasis model assessment of β-cell function (HOMA - B) and insulin resistance (HOMA - IR)

The homeostasis model assessment of β-cell function (HOMA - B) and of insulin resistance (HOMA - IR) were calculated according to Matthews et al. (1985) by means of fasting blood glucose and plasma insulin levels determined in 4.5-month-old *INS*^{C94Y} transgenic pigs (n=6) in comparison with their wild-type littermates (n=6). HOMA - B indices were significantly reduced in 4.5-month-old *INS*^{C94Y} transgenic pigs indicating disturbed glucose-stimulated baseline insulin secretion (1.8 ± 0.39 vs. 47.2 ± 10.45; p< 0.01) (Figure 16). HOMA - IR indices were significantly elevated in *INS*^{C94Y} transgenic pigs at 4.5 months of age (2.4 ± 0.48 vs. 1.2 ± 0.24; p<0.05) suggestive of insulin resistance (Figure 16).

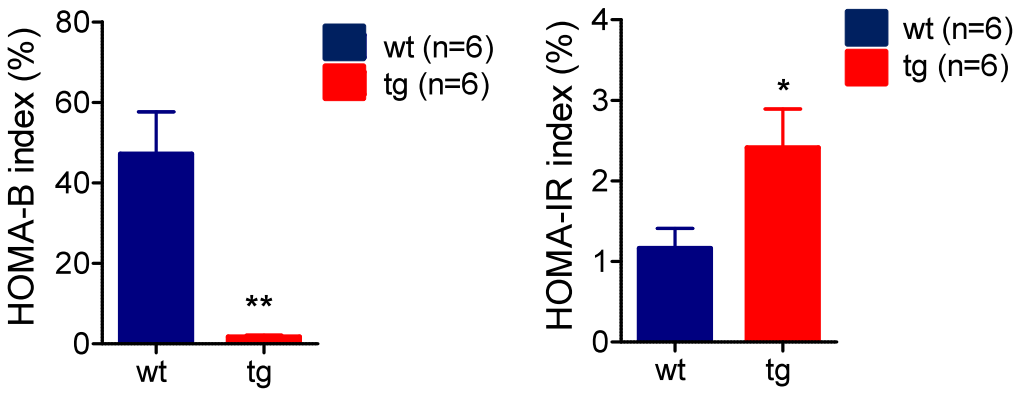

Figure 16: Homeostasis model assessment of baseline insulin secretion (HOMA-B) and of insulin resistance (HOMA-IR) of *INS*^{C94Y} transgenic pigs

4.5-month-old *INS*^{C94Y} transgenic pigs revealed significantly reduced baseline insulin secretion (left panel) and significantly increased insulin resistance indices (tg) compared to littermate controls (right panel). Data indicated as means ± SEM; *: p<0.05; **: p<0.01 vs. control; n: number of animals investigated; published by Renner et al. (2012); "Copyright 2012 American Diabetes Association From Diabetes®, Vol. 61, 2012 Reprinted with permission from the *American Diabetes Association*."

4.2.5. Plasma glucagon levels

In randomly fed 8-day-old *INS*^{C94Y} transgenic pigs, basal plasma glucagon levels were determined by a commercial glucagon radioimmunoassay and revealed a marked but not yet significant increase compared to non-transgenic littermates (192.98 ± 41.91 vs. 154.99 ± 6.64 pg/ml; n=4 per group; p=0.687) (Figure 17; left panel). Fasting plasma glucagon levels of *INS*^{C94Y} transgenic pigs at the age of 4.5 months were likewise noticeably but not significantly higher than in age-matched wild-type controls (101.25 ± 6.8 vs. 82.3 ± 10.35 pg/ml; n=7 per group; p=0.262) (Figure 17; right panel).

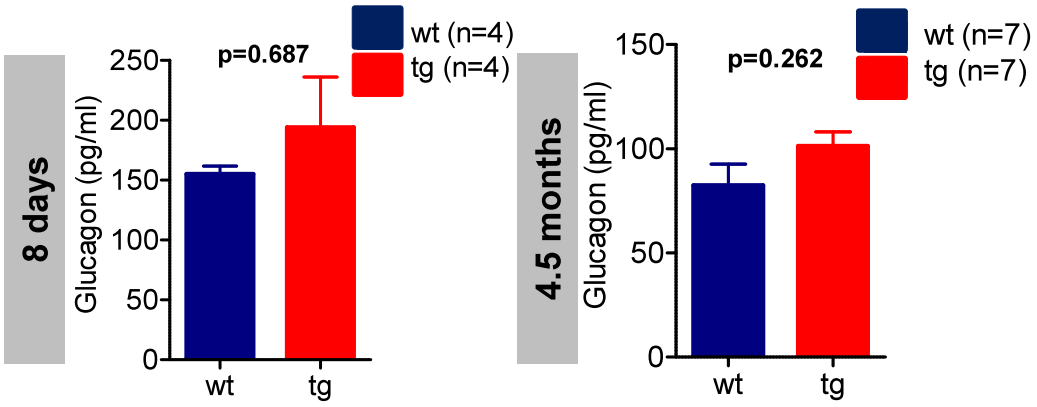

Figure 17: Basal and fasting glucagon levels of 8-day-old and 4.5-month-old *INS*^{C94Y} transgenic pigs and wild-type littermates

Basal plasma glucagon levels of 8-day-old (left panel) and fasting plasma glucagon levels of 4.5-months-old *INS*^{C94Y} transgenic pigs (tg) (right panel) were slightly but not significantly increased in comparison to wild-type littermates (wt) (p=0.687 and p=0.262 respectively); Data indicated as means ± SEM; n: number of animals investigated.

5. Morphological evaluation of the endocrine pancreas

Pancreata of 8-day-old and 4.5-month-old *INS*^{C94Y} transgenic pigs and related non-transgenic littermates were investigated by immunohistochemistry, quantitative stereological analyzes and transmission electron microscopy to determine, if *INS*^{C94Y} transgene expression affects cellular islet composition and ultrastructural architecture of pancreatic β-cells.

5.1. Absolute pancreas weight

Following explantation, pancreas was weighed to the nearest gram. Absolute pancreas weights were unaltered in *INS*^{C94Y} transgenic pigs compared to non-transgenic controls (n=4 per group) at the age of 8 days (4.4 ± 0.6 vs. 4.9 ± 0.4 g; p=0.49) (Figure 18, left panel). Absolute pancreas weights of 4.5-month-old *INS*^{C94Y} transgenic pigs were significantly decreased compared to wild-type controls (79 ± 6 vs. 134 ± 5 g; p<0.001) (Figure 18, right panel). The reduction of the absolute pancreas weights in 4.5-month-old *INS*^{C94Y} transgenic pigs was in proportion to the lower body weight at 4.5 months of age (Figure 12 B).

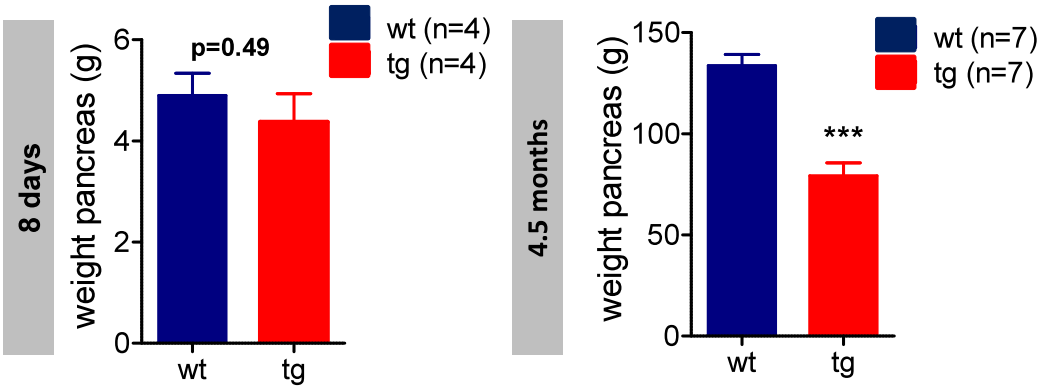

Figure 18: Absolute pancreas weights of *INS*^{C94Y} transgenic and wild-type littermates

8-day-old *INS*^{C94Y} transgenic pigs (tg) and non-transgenic controls (wt) revealed similar absolute pancreas weights (left panel). 4.5-month-old *INS*^{C94Y} transgenic pigs revealed a significant reduction of the absolute pancreas weight compared to their non-transgenic littermates (right panel). Data indicated as means ± SEM;

***: p<0.001 vs. control; n: number of animals investigated; published by Renner et al. (2012); "Copyright 2012 American Diabetes Association From Diabetes®, Vol. 61, 2012 Reprinted with permission from the *American Diabetes Association*."

5.2. Qualitative histological and quantitative stereological analyzes of the endocrine pancreas

Pancreatic sections of 8-day-old *INS*^{C94Y} transgenic pigs and non-transgenic controls (n=4 per group) underwent single immunostaining detecting insulin. Sections of pancreatic tissue of seven 4.5-month-old *INS*^{C94Y} transgenic pigs and seven littermate controls obtained by systematic random sampling were immunhistochemically stained for insulin containing cells and glucagon, somatostatin and pancreatic polypeptide positive cells, referred to as non-β-cells. Furthermore a single immunostaining for glucagon containing cells was performed on pancreatic sections of respective 4.5-month-old *INS*^{C94Y} transgenic pigs and non-transgenic littermate controls.

5.2.1. Histological evaluation of the endocrine pancreas

Qualitative histology on pancreatic tissue of 8-day-old *INS*^{C94Y} transgenic pigs indicated predominantly a great quantity of scattered, single β-cells and age-appropriate small clusters of β-cells with equal staining intensity. Histological evaluation of 8-day-old non-transgenic controls presented likewise regarding equal amounts and distribution of insulin-positive cells (Figure 19 A). At the age of 4.5 months, non-transgenic littermates revealed typical porcine islet composition and distribution of the endocrine cells. Porcine islets were irregularly shaped and insulin positive β-cells were located as major fraction in the central area of the islets surrounded by non-β-cells. Some non-β-cells were also dispersed as single cells in the adjacent exocrine pancreatic tissue (Figure 19 B). Compared to littermate controls, pancreas sections of 4.5-month-old *INS*^{C94Y} transgenic pigs demonstrated a notably reduced number of insulin positive β-cells, mostly presented as single, scattered β-cells or small β-cell clusters up to medium-sized islets. Islet-like structures with few β-cell nuclear profiles surrounded by a proportionately larger number of non-β-cells were also interpreted as islets.

Staining intensity of β-cells was less pronounced in 4.5-month-old *INS*^{C94Y} transgenic pigs indicating decreased insulin content compared to controls (Figure 19B).

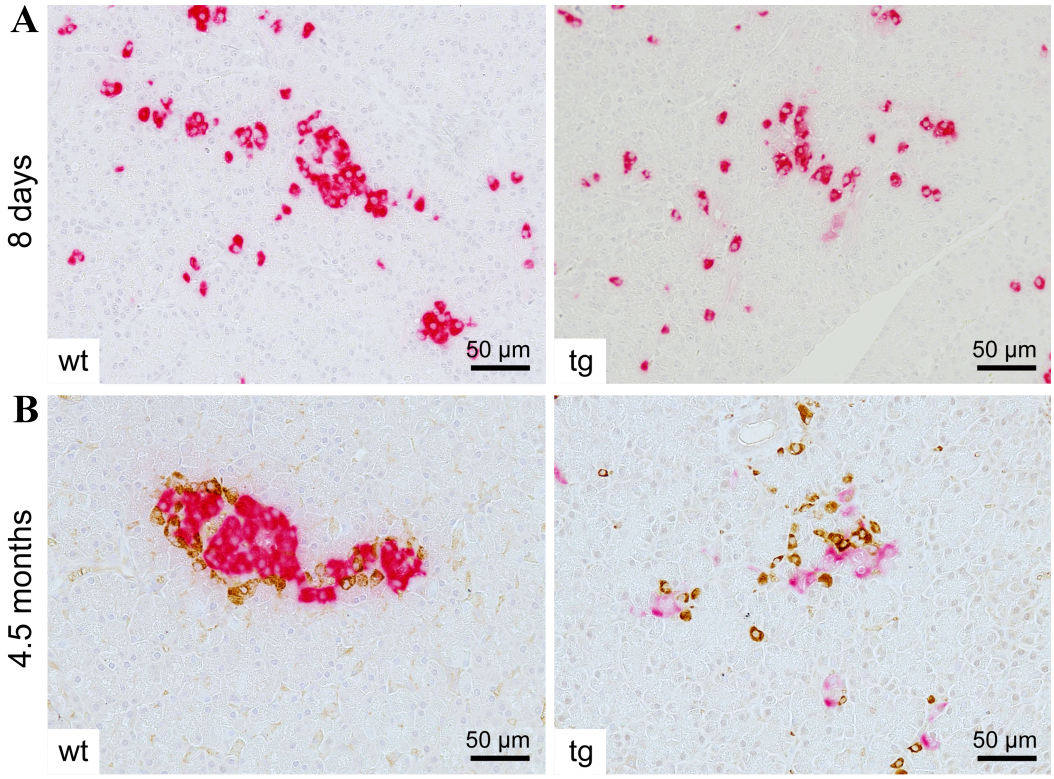

Figure 19: Representative histological sections of pancreatic tissue of an 8-day-old and a 4.5-month-old *INS*^{C94Y} transgenic pig and age-matched controls

(A) Immunohistochemical staining for insulin on pancreatic tissue of an 8-day-old *INS*^{C94Y} transgenic pig (tg) and a littermate control (wt) demonstrating age-appropriate β-cell formation. **(B)** Double immunohistochemical staining for insulin (pink) and glucagon, somatostatin and pancreatic polypeptide (brown) of a 4.5-month-old *INS*^{C94Y} transgenic pig (tg) and a non-transgenic control pig (wt) showing markedly altered islet composition in the transgenic pig. Scale bar = 50 µm; published by Renner et al. (2012); "Copyright 2012 American Diabetes Association From Diabetes®, Vol. 61, 2012 Reprinted with permission from the *American Diabetes Association*."

5.2.2. Quantitative stereological evaluation of the volume density and the total volume of β-cells in the pancreas

In addition quantitative stereological evaluation of the endocrine pancreas was accomplished in order to determine the volume density of β-cells in the pancreas ($Vv_{(\beta\text{-cell/Pan})}$) and the total β-cell volume ($V_{(\beta\text{-cell, Pan})}$) in 8-day-old and 4.5-month-old INS^{C94Y} transgenic pigs and non-transgenic littermates. In accordance with qualitative histological findings, neither $Vv_{(\beta\text{-cell/Pan})}$ (3.18 ± 0.4 vs. 2.98 ± 0.1%; p=1.0) nor $V_{(\beta\text{-cell, Pan})}$ (136.7 ± 36.5 vs. 137.2 ± 14.8 mm^3; p=0.682) were altered in 8-day-old INS^{C94Y} transgenic piglets (n=4) compared to wild-type control piglets (n=4) (Figure 20 A). At the age of 4.5 months, $Vv_{(\beta\text{-cell/Pan})}$ was significantly reduced by 54% (0.54 ± 0.05 vs. 1.18 ± 0.17%; p<0.01) in INS^{C94Y} transgenic pigs (n=7) in comparison to non-transgenic littermates (n=7). Moreover, $V_{(\beta\text{-cell, Pan})}$ was significantly diminished by 72% (409.2 ± 54.7 vs. 1476.7 ± 228.03 mm^3; p<0.001) (Figure 20 B). Due to the growth retardation in general and the proportional lower absolute pancreas weights in 4.5-month-old INS^{C94Y} transgenic pigs, $V_{(\beta\text{-cell, Pan})}$ was additionally calculated in relation to the body weight ($V_{(\beta\text{-cell, Pan})}$/BW ($mm^3$/kg)). $V_{(\beta\text{-cell, Pan})}$/BW was significantly reduced by 53% compared to control littermates (8.95 ± 0.96 vs. 18.84 ± 2.61 mm^3/kg; p<0.01) (Figure 21).

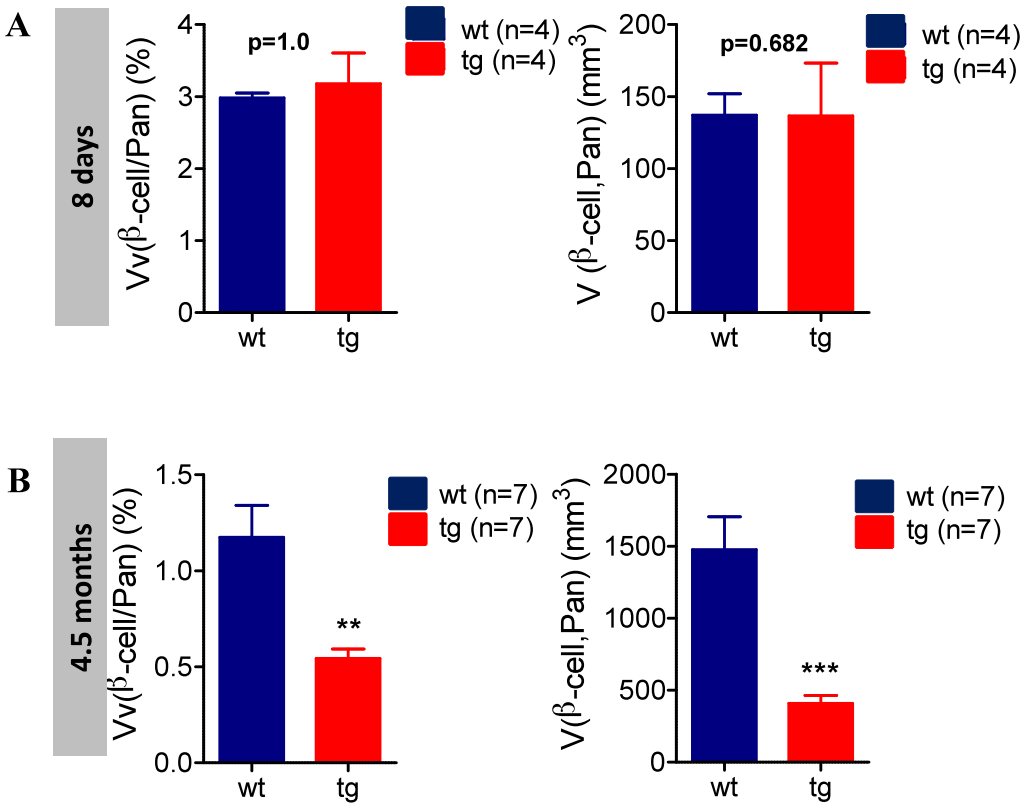

Figure 20: Quantitative stereological analyzes of islet parameters of 8-day-old and 4.5-month-old *INS*^{C94Y} transgenic and wild-type littermates

The volume density of β-cells in the pancreas (Vv $_{(\beta\text{-cell/Pan})}$) and the total β-cell volume (V$_{(\beta\text{-cell, Pan})}$) were determined in 8-day-old and 4.5-month-old *INS*^{C94Y} transgenic pigs (tg) and control littermates (wt). **(A)** Volume density of β-cells in the pancreas and the total β-cell volume did not differ between 8-day-old *INS*^{C94Y} transgenic pigs and controls (p=1.0 and p=0.68 respectively). **(B)** Significant reduction of the volume density of β-cells in the pancreas and the total β-cell volume in 4.5-month-old *INS*^{C94Y} transgenic pigs compared to control littermates (**: p<0.01; ***: p<0.001). **(A/B)** Data indicated as means ± SEM; n: number of animals investigated; Parameter V$_{(\beta\text{-cell, Pan})}$ of 8-day-old and 4.5-month-old *INS*^{C94Y} transgenic pigs and controls were published by Renner at el. (2012); "Copyright 2012 American Diabetes Association From Diabetes®, Vol. 61, 2012 Reprinted with permission from the *American Diabetes Association*."

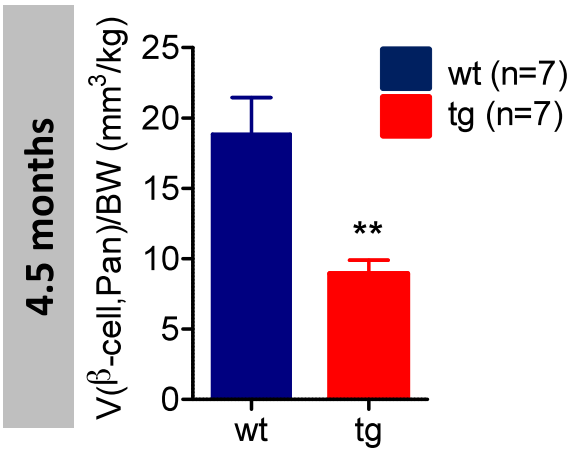

Figure 21: The total β-cell volume in relation to body in 4.5-month-old *INS*^{C94Y} transgenic pigs and non-transgenic littermates

The total β-cell volume in relation to body weight ($V_{(\beta\text{-cell, Pan})}$/BW) indicated a significant reduction by 53% in *INS*^{C94Y} transgenic pigs (tg) compared to non-transgenic control pigs (wt); Data indicated as means ± SEM; n: number of animals investigated; published by Renner et al. (2012); "Copyright 2012 American Diabetes Association From Diabetes®, Vol. 61, 2012 Reprinted with permission from the *American Diabetes Association*."

5.2.3. Qualitative histological and quantitative stereological evaluation of the total α-cell volume

For qualitative histological evaluation, pancreatic sections of 4.5-month-old *INS*^{C94Y} transgenic pigs and non-transgenic littermate pigs were stained for glucagon containing cells. Non-transgenic pigs revealed physiological distribution of α-cells, which were mainly located in a narrow mantle in the periphery of the islet, but also dispersed as minor fraction in the adjacent exocrine tissue (Figure 22; left panel). In *INS*^{C94Y} transgenic pigs, glucagon-positive area appeared enlarged and completely disordered in α-cell conglomerates (Figure 22; right panel).

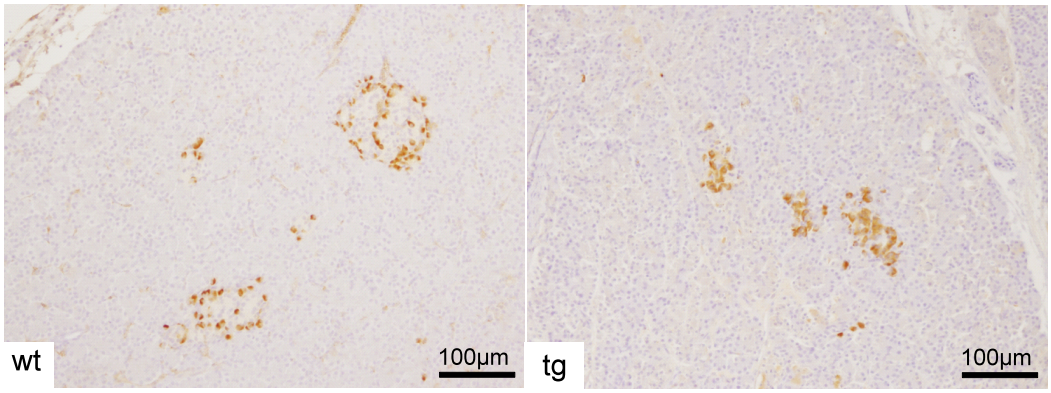

Figure 22: Immunohistochemical staining for glucagon containing cells in 4.5-month-old *INS*^{C94Y} transgenic pigs and non-transgenic littermates

Representative histological sections of pancreatic tissue of a 4.5-month-old *INS*^{C94Y} transgenic pig (tg) and a non-trangenic littermate (wt). Immunhistochemical staining for glucagon revealed an altered islet composition with formation of α-cell conglomerates in 4.5-month-old *INS*^{C94Y} transgenic pigs. Scale bar = 100 µm.

Furthermore the total α-cell volume in the pancreas ($V_{(\alpha\text{-cell, Pan})}$) and the total α-cell volume in relation to body weight ($V_{(\alpha\text{-cell, Pan})}$/BW) was determined in 4.5-month-old *INS*^{C94Y} transgenic pigs and non-transgenic littermates by means of quantitative stereological analyzes. The total α-cell volume in the pancreas ($V_{(\alpha\text{-cell, Pan})}$) was nearly unaltered in 4.5-month-old *INS*^{C94Y} transgenic pigs compared to wild-type littermates (187.03 ± 78.47 vs. 213.38 ± 20.59 mm^3; p=0.075; n=7 per group) (Figure 23 A). However the total α-cell volume in relation to body weight ($V_{(\alpha\text{-cell, Pan})}$/BW) was markedly but not yet significantly increased in 4.5-month-old *INS*^{C94Y} transgenic pigs compared to wild-type littermates (4.26 ± 1.84 vs. 2.74 ± 0.184 mm^3/kg; p=0.538; n=7 per group) (Figure 23 B).

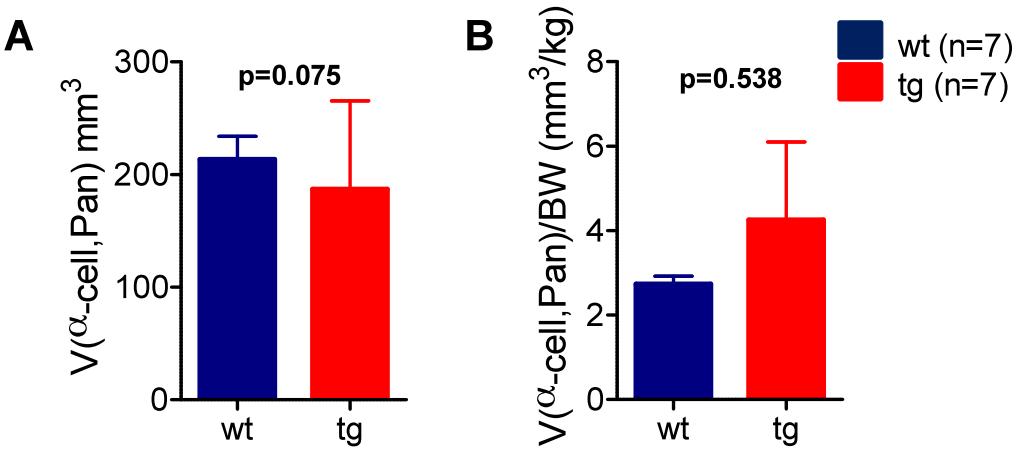

Figure 23: Quantitative stereological analyzes of the total α-cell volume in 4.5-month-old *INS*^{C94Y} transgenic pigs and non-transgenic littermates

The total α-cell volume ($V_{(\alpha\text{-cell, Pan})}$) in the pancreas and the total α-cell volume in relation to body weight ($V_{(\alpha\text{-cell, Pan})}$/BW) were determined in 4.5-month-old *INS*^{C94Y} transgenic pigs (tg) and non-transgenic littermates (wt). There was no difference in the total α-cell volume ($V_{(\alpha\text{-cell, Pan})}$) between *INS*^{C94Y} transgenic pigs and non-transgenic littermates at the age of 4.5 months (A), whereas the total α-cell volume in relation to body weight ($V_{(\alpha\text{-cell, Pan})}$/BW) was marginally increased (B); Data indicated as means ± SEM; n: number of animals investigated.

5.3. Ultrastructural morphology of β-cells

Ultrathin sections of pancreatic tissue of *INS*^{C94Y} transgenic and non-transgenic 8-day-old and 4.5-month-old pigs were subjected to electron microscopy concerning the ultrastructural architecture of pancreatic β-cells to evidence pathological mechanisms of diabetes mellitus present in *INS*^{C94Y} transgenic pigs. In 8-day-old *INS*^{C94Y} transgenic pigs, insulin secretory granules were still apparent in noticeable quantity in β-cells, which exhibited dilation of the endoplasmic reticulum (Figure 24 A). Electron microscopy of representative 4.5-month-old wild-type pigs indicated high number of insulin secretory granules in the cytoplasm of pancreatic β-cells, while cytoplasm of the β-cells of *INS*^{C94Y} transgenic pigs at the age of 4.5 months were nearly devoid of insulin secretory granules. Insulin secretory granules were consistently characterized by an irregularly shaped, electron-dense core with surrounding wide lucent halo. However, the core of insulin secretory granules in 4.5-month-old *INS*^{C94Y} transgenic pigs appeared less electron-dense as

compared to wild-type control. Furthermore endoplasmic reticulum (ER) was seriously enlarged in 4.5-month-old *INS*^{C94Y} transgenic pigs indicated by numerous cross-sectional areas of the endoplasmic reticulum (Figure 24 B).

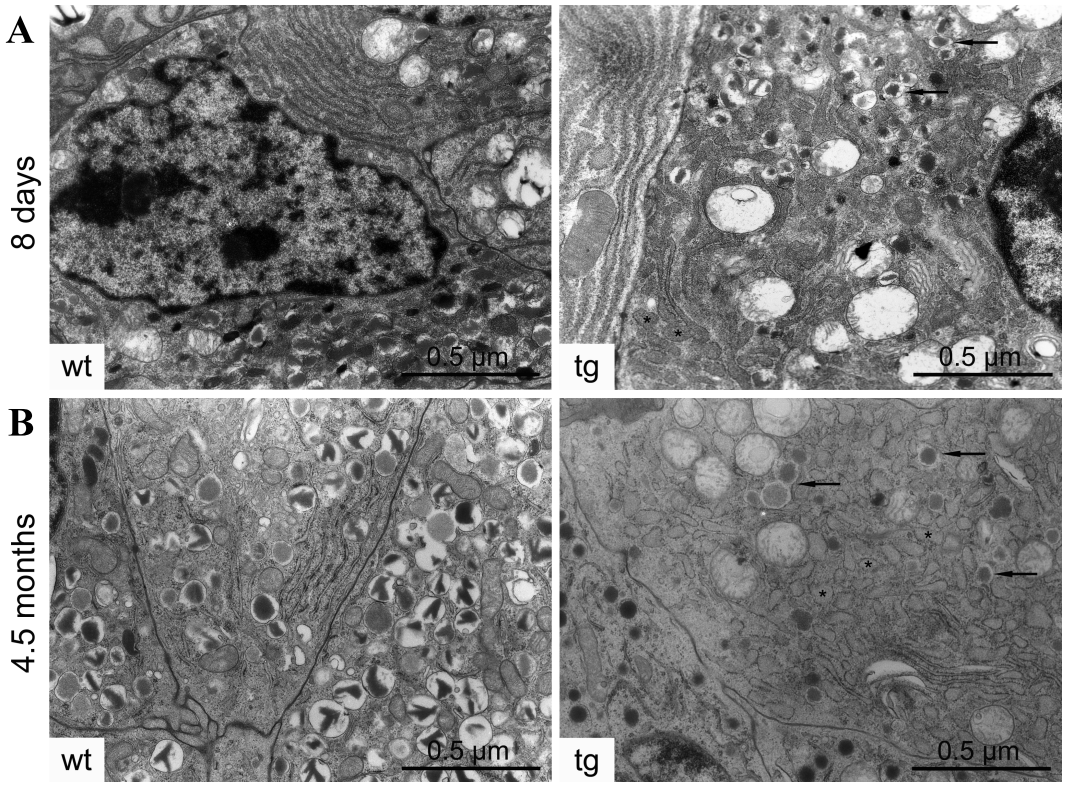

Figure 24: Representative transmission electron micrographs of pancreatic β-cell profiles of 8-day-old and 4.5-month-old *INS*^{C94Y} transgenic pigs and age-matched wild-type pigs

(A) In 8-day-old *INS*^{C94Y} transgenic pigs, β-cells exhibited nearly unaltered density of insulin secretory granules (arrow) but the endoplasmic reticulum was already dilated (asterisk). **(B)** β-cells represented in 4.5-month-old wild-type pigs (wt) revealed high density of insulin secretory granules and regular lamellae of the endoplasmic reticulum, in contrast to highly reduced number of insulin secretory granules (arrow) and severe dilation of the endoplasmic reticulum (asterisk) in the *INS*^{C94Y} transgenic pig. Scale bar = 0.5 µm; published by Renner et al. (2012); "Copyright 2012 American Diabetes Association From Diabetes®, Vol. 61, 2012 Reprinted with permission from the *American Diabetes Association*."

6. Evaluation of diabetes-associated secondary alterations in *INS*^{C94Y} transgenic pigs

Diabetes-associated morphological and functional secondary alterations in the kidney and in peripheral nerves of *INS*^{C94Y} transgenic pigs compared to non-transgenic littermates were investigated by means of histology, quantitative stereological methods and functional analyzes at 4.5 months of age. To evaluate complications of longstanding diabetes mellitus, 1-year-old cloned diabetic *INS*^{C94Y} transgenic pigs were scrutinised for evidence of diabetic kidney disease. To investigate time dependent progression of diabetic nephropathy and diabetic neuropathy likewise, diabetic *INS*^{C94Y} transgenic founder boar 9747 at the age of three years and an age-matched non-transgenic boar were examined for peculiarities of diabetes-associated alterations in respective organs.

6.1. Absolute organ weights

Mean absolute and relative organ weights (% of body weight) in 8-day-old and 4.5-month-old *INS*^{C94Y} transgenic pigs and respective non-transgenic controls are summarized in Table 16 and Table 17.

At the age of 8 days, *INS*^{C94Y} transgenic piglets showed only a slight tendency towards reduced absolute weights of most organs compared with age-matched wild-type piglets. Indeed, the absolute weight of the hearts was already significantly reduced in *INS*^{C94Y} transgenic piglets compared to wild-type littermates (31.3 ± 0.96 vs. 25.1 ± 2.1 g; $p<0.05$; n= 4 per group) (Table 16). As the mean body weight was significantly reduced in 4.5-month-old *INS*^{C94Y} transgenic pigs (Figure 12), the absolute weights of most organs were proportionately decreased in comparison to non-transgenic littermate controls (Table 17).

Table 16: Absolute and relative organ weights of 8-day-old *INS*^{C94Y} transgenic pigs and wild-type littermates

n= 4 per group		Absolute organ weights [g]			Relative organ weights [%/BW]		
Organs	**Genotype**	**mean**	**SEM**	***P*-values**	**mean**	**SEM**	***P*-values**
liver	**wt**	**105.6**	**5.8**	**0.2**	**5.42**	**0.23**	**0.57**
	tg	**94.1**	**5.5**		**5.1**	**0.47**	
pancreas	**wt**	**4.9**	**0.4**	**0.49**	**0.25**	**0.01**	**0.24**
	tg	**4.4**	**0.6**		**0.23**	**0.01**	
lungs	**wt**	**84.9**	**7.5**	**0.46**	**4.31**	**0.03**	**0.31**
	tg	**73.2**	**12.7**		**3.79**	**0.46**	
heart	**wt**	**31.3**	**0.96**	*	**1.63**	**0.16**	**0.2**
	tg	**25.1**	**2.1**		**1.35**	**0.11**	
Kidneys (cumulative)	**wt**	**21.5**	**2.57**	**0.92**	**1.08**	**0.04**	**0.62**
	tg	**22.2**	**4.1**		**1.06**	**0.08**	

n: number of investigated animals; BW: Body weight; SEM: standard error of mean
P-values: levels of significance; *:p<0.05

Table 17: Absolute and relative organ weights of 4.5-month-old *INS*^{C94Y} transgenic pigs and wild-type controls

n= 7 per group		Absolute organ weights [g]			Relative organ weights [%/BW]		
Organs	**Genotype**	**mean**	**SEM**	***P*-values**	**mean**	**SEM**	***P*-values**
liver	**wt**	**1887.9**	**177.4**	*	**2.5**	**0.2**	**0.059**
	tg	**1347.6**	**105.1**		**3.03**	**0.1**	
pancreas	**wt**	**133.7**	**5.5**	****	**0.2**	**0.01**	**0.83**
	tg	**79.3**	**6.3**		**0.18**	**0.012**	
stomach	**wt**	**553,3**	**15.7**	**	**0.75**	**0.04**	**0.622**
	tg	**364.4**	**39.5**		**0.8**	**0.04**	
spleen	**wt**	**494,1**	**57.6**	***	**0.7**	**0.07**	**
	tg	**168.1**	**13.5**		**0.4**	**0.08**	
lungs	**wt**	**611.6**	**33.5**	**	**0.8**	**0.04**	**0.502**
	tg	**406.8**	**36.8**		**0.9**	**0.05**	
heart	**wt**	**299**	**10.2**	****	**0.4**	**0.01**	**0.513**
	tg	**174.6**	**11.8**		**0.4**	**0.02**	
Kidneys (cumulative)	**wt**	**371.7**	**10.3**	**0.058**	**0.5**	**0.06**	***
	tg	**314.3**	**21.9**		**0.7**	**0.07**	

n: number of investigated animals; BW: Body weight; SEM: standard error of mean
P-values: levels of significance; *:p<0.05; **:p<0.01; ***:p<0.001; ****:p<0.0001

6.2. Evaluation of diabetic nephropathy

6.2.1. Absolute and relative kidney weights

Aberrant from the significantly decreased absolute weights of the other organs by at least 30% (Table 17), the absolute weight of the kidneys, cumulatively calculated from the weights of both kidneys, were diminished by only 15% in *INS*^{C94Y} transgenic pigs at 4.5 months of age in comparison to non-transgenic littermates (314.29 ± 21.93 vs. 371.71 ± 10.26 g; p=0.058) (Figure 25; left panel). Thus, relative kidney weights, indicated as the cumulative weight of both kidneys as percent of body weight, were significantly increased compared to non-transgenic littermates (0.7 ± 0.07 vs. 0.5 ± 0.06%; p<0.01) (Figure 25; right panel).

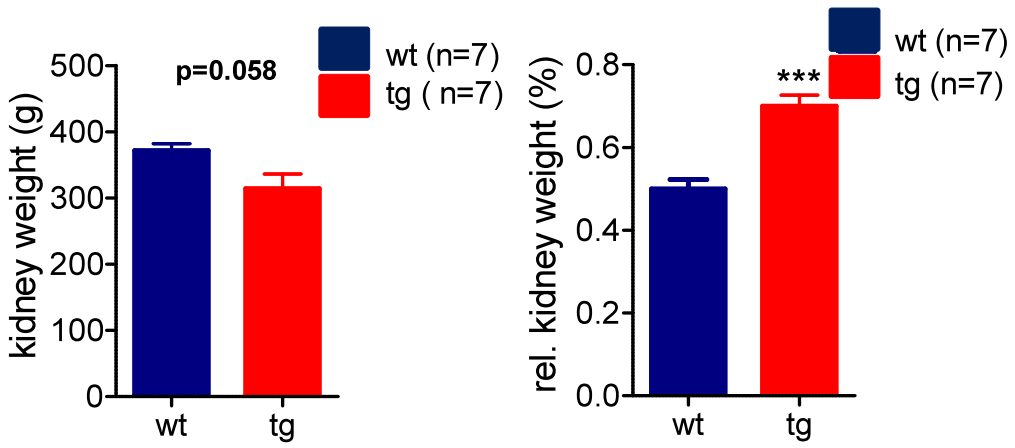

Figure 25: Absolute and relative kidney weights of 4.5-month-old *INS*^{C94Y} transgenic and non-transgenic littermates

Absolute kidney weight of 4.5-month-old *INS*^{C94Y} transgenic pigs (tg) demonstrates a reduction by 15% compared to non-transgenic littermates (wt) (314.29 ± 21.93 vs. 371.71 ± 10.26 g; p=0.058) (left panel). The relative weight (% of body weight) of both kidneys was significantly increased in 4.5-month-old *INS*^{C94Y} transgenic pigs in comparison with their corresponding non-transgenic controls (right panel); Data indicated as means ± SEM; ***: p<0.001 vs. control; n: number of animals investigated; published by Renner et al. (2012); "Copyright 2012 American Diabetes Association From Diabetes®, Vol. 61, 2012 Reprinted with permission from the *American Diabetes Association*."

6.2.2. Glomerular histology and quantitative stereological analyzes of the kidneys

Histopathological analyzes on perfused renal tissue of *INS*^{C94Y} transgenic and non-transgenic control pigs were accomplished following plastic embedding (glycolmethacrylate and methyl-methacrylate (GMA/MMA), hematoxylin and eosin staining (HE) (Figure 26 A) as well as periodic acid silver methenamine staining (PASM) (Figure 26 B). Glomerula were investigated with regard to glomerular hypertrophy, expansion of the mesangial matrix and pathological alterations displaying glomerulosclerosis, which included hyalinosis and obliterations of capillaries. Investigated sections of diabetic *INS*^{C94Y} transgenic pigs at 4.5 months of age and severely diabetic 1-year-old cloned *INS*^{C94Y} transgenic pigs alike did not provide evidence for diabetes-associated kidney disease. Furthermore histological sections of *INS*^{C94Y} transgenic pigs were examined comparatively with non-transgenic controls for the presence of atrophic tubuli, interstitial fibrosis or tubular protein sediments without detecting any noticeable alterations (Figure 26 A/B).

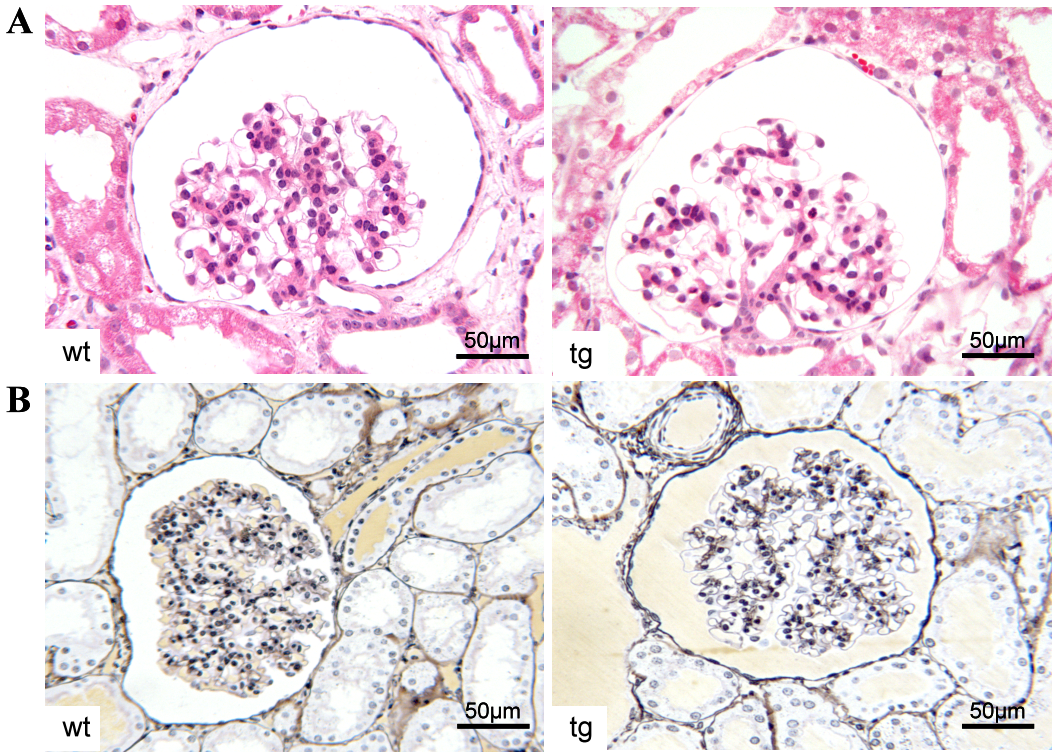

Figure 26: Representative histological sections of renal tissue of a 4.5-month-old *INS*^{C94Y} transgenic pig and a non-transgenic littermate

Light microscopy on cross sections at the equator level of representative glomerula of an *INS*^{C94Y} transgenic pig (tg) and a non-transgenic littermate (wt) at 4.5 months of age without evidence of morphological alterations suggestive of diabetic kidney disease; **(A/B)** GMA/MMA embedded renal tissue; **(A)** HE-staining; **(B)** PASM-staining; Scale bar = 50 µm; Data provided by Dr. Andreas Blutke, Intitute of Veterinary Pathology, Ludwig-Maximilians-University, Munich, Research Group Prof. Dr. Rüdiger Wanke.

The mean glomerular volume ($V_{(glom)}$) was determined by means of planimetric measurements of the mean glomerular profile areas on kidney tissue of 4.5 months old *INS*^{C94Y} transgenic pigs and non-transgenic littermates (144 ± 8 glomerular profiles per animal) and the mean glomerular volume to body weight (BW) ratio ($V_{(glom)}$/BW (mm^3/kg)x10^{-3}) was calculated. The mean glomerular volume to body weight (BW) ratio ($V_{(glom)}$/BW (mm^3/kg)x10^{-3}) was significantly increased by 30% on the average in comparison to corresponding age-matched control pigs (41.68 ± 6.71 vs. 32.05 ± 5.56 (mm^3/kg)x10^{-3}; $p<0.01$ vs. control) (Figure 27).

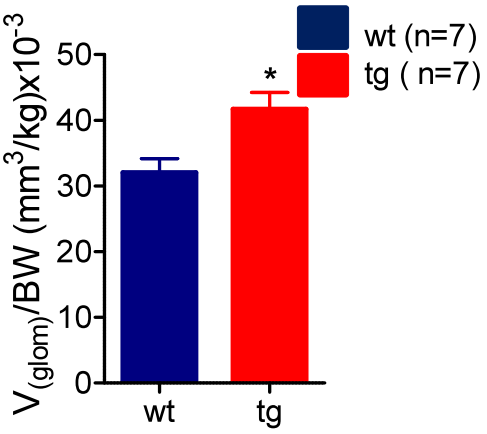

Figure 27: Mean glomerular volume to body weight ratio ($V_{(glom)}$/BW (mm^3/kg)x10^{-3}) in 4.5-month-old *INS^{C94Y}* transgenic and littermate control pigs

4.5-month-old *INS^{C94Y}* transgenic pigs (tg) displayed a significant increase of their mean glomerular volume to body weight ratio ($V_{(glom)}$/BW (mm^3/kg)x10^{-3} as compared to non-transgenic control pigs (wt). Data indicated as means ± SEM; *: $p<0.05$ vs. control; n: number of animals investigated; Data provided by Dr. Andreas Blutke, Intitute of Veterinary Pathology, Ludwig-Maximilians-University, Munich, Research Group Prof. Dr. Rüdiger Wanke; published by Renner et al. (2012); "Copyright 2012 American Diabetes Association From Diabetes®, Vol. 61, 2012 Reprinted with permission from the *American Diabetes Association*."

6.2.3. Transmission electron microscopy of glomerular structures and thickness of the glomerular basement membrane (ThGBM)

Transmission electron microscopy (TEM) was achieved on cortical kidney tissue derived from 4.5-month-old *INS^{C94Y}* transgenic pigs and non-transgenic littermates (three females per group). The true harmonic mean thickness of the glomerular basement membrane (ThGBM) was determined using transmission electronical micrographs of peripheral glomerular capillary loops of the respective pigs. Investigated glomerular cross section profiles of *INS^{C94Y}* transgenic pigs did not indicate any morphological alterations of glomerular capillary structures compared to non-transgenic controls, including podocytes, podocyte foot processes as well as the endothelium (Figure 28; left panel). *INS^{C94Y}* transgenic

animals revealed a nearly identical true harmonic mean thickness (Th) of the glomerular basement membrane (GBM) of peripheral glomerular capillary loops as compared to respective non-transgenic controls (126.52 ± 2.37 vs. 126.66 ± 2.42 nm; p=0.9 vs. control; n=3 per group) (Figure 28; right panel).

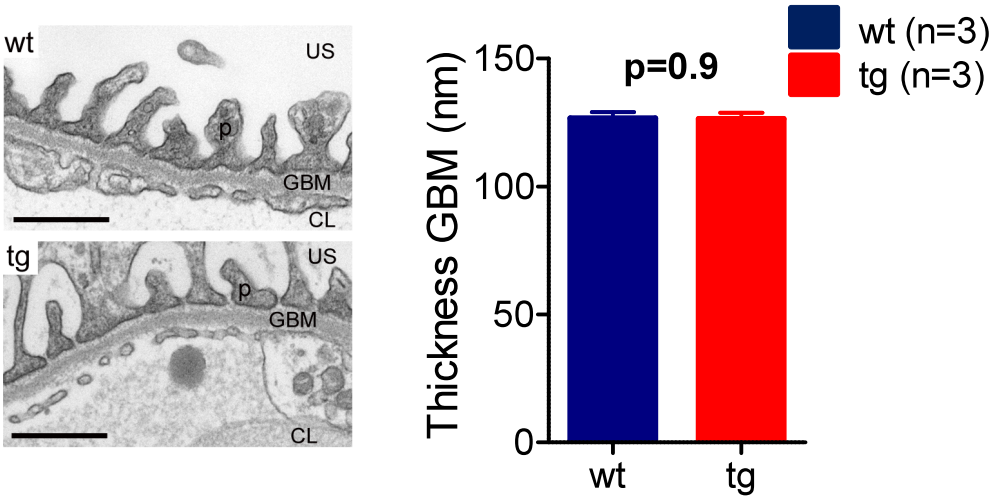

Figure 28: Thickness of the glomerular basement membrane (GBM) in 4.5-month-old *INS*^{C94Y} transgenic pigs and littermate controls

Representative transmission electron micrographs (TEM) of peripheral glomerular capillary loops of an *INS*^{C94Y} transgenic pig (tg) at 4.5 months of age and a control pig (wt) representing unaltered thickness of the glomerular basement membrane (ThGBM) in the transgenic pig; US: urinary space; CL: glomerulary capillary lumen; p: podocyte foot process; scale bar: 500 nm; (left panel). Identical true harmonic mean thickness (Th) of the glomerular basement membrane (GBM) of peripheral glomerular capillary loops of *INS*^{C94Y} transgenic pigs (tg) and control littermates (wt); Data indicated as means ± SEM; p= 0.9 vs. control; n: number of animals investigated; Data provided by Dr. Andreas Blutke, Intitute of Veterinary Pathology, Ludwig-Maximilians-University, Munich, Research Group Prof. Dr. Rüdiger Wanke; published by Renner et al. (2012); "Copyright 2012 American Diabetes Association From Diabetes®, Vol. 61, 2012 Reprinted with permission from the *American Diabetes Association*."

6.2.4. Urine protein excretion patterns

In order to investigate diabetes-associated functional kidney failure in *INS*^{C94Y} transgenic pigs, urine samples of seven representative *INS*^{C94Y} transgenic pigs (3 males and 4 females) and three non-transgenic littermates (2 females and 1 male) at the age of 4.5 months were assayed for the onset of albuminuria in general. Urine samples of 1-year-old cloned diabetic *INS*^{C94Y} transgenic pigs were additionally evaluated to acquire insights in the possible progression of albuminuria in the course of time, when hyperglycemia was left untreated. Urine samples of the insulin-treated diabetic *INS*^{C94Y} transgenic founder boar 9747 and a F1-female (9901), collected at the day of necropsy at the age of three years both, were analyzed likewise for evidence of albuminuria due to prolonged disease duration. An age-matched non-transgenic boar and a female served as wild-type controls for urine analyzes. Gel bands of approximately 66 kDa corresponding to the molecular weight of bovine serum albumin (BSA) standard (66.5 kDa) were compared with related age-matched, non-transgenic controls. Noticeable albuminuria did not become evident in *INS*^{C94Y} transgenic pigs at any time point investigated (Figure 29 A/B). However, one male *INS*^{C94Y} transgenic pig at 4.5-month of age (9900) revealed a slight tendency towards a broadening of the 66 kDa band compared to age-matched, non-transgenic controls (Figure 29 A).

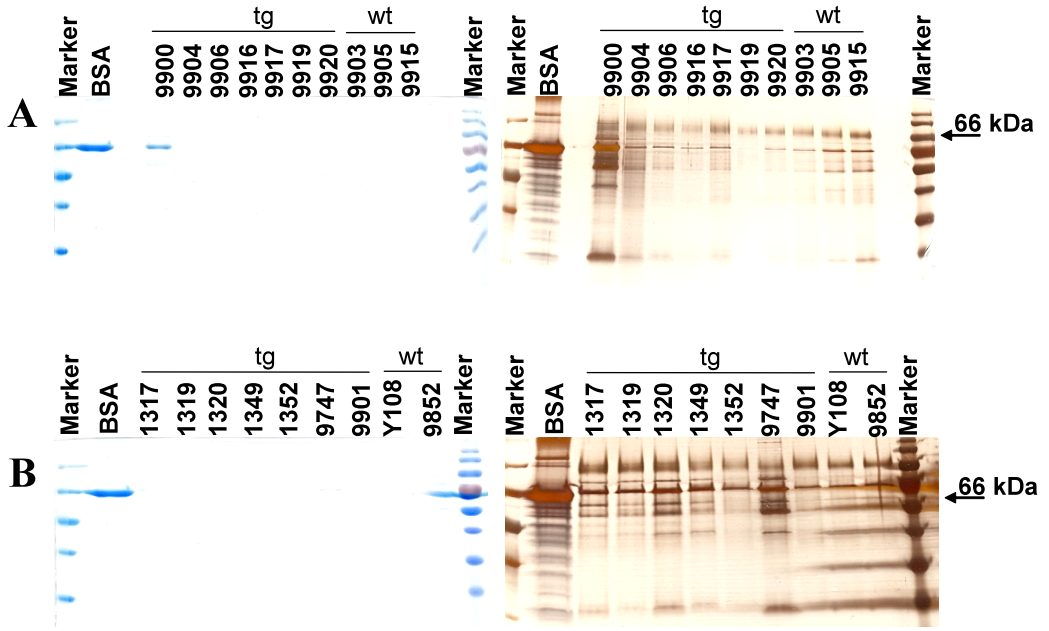

Figure 29: SDS-PAGE urine protein analyzes of *INS*^{C94Y} transgenic pigs and age-matched wild-type pigs

Urine protein fractions were separated by electrophoresis in a 12% SDS polyacrylamide gel followed by Coomassie staining (left panel) and silver staining (right panel) of SDS gels detecting bands of 66 kDa corresponding to the molecular weight of BSA standard (66.5 kDa); urine samples were diluted each to a creatinine level of 1500 µmol/l irrespective of the investigated age group. **(A)** Same urine protein excretion patterns in 4.5-month-old *INS*^{C94Y} transgenic pigs (tg) and representative non-transgenic littermates (wt) without evidence of albuminuria; **(B)** Urine analyzes of diabetic *INS*^{C94Y} transgenic pigs at the age of 1 year (1317, 1319, 1320, 1349, 1352) (tg), one 3-year-old *INS*^{C94Y} transgenic female as well as the 3-year-old *INS*^{C94Y} transgenic founder boar (9747) (tg) were unsuggestive of albuminuria compared to their representative age-matched controls (Y108, 9852) (wt); **(A/B)** Marker: PageRuler^{TM} Prestained Protein Ladder with visible marker-bands indicating the molecular weight of protein standards of 170 kDa to 15 kDa from top to bottom; BSA: bovine serum albumine standard (600 ng/lane); spacing lane: H_20.

6.3. Evaluation of diabetic neuropathy

For histological examination of peripheral nervous tissue a segment of the tibial nerve of representative 4.5-month-old *INS*^{C94Y} transgenic pigs and corresponding non-transgenic littermates was separated immediately after euthanasia and routinely processed for epon embedding. Comparative azur II-methylene blue-safranin staining of tibial nerve fascicle profiles of diabetic *INS*^{C94Y} transgenic pigs and corresponding controls at the age of 4.5 months revealed an unaltered fiber density with physiological homogenous myelination of the fiber caliber and inconspicuous vasculature. A pathognomonic loss of myelinated fibers was not detectable in 4.5-month-old *INS*^{C94Y} transgenic pigs. In addition, higher magnification levels did likewise not adduce light microscopic evidence of axonal degeneration as well as demyelination processes indicated by a high percentage of thin myelin sheaths. Therefore, nerve biopsies of 4.5-month-old *INS*^{C94Y} transgenic pigs did not furnish proof of diabetes-induced injury of nervous tissue (Figure 30). Histological evaluation of nervous tissue of the insulin-treated *INS*^{C94Y} transgenic founder boar at the age of three years also revealed unchanged morphology compared to an age-matched wild-type boar.

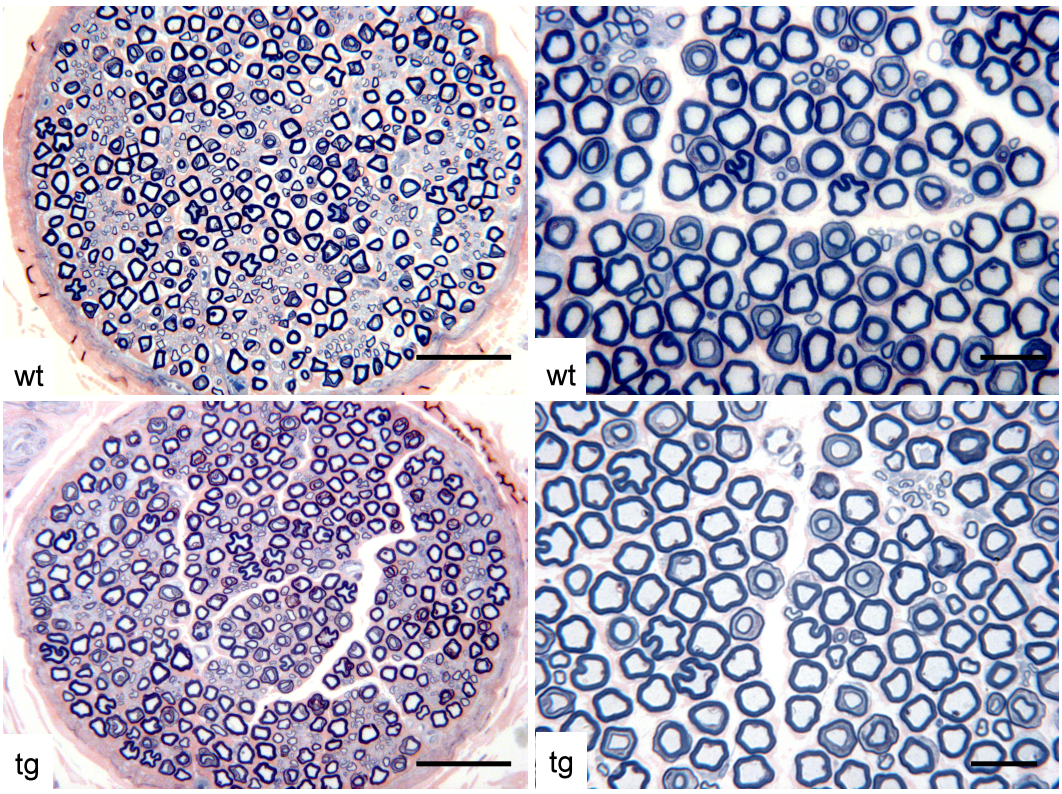

Figure 30: Representative histological sections of a tibial nerve fascicle of a 4.5-month-old *INS*^{C94Y} transgenic pig and a non-transgenic littermate

Light microscopy of semithin sections of a tibial nerve fascicle of an *INS*^{C94Y} transgenic pig (tg) and a non-transgenic control littermate (wt) at 4.5 months of age revealing physiological fiber density unsuggestive of diabetes-induced myelinopathy and axonal atrophy; Azur II-methylene blue-safranin staining on semithin sections illustrated at different magnification levels; Scale bar = 100 µm; Data provided by Dr. Daniela Emrich, Intitute of Veterinary Pathology, Ludwig-Maximilians-University, Munich, Research Group Prof. Dr. Kaspar Matiasek; published by Renner et al. (2012); "Copyright 2012 American Diabetes Association From Diabetes®, Vol. 61, 2012 Reprinted with permission from the *American Diabetes Association*."

Furthermore single fiber teasing on tibial nerve biopsies of 4.5-month-old *INS*^{C94Y} transgenic pigs was accomplished and evaluated for the presence of segmental or paranodal demyelination as well as signs of Wallerian degeneration without detecting any remarkable structural abnormalities compared to non-transgenic littermates.

Teased fibers showed homogenous physiological myelinization of the internodes devoid of structural alterations of the nodes of Ranvier (Figure 31).

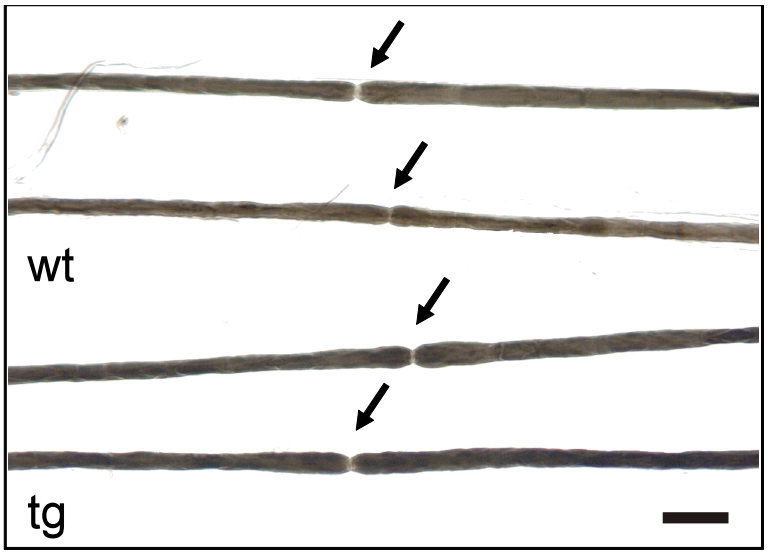

Figure 31: Single fiber teasing of a tibial nerve fascicle of a 4.5-month-old *INS*^{C94Y} transgenic pig and a non-transgenic littermate

Teased fibers sampled from the tibial nerve fascicle evidenced homogenous physiological myelinization without structural alterations of nodular architecture; Scale bar = 100 µm; Data provided by Dr. Daniela Emrich, Intitute of Veterinary Pathology, Ludwig-Maximilians-University, Munich, Research Group Prof. Dr. Kaspar Matiasek; published by Renner et al. (2012); "Copyright 2012 American Diabetes Association From Diabetes®, Vol. 61, 2012 Reprinted with permission from the *American Diabetes Association*."

6.4. Progressive cataract in *INS*^{C94Y} transgenic pigs

A cataract of the eye lenses was already observed in 8-day-old *INS*^{C94Y} transgenic pigs, progressing with increasing age. However, diabetic cataract in *INS*^{C94Y} transgenic pigs turned out being reversible with exogenous insulin replacement and vision could be recovered (Figure 32). At the age of 8 days, lenses revealed incipient opacity at the edges, while in 4.5-month-old *INS*^{C94Y} transgenic pigs the entire lenses were tarnished, which would have led to a deterioration of the visual acuity in all probability (Figure 33).

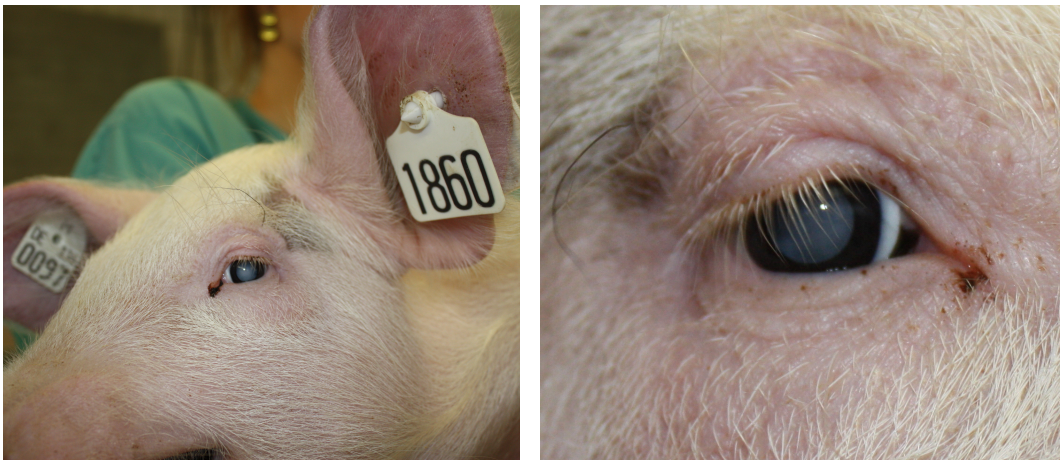

Figure 32: Progressive cataract in *INS*^{C94Y} transgenic pigs

Representative photographs of a 3-month-old *INS*^{C94Y} transgenic pig showing almost completely opaque lenses indicating an advanced state of diabetes-induced cataract.

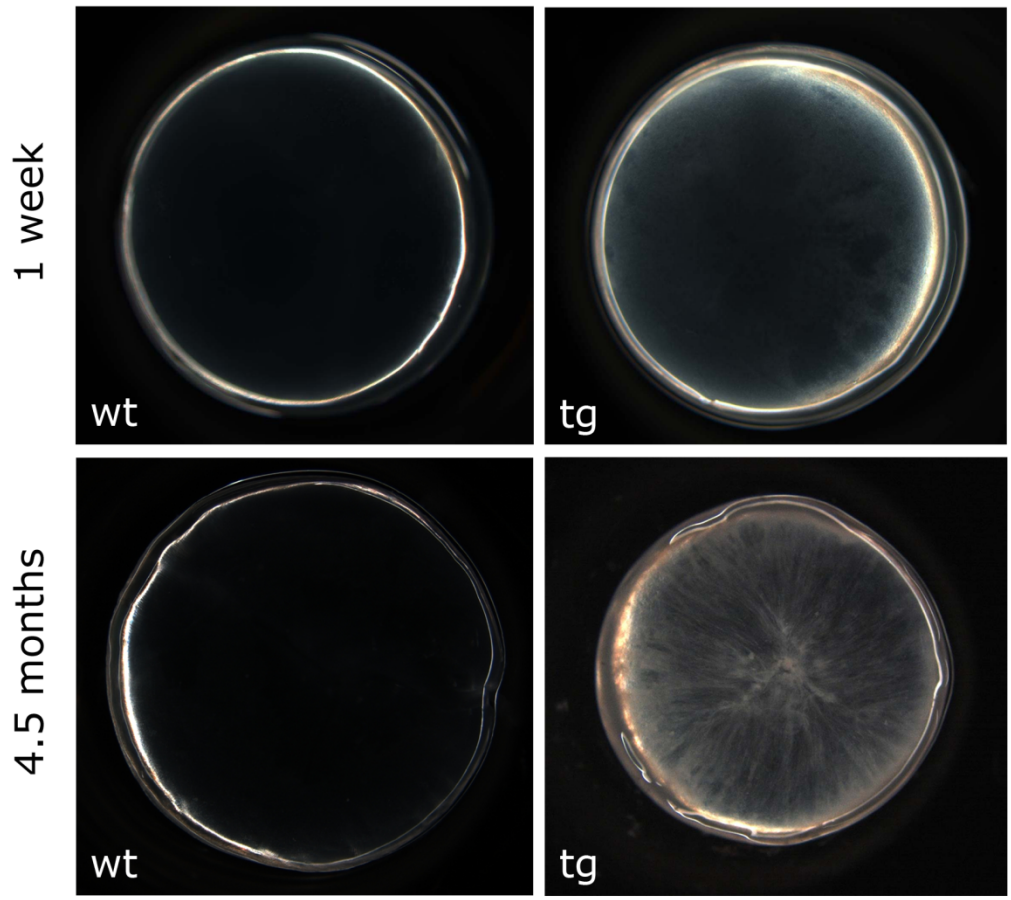

Figure 33: Progressive diabetic cataract in *INS*^{C94Y} transgenic pigs and wild-type littermates

Light microscopy on eye lenses of a representative 8-day-old and a 4.5-month-old *INS*^{C94Y} transgenic pig (tg) and a non-transgenic littermate (wt). Microscopical pictures demonstrate incipient cataract in the transgenic pig at 8 days of age with progression until the whole lens was affected at 4.5 months of age; Data provided by Dr. Oliver Puk, Helmholtz Center Munich-German Research Center for Environmental Health, Institute of Developmental Genetics, Neuherberg, Research group of Prof. Dr. Jochen Graw; published by Renner et al. (2012); "Copyright 2012 American Diabetes Association From Diabetes®, Vol. 61, 2012 Reprinted with permission from the *American Diabetes Association*."

7. Evaluation of endoplasmic reticulum stress in *INS*^{C94Y} transgenic pigs

The presence of endoplasmic reticulum stress in 8-day-old *INS*^{C94Y} transgenic pigs was evaluated by Western blot analysis of isolated pancreatic islets derived from a neonatal *INS*^{C94Y} transgenic piglet in comparison with a non-transgenic littermate. Three independent islet lysates of an *INS*^{C94Y} transgenic piglet and of a non-transgenic littermate were used in each case. Endoplasmic reticulum stress markers were identified by specific antibodies and the fragment size was compared to the molecular weight standard. Quantification was accomplished by normalizing their optical densities with that of β-actin (43 kDa).

7.1. C/EBP-homologous protein 10 (CHOP-10)

The proapoptotic endoplasmic reticulum stress marker CHOP-10, also referred to as Growth arrest and DNA damage protein 153 (GADD 153) was characterized by a specific band of 20 kDa, which was detectable in the *INS*^{C94Y} transgenic piglet as well as in the non-transgenic control. However, the *INS*^{C94Y} transgenic piglet demonstrated a clearly higher optical density of CHOP/β-actin compared to the non-transgenic control (0.196 ± 0.05 vs. 0.076 ± 0.02) indicating upregulation of CHOP-10 expression (Figure 34).

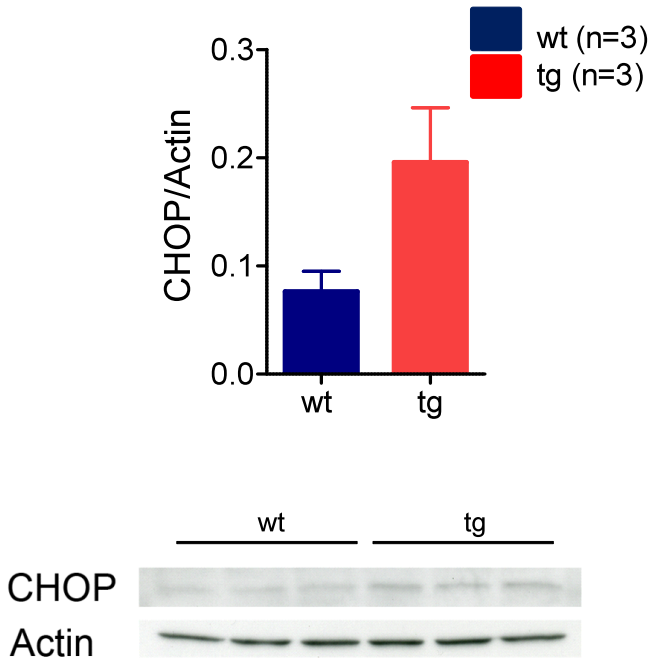

Figure 34: Optical density of CHOP/β-actin in isolated islets of a neonatal *INS*^{C94Y} transgenic pig and a non-transgenic littermate

Western blot analysis of a neonatal *INS*^{C94Y} transgenic pig and non-transgenic control indicated a band of 20 kDa, which meets the molecular weight specific for CHOP-10. The mean optical density of CHOP/β-actin was clearly elevated in the *INS*^{C94Y} transgenic piglet (tg) compared to the non-transgenic control (wt); n: number of investigated islet lysates of an *INS*^{C94Y} transgenic pig and a non-transgenic control; data indicated by means ± SEM.

7.2. Phosphorylated eucaryotic translation initiation factor 2α (PeIF2α)

Evidence of the phosphorylated eukaryotic translation initiation factor 2α (PeIF2α) was visualized in isolated islets of an *INS*^{C94Y} transgenic piglet and of a non-transgenic littermate by a specific band of 36 kDa. The optical density of PeIF2α/β-actin was slightly decreased in the *INS*^{C94Y} transgenic piglet compared to the non-transgenic control (Figure 35).

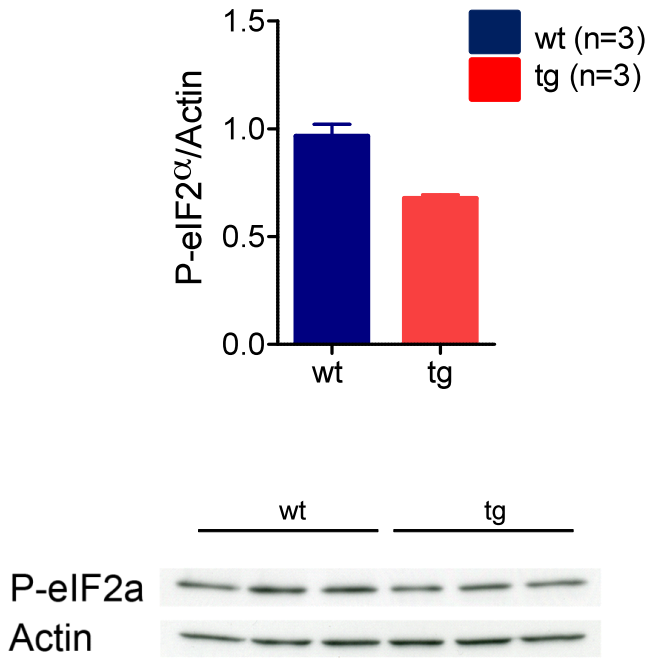

Figure 35: Optical density of PeIF2α/β-actin in isolated islets of a neonatal *INS*^{C94Y} transgenic pig and a non-transgenic littermate

The presence of PeIF2α in isolated islets of a neonatal *INS*^{C94Y} transgenic pig and a non-transgenic control was reflected by a distinct band of 36 kDa. The *INS*^{C94Y} transgenic piglet (tg) revealed a diminished mean optical density of PeIF2α/β-actin compared to the non-transgenic control pig (wt); n: number of investigated islet lysates of an *INS*^{C94Y} transgenic pig and a non-transgenic control; data indicated by means ± SEM.

7.3. Glucose regulated protein 78 (Grp78)

A specific and clearly visible band of 78 kDa, associated with the molecular weight of the glucose regulated protein 78 (Grp78), also synonymously known as binding Ig protein (BiP), could be detected in the *INS*^{C94Y} transgenic pig and in the non-transgenic control likewise. The *INS*^{C94Y} transgenic pig showed a similar optical density of GRP78/β-actin compared to the non-transgenic control indicating unaltered expression levels of Grp78 (Figure 36).

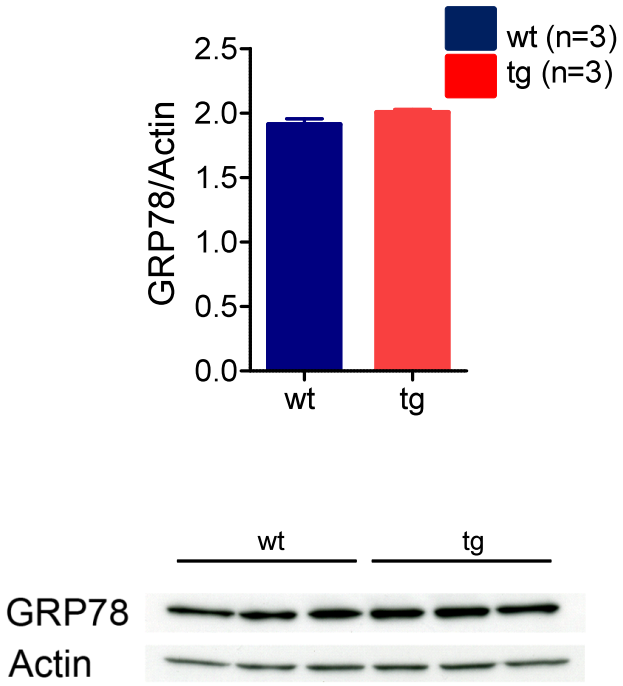

Figure 36: Optical density of GRP78/β-actin in isolated islets of a neonatal *INS*^{C94Y} transgenic pig and a non-transgenic littermate

Grp78, indicated by a band of 78 kDa, was present in isolated islets of a neonatal *INS*^{C94Y} transgenic pig (tg) and a non-transgenic control (wt). The optical density of GRP78/β-actin was unaltered in the *INS*^{C94Y} transgenic piglet compared to the non-transgenic control; n: number of investigated islet lysates of an *INS*^{C94Y} transgenic pig and a non-transgenic control; data indicated by means ± SEM.

V. DISCUSSION

The present study included the generation and characterization of the first genetically engineered porcine animal model of permanent neonatal diabetes mellitus. Severe diabetes mellitus in hemizygous *INS*^{C94Y} transgenic pigs is triggered by expression of a mutated *INS* gene (*INS*^{C94Y}), resembling the *INS*^{C96Y} mutation identified in human and the *Ins2*^{C96Y} mutation of the Akita mouse model (Colombo et al., 2008; Stoy et al., 2007; Yoshioka et al., 1997).

1. Generation of *INS*^{C94Y} transgenic pigs using somatic cell nuclear transfer

INS^{C94Y} transgenic pigs were generated by somatic cell nuclear transfer (SCNT) using pools of donor cells stably nucleofected with the porcine *INS*^{C94Y} expression vector. Using this strategy it is possible to obtain a high proportion of transgenic founder animals with different integration sites and expression levels (Aigner et al., 2010). SCNT and transfer of reconstructed embryos into estrus synchronized recipient gilts resulted in seven live offspring derived from 237 transferred embryos equivalent to a reasonable cloning efficiency of 3% within the expected range (Klymiuk et al., 2012; Kurome et al., 2008; Polejaeva et al., 2000; Umeyama et al., 2009; Vajta et al., 2007). Southern blot analysis using a probe specific for the neomycin resistance cassette attached to the *INS*^{C94Y} expression cassette identified all seven cloned piglets as transgenic and suggested that each founder had a single transgene integration site at a different chromosomal locus, as expected after using pools of stable nucleofected cell clones for SCNT. Therefore it is not surprising, that the *INS*^{C94Y} transgenic founder boars revealed different expression levels of the *INS*^{C94Y} transgene attributable to chromosomal position effects resulting from the chromatin status of neighboring DNA (Clark et al., 1994; Recillas-Targa, 2006; Wolf et al., 2000). Maintenance of *INS*^{C94Y} transgene integrity as well as germ line transmission adhering to mendelian rules was proven by Southern blot analysis of the *INS*^{C94Y} transgenic offspring of the diabetic founder boar 9747 showing the same transgene integration pattern and similar levels of transgene expression as their transgenic sire. Indeed, the diabetic phenotype was exceedingly stable in the

INS^{C94Y} transgenic progeny, which is an important advantage for their future use as a large animal model.

2. Progressive diabetic phenotype in *INS*^{C94Y} transgenic pigs

2.1. Disturbed glycemic control in *INS*^{C94Y} transgenic pigs

The *INS*^{C94Y} transgenic founder boar 9747 as well as the *INS*^{C94Y} transgenic offspring exhibited blood glucose levels significantly exceeding the reference range specified for pigs (70-115 mg/dl depending on the laboratory) indicative of disturbed glucose homeostasis. *INS*^{C94Y} transgenic offspring became hyperglycemic within 24 hours after birth, reaching blood glucose levels over 400 mg/dl at the age of 115 days. Disturbance of β-cell function during the fetal period was unlikely as blood glucose concentrations were unaltered prior to the first colostrum ingestion but cannot be completely excluded. In neonatal humans suffering from PNDM blood glucose levels over 600 mg/dl were reported (Hutchison et al., 1962; Shield et al., 1997; Stoy et al., 2007). The clinical appearance of heterozygous Akita *Ins2*^{C96Y} mutant mice is in line with diagnostic findings relevant for the corresponding *INS*^{C94Y} transgenic pig model (Izumi et al., 2003; Wang et al., 1999). Male heterozygous Akita *Ins2*^{C96Y} mutant mice revealed significantly increased randomly fed blood glucose levels of 280 mg/dl at 4 weeks of age progressing steadily up to over 500 mg/dl, demonstrating the highly diabetogenic impact of one mutated *Ins2* allele in spite of the presence of one wild-type *Ins2* and two wild-type *Ins1* alleles in rodents (Wang et al., 1999; Yoshioka et al., 1997). Moreover, male heterozygous Munich *Ins2*^{C95S} mutant mice, which feature a point mutation in the *Ins2* gene disrupting the C95(A6)-C100(A11) intrachain disulfide bond, likewise developed significantly elevated blood glucose levels of more than 300 mg/dl, confirming the dominant-negative/toxic effect of the mutated *Ins2* allele on β-cell function (Herbach et al., 2007). However, heterozygous Akita *Ins2*^{C96Y} as well as heterozygous Munich *Ins2*^{C95S} mutant mice remained normoglycemic until the age of almost 4 weeks compared to wild-type controls (Herbach et al., 2007; Yoshioka et al., 1997). On the contrary, significantly elevated random blood glucose levels in *INS*^{C94Y} transgenic pigs were detectable within 24 hours postpartum. Both heterozygous Akita *Ins2*^{C96Y} and Munich *Ins2*^{C95S} mutant mice displayed a distinct gender dimorphism with a less pronounced diabetic phenotype in females,

explainable by the protective effect of estrogen on β-cells (Herbach et al., 2007; Louet et al., 2004; Schuster, 2011; Yoshioka et al., 1997). Untreated *INS*^{C94Y} transgenic pigs did not show any sex-related differences in the severity of diabetes and associated symptoms within the observation period of 4.5 months, potentially due to their sexual immaturity.

The fact that only one *INS*^{C94Y} transgenic founder boar (9747) became clinically diabetic, while the other six exhibited normoglycemia suggested a dose-dependent effect of mutant insulin due to different transgene expression levels. To proof this hypothesis and correct for the variation in β-cell content of arbitrarily taken pancreas specimens, the ratio of mutant *INS*^{C94Y} and endogenous *INS* cDNA amplicons was determined. Expression of *INS*^{C94Y} transcripts at a level of 75% of endogenous *INS* transcripts in pancreatic tissue of the diabetic *INS*^{C94Y} transgenic founder boar 9747 as well as in the transgenic offspring most likely contributed to the development of the distinct diabetic phenotype and was supposedly even sufficient to provoke hyperglycemia already in postnatal transgenic piglets, particularly as the total β-cell volume was initially unaltered. The positive correlation of *INS*^{C94Y} mRNA levels with the respective clinical picture approved the dose-dependent effect of mutant *INS*^{C94Y} gene expression.

Furthermore untreated 4.5-month-old *INS*^{C94Y} transgenic pigs exhibited significantly reduced fasting plasma insulin levels compared to non-transgenic littermates. Likewise, male heterozygous Akita *Ins2*^{C96Y} mice revealed a 60% reduction in immunoreactive plasma insulin levels compared to age- and sex-matched control mice at the age of seven weeks (Yoshioka et al., 1997). The molecular mechanism underlying insulin secretory failure in heterozygous Akita *Ins2*^{C96Y} mice has been intensively investigated and is based upon drastic steric rearrangement of the mutant proinsulin polypeptide abetted through disturbed integrity of the C96(A7)-C31(B7) intramolecular disulfide bond (Wang et al., 1999; Yoshinaga et al., 2005). Wild-type proinsulin molecules feature a hydrophobic core with non-polar amino acid residues kept inwardly (Baker et al., 1988; Mayer et al., 2007). Therefore mutant proinsulin is inclined to aggregate promoted through its increased hydrophobicity and incorrect disulfide pairing (Wang et al., 1999; Yoshinaga et al., 2005). Furthermore hydrophobic interaction with the molecular chaperone binding Ig protein (BiP) through fractionally exposed hydrophobic regions and an unpaired cysteine residue mediating

entrapment in the ER was depicted in mutant *Ins2*^{C96Y} transfected CHO cell lines (Wang et al., 1999). Effective secretion of synchronously expressed wild-type proinsulin molecules is also hampered due to the formation of covalent intermolecular protein complexes with highly reactive hydrophobic mutant proinsulin (Hodish et al., 2010; Liu et al., 2007; Park et al., 2010; Wang et al., 1999; Yoshinaga et al., 2005). Therefore, mutant misfolded proinsulin additionally retains wild-type insulin in the ER, acuminating ER-stress (Hodish et al., 2010). Despite early significant hyperglycemia, basal plasma insulin levels of randomly fed 8-day-old *INS*^{C94Y} transgenic pigs were almost unaltered compared to age-matched control piglets. Consonantly, untreated heterozygous Munich *Ins2*^{C95S} mice, regardless of gender, showed similar fasted and postprandial serum insulin levels compared to corresponding controls at the age of one month. However, after oral glucose challenge, serum insulin levels of Munich *Ins2*^{C95S} mice were significantly reduced in comparison to controls, demonstrating disturbed glucose-stimulated insulin secretion (Herbach et al., 2007). For that reason, consequences of glucose challenge need to be evaluated in postnatal *INS*^{C94Y} transgenic pigs to verify initial insulin secretory deficiency preceding absolute insulin deficiency through clinically relevant loss of functional β-cells.

Another factor contributing to the early onset of diabetes in *INS*^{C94Y} transgenic pigs may be an autocrine stimulatory influence of insulin on its own secretion through binding to the insulin receptor present on the surface of pancreatic β-cells. Besides glucose, autocrine insulin-stimulated exocytosis presumably assists the agitated first instance insulin release (Aspinwall et al., 1999; Borelli et al., 2004; Verspohl and Ammon, 1980). Moreover, there is increasing evidence that insulin biosynthesis is likewise translationally regulated through autocrine action of endogenous insulin mediated by the cytoplasmic tyrosine-kinase domain of insulin receptors of pancreatic β-cells (Hubbard, 2013; Lemmon and Schlessinger, 2010; Xu et al., 1998). *In vitro* studies using βTC-F7 cell lines and isolated pancreatic islets derived from male Sprague Dawley rats confirmed insulin-stimulated activating phosphorylation of PHAS-I (phosphorylated heat- and acid stable eIF-4E binding protein regulated by insulin I) bound to the eukaryotic translation initiation factor 4E in the unphosphorylated state in order to repress translation initiation (Xu et al., 1998). Thus a secondary

negative feedback on insulin secretion and biosynthesis emanated from absent autocrine stimulus may contribute to the inherently deficient insulin release in *INS*^{C94Y} transgenic pigs. In order to exemplify the existing disturbed β-cell function, homeostasis model of baseline insulin secretion index (HOMA-B) was determined by means of fasting plasma insulin and glucose levels reflective of the relationship between hepatic gluconeogenesis and insulin secretion in the fasting subject (Matthews et al., 1985; Turner et al., 1979). HOMA-B indices in 4.5-month-old *INS*^{C94Y} transgenic pigs were tremendously decreased by 96% in comparison to age-matched non-transgenic controls, indicating virtually no residual steady-state β-cell function. 20% remaining β-cell function has been referred to as the critical threshold of sufficient glycemic control (Turner et al., 1982). Significantly reduced HOMA-B indices were previously calculated for heterozygous Munich *Ins*^{C95S} mice from the earliest time point investigated (1 month), supporting our findings in *INS*^{C94Y} transgenic pigs (Herbach et al., 2007). Nevertheless, since HOMA-B index was developed for and validated only in humans, the data from animal models need to be considered with care (Wallace et al., 2004).

The homeostasis model assessment of insulin resistance index (HOMA-IR) according to Matthews et al. (1985) is a surrogate index to quantify insulin resistance *in vivo* largely correlating with the hyperinsulinemic euglycemic clamp technique in humans (DeFronzo et al., 1979; Lee et al., 2008; Wallace et al., 2004). Although defined for human metabolism, HOMA-IR indices have proven applicable to a certain degree in insulin resistant mice and revealed reasonable correlation to comparative glucose clamp studies (Lee et al., 2008). Thus, significantly elevated HOMA-IR indices in 4.5-month-old *INS*^{C94Y} transgenic pigs compared to age-matched wild-type controls most likely reflect accompanying insulin resistance. Dysregulation of glycemic control in type 2 diabetes mellitus is mainly expedited by obesity-induced peripheral and hepatic insulin resistance gradually triggering β-cell exhaustion and eventually overt diabetic symptoms (Johnson and Olefsky, 2013). The existence of autocrine feedback loops between insulin production, subsequent insulin secretion and percentage of endogenous insulin molecules bound to eligible receptors on pancreatic β-cells are supposed to implicate insulin resistance in lean, insulin-dependent subjects (Aspinwall et al., 1999). X-ray crystallography recently clarified the three-dimensional structure of

the insulin-insulin receptor complex and underlined importance of proper steric arrangement of the mature insulin molecule for receptor binding affinity (Menting et al., 2013). Absolute necessity of the three highly conserved disulfide bonds for stability of the secondary structure and in consequence for receptor binding affinity of the insulin molecule was emphasized by *in vitro* studies using mutants of human insulin, each lacking one of the three disulfide bonds (Chang et al., 2003). In addition, receptor binding affinity was barely detectable following A7-B7 disulfide deletion of the insulin polypeptide in yeast (Guo and Feng, 2001). Therefore altered binding affinity of mutant porcine C94Y insulin causing steric rearrangement due to the lack of the stabilizing C94(A7)-C31(B7) intramolecular disulfide linking would not be astonishing. *In vitro* studies using the β-cell line HIT-T15 concluded that chronic exposure to high glucose levels increases intracellular reactive oxygen species (ROS) and concurrently decreases *INS* promoter activity through downregulation of the pancreatic and duodenal homeodomain transcription factor 1 (PDX1) and pancreatic β-cell-specific transcriptional activator (MAFA), disturbing insulin expression on the transcriptional level (Houstis et al., 2006; Melloul et al., 1993; Robertson, 2004; Robertson et al., 1992; Sharma et al., 1995). As pancreatic islets are poorly featured with antioxidative defence mechanisms, oxidative stress is barely warded off (Robertson, 2004). Glucotoxicity has also been validated as underlying cause of insulin resistance in humans (Vuorinen-Markkola et al., 1992; Yki-Jarvinen et al., 1987). In accordance, hyperglycemic male heterozygous $Ins2^{C96Y}$ mutant mice exhibited peripheral insulin resistance, which could be rescued by phlorizin application lowering blood glucose levels. Glucose transporter 4 (*Glut4*) expression was found to be downregulated in these insulin-resistant mice and therefore presumably entangled in the pathogenesis of impaired peripheral insulin sensitivity in male heterozygous Akita $Ins2^{C96Y}$ mutant mice (Hong et al., 2007). Amelioration of insulin resistance in male heterozygous Munich $Ins2^{C95S}$ mutant mice through exogenous insulin supplementation places emphasis on glucotoxicity as determinant of insulin resistance (Kautz, 2011). On these grounds, impaired insulin sensitivity and glucose-stimulated insulin secretion involved in deficient glycemic control in untreated INS^{C94Y} transgenic pigs are presumably driven by chronically elevated blood glucose levels exerting chronic oxidative stress on pancreatic β-cells.

However *in vitro* studies awoke reasonable doubts if mutant proinsulin lacking C96(A7)-C31(B7) disulfide bond can be secreted by pancreatic β-cells at all or if a general failure of glucose-stimulated exocytosis impedes sufficient insulin secretion. For instance, transfected HEK293 cells expressing recombinant mutant C96Y proinsulin polypeptide, following site-directed mutagenesis of human proinsulin cDNA, revealed a drastically decreased secretion of mutant proinsulin compared to control HEK293 cells transfected with an expression vector for wild-type proinsulin. Moreover mutant proinsulin was very likely subjected to intracellular proteolysis (Colombo et al., 2008). The same observations were stated for CHO cell lines exhibiting retarded secretion of mutant proinsulin into the cell culture media after mutant *Ins2*^{C96Y} tranfection in comparison to wild-type *Ins2* tranfected CHO cells. Intracellular degradation of mutant proinsulin molecules was likewise supposed (Wang et al., 1999). Experiments using transfected 293T cells even ascertained completely absent secretion of ^{35}S-labeled mutant C96Y proinsulin (Liu et al., 2005). Transfected MIN6 mouse insulinoma cells expressing mutant C96Y proinsulin provided with a selectable green fluorescent protein (GFP) reporter in the C-peptide, showed undetectable GFP-C peptide levels indicating outright failure of endoproteolytic cleavage and exocytosis of the mutant variant (Rajan et al., 2010). So far, it remains to be clarified if the mutant porcine C94Y insulin is at all secreted from pancreatic β-cells of *INS*^{C94Y} transgenic pigs.

Hyperglucagonemia was found to be a concomitant phenomenon in insulin-deficient diabetic patients and is therefore likely to redound to the pathogenesis of diabetes mellitus through augmented hepatic glucose production (Quesada et al., 2008). Glucagon secretion was accelerated in chronically hyperglycemic patients presumably triggered by defective glucose sensing of α-cells and absent insulin repression (Gromada et al., 2007; Jacobson et al., 2009; Unger et al., 1970). Thus, hyperglycemic male heterozygous Munich *Ins2*^{C95S} mutant mice developed elevated randomly fed glucagon levels compared to mild hyperglycemic female heterozygous *Ins2*^{C95S} mutant mice and sex-matched normoglycemic wild-type mice, presumably worsening hyperglycemia by accelerating hepatic glucose supply. Paradoxically stimulated glucose-decoupled glucagon secretion in male heterozygous Munich *Ins2*^{C95S} mutant mice emphasizes potentially disturbed glucose sensing of α-cells in the context of chronically elevated blood glucose

levels as hyperglucagonemia was ameliorated by insulin treatment (Kautz, 2011; Salehi et al., 2006). Basal plasma glucagon levels in randomly fed 8-day-old *INS*^{C94Y} transgenic piglets and fasting plasma glucagon levels in 4.5-month-old *INS*^{C94Y} transgenic pigs were determined by radioimmunoassay and compared to the levels of age-matched non-transgenic control pigs. 8-day-old *INS*^{C94Y} transgenic pigs revealed noticeable higher randomly fed plasma glucagon levels than age-matched control littermates. Similarly, 4.5-month-old *INS*^{C94Y} transgenic pigs exhibited mild hyperglucagonemia in the fasting state compared to age-related controls. In both age groups effects were clearly visible but not significant, arguing against a dominant role of glucagon in the disturbed glucose homeostasis of *INS*^{C94Y} transgenic pigs. Furthermore large-scale comparative oral glucose tolerance tests in human type 2 diabetics demonstrated exceedingly decreased suppression of glucose-stimulated glucagon release during glucose challenge, despite unaltered fasting glucagon levels in these probands (Abdul-Ghani and DeFronzo, 2007). Therefore the relative changes of plasma glucagon levels during glucose challenge may enlighten the actual contribution of glucagon signaling in maintaining hyperglycemia in *INS*^{C94Y} transgenic pigs.

In conclusion, the disturbed glycemic control in *INS*^{C94Y} transgenic pigs is triggered by a complex interaction of pathogenetic factors finally acuminating in the progressive diabetic phenotype observed in these pigs. Chronic hyperglycemia in *INS*^{C94Y} transgenic pigs seems to be based upon the dominant-negative/toxic effect of *INS*^{C94Y} transgene expression impeding adequate glucose-stimulated insulin secretion. Furthermore accompanying peripheral insulin resistance presumably contributes to the pathogenesis of disturbed glycemic control in *INS*^{C94Y} transgenic pigs. With increasing age, the progressive loss of functional β-cells is a factor to be taken into account. The *INS*^{C94Y} transgenic pig model reflects clinical features and underlying disease mechanisms previously demonstrated in diabetic *Ins2* mutant mice. Beyond diabetic rodents, characteristics of human permanent neonatal diabetes have been observed and validated in *INS*^{C94Y} transgenic pigs.

2.2. Growth retardation in *INS*^{C94Y} transgenic pigs

Intrauterine growth retardation (IUGR) and reduced birth weights are characteristic clinical features of humans born with PNDM attributed to the absence of insulin *in utero* as fetal growth factor (Cave et al., 2000; Polak and

Cave, 2007). In contrast, *INS*^{C94Y} transgenic pigs did not exhibit reduced growth compared to non-transgenic littermates until weaning. This discrepancy possibly resulted from different fetal growth kinetics throughout gestation between pigs and humans. In the pig, the highest fetal growth rates are observed around birth, whereas the main fetal growth phase in humans is almost completed within 30 to 36 weeks and potentially declines thereafter. (Litten-Brown et al., 2010). The onset of endogenous mutant *INS* expression in humans might differ from onset of *INS*^{C94Y} transgene expression in the fetal pig and eventually falls in this sensitive phase during late gestation. After weaning, untreated *INS*^{C94Y} transgenic pigs exhibited reduced growth rates resulting in a significantly decreased body weight at the age of 4.5 months as compared to wild-type littermates. Impaired growth was also observed in male heterozygous Akita *Ins2*^{C96Y} mutant mice indicating a detrimental influence of *Ins2*^{C96Y} expression on weight gain (Yoshioka et al., 1997). Furthermore, these findings are concordant with decelerated growth of prepuberal children diagnosed with diabetes mellitus and receiving insufficient glycemic control (Edelsten et al., 1981; Jackson, 1984; Salardi et al., 1987; Tattersall and Pyke, 1973). An important aspect of growth disturbance in hypoinsulinemic subjects is the incompetence of sufficient glucose uptake implicating consecutive cellular glucose deprivation and limiting anabolic processes including linear bone growth (Bereket et al., 1995; reviewed in Martin et al., 1984). Furthermore an absolute insulin deficiency impinges growth upon regulation of the growth hormone (GH)-insulin-like growth factor (IGF) system as already clarified in diabetic mice. Therefore decreased hepatic growth hormone (GH) receptor density and decreased levels of insulin-like growth factor I (IGF-I) were found in poorly controlled diabetic patients (Bereket et al., 1995; Bereket et al., 1999; Clayton et al., 1994; Maes et al., 1986; Strasser-Vogel et al., 1995). However, the remarkable 41% reduction of the body weight in 4.5-months-old *INS*^{C94Y} transgenic pigs compared to non-transgenic controls suggests that the effect of reduced insulin secretion on weight gain and linear growth is exceptionally remarkable in a thriving species like the pig, reflecting conditions during the pubertal growth spurt in humans. Accordant with the reversal of growth delay by adequate insulin therapy in adolescent humans, *INS*^{C94Y} transgenic pigs could be likewise rescued from growth retardation by exogenous insulin supplementation, emphasizing the role of insulin as anabolic promoter of juvenile growth (Bereket et al., 1999; Rudolf et al., 1982). As insulin

is directly involved in osteoblastogenesis and bone mineralization, alterations of skeletal architecture related to insulin-deficiency are frequently diagnosed even in young diabetic patients (Engelhart and G., 2010; Gunczler et al., 1998; reviewed in Thrailkill et al., 2005; Santiago et al., 1977; Wiske et al., 1982). Therefore impact of *INS*^{C94Y} transgene expression on bone growth and composition in adolescent pigs needs to be clarified.

2.3. Evidence for endoplasmic reticulum stress in *INS*^{C94Y} transgenic pigs

To elucidate the involvement of endoplasmic reticulum stress in the pathogenesis of mutant *INS*^{C94Y} gene-induced diabetes mellitus in *INS*^{C94Y} transgenic pigs, the abundance of endoplasmic reticulum stress markers CCAAT/enhancer-binding protein (C/EBP) homologous protein 10 (CHOP-10), phosphorylated eukaryotic translation initiation factor 2α (PeIFα) and binding Ig protein (BiP) was evaluated in isolated pancreatic islets derived from a neonatal *INS*^{C94Y} transgenic piglet and a corresponding non-transgenic control piglet. Three independently sonicated islet lysates of an *INS*^{C94Y} transgenic piglet and a non-transgenic control were used in each case in default of further viable islet samples after isolation process. Due to the limited number of animals being investigated, the data were not statistically evaluated. Islet isolation yielded physiological age-appropriate islet-like cell clusters from the neonatal *INS*^{C94Y} transgenic piglet as well as from the age-matched wild-type control piglet respectively. Western blot analyzes regarding the abundance of ER stress markers in neonatal *INS*^{C94Y} transgenic pigs may serve as first appraisement, but need to be interpreted carefully. Hence, the protocol for Western immunoblot analyzes has been proven applicable for porcine tissue. The proapoptotic ER stress marker CHOP-10 was found to be twofold increased in islet lysates of the *INS*^{C94Y} transgenic piglet compared to those of the age-matched wild-type control piglet, whereas PeIF2α and BiP were roughly unaltered compared to corresponding control islet sonicates. Accumulation of irreversibly misfolded mutant proinsulin polypeptides in the luminal space of the endoplasmic reticulum initiates a complex adaptive signaling pathway to overcome advancing accumulation of client polypeptides on the translational and transcriptional level anticipating chronic stress on the ER (Araki et al., 2003; Eizirik et al., 2008). The unfolded protein response pathway (UPR) is a balancing act between cell survival and cell demise mainly regulated by the stress-regulated transcription factors

IRE1α, PERK and ATF6, kept in the inactive state through complexing with the molecular chaperone BiP (Bertolotti et al., 2000; Harding et al., 1999; Haze et al., 2001; Scheuner and Kaufman, 2008; Shi et al., 1998; Tirasophon et al., 1998; Wu et al., 2007). Beyond functioning as ER sensing determinant, BiP binds folding intermediates and facilitates retention of unfolded substrates in the secretory pathway exerting for complete folding (Araki et al., 2003; Flynn et al., 1989). Therefore, BiP was found to be upregulated upon ER stress in pancreatic islets of human type 2 diabetic subjects in comparison to non-diabetic controls indicated by specifically increased immunostaining intensity (Laybutt et al., 2007). Furthermore mutant proinsulin 2 revealed increased propensities to constitute intermolecular protein complexes within the enlarged ER lumen of islets isolated from heterozygous Akita *Ins2*^{C96Y} mutant mice implying BiP, which was therefore markedly upregulated (Allen et al., 2004; Wang et al., 1999). In contrast, induction of BiP expression was unexpectedly not observed in pancreatic islet protein lysates of untreated heterozygous Munich *Ins2*^{C95S} mutant mice (Kautz, 2011). Convincing conclusions concerning abundance of BiP in pancreatic islets of *INS*^{C94Y} transgenic pigs might be drawn through analyzes of a statistically relevant number of respective pigs. Activated PERK mediates ER stress-induced mRNA translation attenuation in order to adjust new protein synthesis to the instantaneous functional capacity of the ER by phosphorylation of the eukaryotic initiation factor 2 α (Harding et al., 1999; Samuel, 1993; Shi et al., 1998; Vachon et al., 1990). Phosphorylated eIF2α lacks the ability to interconnect with the translation initiator methionyl tRNA (Met-RNA) and to bind to the 40S ribosomal subunit preventing translation initiation of client mRNAs (de Haro et al., 1996; Harding et al., 2000; Pain, 1996; Samuel, 1993). Upregulated PeIF2α associated with curtailed new protein synthesis was not detected in heterozygous Munich *Ins2*^{C95S} mutant mice compared to control mice (Kautz, 2011). *In vitro* studies using a transfected CHO cell lineage expressing *Ins2*^{C96Y} mutant gene revealed likewise unchanged protein biosynthesis activity compared to control CHO cells expressing wild-type *Ins2*. Thus, expression of *Ins2*^{C96Y} mutant gene might presumably not interfere with protein biosynthesis *in vivo* (Izumi et al., 2003). On these grounds unaltered ratio of PeIF2α in neonatal *INS*^{C94Y} transgenic pigs compared to age-related wild-type control pigs could be possible but needs to be further elucidated. Sustained and insuperable endoplasmic reticulum stress

induces programmed cell death successively acuminating in disturbed tissue function (Kaufman, 2002; Kim et al., 2008; Szegezdi et al., 2006; van der Kallen et al., 2009). Overexpression of CHOP-10 is tightly linked to the initiation of apoptosis in response to chronic ER stress (Marciniak et al., 2004; Oyadomari and Mori, 2004; Zinszner et al., 1998). Heterozygous Akita *Ins2*^{C96Y} mutant mice revealed markedly increased *Chop* mRNA levels compared to corresponding wild-type mice indicating initiation of ER stress-induced apoptosis in pancreatic β-cells and corroborating the dominant-negative/toxic effect of *Ins2*^{C96Y} expression in these mice (Oyadomari et al., 2002). In contrast, in double-mutant heterozygous Akita *Ins2*^{C96Y} mutant mice, additionally bearing a heterozygous or homozygous disrupted *Chop* gene, progression of diabetic symptoms was specifically decelerated or even prevented (Oyadomari et al., 2002). In general, *Chop*-null mutation was shown to ameliorate severe β-cell dysfunction in a variety of rodent models of diabetes (Song et al., 2008). The optical density of CHOP-10/β-actin was significantly increased in islet sonicates of untreated male heterozygous Munich *Ins2*^{C95S} mutant mice compared to corresponding controls, indicating ER stress mediated CHOP-10-induced apoptosis of β-cells (Kautz, 2011). Therefore, the high-level expression of mutant *INS*^{C94Y} gene in the *INS*^{C94Y} transgenic pig model and the supposedly interminable accumulation of misfolded mutant proinsulin polypeptides in the ER is likely to gradually culminate in β-cell apoptosis following exhaustion of the compensatory abilities of the UPR by chronic ER stress. This presumption is underlined by a considerable increase in the optical density of CHOP-10/β-actin in isolated islets of the *INS*^{C94Y} transgenic piglet compared to those of the age-related control piglet.

Preliminary findings achieved by Western blot analysis of ER stress markers in isolated pancreatic islet of *INS*^{C94Y} transgenic pigs and respective control pigs are in line with the results of immunohistochemistry as well as electron microscopy of β-cells revealing insulin deficiency and drastic ER stress-induced β-cell demise. Therefore ER stress in pancreatic β-cells, likely triggering apoptosis of respective perturbed cells, might be a conceivable corollary of *INS*^{C94Y} transgene expression and in most instances responsible for the restrained insulin supply and full-blown clinical diabetes mellitus in these pigs. A larger cohort of *INS*^{C94Y} transgenic pigs and corresponding controls imperatively needs to be investigated to achieve reliable results in this case.

3. Morphological consequences of *INS*^{C94Y} transgene expression

3.1. Altered cellular composition of the endocrine pancreas in 4.5-month-old *INS*^{C94Y} transgenic pigs

Pancreata of 8-day-old *INS*^{C94Y} transgenic pigs and 4.5-month-old *INS*^{C94Y} transgenic pigs were investigated by means of immunohistochemistry and quantitative stereological analyzes using state-of-the-art unbiased model-independent stereological methods (Gundersen et al., 1988; Gundersen and Jensen, 1987; Wanke, 1994).

Pancreatic sections of 8-day-old *INS*^{C94Y} transgenic pigs and age-matched non-transgenic controls were stained for insulin containing β-cells and revealed homogeneously evenly distributed single β-cells and small islet-like cell clusters of constant staining intensity. The qualitative histological findings were confirmed by an almost identical volume density of β-cells ($Vv_{(\beta\text{-cell/Pan})}$) and an unaltered total β-cell volume ($V_{(\beta\text{-cell, Pan})}$) of the endocrine pancreas of 8-day-old *INS*^{C94Y} transgenic pigs in comparison to age-matched wild-type pigs. This is in line with insights achieved in sex-matched postnatal heterozygous Akita *Ins2*^{C96Y} mutant mice exhibiting unaltered insulin-positive areas suggesting postnatal disturbance of β-cells (Kayo and Koizumi, 1998; Liu et al., 2010). However, alterations of the ultrastructural architecture of β-cells were already noticeable in heterozygous Akita *Ins2*^{C96Y} mutant mice (Kayo and Koizumi, 1998; Liu et al., 2010) as well as in *INS*^{C94Y} transgenic pigs at this early postnatal stage. However, *INS*^{C94Y} transgenic pigs already exhibited severe hyperglycemia in contrast to still normoglycemic heterozygous Akita *Ins2*^{C96Y} mutant mice (Kayo and Koizumi, 1998).

Double immunohistochemical staining of pancreatic tissue of 4.5-month-old *INS*^{C94Y} transgenic pigs and age-matched non-transgenic littermate controls visualizing insulin-positive β-cells on the one hand and glucagon, somatostatin as well as pancreatic polypeptide containing cells, referred to as non-β-cells, on the other hand revealed markedly altered islet composition in the transgenic pigs. Compared to age-matched non-transgenic control pigs, pancreas sections of 4.5-month-old *INS*^{C94Y} transgenic pigs comprise visibly less insulin-positive cells with notably weaker staining intensity suggesting decreased insulin content within the

β-cells. This is in line with a highly reduced number of insulin secretory granules in the cytoplasm of pancreatic β-cells of 4.5-month-old *INS*^{C94Y} transgenic pigs compared to non-transgenic control pigs ascertained by means of electron microscopy. Mainly scattered single β-cells, small β-cell clusters and at most medium-sized islets were observed in the endocrine pancreas of 4.5-month-old *INS*^{C94Y} transgenic pigs, whereas wild-type pigs revealed typical large, irregularly shaped pancreatic islets with a core of insulin-positive cells surrounded by a narrow mantle of non-β-cells. Quantitative stereological examination of the endocrine compartment of the pancreas of 4.5-month-old *INS*^{C94Y} transgenic pigs and corresponding non-transgenic littermates revealed a significant 54% reduction of the volume density of β-cells in the pancreas ($Vv_{(\beta\text{-cell/Pan})}$) in the transgenic pigs, therefore representing less than 0.5% volume fraction of the pancreas. The visual perception of successive β-cell abatement received in *INS*^{C94Y} transgenic pigs at the age of 4.5 months was quantitatively accredited by a 72% reduction of the total β-cell volume ($V_{(\beta\text{-cell, Pan})}$) in comparison to non-transgenic controls. Due to the significantly lowered absolute pancreas weights correlative with the remarkable overall growth deceleration, the total β-cell volume related to body weight ($V_{(\beta\text{-cell, Pan})}$/BW ($mm^3$/kg)) was reduced by only 53% and therefore proportionately lower compared to $V_{(\beta\text{-cell, Pan})}$. As insulin staining was used to identify β-cells and a large number of β-cells of *INS*^{C94Y} transgenic pigs were extensively degranulated, underestimation of the proportion of β-cells in the endocrine pancreas of 4.5-months-old *INS*^{C94Y} transgenic pigs needs to be considered. In accordance, the volume fraction of insulin-positive cells in the islets was diminished by approximately 90% in proportion to an unaltered relative area of islets in the endocrine pancreas of male heterozygous Akita *Ins2*^{C96Y} mutant mice compared to age- and sex-related control mice at the age of 30 weeks (Yoshioka et al., 1997). The total β-cell volume ($V_{(\beta\text{-cell, Islet})}$) in the pancreatic islets and the volume density of β-cells in the islets ($Vv_{(\beta\text{-cell/Islet})}$) of hyperglycemic, male heterozygous Munich *Ins2*^{C95S} mutant mice were significantly decreased by around 80% compared to corresponding control mice (Herbach et al., 2007). Rodents feature the capability of extensive β-cell regeneration. In comparison to humans and pigs, where β-cell replication plays a minor role, β-cell content in the rodent pancreas is much more dynamically regulated and on demand through proliferation, neogenesis and apoptosis

(Bonner-Weir, 2000; Bonner-Weir et al., 1983; Butler et al., 2003; Chick and Like, 1970; Finegood et al., 1995; Menge et al., 2008; Tyrberg et al., 2001). Nevertheless a decrease in β-cell mass by 50% was stated to effectually decrease insulin supply accompanied by impaired glucose tolerance and even overt hyperglycemia in pigs and in humans (Butler et al., 2003; Kendall et al., 1990; Kjems et al., 2001; Kloppel et al., 1985; Renner et al., 2010). Several *in vivo* and *in vitro* studies certificated a pro-apoptotic effect of long-standing hyperglycemia on pancreatic β-cells devoid of compensatory β-cell proliferation and neogenesis. Vice versa successive diminishment of residual β-cell exert detrimental impact on glycemic control (Donath and Halban, 2004; Kaiser et al., 2003). Although feasible stereological data of the human pancreas are rare due to restricted availability of adequate human pancreatic tissue from postmortem examinations, there is a clear agreement, that overt hyperglycemia in humans suffering from type 2 diabetes mellitus is attended or rather initiated by a reduced percentage of functional β-cells compared to non-diabetic controls aggravating with increasing body mass index (Butler et al., 2003; Cnop et al., 2005; Kloppel et al., 1985; Yoon et al., 2003). Furthermore viability of isolated islets from human donors impinged upon high glucose dosage, mimicking diabetic conditions and a considerable higher fraction of apoptotic cells was detected compared to culture conditions at a normal glucose concentration (Federici et al., 2001; Maedler et al., 2008). In addition high glucose-induced oxidative stress was found to be deleteriously effective on β-cell survival and could therefore account for β-cell apoptosis in severe diabetic INS^{C94Y} transgenic pigs (Ihara et al., 1999; Kaiser et al., 2003; Laybutt et al., 2002). Perpetual ER stress is very likely to represent another determinant of significantly reduced total β-cell volume in the pancreas of INS^{C94Y} transgenic pigs. As described above, hydrophobic mutant proinsulin is presumably prone to accumulate within the ER of INS^{C94Y} transgenic pigs and may provoke chronic ER-stress through activation of the unfolded protein response ultimately triggering progressive β-cell demise via programmed cell death.

Furthermore 4.5-month-old INS^{C94Y} transgenic pigs and corresponding age-related non-transgenic control pigs underwent a single immunohistochemical staining detecting glucagon-positive α-cells. Histological pancreas sections were evaluated for presence of a compensatory increase in the percentage of glucagon-producing

α-cells. As underlined by the qualitative histological appearance, the total α-cell volume in relation to body weight ($V_{(\alpha\text{-cell, Pan})}$/BW) revealed a twofold but not yet significant increase in *INS*^{C94Y} transgenic pigs compared to age-matched non-transgenic controls, indicating a visible trend of compensatory enlargement of functional α-cell volume fraction in the transgenic pigs. The total α-cell volume ($V_{(\alpha\text{-cell, Pan})}$) in the pancreas of 4.5-month-old *INS*^{C94Y} transgenic pigs was almost unaltered compared to corresponding wild-type controls explainable by the significantly reduced body weight and the correspondingly decreased absolute pancreas weights in the transgenic pigs. Pancreata of human donors diagnosed with type 2 diabetes mellitus in their lifetime, correspondingly revealed a twofold increase in the relative α-cell volume (Yoon et al., 2003). An almost threefold increased proportion of glucagon-positive area was found in the islets of heterozygous Akita *Ins2*^{C96Y} mutant mice compared to sex-matched wild-type controls in fact one day postpartum onwards (Kayo and Koizumi, 1998). In islets of untreated male heterozygous Munich *Ins2*^{C95S} mutant mice the total volume of non-β-cells was notably increased compared to related wild-type mice (Kautz, 2011). On equal term with the extensive β-cell replication in response to hyperglycemia, the higher percentage increase of the functional α-cell fraction in diabetic rodents is likewise ascribed to the generally higher regeneration potency in rodents (Butler et al., 2003; Menge et al., 2008). Indeed, the increase in the total volume of non-β-cells in untreated male heterozygous Munich *Ins2*^{C95S} mutant mice was chiefly represented through expansion of the total α-cell volume (Herbach et al., 2007). Therefore stereological investigations on α-cell turnover in response to progressive β-cell demise in humans and in diabetic *Ins2* mutant mice accredited that α-cell expansion is a regularly observed phenomenon following dramatic β-cell loss in humans and in mice, presumably contributing to paradoxically glucose-decoupled hyperglucagonemia in diabetic subjects (Herbach et al., 2007; Kautz, 2011; Kayo and Koizumi, 1998; Rahier et al., 1983; Yoon et al., 2003). As already mentioned, chronic exposure to high glucose concentrations is implicated in the transcriptional downregulation and disturbed biological activity of pancreatic and duodenal homeodomain transcription factor 1 (PDX-1) (Harmon et al., 1999; Sharma et al., 1995). Reduced *Pdx-1* mRNA levels were shown to increase the volume density of glucagon-positive cells in transgenic mice (Harmon et al., 1999; Lottmann et al.,

2001; Sharma et al., 1995). Furthermore, *in vitro* studies using eagerly differentiating rat insulinoma INSrβ cells affirmed the assumption that suppression of *Pdx-1* expression leads to the development of an α-cell-specific phenotype in a previously insulin producing β-cell lineage, indicated by increased glucagon mRNA levels and attenuation of *Ins* gene transcription. Opposed results were achieved by *Pdx-1* overexpression in these cells facilitating insulin biosynthesis and maturation of insulin granules (Wang et al., 2001). On these grounds, slightly increased total α-cell volume in relation to body weight ($V_{(\alpha\text{-cell, Pan})}$/BW) and the trend of increased fasting plasma glucagon levels in 4.5-month-old INS^{C94Y} transgenic pigs compared to age-matched non-transgenic controls might be based on a moderate, incremental shift of progenitor cells towards α-cell differentiation triggered by chronic hyperglycemia present in these pigs. Further investigations are needed on this complex issue.

3.2. Altered ultrastructural architecture of pancreatic β-cells in INS^{C94Y} transgenic pigs

To evidence pathological impact of INS^{C94Y} transgene expression on the ultrastructural architecture of pancreatic β-cells, pancreatic tissue of 8-day-old and 4.5-month-old INS^{C94Y} transgenic pigs was subjected to transmission electron microscopy. Despite quantitative stereological evaluation on immunohistochemically stained pancreatic sections of pancreatic tissue of 8-day-old INS^{C94Y} transgenic pigs revealed an unaltered volume density of insulin-positive cells ($Vv_{(\beta\text{-cell/Pan})}$), an unaltered total volume of insulin-positive cells ($V_{(\beta\text{-cell, Pan})}$) and a similar staining intensity of insulin-positive cells in comparison to age-related wild-type pigs, ultrastructural correlates of β-cell disturbance were already evident. At the age of 8 days, the number of insulin secretory granules appeared to be moderately decreased compared to age-matched controls but granules were still present in a considerable quantity suggesting still satisfactory but successively abating trafficking of proinsulin molecules and maturation of insulin secretory granules. This is also in line with the unaltered randomly fed basal plasma insulin levels compared to related non-transgenic controls at this age. Hyperglycemia in 8-day-old INS^{C94Y} transgenic pigs might therefore arise from disturbed glucose-induced insulin secretion. However, dilation of the endoplasmic reticulum was already present in 8-day-old INS^{C94Y} transgenic pigs indicating early disturbance of endoplasmic reticulum integrity and already

initiated impairment of the secretory pathway of pancreatic β-cells at this early stage. In accordance, sex-matched heterozygous Akita *Ins2*^{C96Y} mutant mice showed relevant structural alterations of pancreatic β-cells on the electron microscopic level including remarkable enlargement of the endoplasmic reticulum and partial degranulation, whereas stereologically determined insulin-positive and relative islet area were initially unaltered compared to corresponding control mice (Kayo and Koizumi, 1998; Liu et al., 2010). In 4.5-month-old *INS*^{C94Y} transgenic pigs ultrastructural changes of the β-cell architecture were more pronounced. The highly reduced number of insulin secretory granules in the cytoplasm of pancreatic β-cells in 4.5-month-old *INS*^{C94Y} transgenic pigs is likely responsible for the weaker staining intensity of insulin-positive cells on immunhistochemically stained pancreas sections of respective pigs. Pancreatic β-cells of heterozygous Munich *Ins2*^{C95S} mutant mice were correspondingly almost devoid of insulin secretory granules or contained few remaining secretory granules of altered size and organization (Herbach et al., 2007; Kautz, 2011). Diminished density of insulin secretory granules was also stated for heterozygous Akita *Ins2*^{C96Y} mutant mice (Wang et al., 1999; Zuber et al., 2004). Additionally, the transcripts of E3 ubiquitin-protein ligase 3-hydroxy-3-methylglutaryl-coenzyme (HMG-coA) reductase degradation 1 (*Hrd1*), an orthologue of yeast *Hrd1p* imperatively involved in ER-stress associated degradation (ERAD) of misfolded proteins, was found to be upregulated in pancreatic islets of heterozygous Akita *Ins2*^{C96Y} mutant mice likely contributing to protective degradation of misfolded mutant proinsulin 2 of Akita mice in an endeavour to decrease the load on the ER (Allen et al., 2004; Kaneko et al., 2002; Kikkert et al., 2004; Nadav et al., 2003). For that reason mutant proinsulin could likewise be partially degraded in pancreatic β-cells of *INS*^{C94Y} transgenic pigs and not be efficiently delivered to secretory granules. This might also account for reduced density of secretory granules in β-cells of *INS*^{C94Y} transgenic pigs. Indeed, the previously quoted hypothesis of decreased insulin content within the β-cells of 4.5-month-old *INS*^{C94Y} transgenic pigs based upon disturbed insulin biosynthesis is supported by relevant morphological alteration. Conspicuous distension of the rough endoplasmic reticulum, characterized by vacuole-like appearance, was incessantly observed in β-cells of heterozygous Akita *Ins2*^{C96Y} mutant mice as well as in heterozygous Munich *Ins2*^{C95S} mutant mice, progressing with increasing

age and was associated with drastic impairment of the secretory pathway in these *Ins2* mutant mice (Herbach et al., 2007; Izumi et al., 2003; Kautz, 2011; Wang et al., 1999; Zuber et al., 2004). Further, accumulated proinsulin 2 was *de facto* identified in the lumen of the ER by immunogold-labeling of pancreatic β-cells of Akita mice (Wang et al., 1999; Zuber et al., 2004). Endoplasmic reticulum of 4.5-month-old INS^{C94Y}transgenic pigs appeared to be seriously enlarged. Numerous cross-sectional profiles of the ER appeared to completely fill the cytoplasm of pancreatic β-cells of 4.5-month-old INS^{C94Y}transgenic pigs superseding insulin secretory granules in representative age-related wild-type control pigs. The suspicion of severe ER dysfunction based upon ER stress triggered by mutant C94Y proinsulin entrapped in the early secretory compartment of pancreatic β-cells in INS^{C94Y} transgenic pigs seems to be substantiated.

3.3. Diabetes-associated secondary alterations in INS^{C94Y} transgenic pigs

Histology, quantitative stereological methods and functional analyzes were applied in order to evaluate longstanding complications of mutant INS^{C94Y} gene-induced diabetes mellitus on diverse organs of INS^{C94Y} transgenic pigs. As a result of stagnant growth indicating detrimental influence of INS^{C94Y} transgene expression on weight gain, absolute weights of most organs were proportionately decreased in untreated INS^{C94Y} transgenic pigs at the age of 4.5 months in comparison to age-matched non-transgenic control pigs. Thus, relative organ weights (% of body weight) with a few exceptions were almost unaltered compared to corresponding controls. By way of an exception, the relative liver weights of untreated 4.5-month-old INS^{C94Y} transgenic pigs were significantly higher than those of age-related non-transgenic pigs. Hepatomegaly is a well-known complication in poorly controlled juvenile-onset human diabetics (Chatila and West, 1996; Sayuk et al., 2007; Torres and Lopez, 2001). Chronically elevated blood glucose levels gradually cause hepatocellular glycogen deposition as a result of insulin-independent hepatocellular entry of glucose, whereby hepatic glycogen production and storage is stimulated despite insulin-deficiency (Carcione et al., 2003; Evans et al., 1955; Torbenson et al., 2006; Torres and Lopez, 2001). Further complicating matters, glycogenolysis is decelerated by high blood glucose levels further raising hepatocellular glycogen levels and distending hepatocytes (Chatila and West, 1996; Sayuk et al., 2007; Stone and Van Thiel, 1985). Hepatic steatosis as a cause of hepatomegaly in humans with diabetes

mellitus is mainly ascribed to obese patients diagnosed with type 2 diabetes mellitus accompanied by peripheral insulin resistance and hypertriglyceridaemia (Clark and Diehl, 2002; Toledo et al., 2006). As hepatic steatosis is rare with type 1 diabetics of normal weight, hepatic glycogenosis is more likely to contribute to the modest hepatomegaly observed in non-obese 4.5-month-old INS^{C94Y} transgenic pigs (Torbenson et al., 2006). Accomplishment of glycogen staining detecting glycogen deposits in liver tissue might offer valuable clues about the origin of elevated liver weights in INS^{C94Y} transgenic pigs in comparison to related controls.

Whereas absolute weights of most organs revealed an at least 30% reduction compared to age-matched non-transgenic controls, cumulative absolute kidney weights in 4.5-month-old INS^{C94Y} transgenic pigs were diminished by only 15% as a notable exception. In consequence, cumulative kidney weights as percent of body weight were significantly increased in 4.5-month-old INS^{C94Y} transgenic pigs compared to non-transgenic littermate controls. Moreover, planimetric measurements of the mean glomerular profile areas on kidney tissue of 4.5-month-old INS^{C94Y} transgenic pigs and age-matched non-transgenic controls evinced a significant increase of the mean glomerular volume to body weight ratio ($V_{(glom)}$/BW) by 30% on the average. Renal and glomerular hypertrophy was also found in humans diagnosed with diabetes mellitus as an early pathological indicator of diabetic kidney disease (Cortes et al., 1987; Mahimainathan et al., 2006; Mogensen et al., 1983; Osterby and Gundersen, 1975; Seyer-Hansen et al., 1980). In correspondence, heterozygous male Munich $Ins2^{C95S}$ mutant mice revealed elevated kidney weights in comparison to associated wild-type controls as well as insulin-treated mutants. Diabetes-associated pathological alterations of the kidney have not been investigated in the Munich $Ins2^{C95S}$ mouse model so far (Kautz, 2011). Transgenic mice expressing a dominant-negative glucose-dependent insulintropic polypeptide receptor ($GIPR^{dn}$) demonstrated significantly increased kidney weights progressing with increasing age in comparison to age- and sex-matched control mice. Diabetic $GIPR^{dn}$ transgenic females were diagnosed with renal hypertrophy at 8 weeks of age, followed by detection of pronounced glomerular alterations at 20 weeks of age. Therefore early phase of diabetic kidney disease is recapitulated in this model (Herbach et al., 2009). Whereas $GIPR^{dn}$ transgenic mice developed pronounced changes in the

tubulointerstitial and glomerular architecture accompanied by remarkable albuminuria through podocyte abnormalities directly linked to high glucose level-induced damage of renal tissue (Herbach et al., 2009), histopathological examination of renal tissue from 4.5-month-old *INS*^{C94Y} transgenic pigs did not provide evidence for diabetes-associated kidney disease. Furthermore glomerular cross section profiles of *INS*^{C94Y} transgenic pigs did not indicate evidence for podocyte injury. Consequently it was not surprising that *INS*^{C94Y} transgenic pigs did not show albuminuria at any time point investigated. Although renal and glomerular hypertrophy was regularly observed in heterozygous Akita *Ins2*^{C96Y} mutant mice, pathological alterations were rarely detectable and mild (Gurley et al., 2006; Gurley et al., 2010). A thickening of the glomerular basement membrane reliably indicates early-stage diabetes-associated renal disease in mice (Herbach et al., 2009). However, transmission electron microsopy of peripheral glomerular capaillary loops detected an unaltered true harmonic mean thickness of the glomerular basement membrane in *INS*^{C94Y} transgenic pigs compared to respective non-transgenic control pigs at the age of 4.5 months. In human diabetes patients, thickening of the glomerular basement membrane necessitates years of progression until morphological alterations become detectable and even more until diabetes-induced nephropathy becomes clinically relevant. Moreover, the course of the disease can be decelerated by adequate insulin treatment (Mason and Wahab, 2003; Mogensen et al., 1983; Pagtalunan et al., 1997; Wolf, 2004). Therefore, it is not surprising that *INS*^{C94Y} transgenic pigs did not demonstrate morphological alterations diagnostic for diabetic nephropathy within the observation period. Studies on Munich-Wistar rats with streptozotocin-induced diabetes mellitus and non-diabetic control rats have shown that chronic hyperglycemia was solely not enough to induce and advance glomerular kidney injury (Zatz et al., 1985). Therefore complicating factors including high-protein diet or elevated blood pressure might be able to initiate and expedite diabetic kidney lesions in *INS*^{C94Y} transgenic pigs.

Periperal sensorimotor and autonomic polyneuropathy, mainly affecting myelinated nerve fibers, are well-known complications of sustained uncontrolled diabetes mellitus in humans (Mizisin et al., 2007). However, histology on semithin section as well as single fiber teasing of tibial nerve fascicles of *INS*^{C94Y} transgenic pigs and non-transgenic control pigs revealed homogenous,

physiological myelinization unsuggestive of axonal degeneration. Accordingly, histological examinations on transverse sections of sciatic nerve fascicles of diabetic male heterozygous Akita *Ins2*^{C96Y} mutant mice and non-diabetic control mice likewise did not show any indications for diabetes-induced nerve pathology (Yaguchi et al., 2003). In humans, emergence of diabetes-induced peripheral polyneuropathy is directly linked to the duration of chronic hyperglycemia (Tesfaye et al., 2005). Thus, development of chronic diabetic sensorimotor polyneuropathy in *INS*^{C94Y} transgenic pigs is presumably highly time-dependent and may occur with increasing age.

Similar to human, progressive cataract of the eye lenses was regularly observed in *INS*^{C94Y} transgenic pigs attended by vision impairment in all likelihood (Stefek and Karasu, 2011). Since incipient cataract was already present at 8 days of age, diabetic cataract formation seems to be rather a matter of the severity of hyperglycemia than a matter of the duration of the exposure to high blood glucose levels. This hypothesis was confirmed as lens opacification was reversible with insulin therapy and reconstitution of physiological glycemic conditions in *INS*^{C94Y} transgenic pigs. Since excessive amounts of glucose are supplied to the aqueous humor in response to chronic hyperglycemia, a high percentage is subjected to the polyol pathway and converted to sorbitol through aldose reductase action. Sorbitol accumulation triggers detrimental rearrangement of collagen fibers by increased osmotic water consumption into the lens and ultimately lens opacity (Kinoshita et al., 1979; Petrash, 2004). This mechanism was clearly enlightened by the protective pharmaceutical impact of aldose reductase inhibitors on cataract formation in young rats with streptozotocin-induced diabetes mellitus (Kador et al., 2000). In contrast, the phenomenon of diabetes-induced lens opacification has never been observed in diabetic mice, presumably related to lower aldose reductase activity in lenses of mice in comparison with humans and rats (Chand et al., 1982; Petrash, 2004; Varma and Kinoshita, 1974). However, the underlying pathogenic mechanism of diabetes-associated cataract formation in *INS*^{C94Y} transgenic pigs remains to be elucidated.

VI. CONCLUDING REMARKS AND PERSPECTIVES

INS^{C94Y} transgenic pigs exhibit a progressive diabetic phenotype characterized by chronically elevated randomly fed and fasting blood glucose levels as well as excessive growth retardation. The dominant-negative/toxic effect of *INS*^{C94Y} transgene expression leads to early-onset hyperglycemia through a clinically relevant impairment of β-cells. Insufficient glucose-stimulated insulin secretion and impaired peripheral glucose sensing are probably the initial causes of disturbed glycemic control in *INS*^{C94Y} transgenic pigs, preceding insulin deficiency gradually evolving from loss of functional β-cells. In addition, chronic ER stress, perpetuated by interminable entrapment of unfolded mutant proinsulin polypeptides, ultimately contributes to insulin deficiency in *INS*^{C94Y} transgenic pigs at the age of 4.5 months by progressive reduction of the total volume of functional β-cells via programmed cell death. Accompanying peripheral insulin resistance, presumably mediated by long-term glucose toxicity and altered insulin receptor binding potency of mutant porcine C94Y insulin, seems to exert remarkable impact on the severity of diabetic symptoms present in *INS*^{C94Y} transgenic pigs. Nevertheless clinical features and underlying disease mechanisms, intensively investigated in diabetic *Ins2* mutant mice, were likewise demonstrated in the *INS*^{C94Y} transgenic pig model and diagnostic findings of human permanent neonatal diabetes mellitus have been observed and validated in *INS*^{C94Y} transgenic pigs. Interestingly, *INS*^{C94Y} transgenic pigs responded highly satisfactorily to exogenous insulin supplementation and could be raised to sexual maturity allowing for conventional breeding. Considerably mimicking the human conditions, the *INS*^{C94Y} transgenic pig model has proven eligible for interesting questions of translational diabetes research. The consistent diabetic phenotype and its rescue by insulin supplementation make the *INS*^{C94Y} transgenic pig a promising animal model for reliable preclinical testing of novel therapeutic and regenerative approaches. The accurately quantified and reproducible reduction of the total volume of functional β-cells related to a well-defined pecularity of diabetic symptoms in *INS*^{C94Y} transgenic pigs constitutes a standardized system for testing putatively preservative or proliferative effects of anti-diabetic pharmaceuticals. Furthermore, the *INS*^{C94Y} pig is a useful animal model for the development of imaging techniques to monitor β-cells *in vivo*. Resembling human body weight

and size, the *INS*^{C94Y} transgenic pig enables application of standard diagnostic and surgical techniques of human medicine. Therefore, the *INS*^{C94Y} transgenic pig model complies with the requirements for islet transplantation studies. Thus, practicability of the respective surgical procedure as well as the functionality of inserted pancreatic islet allografts can be evaluated in a genetically engineered diabetic pig model exhibiting robust hyperglycemia. Consequences of maternal diabetes on the developing organism and long-term effects on offspring mediated by intrauterine programming are other interesting questions in this field. Important aspects of oocyte maturation, early embryonic development and developmental stage at birth are almost comparable between humans and pigs (Prather et al., 2009). Furthermore, female *INS*^{C94Y} transgenic pigs are adapted to estrus synchronization and have already proven to be able to establish and maintain pregnancy. Thus, the *INS*^{C94Y} transgenic pig offers the possibility to study developmental consequences of pre-conceptional diabetes mellitus on oocyte maturation, embryonic development, fetal programming as well as offspring metabolism and growth in an organism considerably reflecting human reproductive biology.

VII. SUMMARY

Genotypic and phenotypic characterization of *INS*^{C94Y} trangenic pigs – a novel large animal model for permanent neonatal diabetes mellitus

Different mutations in the human insulin (*INS*) gene have been described as a cause of non-autoimmune permanent neonatal diabetes mellitus (PNDM). Studies on heterozygous Akita *Ins2*^{C96Y} and Munich *Ins2*^{C95S} mutant mice already clarified fundamental mechanisms of the disease but have limitations for translational research. To establish a preclinical animal model of PNDM, considerably mimicking the human conditions, we generated *INS*^{C94Y} transgenic pigs that correspond to the human *INS*^{C96Y} mutation and the *Ins2* mutation of the Akita mouse model. Transgenic pigs expressing high levels of *INS*^{C94Y} mRNA (70–86% of endogenous *INS* transcripts) showed significantly elevated blood glucose levels within 24 hours after birth and exhibited reduced growth. Furthermore fasting insulin levels were significantly reduced by 60% in 4.5-month-old *INS*^{C94Y} transgenic pigs compared to littermate controls. Despite the early onset of hyperglycemia, total β-cell volume of 8-day-old *INS*^{C94Y} transgenic pigs was unaltered compared to littermate controls. However quantitative-stereological analyzes of pancreatic tissue of 4.5-month-old *INS*^{C94Y} transgenic pigs revealed a 72% reduction of the total β-cell volume and a 53% reduction of the total β-cell volume related to body weight. A highly reduced number of insulin secretory granules and severe dilation of the endoplasmic reticulum was detected by electron microscopy of pancreatic β-cells. Diabetes-induced pathological alterations of kidney and peripheral nerves were not detected within one year but a remarkable cataract was regularly observed.

In summary**,** we have generated the first genetically modified diabetic pig model, which can be propagated by conventional breeding. The consistent diabetic phenotype and its rescue by insulin supplementation make the *INS*^{C94Y} transgenic pig a promising animal model for reliable preclinical testing of novel therapeutic and regenerative approaches including islet transplantation. Moreover

the *INS*^{C94Y} transgenic pig model is implementable for the characterization of developmental consequences of pre-conceptional maternal diabetes mellitus on embryos, fetuses and offspring. Therefore the *INS*^{C94Y} transgenic pig is a clinically relevant large animal model and has proven to be useful for a plethora of research options for translational medicine.

VIII. ZUSAMMENFASSUNG

Genotypische und phänotypische Charakterisierung von *INS*^{C94Y} transgenen Schweinen – ein neues Großtiermodell für den permanent neonatalen Diabetes mellitus

Verschiedene Mutationen des humanen Insulin-Gens (*INS*) wurden als Ursache eines nicht-autoimmun bedingten permanenten neonatalen Diabetes mellitus beschrieben. Durch Studien an heterozygoten Akita *Ins2*^{C96Y} und Munich *Ins2*^{C95S} Mausmutanten konnten bereits grundlegende Mechanismen der Erkrankung aufgeklärt werden. Diese Mausmodelle weisen allerdings gewisse Beschränkungen im Hinblick auf die translationale Forschung auf. Um ein Großtiermodell zu erstellen, das die Gegebenheiten beim Menschen sehr gut widerspiegelt, wurden *INS*^{C94Y} transgene Schweine generiert. Das *INS*^{C94Y} transgene Schweinemodell stellt das korrespondierende Großtiermodell der *Ins2* Mutation der Akita Maus sowie der humanen *INS*^{C96Y} Mutation dar. Bei *INS*^{C94Y} transgenen Schweinen mit hoher *INS*^{C94Y} mRNA Expression (70-86% der endogenen *INS* Transkripte) waren bereits einen Tag nach der Geburt, signifikant erhöhte Blutglukosewerte und nach dem Absetzen ein massiv verzögertes Wachstum zu beobachten. Darüber hinaus waren die gefasteten Insulinspiegel im Plasma 4,5 Monate alter *INS*^{C94Y} transgener Schweine im Vergleich zu den nichttransgenen Wurfgeschwistern signifikant um 60% reduziert. Obwohl *INS*^{C94Y} transgene Schweine im Alter von 8 Tagen bereits eine schwere Hyperglykämie zeigten, war das Gesamt-β-Zellvolumen im Vergleich zu nichttransgenen Wurfgeschwistern noch unverändert. Dahingegen zeigten quantitativ-stereologische Analysen des pankreatischen Gewebes *INS*^{C94Y} transgener Schweine im Alter von 4,5 Monaten eine Reduktion des Gesamt-β-Zellvolumens um 72%. Die körpergewichtsbezogene Reduktion des Gesamt-β-Zellvolumens betrug 53%. Eine stark reduzierte Anzahl sekretorischer Insulingranula und eine massive Erweiterung des endoplasmatischen Retikulums konnte mittels Elektronenmikroskopie pankreatischer β-Zellen 4,5 Monate alter *INS*^{C94Y} transgener Schweine gezeigt werden. Diabetes-bedingte pathologische

Nierenveränderungen sowie Schädigung peripherer Nerven waren im Untersuchungszeitraum von einem Jahr nicht feststellbar. Allerdings zeigten *INS*^{C94Y} transgene Schweine eine regelmäßige Kataraktentwicklung. Zusammenfassend gesagt, haben wir das erste genetisch modifizierte diabetische Schweinemodell entwickelt, das unter Insulinbehandlung konventionell vermehrt werden kann. Der konstante diabetische Phänotyp des *INS*^{C94Y} transgenen Schweins, der durch Insulinsupplementierung gemildert werden kann, zeichnet es als vielversprechendes Tiermodell für die translationale Diabetesforschung aus. Neue therapeutische und regenerative Ansätze, die auch die Transplantation pankreatischer Inseln beinhalten, können an diesem diabetischen Großtiermodell validiert werden. Darüber hinaus ist das *INS*^{C94Y} transgene Schweinemodell geeignet, um entwicklungsbiologische Auswirkungen eines präkonzeptionellen maternalen Diabetes mellitus auf Embryonen, Feten und Nachkommen zu charakterisieren. Aus diesem Grund ist das *INS*^{C94Y} transgene Schweinemodell ein klinisch relevantes Großtiermodell und eröffnet vielfältige Forschungsmöglichkeiten für die translationale Medizin.

IX. INDEX OF FIGURES

X. INDEX OF TABLES

XI. REFERENCE LIST

Abdul-Ghani, M., and DeFronzo, R. A. (2007). Fasting hyperglycemia impairs glucose- but not insulin-mediated suppression of glucagon secretion. *J Clin Endocrinol Metab* **92**, 1778-84.

ADA (2008). Economic costs of diabetes in the U.S. in 2007 - American Diabetes Association. *Diabetes Care* **31**, 596-615.

ADA (2013). Diagnosis and classification of diabetes mellitus - American Diabetes Association (ADA). *Diabetes Care* **36 Suppl 1**, S67-74.

Adesnik, M., Lande, M., Martin, T., and Sabatini, D. D. (1976). Retention of mRNA on the endoplasmic reticulum membranes after in vivo disassembly of polysomes by an inhibitor of initiation. *J Cell Biol* **71**, 307-13.

Aguilar-Bryan, L., and Bryan, J. (2008). Neonatal diabetes mellitus. *Endocr Rev* **29**, 265-91.

Aigner, B., Rathkolb, B., Herbach, N., Hrabe de Angelis, M., Wanke, R., and Wolf, E. (2008). Diabetes models by screen for hyperglycemia in phenotype-driven ENU mouse mutagenesis projects. *Am J Physiol Endocrinol Metab* **294**, E232-40.

Aigner, B., Renner, S., Kessler, B., Klymiuk, N., Kurome, M., Wunsch, A., and Wolf, E. (2010). Transgenic pigs as models for translational biomedical research. *J Mol Med* **88**, 653-64.

Alberti, K. G., and Zimmet, P. Z. (1998). Definition, diagnosis and classification of diabetes mellitus and its complications. Part 1: diagnosis and classification of diabetes mellitus provisional report of a WHO consultation. *Diabet Med* **15**, 539-53.

Allen, J. R., Nguyen, L. X., Sargent, K. E., Lipson, K. L., Hackett, A., and Urano, F. (2004). High ER stress in beta-cells stimulates intracellular degradation of misfolded insulin. *Biochem Biophys Res Commun* **324**, 166-70.

Araki, E., Oyadomari, S., and Mori, M. (2003). Impact of endoplasmic reticulum stress pathway on pancreatic beta-cells and diabetes mellitus. *Exp Biol Med (Maywood)* **228**, 1213-7.

Arima, T., Drewell, R. A., Arney, K. L., Inoue, J., Makita, Y., Hata, A., Oshimura, M., Wake, N., and Surani, M. A. (2001). A conserved imprinting control region at the HYMAI/ZAC domain is implicated in transient neonatal diabetes mellitus. *Hum Mol Genet* **10**, 1475-83.

Arima, T., Drewell, R. A., Oshimura, M., Wake, N., and Surani, M. A. (2000). A novel imprinted gene, HYMAI, is located within an imprinted domain on human chromosome 6 containing ZAC. *Genomics* **67**, 248-55.

Aspinwall, C. A., Lakey, J. R., and Kennedy, R. T. (1999). Insulin-stimulated insulin secretion in single pancreatic beta cells. *J Biol Chem* **274**, 6360-5.

Babenko, A. P., Polak, M., Cave, H., Busiah, K., Czernichow, P., Scharfmann, R., Bryan, J., Aguilar-Bryan, L., Vaxillaire, M., and Froguel, P. (2006). Activating mutations in the ABCC8 gene in neonatal diabetes mellitus. *N Engl J Med* **355**, 456-66.

Bach, J. F. (1994). Insulin-dependent diabetes mellitus as an autoimmune disease. *Endocr Rev* **15**, 516-42.

Bahr, A., and Wolf, E. (2012). Domestic animal models for biomedical research. *Reprod Domest Anim* **47 Suppl 4**, 59-71.

Baker, E. N., Blundell, T. L., Cutfield, J. F., Cutfield, S. M., Dodson, E. J., Dodson, G. G., Hodgkin, D. M., Hubbard, R. E., Isaacs, N. W., Reynolds, C. D., and et al. (1988). The structure of 2Zn pig insulin crystals at 1.5 A resolution. *Philos Trans R Soc Lond B Biol Sci* **319**, 369-456.

Benech-Kieffer, F., Wegrich, P., Schwarzenbach, R., Klecak, G., Weber, T., Leclaire, J., and Schaefer, H. (2000). Percutaneous absorption of sunscreens in vitro: interspecies comparison, skin models and reproducibility aspects. *Skin Pharmacol Appl Skin Physiol* **13**, 324-35.

Bennett, C. L., Christie, J., Ramsdell, F., Brunkow, M. E., Ferguson, P. J., Whitesell, L., Kelly, T. E., Saulsbury, F. T., Chance, P. F., and Ochs, H. D. (2001). The immune dysregulation, polyendocrinopathy, enteropathy, X-linked syndrome (IPEX) is caused by mutations of FOXP3. *Nat Genet* **27**, 20-1.

Bennett, R. A., and Pegg, A. E. (1981). Alkylation of DNA in rat tissues following administration of streptozotocin. *Cancer Res* **41**, 2786-90.

Bereket, A., Lang, C. H., Blethen, S. L., Gelato, M. C., Fan, J., Frost, R. A., and Wilson, T. A. (1995). Effect of insulin on the insulin-like growth factor system in children with new-onset insulin-dependent diabetes mellitus. *J Clin Endocrinol Metab* **80**, 1312-7.

Bereket, A., Lang, C. H., and Wilson, T. A. (1999). Alterations in the growth hormone-insulin-like growth factor axis in insulin dependent diabetes mellitus. *Horm Metab Res* **31**, 172-81.

Bernales, S., Papa, F. R., and Walter, P. (2006). Intracellular signaling by the unfolded protein response. *Annu Rev Cell Dev Biol* **22**, 487-508.

Bertolotti, A., Zhang, Y., Hendershot, L. M., Harding, H. P., and Ron, D. (2000). Dynamic interaction of BiP and ER stress transducers in the unfolded-protein response. *Nat Cell Biol* **2**, 326-32.

Besenfelder, U., Modl, J., Muller, M., and Brem, G. (1997). Endoscopic embryo collection and embryo transfer into the oviduct and the uterus of pigs. *Theriogenology* **47**, 1051-60.

Besnard, A., Galan-Rodriguez, B., Vanhoutte, P., and Caboche, J. (2011). Elk-1 a transcription factor with multiple facets in the brain. *Front Neurosci* **5**, 35.

Betsholtz, C., Svensson, V., Rorsman, F., Engstrom, U., Westermark, G. T., Wilander, E., Johnson, K., and Westermark, P. (1989). Islet amyloid polypeptide (IAPP):cDNA cloning and identification of an amyloidogenic region associated with the species-specific occurrence of age-related diabetes mellitus. *Exp Cell Res* **183**, 484-93.

Blundell, T. L., Cutfield, J. F., Cutfield, S. M., Dodson, E. J., Dodson, G. G., Hodgkin, D. C., and Mercola, D. A. (1972). Three-dimensional atomic structure of insulin and its relationship to activity. *Diabetes* **21**, 492-505.

Bogardus, C., Lillioja, S., Mott, D. M., Hollenbeck, C., and Reaven, G. (1985). Relationship between degree of obesity and in vivo insulin action in man. *Am J Physiol* **248**, E286-91.

Bogoyevitch, M. A., and Kobe, B. (2006). Uses for JNK: the many and varied substrates of the c-Jun N-terminal kinases. *Microbiol Mol Biol Rev* **70**, 1061-95.

Bogue, M. (2003). Mouse Phenome Project: understanding human biology through mouse genetics and genomics. *J Appl Physiol* **95**, 1335-7.

Bonfanti, R., Colombo, C., Nocerino, V., Massa, O., Lampasona, V., Iafusco, D., Viscardi, M., Chiumello, G., Meschi, F., and Barbetti, F. (2009). Insulin gene mutations as cause of diabetes in children negative for five type 1 diabetes autoantibodies. *Diabetes Care* **32**, 123-5.

Bonner-Weir, S. (2000). Islet growth and development in the adult. *J Mol Endocrinol* **24**, 297-302.

Bonner-Weir, S., Trent, D. F., and Weir, G. C. (1983). Partial pancreatectomy in the rat and subsequent defect in glucose-induced insulin release. *J Clin Invest* **71**, 1544-53.

Borelli, M. I., Francini, F., and Gagliardino, J. J. (2004). Autocrine regulation of glucose metabolism in pancreatic islets. *Am J Physiol Endocrinol Metab* **286**, E111-5.

Brandhorst, D., Brandhorst, H., Hering, B. J., Federlin, K., and Bretzel, R. G. (1995). Islet isolation from the pancreas of large mammals and humans: 10 years of experience. *Exp Clin Endocrinol Diabetes* **103 Suppl 2**, 3-14.

Bromberg, J. S., and LeRoith, D. (2006). Diabetes cure--is the glass half full? *N Engl J Med* **355**, 1372-4.

Broughton, D. L., and Taylor, R. (1991). Review: deterioration of glucose tolerance with age: the role of insulin resistance. *Age Ageing* **20**, 221-5.

Brown, M. S., Ye, J., Rawson, R. B., and Goldstein, J. L. (2000). Regulated intramembrane proteolysis: a control mechanism conserved from bacteria to humans. *Cell* **100**, 391-8.

Butler, A. E., Janson, J., Bonner-Weir, S., Ritzel, R., Rizza, R. A., and Butler, P. C. (2003). Beta-cell deficit and increased beta-cell apoptosis in humans with type 2 diabetes. *Diabetes* **52**, 102-10.

Byrne, M. M., Sturis, J., Menzel, S., Yamagata, K., Fajans, S. S., Dronsfield, M. J., Bain, S. C., Hattersley, A. T., Velho, G., Froguel, P., Bell, G. I., and Polonsky, K. S. (1996). Altered insulin secretory responses to glucose in diabetic and nondiabetic subjects with mutations in the diabetes susceptibility gene MODY3 on chromosome 12. *Diabetes* **45**, 1503-10.

Cabrera, O., Berman, D. M., Kenyon, N. S., Ricordi, C., Berggren, P. O., and Caicedo, A. (2006). The unique cytoarchitecture of human pancreatic islets has implications for islet cell function. *Proc Natl Acad Sci U S A* **103**, 2334-9.

Calfon, M., Zeng, H., Urano, F., Till, J. H., Hubbard, S. R., Harding, H. P., Clark, S. G., and Ron, D. (2002). IRE1 couples endoplasmic reticulum load to secretory capacity by processing the XBP-1 mRNA. *Nature* **415**, 92-6.

Canavan, J. P., Flecknell, P. A., New, J. P., Alberti, K. G., and Home, P. D. (1997). The effect of portal and peripheral insulin delivery on carbohydrate and lipid metabolism in a miniature pig model of human IDDM. *Diabetologia* **40**, 1125-34.

Carcione, L., Lombardo, F., Messina, M. F., Rosano, M., and De Luca, F. (2003). Liver glycogenosis as early manifestation in type 1 diabetes mellitus. *Diabetes Nutr Metab* **16**, 182-4.

Carroll, R. J., Hammer, R. E., Chan, S. J., Swift, H. H., Rubenstein, A. H., and Steiner, D. F. (1988). A mutant human proinsulin is secreted from islets of Langerhans in increased amounts via an unregulated pathway. *Proc Natl Acad Sci U S A* **85**, 8943-7.

Cave, H., Polak, M., Drunat, S., Denamur, E., and Czernichow, P. (2000). Refinement of the 6q chromosomal region implicated in transient neonatal diabetes. *Diabetes* **49**, 108-13.

Chaib, E., Galvao, F. H., Rocha-Filho, J. A., Silveira, B. L., Chen, L., de, C. C. M. P., Pariz, C. E., de Almeida, F. S., Waisberg, D. R., de Souza, Y. E., Machado, M. C., and D'Albuquerque, L. A. (2011). Total pancreatectomy: porcine model for inducing diabetes - anatomical assessment and surgical aspects. *Eur Surg Res* **46**, 52-5.

Chan, S. J., Seino, S., Gruppuso, P. A., Schwartz, R., and Steiner, D. F. (1987). A mutation in the B chain coding region is associated with impaired proinsulin conversion in a family with hyperproinsulinemia. *Proc Natl Acad Sci U S A* **84**, 2194-7.

Chand, D., El-Aguizy, H. K., Richards, R. D., and Varma, S. D. (1982). Sugar cataracts in vitro: implications of oxidative stress and aldose reductase I. *Exp Eye Res* **35**, 491-7.

Chang, S. G., Choi, K. D., Jang, S. H., and Shin, H. C. (2003). Role of disulfide bonds in the structure and activity of human insulin. *Mol Cells* **16**, 323-30.

Chatila, R., and West, A. B. (1996). Hepatomegaly and abnormal liver tests due to glycogenosis in adults with diabetes. *Medicine (Baltimore)* **75**, 327-33.

Chen, X., Shen, J., and Prywes, R. (2002). The luminal domain of ATF6 senses endoplasmic reticulum (ER) stress and causes translocation of ATF6 from the ER to the Golgi. *J Biol Chem* **277**, 13045-52.

Chick, W. L., and Like, A. A. (1970). Studies in the diabetic mutant mouse. 3. Physiological factors associated with alterations in beta cell proliferation. *Diabetologia* **6**, 243-51.

Clark, A., Charge, S. B., Badman, M. K., and de Koning, E. J. (1996). Islet amyloid in type 2 (non-insulin-dependent) diabetes. *APMIS* **104**, 12-8.

Clark, A. J., Bissinger, P., Bullock, D. W., Damak, S., Wallace, R., Whitelaw, C. B., and Yull, F. (1994). Chromosomal position effects and the modulation of transgene expression. *Reprod Fertil Dev* **6**, 589-98.

Clark, J. M., and Diehl, A. M. (2002). Hepatic steatosis and type 2 diabetes mellitus. *Curr Diab Rep* **2**, 210-5.

Clayton, K. L., Holly, J. M., Carlsson, L. M., Jones, J., Cheetham, T. D., Taylor, A. M., and Dunger, D. B. (1994). Loss of the normal relationships between growth hormone, growth hormone-binding protein and insulin-like growth factor-I in adolescents with insulin-dependent diabetes mellitus. *Clin Endocrinol (Oxf)* **41**, 517-24.

Clee, S. M., and Attie, A. D. (2007). The genetic landscape of type 2 diabetes in mice. *Endocr Rev* **28**, 48-83.

Clemens, M. J. (1994). Regulation of eukaryotic protein synthesis by protein kinases that phosphorylate initiation factor eIF-2. *Mol Biol Rep* **19**, 201-10.

Cnop, M., Welsh, N., Jonas, J. C., Jorns, A., Lenzen, S., and Eizirik, D. L. (2005). Mechanisms of pancreatic beta-cell death in type 1 and type 2 diabetes: many differences, few similarities. *Diabetes* **54 Suppl 2**, S97-107.

Collinet, M., Berthelon, M., Benit, P., Laborde, K., Desbuquois, B., Munnich, A., and Robert, J. J. (1998). Familial hyperproinsulinaemia due to a mutation substituting histidine for arginine at position 65 in proinsulin: identification of the mutation by restriction enzyme mapping. *Eur J Pediatr* **157**, 456-60.

Colombo, C., Porzio, O., Liu, M., Massa, O., Vasta, M., Salardi, S., Beccaria, L., Monciotti, C., Toni, S., Pedersen, O., Hansen, T., Federici, L., Pesavento, R., Cadario, F., Federici, G., Ghirri, P., Arvan, P., Iafusco, D., Barbetti, F., Early Onset Diabetes Study Group of the Italian Society of Pediatric, E., and Diabetes (2008). Seven mutations in the human insulin gene linked to permanent neonatal/infancy-onset diabetes mellitus. *J Clin Invest* **118**, 2148-56.

Connolly, T., and Gilmore, R. (1989). The signal recognition particle receptor mediates the GTP-dependent displacement of SRP from the signal sequence of the nascent polypeptide. *Cell* **57**, 599-610.

Cortes, P., Dumler, F., Goldman, J., and Levin, N. W. (1987). Relationship between renal function and metabolic alterations in early streptozocin-induced diabetes in rats. *Diabetes* **36**, 80-7.

Cudworth, A. G., and Woodrow, J. C. (1975). HL-A system and diabetes mellitus. *Diabetes* **24**, 345-9.

Davis, R. J. (1999). Signal transduction by the c-Jun N-terminal kinase. *Biochem Soc Symp* **64**, 1-12.

Davis, R. J. (2000). Signal transduction by the JNK group of MAP kinases. *Cell* **103**, 239-52.

de Haro, C., Mendez, R., and Santoyo, J. (1996). The eIF-2alpha kinases and the control of protein synthesis. *FASEB J* **10**, 1378-87.

DeFronzo, R. A. (2004). Pathogenesis of type 2 diabetes mellitus. *Med Clin North Am* **88**, 787-835, ix.

DeFronzo, R. A., Tobin, J. D., and Andres, R. (1979). Glucose clamp technique: a method for quantifying insulin secretion and resistance. *Am J Physiol* **237**, E214-23.

Delepine, M., Nicolino, M., Barrett, T., Golamaully, M., Lathrop, G. M., and Julier, C. (2000). EIF2AK3, encoding translation initiation factor 2-alpha kinase 3, is mutated in patients with Wolcott-Rallison syndrome. *Nat Genet* **25**, 406-9.

Derewenda, U., Derewenda, Z., Dodson, G. G., Hubbard, R. E., and Korber, F. (1989). Molecular structure of insulin: the insulin monomer and its assembly. *Br Med Bull* **45**, 4-18.

Dische, F. E. (1992). Measurement of glomerular basement membrane thickness and its application to the diagnosis of thin-membrane nephropathy. *Arch Pathol Lab Med* **116**, 43-9.

Donath, M. Y., and Halban, P. A. (2004). Decreased beta-cell mass in diabetes: significance, mechanisms and therapeutic implications. *Diabetologia* **47**, 581-9.

Douglas, W. R. (1972). Of pigs and men and research: a review of applications and analogies of the pig, sus scrofa, in human medical research. *Space Life Sci* **3**, 226-34.

Dufrane, D., van Steenberghe, M., Guiot, Y., Goebbels, R. M., Saliez, A., and Gianello, P. (2006). Streptozotocin-induced diabetes in large animals (pigs/primates): role of GLUT2 transporter and beta-cell plasticity. *Transplantation* **81**, 36-45.

Edelsten, A. D., Hughes, I. A., Oakes, S., Gordon, I. R., and Savage, D. C. (1981). Height and skeletal maturity in children with newly-diagnosed juvenile-onset diabetes. *Arch Dis Child* **56**, 40-4.

Edghill, E. L., Dix, R. J., Flanagan, S. E., Bingley, P. J., Hattersley, A. T., Ellard, S., and Gillespie, K. M. (2006). HLA genotyping supports a nonautoimmune etiology in patients diagnosed with diabetes under the age of 6 months. *Diabetes* **55**, 1895-8.

Edghill, E. L., Flanagan, S. E., and Ellard, S. (2010). Permanent neonatal diabetes due to activating mutations in ABCC8 and KCNJ11. *Rev Endocr Metab Disord* **11**, 193-8.

Edghill, E. L., Flanagan, S. E., Patch, A. M., Boustred, C., Parrish, A., Shields, B., Shepherd, M. H., Hussain, K., Kapoor, R. R., Malecki, M., MacDonald, M. J., Stoy, J., Steiner, D. F., Philipson, L. H., Bell, G. I., Neonatal Diabetes International Collaborative, G., Hattersley, A. T., and Ellard, S. (2008). Insulin mutation screening in 1,044 patients with diabetes: mutations in the INS gene are a common cause of neonatal diabetes but a rare cause of diabetes diagnosed in childhood or adulthood. *Diabetes* **57**, 1034-42.

Edghill, E. L., Gloyn, A. L., Gillespie, K. M., Lambert, A. P., Raymond, N. T., Swift, P. G., Ellard, S., Gale, E. A., and Hattersley, A. T. (2004). Activating mutations in the KCNJ11 gene encoding the ATP-sensitive K+ channel subunit Kir6.2 are rare in clinically defined type 1 diabetes diagnosed before 2 years. *Diabetes* **53**, 2998-3001.

Eizirik, D. L., Cardozo, A. K., and Cnop, M. (2008). The role for endoplasmic reticulum stress in diabetes mellitus. *Endocr Rev* **29**, 42-61.

El-Aouni, C., Herbach, N., Blattner, S. M., Henger, A., Rastaldi, M. P., Jarad, G., Miner, J. H., Moeller, M. J., St-Arnaud, R., Dedhar, S., Holzman, L. B., Wanke, R., and Kretzler, M. (2006). Podocyte-specific deletion of integrin-linked kinase results in severe glomerular basement membrane alterations and progressive glomerulosclerosis. *J Am Soc Nephrol* **17**, 1334-44.

Ellgaard, L., and Helenius, A. (2003). Quality control in the endoplasmic reticulum. *Nat Rev Mol Cell Biol* **4**, 181-91.

Ellgaard, L., Molinari, M., and Helenius, A. (1999). Setting the standards: quality control in the secretory pathway. *Science* **286**, 1882-8.

Engelhart, W. v., and G., B., eds. (2010). "Physiologie der Haustiere," pp. 1-736. Verlag Enke Ferdinand

Eriksson, J., Franssila-Kallunki, A., Ekstrand, A., Saloranta, C., Widen, E., Schalin, C., and Groop, L. (1989). Early metabolic defects in persons at increased risk for non-insulin-dependent diabetes mellitus. *N Engl J Med* **321**, 337-43.

Evans, R. W., Littler, T. R., and Pemberton, H. S. (1955). Glycogen storage in the liver in diabetes mellitus. *J Clin Pathol* **8**, 110-3.

Expert Committee on the Diagnosis and Classification of Diabetes mellitus (2003). Report of the expert committee on the diagnosis and classification of diabetes mellitus. *Diabetes Care* **26 Suppl 1**, S5-20.

Fajans, S. S., Bell, G. I., Bowden, D. W., Halter, J. B., and Polonsky, K. S. (1994). Maturity-onset diabetes of the young. *Life Sci* **55**, 413-22.

Fajans, S. S., Bell, G. I., and Polonsky, K. S. (2001). Molecular mechanisms and clinical pathophysiology of maturity-onset diabetes of the young. *N Engl J Med* **345**, 971-80.

Federici, M., Hribal, M., Perego, L., Ranalli, M., Caradonna, Z., Perego, C., Usellini, L., Nano, R., Bonini, P., Bertuzzi, F., Marlier, L. N., Davalli, A. M., Carandente, O., Pontiroli, A. E., Melino, G., Marchetti, P., Lauro, R., Sesti, G., and Folli, F. (2001). High glucose causes apoptosis in cultured human pancreatic islets of Langerhans: a potential role for regulation of specific Bcl family genes toward an apoptotic cell death program. *Diabetes* **50**, 1290-301.

Finegood, D. T., Scaglia, L., and Bonner-Weir, S. (1995). Dynamics of beta-cell mass in the growing rat pancreas. Estimation with a simple mathematical model. *Diabetes* **44**, 249-56.

Flanagan, S. E., Patch, A. M., Mackay, D. J., Edghill, E. L., Gloyn, A. L., Robinson, D., Shield, J. P., Temple, K., Ellard, S., and Hattersley, A. T. (2007). Mutations in ATP-sensitive K+ channel genes cause transient neonatal diabetes and permanent diabetes in childhood or adulthood. *Diabetes* **56**, 1930-7.

Flores-Le Roux, J. A., Comin, J., Pedro-Botet, J., Benaiges, D., Puig-de Dou, J., Chillaron, J. J., Goday, A., Bruguera, J., and Cano-Perez, J. F. (2011). Seven-year mortality in heart failure patients with undiagnosed diabetes: an observational study. *Cardiovasc Diabetol* **10**, 39.

Flynn, G. C., Chappell, T. G., and Rothman, J. E. (1989). Peptide binding and release by proteins implicated as catalysts of protein assembly. *Science* **245**, 385-90.

Fornace, A. J., Jr., Alamo, I., Jr., and Hollander, M. C. (1988). DNA damage-inducible transcripts in mammalian cells. *Proc Natl Acad Sci U S A* **85**, 8800-4.

Fosel, S. (1995). Transient and permanent neonatal diabetes. *Eur J Pediatr* **154**, 944-8.

Frayling, T. M., Lindgren, C. M., Chevre, J. C., Menzel, S., Wishart, M., Benmezroua, Y., Brown, A., Evans, J. C., Rao, P. S., Dina, C., Lecoeur, C., Kanninen, T., Almgren, P., Bulman, M. P., Wang, Y., Mills, J., Wright-Pascoe, R., Mahtani, M. M., Prisco, F., Costa, A., Cognet, I., Hansen, T., Pedersen, O., Ellard, S., Tuomi, T., Groop, L. C., Froguel, P., Hattersley, A. T., and Vaxillaire, M. (2003). A genome-wide scan in families with maturity-onset diabetes of the young: evidence for further genetic heterogeneity. *Diabetes* **52**, 872-81.

Freedman, R. B. (1989). Protein disulfide isomerase: multiple roles in the modification of nascent secretory proteins. *Cell* **57**, 1069-72.

Fritsche, A., Stefan, N., Hardt, E., Haring, H., and Stumvoll, M. (2000). Characterisation of beta-cell dysfunction of impaired glucose tolerance: evidence for impairment of incretin-induced insulin secretion. *Diabetologia* **43**, 852-8.

Froguel, P., Vaxillaire, M., Sun, F., Velho, G., Zouali, H., Butel, M. O., Lesage, S., Vionnet, N., Clement, K., Fougerousse, F., and et al. (1992). Close linkage of glucokinase locus on chromosome 7p to early-onset non-insulin-dependent diabetes mellitus. *Nature* **356**, 162-4.

Froguel, P., and Velho, G. (1999). Molecular Genetics of Maturity-onset Diabetes of the Young. *Trends Endocrinol Metab* **10**, 142-146.

Gardner, R. J., Mackay, D. J., Mungall, A. J., Polychronakos, C., Siebert, R., Shield, J. P., Temple, I. K., and Robinson, D. O. (2000). An imprinted locus associated with transient neonatal diabetes mellitus. *Hum Mol Genet* **9**, 589-96.

Garin, I., Edghill, E. L., Akerman, I., Rubio-Cabezas, O., Rica, I., Locke, J. M., Maestro, M. A., Alshaikh, A., Bundak, R., del Castillo, G., Deeb, A., Deiss, D., Fernandez, J. M., Godbole, K., Hussain, K., O'Connell, M., Klupa, T., Kolouskova, S., Mohsin, F., Perlman, K., Sumnik, Z., Rial, J. M., Ugarte, E., Vasanthi, T., Neonatal Diabetes International, G., Johnstone, K., Flanagan, S. E., Martinez, R., Castano, C., Patch, A. M., Fernandez-Rebollo, E., Raile, K., Morgan, N., Harries, L. W., Castano, L., Ellard, S., Ferrer, J., Perez de Nanclares, G., and Hattersley, A. T. (2010). Recessive mutations in the INS gene result in neonatal diabetes through reduced insulin biosynthesis. *Proc Natl Acad Sci U S A* **107**, 3105-10.

Gavin, J. R., 3rd (1998). New classification and diagnostic criteria for diabetes mellitus. *Clin Cornerstone* **1**, 1-12.

Gentz, J. C., and Cornblath, M. (1969). Transient diabetes of the newborn. *Adv Pediatr* **16**, 345-63.

Germain, P., Chambon, P., Eichele, G., Evans, R. M., Lazar, M. A., Leid, M., De Lera, A. R., Lotan, R., Mangelsdorf, D. J., and Gronemeyer, H. (2006). International Union of Pharmacology. LX. Retinoic acid receptors. *Pharmacol Rev* **58**, 712-25.

Gething, M. J., and Sambrook, J. (1992). Protein folding in the cell. *Nature* **355**, 33-45.

Ghaemmaghami, S., Huh, W. K., Bower, K., Howson, R. W., Belle, A., Dephoure, N., O'Shea, E. K., and Weissman, J. S. (2003). Global analysis of protein expression in yeast. *Nature* **425**, 737-41.

Gillespie, K. M. (2006). Type 1 diabetes: pathogenesis and prevention. *CMAJ* **175**, 165-70.

Glaser, B., Kesavan, P., Heyman, M., Davis, E., Cuesta, A., Buchs, A., Stanley, C. A., Thornton, P. S., Permutt, M. A., Matschinsky, F. M., and Herold, K. C. (1998). Familial hyperinsulinism caused by an activating glucokinase mutation. *N Engl J Med* **338**, 226-30.

Gloyn, A. L., Pearson, E. R., Antcliff, J. F., Proks, P., Bruining, G. J., Slingerland, A. S., Howard, N., Srinivasan, S., Silva, J. M., Molnes, J., Edghill, E. L., Frayling, T. M., Temple, I. K., Mackay, D., Shield, J. P., Sumnik, Z., van Rhijn, A., Wales, J. K., Clark, P., Gorman, S., Aisenberg, J., Ellard, S., Njolstad, P. R., Ashcroft, F. M., and Hattersley, A. T. (2004). Activating mutations in the gene encoding the ATP-sensitive potassium-channel subunit Kir6.2 and permanent neonatal diabetes. *N Engl J Med* **350**, 1838-49.

Gloyn, A. L., Reimann, F., Girard, C., Edghill, E. L., Proks, P., Pearson, E. R., Temple, I. K., Mackay, D. J., Shield, J. P., Freedenberg, D., Noyes, K., Ellard, S., Ashcroft, F. M., Gribble, F. M., and Hattersley, A. T. (2005). Relapsing diabetes can result from moderately activating mutations in KCNJ11. *Hum Mol Genet* **14**, 925-34.

Gorelick, F. S., and Shugrue, C. (2001). Exiting the endoplasmic reticulum. *Mol Cell Endocrinol* **177**, 13-8.

Gorus, F. K., Malaisse, W. J., and Pipeleers, D. G. (1982). Selective uptake of alloxan by pancreatic B-cells. *Biochem J* **208**, 513-5.

Gottschalk, M. E., Schatz, D. A., Clare-Salzler, M., Kaufman, D. L., Ting, G. S., and Geffner, M. E. (1992). Permanent diabetes without serological evidence of autoimmunity after transient neonatal diabetes. *Diabetes Care* **15**, 1273-6.

Gray, C. S., Scott, J. F., French, J. M., Alberti, K. G., and O'Connell, J. E. (2004). Prevalence and prediction of unrecognised diabetes mellitus and impaired glucose tolerance following acute stroke. *Age Ageing* **33**, 71-7.

Gromada, J., Franklin, I., and Wollheim, C. B. (2007). Alpha-cells of the endocrine pancreas: 35 years of research but the enigma remains. *Endocr Rev* **28**, 84-116.

Gross, A., McDonnell, J. M., and Korsmeyer, S. J. (1999). BCL-2 family members and the mitochondria in apoptosis. *Genes Dev* **13**, 1899-911.

Gunczler, P., Lanes, R., Paz-Martinez, V., Martins, R., Esaa, S., Colmenares, V., and Weisinger, J. R. (1998). Decreased lumbar spine bone mass and low bone turnover in children and adolescents with insulin dependent diabetes mellitus followed longitudinally. *J Pediatr Endocrinol Metab* **11**, 413-9.

Gundersen, H. J., Bendtsen, T. F., Korbo, L., Marcussen, N., Moller, A., Nielsen, K., Nyengaard, J. R., Pakkenberg, B., Sorensen, F. B., Vesterby, A., and et al. (1988). Some new, simple and efficient stereological methods and their use in pathological research and diagnosis. *APMIS* **96**, 379-94.

Gundersen, H. J., and Jensen, E. B. (1987). The efficiency of systematic sampling in stereology and its prediction. *J Microsc* **147**, 229-63.

Guo, Z. Y., and Feng, Y. M. (2001). Effects of cysteine to serine substitutions in the two inter-chain disulfide bonds of insulin. *Biol Chem* **382**, 443-8.

Gurley, S. B., Clare, S. E., Snow, K. P., Hu, A., Meyer, T. W., and Coffman, T. M. (2006). Impact of genetic background on nephropathy in diabetic mice. *Am J Physiol Renal Physiol* **290**, F214-22.

Gurley, S. B., Mach, C. L., Stegbauer, J., Yang, J., Snow, K. P., Hu, A., Meyer, T. W., and Coffman, T. M. (2010). Influence of genetic background on albuminuria and kidney injury in Ins2(+/C96Y) (Akita) mice. *Am J Physiol Renal Physiol* **298**, F788-95.

Halban, P. A. (1994). Proinsulin processing in the regulated and the constitutive secretory pathway. *Diabetologia* **37 Suppl 2**, S65-72.

Hamilton-Shield, J. P. (2007). Overview of neonatal diabetes. *Endocr Dev* **12**, 12-23.

Haneda, M., Chan, S. J., Kwok, S. C., Rubenstein, A. H., and Steiner, D. F. (1983). Studies on mutant human insulin genes: identification and sequence analysis of a gene encoding [SerB24]insulin. *Proc Natl Acad Sci U S A* **80**, 6366-70.

Hansen, T., Urhammer, S. A., and Pedersen, O. B. (2002). [Maturity-onset diabetes of the young--MODY. Molecular-genetic, pathophysiological and clinical characteristics]. *Ugeskr Laeger* **164**, 2017-22.

Harding, H. P., Novoa, I., Zhang, Y., Zeng, H., Wek, R., Schapira, M., and Ron, D. (2000). Regulated translation initiation controls stress-induced gene expression in mammalian cells. *Mol Cell* **6**, 1099-108.

Harding, H. P., and Ron, D. (2002). Endoplasmic reticulum stress and the development of diabetes: a review. *Diabetes* **51 Suppl 3**, S455-61.

Harding, H. P., Zhang, Y., and Ron, D. (1999). Protein translation and folding are coupled by an endoplasmic-reticulum-resident kinase. *Nature* **397**, 271-4.

Harmon, J. S., Gleason, C. E., Tanaka, Y., Oseid, E. A., Hunter-Berger, K. K., and Robertson, R. P. (1999). In vivo prevention of hyperglycemia also prevents glucotoxic effects on PDX-1 and insulin gene expression. *Diabetes* **48**, 1995-2000.

Harris, M. I. (1988). Classification and diagnostic criteria for diabetes mellitus and other categories of glucose intolerance. *Prim Care* **15**, 205-25.

Hattersley, A. T. (2005). Molecular genetics goes to the diabetes clinic. *Clin Med* **5**, 476-81.

Hay, C. W., and Docherty, K. (2006). Comparative analysis of insulin gene promoters: implications for diabetes research. *Diabetes* **55**, 3201-13.

Haze, K., Okada, T., Yoshida, H., Yanagi, H., Yura, T., Negishi, M., and Mori, K. (2001). Identification of the G13 (cAMP-response-element-binding protein-related protein) gene product related to activating transcription factor 6 as a transcriptional activator of the mammalian unfolded protein response. *Biochem J* **355**, 19-28.

Haze, K., Yoshida, H., Yanagi, H., Yura, T., and Mori, K. (1999). Mammalian transcription factor ATF6 is synthesized as a transmembrane protein and activated by proteolysis in response to endoplasmic reticulum stress. *Mol Biol Cell* **10**, 3787-99.

Herbach, N., Rathkolb, B., Kemter, E., Pichl, L., Klaften, M., de Angelis, M. H., Halban, P. A., Wolf, E., Aigner, B., and Wanke, R. (2007). Dominant-negative effects of a novel mutated Ins2 allele causes early-onset diabetes and severe beta-cell loss in Munich Ins2C95S mutant mice. *Diabetes* **56**, 1268-76.

Herbach, N., Schairer, I., Blutke, A., Kautz, S., Siebert, A., Goke, B., Wolf, E., and Wanke, R. (2009). Diabetic kidney lesions of GIPRdn transgenic mice: podocyte hypertrophy and thickening of the GBM precede glomerular hypertrophy and glomerulosclerosis. *Am J Physiol Renal Physiol* **296**, F819-29.

Hermanns, W., Liebig, K., and Schulz, L. C. (1981). Postembedding immunohistochemical demonstration of antigen in experimental polyarthritis using plastic embedded whole joints. *Histochemistry* **73**, 439-46.

Herr, R. R., Jahnke, J. K., and Argoudelis, A. D. (1967). The structure of streptozotocin. *J Am Chem Soc* **89**, 4808-9.

Hinnebusch, A. G. (1997). Translational regulation of yeast GCN4. A window on factors that control initiator-trna binding to the ribosome. *J Biol Chem* **272**, 21661-4.

Hirose, K., Osterby, R., Nozawa, M., and Gundersen, H. J. (1982). Development of glomerular lesions in experimental long-term diabetes in the rat. *Kidney Int* **21**, 689-95.

Hodish, I., Liu, M., Rajpal, G., Larkin, D., Holz, R. W., Adams, A., Liu, L., and Arvan, P. (2010). Misfolded proinsulin affects bystander proinsulin in neonatal diabetes. *J Biol Chem* **285**, 685-94.

Hoenig, M., Hall, G., Ferguson, D., Jordan, K., Henson, M., Johnson, K., and O'Brien, T. (2000). A feline model of experimentally induced islet amyloidosis. *Am J Pathol* **157**, 2143-50.

Hollien, J., Lin, J. H., Li, H., Stevens, N., Walter, P., and Weissman, J. S. (2009). Regulated Ire1-dependent decay of messenger RNAs in mammalian cells. *J Cell Biol* **186**, 323-31.

Hollien, J., and Weissman, J. S. (2006). Decay of endoplasmic reticulum-localized mRNAs during the unfolded protein response. *Science* **313**, 104-7.

Hong, E. G., Jung, D. Y., Ko, H. J., Zhang, Z., Ma, Z., Jun, J. Y., Kim, J. H., Sumner, A. D., Vary, T. C., Gardner, T. W., Bronson, S. K., and Kim, J. K. (2007). Nonobese, insulin-deficient Ins2Akita mice develop type 2 diabetes phenotypes including insulin resistance and cardiac remodeling. *Am J Physiol Endocrinol Metab* **293**, E1687-96.

Hong, M., Luo, S., Baumeister, P., Huang, J. M., Gogia, R. K., Li, M., and Lee, A. S. (2004). Underglycosylation of ATF6 as a novel sensing mechanism for activation of the unfolded protein response. *J Biol Chem* **279**, 11354-63.

Horikawa, Y., Iwasaki, N., Hara, M., Furuta, H., Hinokio, Y., Cockburn, B. N., Lindner, T., Yamagata, K., Ogata, M., Tomonaga, O., Kuroki, H., Kasahara, T., Iwamoto, Y., and Bell, G. I. (1997). Mutation in hepatocyte nuclear factor-1 beta gene (TCF2) associated with MODY. *Nat Genet* **17**, 384-5.

Houstis, N., Rosen, E. D., and Lander, E. S. (2006). Reactive oxygen species have a causal role in multiple forms of insulin resistance. *Nature* **440**, 944-8.

Hu, P., Han, Z., Couvillon, A. D., Kaufman, R. J., and Exton, J. H. (2006). Autocrine tumor necrosis factor alpha links endoplasmic reticulum stress to the membrane death receptor pathway through IRE1alpha-mediated NF-kappaB activation and down-regulation of TRAF2 expression. *Mol Cell Biol* **26**, 3071-84.

Hu, S. Q., Burke, G. T., Schwartz, G. P., Ferderigos, N., Ross, J. B., and Katsoyannis, P. G. (1993). Steric requirements at position B12 for high biological activity in insulin. *Biochemistry* **32**, 2631-5.

Hua, Q. X., Chu, Y. C., Jia, W., Phillips, N. F., Wang, R. Y., Katsoyannis, P. G., and Weiss, M. A. (2002). Mechanism of insulin chain combination. Asymmetric roles of A-chain alpha-helices in disulfide pairing. *J Biol Chem* **277**, 43443-53.

Hua, Q. X., Liu, M., Hu, S. Q., Jia, W., Arvan, P., and Weiss, M. A. (2006a). A conserved histidine in insulin is required for the foldability of human proinsulin: structure and function of an ALAB5 analog. *J Biol Chem* **281**, 24889-99.

Hua, Q. X., Mayer, J. P., Jia, W., Zhang, J., and Weiss, M. A. (2006b). The folding nucleus of the insulin superfamily: a flexible peptide model foreshadows the native state. *J Biol Chem* **281**, 28131-42.

Hua, Q. X., Nakagawa, S., Hu, S. Q., Jia, W., Wang, S., and Weiss, M. A. (2006c). Toward the active conformation of insulin: stereospecific modulation of a structural switch in the B chain. *J Biol Chem* **281**, 24900-9.

Huang, E. S., Basu, A., O'Grady, M., and Capretta, J. C. (2009). Projecting the future diabetes population size and related costs for the U.S. *Diabetes Care* **32**, 2225-9.

Huang, X. F., and Arvan, P. (1994). Formation of the insulin-containing secretory granule core occurs within immature beta-granules. *J Biol Chem* **269**, 20838-44.

Hubbard, S. R. (2013). Structural biology: Insulin meets its receptor. *Nature* **493**, 171-2.

Huge, A., Weber, E., and Ehrlein, H. J. (1995). Effects of enteral feedback inhibition on motility, luminal flow, and absorption of nutrients in proximal gut of minipigs. *Dig Dis Sci* **40**, 1024-34.

Hutchison, J. H., Keay, A. J., and Kerr, M. M. (1962). Congenital temporary diabetes mellitus. *Br Med J* **2**, 436-40.

Hwang, C., Sinskey, A. J., and Lodish, H. F. (1992). Oxidized redox state of glutathione in the endoplasmic reticulum. *Science* **257**, 1496-502.

Ihara, Y., Toyokuni, S., Uchida, K., Odaka, H., Tanaka, T., Ikeda, H., Hiai, H., Seino, Y., and Yamada, Y. (1999). Hyperglycemia causes oxidative stress in pancreatic beta-cells of GK rats, a model of type 2 diabetes. *Diabetes* **48**, 927-32.

Imagawa, A., Hanafusa, T., Miyagawa, J., and Matsuzawa, Y. (2000). A novel subtype of type 1 diabetes mellitus characterized by a rapid onset and an absence of diabetes-related antibodies. Osaka IDDM Study Group. *N Engl J Med* **342**, 301-7.

In 't Veld, P. A., Zhang, F., Madsen, O. D., and Kloppel, G. (1992). Islet amyloid polypeptide immunoreactivity in the human fetal pancreas. *Diabetologia* **35**, 272-6.

Ishihara, M., Inoue, I., Kawagoe, T., Shimatani, Y., Kurisu, S., Hata, T., Nakama, Y., Kijima, Y., and Kagawa, E. (2006). Is admission hyperglycaemia in non-diabetic patients with acute myocardial infarction a surrogate for previously undiagnosed abnormal glucose tolerance? *Eur Heart J* **27**, 2413-9.

Izumi, T., Yokota-Hashimoto, H., Zhao, S., Wang, J., Halban, P. A., and Takeuchi, T. (2003). Dominant negative pathogenesis by mutant proinsulin in the Akita diabetic mouse. *Diabetes* **52**, 409-16.

Jackson, R. L. (1984). Growth and maturation of children with insulin-dependent diabetes mellitus. *Pediatr Clin North Am* **31**, 545-67.

Jacobson, D. A., Wicksteed, B. L., and Philipson, L. H. (2009). The alpha-cell conundrum: ATP-sensitive K+ channels and glucose sensing. *Diabetes* **58**, 304-6.

Jay, T. R., Heald, K. A., Carless, N. J., Topham, D. E., and Downing, R. (1999). The distribution of porcine pancreatic beta-cells at ages 5, 12 and 24 weeks. *Xenotransplantation* **6**, 131-40.

Jensen, E. B., Gundersen, H. J., and Osterby, R. (1979). Determination of membrane thickness distribution from orthogonal intercepts. *J Microsc* **115**, 19-33.

Jimbo, A., Fujita, E., Kouroku, Y., Ohnishi, J., Inohara, N., Kuida, K., Sakamaki, K., Yonehara, S., and Momoi, T. (2003). ER stress induces caspase-8 activation, stimulating cytochrome c release and caspase-9 activation. *Exp Cell Res* **283**, 156-66.

Johnson, A. M., and Olefsky, J. M. (2013). The origins and drivers of insulin resistance. *Cell* **152**, 673-84.

Johnson, K. H., O'Brien, T. D., Hayden, D. W., Jordan, K., Ghobrial, H. K., Mahoney, W. C., and Westermark, P. (1988). Immunolocalization of islet amyloid polypeptide (IAPP) in pancreatic beta cells by means of peroxidase-antiperoxidase (PAP) and protein A-gold techniques. *Am J Pathol* **130**, 1-8.

Jonsson, J., Carlsson, L., Edlund, T., and Edlund, H. (1994). Insulin-promoter-factor 1 is required for pancreas development in mice. *Nature* **371**, 606-9.

Justice, M. J., Noveroske, J. K., Weber, J. S., Zheng, B., and Bradley, A. (1999). Mouse ENU mutagenesis. *Hum Mol Genet* **8**, 1955-63.

Kador, P. F., Lee, J. W., Fujisawa, S., Blessing, K., and Lou, M. F. (2000). Relative importance of aldose reductase versus nonenzymatic glycosylation on sugar cataract formation in diabetic rats. *J Ocul Pharmacol Ther* **16**, 149-60.

Kahn, S. E. (2003). The relative contributions of insulin resistance and beta-cell dysfunction to the pathophysiology of Type 2 diabetes. *Diabetologia* **46**, 3-19.

Kaisaki, P. J., Menzel, S., Lindner, T., Oda, N., Rjasanowski, I., Sahm, J., Meincke, G., Schulze, J., Schmechel, H., Petzold, C., Ledermann, H. M., Sachse, G., Boriraj, V. V., Menzel, R., Kerner, W., Turner, R. C., Yamagata, K., and Bell, G. I. (1997). Mutations in the hepatocyte nuclear factor-1alpha gene in MODY and early-onset NIDDM: evidence for a mutational hotspot in exon 4. *Diabetes* **46**, 528-35.

Kaiser, N., Leibowitz, G., and Nesher, R. (2003). Glucotoxicity and beta-cell failure in type 2 diabetes mellitus. *J Pediatr Endocrinol Metab* **16**, 5-22.

Kaneko, M., Ishiguro, M., Niinuma, Y., Uesugi, M., and Nomura, Y. (2002). Human HRD1 protects against ER stress-induced apoptosis through ER-associated degradation. *FEBS Lett* **532**, 147-52.

Karjalainen, J., Salmela, P., Ilonen, J., Surcel, H. M., and Knip, M. (1989). A comparison of childhood and adult type I diabetes mellitus. *N Engl J Med* **320**, 881-6.

Kaufman, R. J. (2002). Orchestrating the unfolded protein response in health and disease. *J Clin Invest* **110**, 1389-98.

Kautz, S. M. (2011). Mechanisms of β-cell loss in male Munich *Ins2*^{C95S} mutant mice. Inaugural-Dissertation, Ludwig-Maximilians-University, Munich.

Kayo, T., and Koizumi, A. (1998). Mapping of murine diabetogenic gene mody on chromosome 7 at D7Mit258 and its involvement in pancreatic islet and beta cell development during the perinatal period. *J Clin Invest* **101**, 2112-8.

Kemmink, J., Darby, N. J., Dijkstra, K., Nilges, M., and Creighton, T. E. (1997). The folding catalyst protein disulfide isomerase is constructed of active and inactive thioredoxin modules. *Curr Biol* **7**, 239-45.

Kendall, D. M., Sutherland, D. E., Najarian, J. S., Goetz, F. C., and Robertson, R. P. (1990). Effects of hemipancreatectomy on insulin secretion and glucose tolerance in healthy humans. *N Engl J Med* **322**, 898-903.

Kikkert, M., Doolman, R., Dai, M., Avner, R., Hassink, G., van Voorden, S., Thanedar, S., Roitelman, J., Chau, V., and Wiertz, E. (2004). Human HRD1 is an E3 ubiquitin ligase involved in degradation of proteins from the endoplasmic reticulum. *J Biol Chem* **279**, 3525-34.

Kim, A., Miller, K., Jo, J., Kilimnik, G., Wojcik, P., and Hara, M. (2009). Islet architecture: A comparative study. *Islets* **1**, 129-36.

Kim, I., Xu, W., and Reed, J. C. (2008). Cell death and endoplasmic reticulum stress: disease relevance and therapeutic opportunities. *Nat Rev Drug Discov* **7**, 1013-30.

Kinoshita, J. H., Fukushi, S., Kador, P., and Merola, L. O. (1979). Aldose reductase in diabetic complications of the eye. *Metabolism* **28**, 462-9.

Kirk, A. D. (2003). Crossing the bridge: large animal models in translational transplantation research. *Immunol Rev* **196**, 176-96.

Kjems, L. L., Kirby, B. M., Welsh, E. M., Veldhuis, J. D., Straume, M., McIntyre, S. S., Yang, D., Lefebvre, P., and Butler, P. C. (2001). Decrease in beta-cell mass leads to impaired pulsatile insulin secretion, reduced postprandial hepatic insulin clearance, and relative hyperglucagonemia in the minipig. *Diabetes* **50**, 2001-12.

Kloppel, G., Lohr, M., Habich, K., Oberholzer, M., and Heitz, P. U. (1985). Islet pathology and the pathogenesis of type 1 and type 2 diabetes mellitus revisited. *Surv Synth Pathol Res* **4**, 110-25.

Klymiuk, N., Bocker, W., Schonitzer, V., Bahr, A., Radic, T., Frohlich, T., Wunsch, A., Kessler, B., Kurome, M., Schilling, E., Herbach, N., Wanke, R., Nagashima, H., Mutschler, W., Arnold, G. J., Schwinzer, R., Schieker, M., and Wolf, E. (2012). First inducible transgene expression in porcine large animal models. *FASEB J* **26**, 1086-99.

Kokame, K., Agarwala, K. L., Kato, H., and Miyata, T. (2000). Herp, a new ubiquitin-like membrane protein induced by endoplasmic reticulum stress. *J Biol Chem* **275**, 32846-53.

Kokame, K., Kato, H., and Miyata, T. (2001). Identification of ERSE-II, a new cis-acting element responsible for the ATF6-dependent mammalian unfolded protein response. *J Biol Chem* **276**, 9199-205.

Korbutt, G. S., Elliott, J. F., Ao, Z., Smith, D. K., Warnock, G. L., and Rajotte, R. V. (1996). Large scale isolation, growth, and function of porcine neonatal islet cells. *J Clin Invest* **97**, 2119-29.

Kraft W., D. U. M. (2005). Klinische Labordiagnostik in der Tiermedizin. Schattauerverlag, Stuttgart, New York.

Kues, W. A., and Niemann, H. (2004). The contribution of farm animals to human health. *Trends Biotechnol* **22**, 286-94.

Kukreja, A., and Maclaren, N. K. (1999). Autoimmunity and diabetes. *J Clin Endocrinol Metab* **84**, 4371-8.

Kurome, M., Ishikawa, T., Tomii, R., Ueno, S., Shimada, A., Yazawa, H., and Nagashima, H. (2008). Production of transgenic and non-transgenic clones in miniature pigs by somatic cell nuclear transfer. *J Reprod Dev* **54**, 156-63.

Kurome, M., Ueda, H., Tomii, R., Naruse, K., and Nagashima, H. (2006). Production of transgenic-clone pigs by the combination of ICSI-mediated gene transfer with somatic cell nuclear transfer. *Transgenic Res* **15**, 229-40.

Kuzuya, T., Nakagawa, S., Satoh, J., Kanazawa, Y., Iwamoto, Y., Kobayashi, M., Nanjo, K., Sasaki, A., Seino, Y., Ito, C., Shima, K., Nonaka, K., Kadowaki, T., and Committee of the Japan Diabetes Society on the diagnostic criteria of diabetes, m. (2002). Report of the Committee on the classification and diagnostic criteria of diabetes mellitus. *Diabetes Res Clin Pract* **55**, 65-85.

Kwok, S. C., Steiner, D. F., Rubenstein, A. H., and Tager, H. S. (1983). Identification of a point mutation in the human insulin gene giving rise to a structurally abnormal insulin (insulin Chicago). *Diabetes* **32**, 872-5.

Ladias, J. A., Hadzopoulou-Cladaras, M., Kardassis, D., Cardot, P., Cheng, J., Zannis, V., and Cladaras, C. (1992). Transcriptional regulation of human apolipoprotein genes ApoB, ApoCIII, and ApoAII by members of the steroid hormone receptor superfamily HNF-4, ARP-1, EAR-2, and EAR-3. *J Biol Chem* **267**, 15849-60.

Lan, M. S., Wasserfall, C., Maclaren, N. K., and Notkins, A. L. (1996). IA-2, a transmembrane protein of the protein tyrosine phosphatase family, is a major autoantigen in insulin-dependent diabetes mellitus. *Proc Natl Acad Sci U S A* **93**, 6367-70.

Larsen, M. O., Gotfredsen, C. F., Wilken, M., Carr, R. D., Porksen, N., and Rolin, B. (2003a). Loss of beta-cell mass leads to a reduction of pulse mass with normal periodicity, regularity and entrainment of pulsatile insulin secretion in Gottingen minipigs. *Diabetologia* **46**, 195-202.

Larsen, M. O., and Rolin, B. (2004). Use of the Gottingen minipig as a model of diabetes, with special focus on type 1 diabetes research. *ILAR J* **45**, 303-13.

Larsen, M. O., Rolin, B., Wilken, M., Carr, R. D., and Gotfredsen, C. F. (2003b). Measurements of insulin secretory capacity and glucose tolerance to predict pancreatic beta-cell mass in vivo in the nicotinamide/streptozotocin Gottingen minipig, a model of moderate insulin deficiency and diabetes. *Diabetes* **52**, 118-23.

Larsen, M. O., Rolin, B., Wilken, M., Carr, R. D., Svendsen, O., and Bollen, P. (2001). Parameters of glucose and lipid metabolism in the male Gottingen minipig: influence of age, body weight, and breeding family. *Comp Med* **51**, 436-42.

Larsson, K., Elding-Larsson, H., Cederwall, E., Kockum, K., Neiderud, J., Sjoblad, S., Lindberg, B., Lernmark, B., Cilio, C., Ivarsson, S. A., and Lernmark, A. (2004). Genetic and perinatal factors as risk for childhood type 1 diabetes. *Diabetes Metab Res Rev* **20**, 429-37.

Laybutt, D. R., Kaneto, H., Hasenkamp, W., Grey, S., Jonas, J. C., Sgroi, D. C., Groff, A., Ferran, C., Bonner-Weir, S., Sharma, A., and Weir, G. C. (2002). Increased expression of antioxidant and antiapoptotic genes in islets that may contribute to beta-cell survival during chronic hyperglycemia. *Diabetes* **51**, 413-23.

Laybutt, D. R., Preston, A. M., Akerfeldt, M. C., Kench, J. G., Busch, A. K., Biankin, A. V., and Biden, T. J. (2007). Endoplasmic reticulum stress contributes to beta cell apoptosis in type 2 diabetes. *Diabetologia* **50**, 752-63.

Leahy, J. L. (2005). Pathogenesis of type 2 diabetes mellitus. *Arch Med Res* **36**, 197-209.

Lee, A. H., Iwakoshi, N. N., and Glimcher, L. H. (2003). XBP-1 regulates a subset of endoplasmic reticulum resident chaperone genes in the unfolded protein response. *Mol Cell Biol* **23**, 7448-59.

Lee, M. C., Miller, E. A., Goldberg, J., Orci, L., and Schekman, R. (2004). Bi-directional protein transport between the ER and Golgi. *Annu Rev Cell Dev Biol* **20**, 87-123.

Lee, S., Muniyappa, R., Yan, X., Chen, H., Yue, L. Q., Hong, E. G., Kim, J. K., and Quon, M. J. (2008). Comparison between surrogate indexes of insulin sensitivity and resistance and hyperinsulinemic euglycemic clamp estimates in mice. *Am J Physiol Endocrinol Metab* **294**, E261-70.

Lei, K., Nimnual, A., Zong, W. X., Kennedy, N. J., Flavell, R. A., Thompson, C. B., Bar-Sagi, D., and Davis, R. J. (2002). The Bax subfamily of Bcl2-related proteins is essential for apoptotic signal transduction by c-Jun NH(2)-terminal kinase. *Mol Cell Biol* **22**, 4929-42.

Lemmon, M. A., and Schlessinger, J. (2010). Cell signaling by receptor tyrosine kinases. *Cell* **141**, 1117-34.

Lenzen, S. (2008). The mechanisms of alloxan- and streptozotocin-induced diabetes. *Diabetologia* **51**, 216-26.

Lenzen, S., Freytag, S., and Panten, U. (1988). Inhibition of glucokinase by alloxan through interaction with SH groups in the sugar-binding site of the enzyme. *Mol Pharmacol* **34**, 395-400.

Lenzen, S., Tiedge, M., and Panten, U. (1987). Glucokinase in pancreatic B-cells and its inhibition by alloxan. *Acta Endocrinol (Copenh)* **115**, 21-9.

Leppa, S., and Bohmann, D. (1999). Diverse functions of JNK signaling and c-Jun in stress response and apoptosis. *Oncogene* **18**, 6158-62.

Lipson, K. L., Ghosh, R., and Urano, F. (2008). The role of IRE1alpha in the degradation of insulin mRNA in pancreatic beta-cells. *PLoS One* **3**, e1648.

Litten-Brown, J. C., Corson, A. M., and Clarke, L. (2010). Porcine models for the metabolic syndrome, digestive and bone disorders: a general overview. *Animal* **4**, 899-920.

Liu, C. Y., and Kaufman, R. J. (2003). The unfolded protein response. *J Cell Sci* **116**, 1861-2.

Liu, C. Y., Schroder, M., and Kaufman, R. J. (2000). Ligand-independent dimerization activates the stress response kinases IRE1 and PERK in the lumen of the endoplasmic reticulum. *J Biol Chem* **275**, 24881-5.

Liu, C. Y., Wong, H. N., Schauerte, J. A., and Kaufman, R. J. (2002). The protein kinase/endoribonuclease IRE1alpha that signals the unfolded protein response has a luminal N-terminal ligand-independent dimerization domain. *J Biol Chem* **277**, 18346-56.

Liu, M., Hodish, I., Haataja, L., Lara-Lemus, R., Rajpal, G., Wright, J., and Arvan, P. (2010). Proinsulin misfolding and diabetes: mutant INS gene-induced diabetes of youth. *Trends Endocrinol Metab* **21**, 652-9.

Liu, M., Hodish, I., Rhodes, C. J., and Arvan, P. (2007). Proinsulin maturation, misfolding, and proteotoxicity. *Proc Natl Acad Sci U S A* **104**, 15841-6.

Liu, M., Li, Y., Cavener, D., and Arvan, P. (2005). Proinsulin disulfide maturation and misfolding in the endoplasmic reticulum. *J Biol Chem* **280**, 13209-12.

Lohr, M., Lubbersmeyer, J., Otremba, B., Klapdor, R., Grossner, D., and Kloppel, G. (1989). Increase in B-cells in the pancreatic remnant after partial pancreatectomy in pigs. An immunocytochemical and functional study. *Virchows Arch B Cell Pathol Incl Mol Pathol* **56**, 277-86.

Lottmann, H., Vanselow, J., Hessabi, B., and Walther, R. (2001). The Tet-On system in transgenic mice: inhibition of the mouse pdx-1 gene activity by antisense RNA expression in pancreatic beta-cells. *J Mol Med (Berl)* **79**, 321-8.

Louet, J. F., LeMay, C., and Mauvais-Jarvis, F. (2004). Antidiabetic actions of estrogen: insight from human and genetic mouse models. *Curr Atheroscler Rep* **6**, 180-5.

Lu, J., Li, Q., Xie, H., Chen, Z. J., Borovitskaya, A. E., Maclaren, N. K., Notkins, A. L., and Lan, M. S. (1996). Identification of a second transmembrane protein tyrosine phosphatase, IA-2beta, as an autoantigen in insulin-dependent diabetes mellitus: precursor of the 37-kDa tryptic fragment. *Proc Natl Acad Sci U S A* **93**, 2307-11.

Lu, P. D., Harding, H. P., and Ron, D. (2004). Translation reinitiation at alternative open reading frames regulates gene expression in an integrated stress response. *J Cell Biol* **167**, 27-33.

Ludvik, B., Nolan, J. J., Baloga, J., Sacks, D., and Olefsky, J. (1995). Effect of obesity on insulin resistance in normal subjects and patients with NIDDM. *Diabetes* **44**, 1121-5.

Lukinius, A., Korsgren, O., Grimelius, L., and Wilander, E. (1996). Expression of islet amyloid polypeptide in fetal and adult porcine and human pancreatic islet cells. *Endocrinology* **137**, 5319-25.

Lunney, J. K. (2007). Advances in swine biomedical model genomics. *Int J Biol Sci* **3**, 179-84.

Ma, Y., Brewer, J. W., Diehl, J. A., and Hendershot, L. M. (2002). Two distinct stress signaling pathways converge upon the CHOP promoter during the mammalian unfolded protein response. *J Mol Biol* **318**, 1351-65.

Ma, Y., and Hendershot, L. M. (2002). The mammalian endoplasmic reticulum as a sensor for cellular stress. *Cell Stress Chaperones* **7**, 222-9.

Maedler, K., Schulthess, F. T., Bielman, C., Berney, T., Bonny, C., Prentki, M., Donath, M. Y., and Roduit, R. (2008). Glucose and leptin induce apoptosis in human beta-cells and impair glucose-stimulated insulin secretion through activation of c-Jun N-terminal kinases. *FASEB J* **22**, 1905-13.

Maes, M., Underwood, L. E., and Ketelslegers, J. M. (1986). Low serum somatomedin-C in insulin-dependent diabetes: evidence for a postreceptor mechanism. *Endocrinology* **118**, 377-82.

Mahimainathan, L., Das, F., Venkatesan, B., and Choudhury, G. G. (2006). Mesangial cell hypertrophy by high glucose is mediated by downregulation of the tumor suppressor PTEN. *Diabetes* **55**, 2115-25.

Malaisse, W. J. (1982). Alloxan toxicity to the pancreatic B-cell. A new hypothesis. *Biochem Pharmacol* **31**, 3527-34.

Malecki, M. T., Jhala, U. S., Antonellis, A., Fields, L., Doria, A., Orban, T., Saad, M., Warram, J. H., Montminy, M., and Krolewski, A. S. (1999). Mutations in NEUROD1 are associated with the development of type 2 diabetes mellitus. *Nat Genet* **23**, 323-8.

Malecki, M. T., and Mlynarski, W. (2008). Monogenic diabetes: implications for therapy of rare types of disease. *Diabetes Obes Metab* **10**, 607-16.

Marciniak, S. J., Yun, C. Y., Oyadomari, S., Novoa, I., Zhang, Y., Jungreis, R., Nagata, K., Harding, H. P., and Ron, D. (2004). CHOP induces death by promoting protein synthesis and oxidation in the stressed endoplasmic reticulum. *Genes Dev* **18**, 3066-77.

Marquardt, T., and Helenius, A. (1992). Misfolding and aggregation of newly synthesized proteins in the endoplasmic reticulum. *J Cell Biol* **117**, 505-13.

Mason, R. M., and Wahab, N. A. (2003). Extracellular matrix metabolism in diabetic nephropathy. *J Am Soc Nephrol* **14**, 1358-73.

Matschinsky, F. M., Glaser, B., and Magnuson, M. A. (1998). Pancreatic beta-cell glucokinase: closing the gap between theoretical concepts and experimental realities. *Diabetes* **47**, 307-15.

Matsunari, H., and Nagashima, H. (2009). Application of genetically modified and cloned pigs in translational research. *J Reprod Dev* **55**, 225-30.

Matsuoka, T. A., Zhao, L., Artner, I., Jarrett, H. W., Friedman, D., Means, A., and Stein, R. (2003). Members of the large Maf transcription family regulate insulin gene transcription in islet beta cells. *Mol Cell Biol* **23**, 6049-62.

Matthews, D. R., Hosker, J. P., Rudenski, A. S., Naylor, B. A., Treacher, D. F., and Turner, R. C. (1985). Homeostasis model assessment: insulin resistance and beta-cell function from fasting plasma glucose and insulin concentrations in man. *Diabetologia* **28**, 412-9.

Mayer, J. P., Zhang, F., and DiMarchi, R. D. (2007). Insulin structure and function. *Biopolymers* **88**, 687-713.

Maytin, E. V., Ubeda, M., Lin, J. C., and Habener, J. F. (2001). Stress-inducible transcription factor CHOP/gadd153 induces apoptosis in mammalian cells via p38 kinase-dependent and -independent mechanisms. *Exp Cell Res* **267**, 193-204.

McCullough, K. D., Martindale, J. L., Klotz, L. O., Aw, T. Y., and Holbrook, N. J. (2001). Gadd153 sensitizes cells to endoplasmic reticulum stress by down-regulating Bcl2 and perturbing the cellular redox state. *Mol Cell Biol* **21**, 1249-59.

Melloul, D., Ben-Neriah, Y., and Cerasi, E. (1993). Glucose modulates the binding of an islet-specific factor to a conserved sequence within the rat I and the human insulin promoters. *Proc Natl Acad Sci U S A* **90**, 3865-9.

Melo, E. O., Canavessi, A. M., Franco, M. M., and Rumpf, R. (2007). Animal transgenesis: state of the art and applications. *J Appl Genet* **48**, 47-61.

Melville, M. W., Tan, S. L., Wambach, M., Song, J., Morimoto, R. I., and Katze, M. G. (1999). The cellular inhibitor of the PKR protein kinase, P58(IPK), is an influenza virus-activated co-chaperone that modulates heat shock protein 70 activity. *J Biol Chem* **274**, 3797-803.

Menge, B. A., Tannapfel, A., Belyaev, O., Drescher, R., Muller, C., Uhl, W., Schmidt, W. E., and Meier, J. J. (2008). Partial pancreatectomy in adult humans does not provoke beta-cell regeneration. *Diabetes* **57**, 142-9.

Menting, J. G., Whittaker, J., Margetts, M. B., Whittaker, L. J., Kong, G. K., Smith, B. J., Watson, C. J., Zakova, L., Kletvikova, E., Jiracek, J., Chan, S. J., Steiner, D. F., Dodson, G. G., Brzozowski, A. M., Weiss, M. A., Ward, C. W., and Lawrence, M. C. (2013). How insulin engages its primary binding site on the insulin receptor. *Nature* **493**, 241-5.

Merger, S. R., Leslie, R. D., and Boehm, B. O. (2012). The broad clinical phenotype of Type 1 diabetes at presentation. *Diabet Med*.

Metzger, B. E., Buchanan, T. A., Coustan, D. R., de Leiva, A., Dunger, D. B., Hadden, D. R., Hod, M., Kitzmiller, J. L., Kjos, S. L., Oats, J. N., Pettitt, D. J., Sacks, D. A., and Zoupas, C. (2007). Summary and recommendations of the Fifth International Workshop-Conference on Gestational Diabetes Mellitus. *Diabetes Care* **30 Suppl 2**, S251-60.

Meyer, W. (1996). [Comments on the suitability of swine skin as a biological model for human skin]. *Hautarzt* **47**, 178-82.

Miller, E. R., and Ullrey, D. E. (1987). The pig as a model for human nutrition. *Annu Rev Nutr* **7**, 361-82.

Mirmira, R. G., Nakagawa, S. H., and Tager, H. S. (1991). Importance of the character and configuration of residues B24, B25, and B26 in insulin-receptor interactions. *J Biol Chem* **266**, 1428-36.

Mirmira, R. G., and Tager, H. S. (1989). Role of the phenylalanine B24 side chain in directing insulin interaction with its receptor. Importance of main chain conformation. *J Biol Chem* **264**, 6349-54.

Mizisin, A. P., Nelson, R. W., Sturges, B. K., Vernau, K. M., Lecouteur, R. A., Williams, D. C., Burgers, M. L., and Shelton, G. D. (2007). Comparable myelinated nerve pathology in feline and human diabetes mellitus. *Acta Neuropathol* **113**, 431-42.

Mogensen, C. E., Christensen, C. K., and Vittinghus, E. (1983). The stages in diabetic renal disease. With emphasis on the stage of incipient diabetic nephropathy. *Diabetes* **32 Suppl 2**, 64-78.

Molven, A., Ringdal, M., Nordbo, A. M., Raeder, H., Stoy, J., Lipkind, G. M., Steiner, D. F., Philipson, L. H., Bergmann, I., Aarskog, D., Undlien, D. E., Joner, G., Sovik, O., Norwegian Childhood Diabetes Study, G., Bell, G. I., and Njolstad, P. R. (2008). Mutations in the insulin gene can cause MODY and autoantibody-negative type 1 diabetes. *Diabetes* **57**, 1131-5.

Monshouwer, M., and Witkamp, R. F. (2000). Cytochromes and cytokines: changes in drug disposition in animals during an acute phase response: a mini-review. *Vet Q* **22**, 17-20.

Moody, A. J., Thim, L., and Valverde, I. (1984). The isolation and sequencing of human gastric inhibitory peptide (GIP). *FEBS Lett* **172**, 142-8.

Morishima, N., Nakanishi, K., Takenouchi, H., Shibata, T., and Yasuhiko, Y. (2002). An endoplasmic reticulum stress-specific caspase cascade in apoptosis. Cytochrome c-independent activation of caspase-9 by caspase-12. *J Biol Chem* **277**, 34287-94.

Mouse Genome Sequencing, C., Waterston, R. H., Lindblad-Toh, K., Birney, E., Rogers, J., Abril, J. F., Agarwal, P., Agarwala, R., Ainscough, R., Alexandersson, M., et al. (2002). Initial sequencing and comparative analysis of the mouse genome. *Nature* **420**, 520-62.

Murakami, T., Hitomi, S., Ohtsuka, A., Taguchi, T., and Fujita, T. (1997). Pancreatic insulo-acinar portal systems in humans, rats, and some other mammals: scanning electron microscopy of vascular casts. *Microsc Res Tech* **37**, 478-88.

Nadanaka, S., Okada, T., Yoshida, H., and Mori, K. (2007). Role of disulfide bridges formed in the luminal domain of ATF6 in sensing endoplasmic reticulum stress. *Mol Cell Biol* **27**, 1027-43.

Nadanaka, S., Yoshida, H., Kano, F., Murata, M., and Mori, K. (2004). Activation of mammalian unfolded protein response is compatible with the quality control system operating in the endoplasmic reticulum. *Mol Biol Cell* **15**, 2537-48.

Nadav, E., Shmueli, A., Barr, H., Gonen, H., Ciechanover, A., and Reiss, Y. (2003). A novel mammalian endoplasmic reticulum ubiquitin ligase homologous to the yeast Hrd1. *Biochem Biophys Res Commun* **303**, 91-7.

Nakagawa, S. H., Hua, Q. X., Hu, S. Q., Jia, W., Wang, S., Katsoyannis, P. G., and Weiss, M. A. (2006). Chiral mutagenesis of insulin. Contribution of the B20-B23 beta-turn to activity and stability. *J Biol Chem* **281**, 22386-96.

Nakagawa, S. H., and Tager, H. S. (1991). Implications of invariant residue LeuB6 in insulin-receptor interactions. *J Biol Chem* **266**, 11502-9.

Nakagawa, S. H., Zhao, M., Hua, Q. X., Hu, S. Q., Wan, Z. L., Jia, W., and Weiss, M. A. (2005). Chiral mutagenesis of insulin. Foldability and function are inversely regulated by a stereospecific switch in the B chain. *Biochemistry* **44**, 4984-99.

Nakagawa, T., and Yuan, J. (2000). Cross-talk between two cysteine protease families. Activation of caspase-12 by calpain in apoptosis. *J Cell Biol* **150**, 887-94.

Nakagawa, T., Zhu, H., Morishima, N., Li, E., Xu, J., Yankner, B. A., and Yuan, J. (2000). Caspase-12 mediates endoplasmic-reticulum-specific apoptosis and cytotoxicity by amyloid-beta. *Nature* **403**, 98-103.

Nanjo, K., Sanke, T., Miyano, M., Okai, K., Sowa, R., Kondo, M., Nishimura, S., Iwo, K., Miyamura, K., Given, B. D., and et al. (1986). Diabetes due to secretion of a structurally abnormal insulin (insulin Wakayama). Clinical and functional characteristics of [LeuA3] insulin. *J Clin Invest* **77**, 514-9.

Naya, F. J., Stellrecht, C. M., and Tsai, M. J. (1995). Tissue-specific regulation of the insulin gene by a novel basic helix-loop-helix transcription factor. *Genes Dev* **9**, 1009-19.

Neuhof, A., Rolls, M. M., Jungnickel, B., Kalies, K. U., and Rapoport, T. A. (1998). Binding of signal recognition particle gives ribosome/nascent chain complexes a competitive advantage in endoplasmic reticulum membrane interaction. *Mol Biol Cell* **9**, 103-15.

Nicol, D. S., and Smith, L. F. (1960). Amino-acid sequence of human insulin. *Nature* **187**, 483-5.

Nishitoh, H., Matsuzawa, A., Tobiume, K., Saegusa, K., Takeda, K., Inoue, K., Hori, S., Kakizuka, A., and Ichijo, H. (2002). ASK1 is essential for endoplasmic reticulum stress-induced neuronal cell death triggered by expanded polyglutamine repeats. *Genes Dev* **16**, 1345-55.

Nishitoh, H., Saitoh, M., Mochida, Y., Takeda, K., Nakano, H., Rothe, M., Miyazono, K., and Ichijo, H. (1998). ASK1 is essential for JNK/SAPK activation by TRAF2. *Mol Cell* **2**, 389-95.

Njolstad, P. R., Sovik, O., Cuesta-Munoz, A., Bjorkhaug, L., Massa, O., Barbetti, F., Undlien, D. E., Shiota, C., Magnuson, M. A., Molven, A., Matschinsky, F. M., and Bell, G. I. (2001). Neonatal diabetes mellitus due to complete glucokinase deficiency. *N Engl J Med* **344**, 1588-92.

Noguchi, K., Kitanaka, C., Yamana, H., Kokubu, A., Mochizuki, T., and Kuchino, Y. (1999). Regulation of c-Myc through phosphorylation at Ser-62 and Ser-71 by c-Jun N-terminal kinase. *J Biol Chem* **274**, 32580-7.

Noiva, R. (1999). Protein disulfide isomerase: the multifunctional redox chaperone of the endoplasmic reticulum. *Semin Cell Dev Biol* **10**, 481-93.

Notkins, A. L., Lu, J., Li, Q., VanderVegt, F. P., Wasserfall, C., Maclaren, N. K., and Lan, M. S. (1996). IA-2 and IA-2 beta are major autoantigens in IDDM and the precursors of the 40 kDa and 37 kDa tryptic fragments. *J Autoimmun* **9**, 677-82.

Nyengaard, J. R. (1999). Stereologic methods and their application in kidney research. *J Am Soc Nephrol* **10**, 1100-23.

O'Brien, T. D., Butler, P. C., Westermark, P., and Johnson, K. H. (1993). Islet amyloid polypeptide: a review of its biology and potential roles in the pathogenesis of diabetes mellitus. *Vet Pathol* **30**, 317-32.

O'Brien, T. D., Wagner, J. D., Litwak, K. N., Carlson, C. S., Cefalu, W. T., Jordan, K., Johnson, K. H., and Butler, P. C. (1996). Islet amyloid and islet amyloid polypeptide in cynomolgus macaques (Macaca fascicularis): an animal model of human non-insulin-dependent diabetes mellitus. *Vet Pathol* **33**, 479-85.

Okada, T., Yoshida, H., Akazawa, R., Negishi, M., and Mori, K. (2002). Distinct roles of activating transcription factor 6 (ATF6) and double-stranded RNA-activated protein kinase-like endoplasmic reticulum kinase (PERK) in transcription during the mammalian unfolded protein response. *Biochem J* **366**, 585-94.

Oohashi, H., Ohgawara, H., Nanjo, K., Tasaka, Y., Cao, Q. P., Chan, S. J., Rubenstein, A. H., Steiner, D. F., and Omori, Y. (1993). Familial hyperproinsulinemia associated with NIDDM. A case study. *Diabetes Care* **16**, 1340-6.

Orskov, C. (1992). Glucagon-like peptide-1, a new hormone of the entero-insular axis. *Diabetologia* **35**, 701-11.

Osterby, R., and Gundersen, H. J. (1975). Glomerular size and structure in diabetes mellitus. I. Early abnormalities. *Diabetologia* **11**, 225-9.

Oyadomari, S., Koizumi, A., Takeda, K., Gotoh, T., Akira, S., Araki, E., and Mori, M. (2002). Targeted disruption of the Chop gene delays endoplasmic reticulum stress-mediated diabetes. *J Clin Invest* **109**, 525-32.

Oyadomari, S., and Mori, M. (2004). Roles of CHOP/GADD153 in endoplasmic reticulum stress. *Cell Death Differ* **11**, 381-9.

Pagtalunan, M. E., Miller, P. L., Jumping-Eagle, S., Nelson, R. G., Myers, B. D., Rennke, H. G., Coplon, N. S., Sun, L., and Meyer, T. W. (1997). Podocyte loss and progressive glomerular injury in type II diabetes. *J Clin Invest* **99**, 342-8.

Pain, V. M. (1996). Initiation of protein synthesis in eukaryotic cells. *Eur J Biochem* **236**, 747-71.

Park, S. Y., Ye, H., Steiner, D. F., and Bell, G. I. (2010). Mutant proinsulin proteins associated with neonatal diabetes are retained in the endoplasmic reticulum and not efficiently secreted. *Biochem Biophys Res Commun* **391**, 1449-54.

Parodi, A. J. (2000). Protein glucosylation and its role in protein folding. *Annu Rev Biochem* **69**, 69-93.

Patil, C., and Walter, P. (2001). Intracellular signaling from the endoplasmic reticulum to the nucleus: the unfolded protein response in yeast and mammals. *Curr Opin Cell Biol* **13**, 349-55.

Pearson, E. R., Starkey, B. J., Powell, R. J., Gribble, F. M., Clark, P. M., and Hattersley, A. T. (2003). Genetic cause of hyperglycaemia and response to treatment in diabetes. *Lancet* **362**, 1275-81.

Petrash, J. M. (2004). All in the family: aldose reductase and closely related aldo-keto reductases. *Cell Mol Life Sci* **61**, 737-49.

Pociot, F., and McDermott, M. F. (2002). Genetics of type 1 diabetes mellitus. *Genes Immun* **3**, 235-49.

Polak, M., and Cave, H. (2007). Neonatal diabetes mellitus: a disease linked to multiple mechanisms. *Orphanet J Rare Dis* **2**, 12.

Polak, M., Dechaume, A., Cave, H., Nimri, R., Crosnier, H., Sulmont, V., de Kerdanet, M., Scharfmann, R., Lebenthal, Y., Froguel, P., Vaxillaire, M., and French, N. D. S. G. (2008). Heterozygous missense mutations in the insulin gene are linked to permanent diabetes appearing in the neonatal period or in early infancy: a report from the French ND (Neonatal Diabetes) Study Group. *Diabetes* **57**, 1115-9.

Polejaeva, I. A., Chen, S. H., Vaught, T. D., Page, R. L., Mullins, J., Ball, S., Dai, Y., Boone, J., Walker, S., Ayares, D. L., Colman, A., and Campbell, K. H. (2000). Cloned pigs produced by nuclear transfer from adult somatic cells. *Nature* **407**, 86-90.

Potter, K. J., Abedini, A., Marek, P., Klimek, A. M., Butterworth, S., Driscoll, M., Baker, R., Nilsson, M. R., Warnock, G. L., Oberholzer, J., Bertera, S., Trucco, M., Korbutt, G. S., Fraser, P. E., Raleigh, D. P., and Verchere, C. B. (2010). Islet amyloid deposition limits the viability of human islet grafts but not porcine islet grafts. *Proc Natl Acad Sci U S A* **107**, 4305-10.

Prather, R. S., Hawley, R. J., Carter, D. B., Lai, L., and Greenstein, J. L. (2003). Transgenic swine for biomedicine and agriculture. *Theriogenology* **59**, 115-23.

Prather, R. S., Ross, J. W., Isom, S. C., and Green, J. A. (2009). Transcriptional, post-transcriptional and epigenetic control of porcine oocyte maturation and embryogenesis. *Soc Reprod Fertil Suppl* **66**, 165-76.

Quesada, I., Tuduri, E., Ripoll, C., and Nadal, A. (2008). Physiology of the pancreatic alpha-cell and glucagon secretion: role in glucose homeostasis and diabetes. *J Endocrinol* **199**, 5-19.

Qvist, M. H., Hoeck, U., Kreilgaard, B., Madsen, F., and Frokjaer, S. (2000). Evaluation of Gottingen minipig skin for transdermal in vitro permeation studies. *Eur J Pharm Sci* **11**, 59-68.

Rahier, J., Goebbels, R. M., and Henquin, J. C. (1983). Cellular composition of the human diabetic pancreas. *Diabetologia* **24**, 366-71.

Rajan, S., Eames, S. C., Park, S. Y., Labno, C., Bell, G. I., Prince, V. E., and Philipson, L. H. (2010). In vitro processing and secretion of mutant insulin proteins that cause permanent neonatal diabetes. *Am J Physiol Endocrinol Metab* **298**, E403-10.

Ramachandran, A., Snehalatha, C., Latha, E., Manoharan, M., and Vijay, V. (1999). Impacts of urbanisation on the lifestyle and on the prevalence of diabetes in native Asian Indian population. *Diabetes Res Clin Pract* **44**, 207-13.

Ramage, I. J., Howatson, A. G., McColl, J. H., Maxwell, H., Murphy, A. V., and Beattie, T. J. (2002). Glomerular basement membrane thickness in children: a stereologic assessment. *Kidney Int* **62**, 895-900.

Ramji, D. P., and Foka, P. (2002). CCAAT/enhancer-binding proteins: structure, function and regulation. *Biochem J* **365**, 561-75.

Rao, R. V., Ellerby, H. M., and Bredesen, D. E. (2004). Coupling endoplasmic reticulum stress to the cell death program. *Cell Death Differ* **11**, 372-80.

Rao, R. V., Hermel, E., Castro-Obregon, S., del Rio, G., Ellerby, L. M., Ellerby, H. M., and Bredesen, D. E. (2001). Coupling endoplasmic reticulum stress to the cell death program. Mechanism of caspase activation. *J Biol Chem* **276**, 33869-74.

Recillas-Targa, F. (2006). Multiple strategies for gene transfer, expression, knockdown, and chromatin influence in mammalian cell lines and transgenic animals. *Mol Biotechnol* **34**, 337-54.

Rees, D. A., and Alcolado, J. C. (2005). Animal models of diabetes mellitus. *Diabet Med* **22**, 359-70.

Ren, B., Tibbelin, G., de Pascale, D., Rossi, M., Bartolucci, S., and Ladenstein, R. (1998). A protein disulfide oxidoreductase from the archaeon Pyrococcus furiosus contains two thioredoxin fold units. *Nat Struct Biol* **5**, 602-11.

Renner, S., Braun-Reichhart, C., Blutke, A., Herbach, N., Emrich, D., Streckel, E., Wunsch, A., Kessler, B., Kurome, M., Bahr, A., Klymiuk, N., Krebs, S., Puk, O., Nagashima, H., Graw, J., Blum, H., Wanke, R., and Wolf, E. (2012). Permanent Neonatal Diabetes in INSC94Y Transgenic Pigs. *Diabetes*.

Renner, S., Fehlings, C., Herbach, N., Hofmann, A., von Waldthausen, D. C., Kessler, B., Ulrichs, K., Chodnevskaja, I., Moskalenko, V., Amselgruber, W., Goke, B., Pfeifer, A., Wanke, R., and Wolf, E. (2010). Glucose intolerance and reduced proliferation of pancreatic beta-cells in transgenic pigs with impaired glucose-dependent insulinotropic polypeptide function. *Diabetes* **59**, 1228-38.

reviewed in Martin, R. J., Ramsay, T. G., and Harris, R. B. S. (1984). Central role of insulin in growth and development. *Domestic Animal Endocrinology* **1**, 89-104.

reviewed in Thrailkill, K. M., Lumpkin, C. K., Jr., Bunn, R. C., Kemp, S. F., and Fowlkes, J. L. (2005). Is insulin an anabolic agent in bone? Dissecting the diabetic bone for clues. *Am J Physiol Endocrinol Metab* **289**, E735-45.

Reynolds, E. S. (1963). The use of lead citrate at high pH as an electron-opaque stain in electron microscopy. *J Cell Biol* **17**, 208-12.

Roberts, R. M., Smith, G. W., Bazer, F. W., Cibelli, J., Seidel, G. E., Jr., Bauman, D. E., Reynolds, L. P., and Ireland, J. J. (2009). Research priorities. Farm animal research in crisis. *Science* **324**, 468-9.

Robertson, R. P. (2004). Chronic oxidative stress as a central mechanism for glucose toxicity in pancreatic islet beta cells in diabetes. *J Biol Chem* **279**, 42351-4.

Robertson, R. P., Zhang, H. J., Pyzdrowski, K. L., and Walseth, T. F. (1992). Preservation of insulin mRNA levels and insulin secretion in HIT cells by avoidance of chronic exposure to high glucose concentrations. *J Clin Invest* **90**, 320-5.

Rogatsky, I., Logan, S. K., and Garabedian, M. J. (1998). Antagonism of glucocorticoid receptor transcriptional activation by the c-Jun N-terminal kinase. *Proc Natl Acad Sci U S A* **95**, 2050-5.

Roglic, G., and Unwin, N. (2010). Mortality attributable to diabetes: estimates for the year 2010. *Diabetes Res Clin Pract* **87**, 15-9.

Ron, D. (2002). Translational control in the endoplasmic reticulum stress response. *J Clin Invest* **110**, 1383-8.

Ron, D., and Habener, J. F. (1992). CHOP, a novel developmentally regulated nuclear protein that dimerizes with transcription factors C/EBP and LAP and functions as a dominant-negative inhibitor of gene transcription. *Genes Dev* **6**, 439-53.

Rosenthal, M., Doberne, L., Greenfield, M., Widstrom, A., and Reaven, G. M. (1982). Effect of age on glucose tolerance, insulin secretion, and in vivo insulin action. *J Am Geriatr Soc* **30**, 562-7.

Roy, B., and Lee, A. S. (1999). The mammalian endoplasmic reticulum stress response element consists of an evolutionarily conserved tripartite structure and interacts with a novel stress-inducible complex. *Nucleic Acids Res* **27**, 1437-43.

Rubio-Cabezas, O., Edghill, E. L., Argente, J., and Hattersley, A. T. (2009). Testing for monogenic diabetes among children and adolescents with antibody-negative clinically defined Type 1 diabetes. *Diabet Med* **26**, 1070-4.

Rudolf, M. C., Sherwin, R. S., Markowitz, R., Bates, S. E., Genel, M., Hochstadt, J., and Tamborlane, W. V. (1982). Effect of intensive insulin treatment on linear growth in the young diabetic patient. *J Pediatr* **101**, 333-9.

Russell, W. L., Kelly, E. M., Hunsicker, P. R., Bangham, J. W., Maddux, S. C., and Phipps, E. L. (1979). Specific-locus test shows ethylnitrosourea to be the most potent mutagen in the mouse. *Proc Natl Acad Sci U S A* **76**, 5818-9.

Rutkowski, D. T., and Kaufman, R. J. (2004). A trip to the ER: coping with stress. *Trends Cell Biol* **14**, 20-8.

Salardi, S., Tonioli, S., Tassoni, P., Tellarini, M., Mazzanti, L., and Cacciari, E. (1987). Growth and growth factors in diabetes mellitus. *Arch Dis Child* **62**, 57-62.

Salehi, A., Vieira, E., and Gylfe, E. (2006). Paradoxical stimulation of glucagon secretion by high glucose concentrations. *Diabetes* **55**, 2318-23.

Samuel, C. E. (1993). The eIF-2 alpha protein kinases, regulators of translation in eukaryotes from yeasts to humans. *J Biol Chem* **268**, 7603-6.

Sanger, F. (1959). Chemistry of insulin; determination of the structure of insulin opens the way to greater understanding of life processes. *Science* **129**, 1340-4.

Santiago, J. V., McAlister, W. H., Ratzan, S. K., Bussman, Y., Haymond, M. W., Shackelford, G., and Weldon, V. V. (1977). Decreased cortical thickness & osteopenia in children with diabetes mellitus. *J Clin Endocrinol Metab* **45**, 845-8.

Sayeed, A., and Ng, D. T. (2005). Search and destroy: ER quality control and ER-associated protein degradation. *Crit Rev Biochem Mol Biol* **40**, 75-91.

Sayuk, G. S., Elwing, J. E., and Lisker-Melman, M. (2007). Hepatic glycogenosis: an underrecognized source of abnormal liver function tests? *Dig Dis Sci* **52**, 936-8.

Scherle, W. (1970). A simple method for volumetry of organs in quantitative stereology. *Mikroskopie* **26**, 57-60.

Scheuner, D., and Kaufman, R. J. (2008). The unfolded protein response: a pathway that links insulin demand with beta-cell failure and diabetes. *Endocr Rev* **29**, 317-33.

Schnedl, W. J., Ferber, S., Johnson, J. H., and Newgard, C. B. (1994). STZ transport and cytotoxicity. Specific enhancement in GLUT2-expressing cells. *Diabetes* **43**, 1326-33.

Schreiber, M., Kolbus, A., Piu, F., Szabowski, A., Mohle-Steinlein, U., Tian, J., Karin, M., Angel, P., and Wagner, E. F. (1999). Control of cell cycle progression by c-Jun is p53 dependent. *Genes Dev* **13**, 607-19.

Schroder, M., and Kaufman, R. J. (2005). ER stress and the unfolded protein response. *Mutat Res* **569**, 29-63.

Schuster, M. S. (2011). Impact of 17βEstradiol on β-cell survival of female Munich *Ins2*^{C95S} mutant mice. Inaugural Dissertation, Ludwig Maximilians Universität, Munich.

Scorrano, L., Oakes, S. A., Opferman, J. T., Cheng, E. H., Sorcinelli, M. D., Pozzan, T., and Korsmeyer, S. J. (2003). BAX and BAK regulation of endoplasmic reticulum Ca2+: a control point for apoptosis. *Science* **300**, 135-9.

Scully, T. (2012). Diabetes in numbers. *Nature* **485**, S2-3.

Sellick, G. S., Barker, K. T., Stolte-Dijkstra, I., Fleischmann, C., Coleman, R. J., Garrett, C., Gloyn, A. L., Edghill, E. L., Hattersley, A. T., Wellauer, P. K., Goodwin, G., and Houlston, R. S. (2004). Mutations in PTF1A cause pancreatic and cerebellar agenesis. *Nat Genet* **36**, 1301-5.

Senee, V., Chelala, C., Duchatelet, S., Feng, D., Blanc, H., Cossec, J. C., Charon, C., Nicolino, M., Boileau, P., Cavener, D. R., Bougneres, P., Taha, D., and Julier, C. (2006). Mutations in GLIS3 are responsible for a rare syndrome with neonatal diabetes mellitus and congenital hypothyroidism. *Nat Genet* **38**, 682-7.

Seyer-Hansen, K., Hansen, J., and Gundersen, H. J. (1980). Renal hypertrophy in experimental diabetes. A morphometric study. *Diabetologia* **18**, 501-5.

Sharma, A., Olson, L. K., Robertson, R. P., and Stein, R. (1995). The reduction of insulin gene transcription in HIT-T15 beta cells chronically exposed to high glucose concentration is associated with the loss of RIPE3b1 and STF-1 transcription factor expression. *Mol Endocrinol* **9**, 1127-34.

Shaw, J. E., Sicree, R. A., and Zimmet, P. Z. (2010). Global estimates of the prevalence of diabetes for 2010 and 2030. *Diabetes Res Clin Pract* **87**, 4-14.

Shen, J., Chen, X., Hendershot, L., and Prywes, R. (2002). ER stress regulation of ATF6 localization by dissociation of BiP/GRP78 binding and unmasking of Golgi localization signals. *Dev Cell* **3**, 99-111.

Shen, J., Snapp, E. L., Lippincott-Schwartz, J., and Prywes, R. (2005). Stable binding of ATF6 to BiP in the endoplasmic reticulum stress response. *Mol Cell Biol* **25**, 921-32.

Shi, Y., Vattem, K. M., Sood, R., An, J., Liang, J., Stramm, L., and Wek, R. C. (1998). Identification and characterization of pancreatic eukaryotic initiation factor 2 alpha-subunit kinase, PEK, involved in translational control. *Mol Cell Biol* **18**, 7499-509.

Shield, J. P. (2000). Neonatal diabetes: new insights into aetiology and implications. *Horm Res* **53 Suppl 1**, 7-11.

Shield, J. P., Gardner, R. J., Wadsworth, E. J., Whiteford, M. L., James, R. S., Robinson, D. O., Baum, J. D., and Temple, I. K. (1997). Aetiopathology and genetic basis of neonatal diabetes. *Arch Dis Child Fetal Neonatal Ed* **76**, F39-42.

Slingerland, A. S. (2006). Monogenic diabetes in children and young adults: Challenges for researcher, clinician and patient. *Rev Endocr Metab Disord* **7**, 171-85.

Song, B., Scheuner, D., Ron, D., Pennathur, S., and Kaufman, R. J. (2008). Chop deletion reduces oxidative stress, improves beta cell function, and promotes cell survival in multiple mouse models of diabetes. *J Clin Invest* **118**, 3378-89.

Sonnenberg, G. E., and Berger, M. (1983). Human insulin: much ado about one amino acid? *Diabetologia* **25**, 457-9.

Sousa, M., and Parodi, A. J. (1995). The molecular basis for the recognition of misfolded glycoproteins by the UDP-Glc:glycoprotein glucosyltransferase. *EMBO J* **14**, 4196-203.

Sousa, M. C., Ferrero-Garcia, M. A., and Parodi, A. J. (1992). Recognition of the oligosaccharide and protein moieties of glycoproteins by the UDP-Glc:glycoprotein glucosyltransferase. *Biochemistry* **31**, 97-105.

Spengler, D., Villalba, M., Hoffmann, A., Pantaloni, C., Houssami, S., Bockaert, J., and Journot, L. (1997). Regulation of apoptosis and cell cycle arrest by Zac1, a novel zinc finger protein expressed in the pituitary gland and the brain. *EMBO J* **16**, 2814-25.

Srinivasan, K., and Ramarao, P. (2007). Animal models in type 2 diabetes research: an overview. *Indian J Med Res* **125**, 451-72.

Stefek, M., and Karasu, C. (2011). Eye lens in aging and diabetes: effect of quercetin. *Rejuvenation Res* **14**, 525-34.

Steiner, D. F., Tager, H. S., Chan, S. J., Nanjo, K., Sanke, T., and Rubenstein, A. H. (1990). Lessons learned from molecular biology of insulin-gene mutations. *Diabetes Care* **13**, 600-9.

Steiner, D. J., Kim, A., Miller, K., and Hara, M. (2010). Pancreatic islet plasticity: interspecies comparison of islet architecture and composition. *Islets* **2**, 135-45.

Stoffel, M., and Duncan, S. A. (1997). The maturity-onset diabetes of the young (MODY1) transcription factor HNF4alpha regulates expression of genes required for glucose transport and metabolism. *Proc Natl Acad Sci U S A* **94**, 13209-14.

Stoffers, D. A., Ferrer, J., Clarke, W. L., and Habener, J. F. (1997a). Early-onset type-II diabetes mellitus (MODY4) linked to IPF1. *Nat Genet* **17**, 138-9.

Stoffers, D. A., Zinkin, N. T., Stanojevic, V., Clarke, W. L., and Habener, J. F. (1997b). Pancreatic agenesis attributable to a single nucleotide deletion in the human IPF1 gene coding sequence. *Nat Genet* **15**, 106-10.

Stone, B. G., and Van Thiel, D. H. (1985). Diabetes mellitus and the liver. *Semin Liver Dis* **5**, 8-28.

Stoy, J., Edghill, E. L., Flanagan, S. E., Ye, H., Paz, V. P., Pluzhnikov, A., Below, J. E., Hayes, M. G., Cox, N. J., Lipkind, G. M., Lipton, R. B., Greeley, S. A., Patch, A. M., Ellard, S., Steiner, D. F., Hattersley, A. T., Philipson, L. H., and Bell, G. I. (2007). Insulin gene mutations as a cause of permanent neonatal diabetes. *Proc Natl Acad Sci U S A* **104**, 15040-4.

Stoy, J., Steiner, D. F., Park, S. Y., Ye, H., Philipson, L. H., and Bell, G. I. (2010). Clinical and molecular genetics of neonatal diabetes due to mutations in the insulin gene. *Rev Endocr Metab Disord* **11**, 205-15.

Strasser-Vogel, B., Blum, W. F., Past, R., Kessler, U., Hoeflich, A., Meiler, B., and Kiess, W. (1995). Insulin-like growth factor (IGF)-I and -II and IGF-binding proteins-1, -2, and -3 in children and adolescents with diabetes mellitus: correlation with metabolic control and height attainment. *J Clin Endocrinol Metab* **80**, 1207-13.

Stump, K. C., Swindle, M. M., Saudek, C. D., and Strandberg, J. D. (1988). Pancreatectomized swine as a model of diabetes mellitus. *Lab Anim Sci* **38**, 439-43.

Sundar Rajan, S., Srinivasan, V., Balasubramanyam, M., and Tatu, U. (2007). Endoplasmic reticulum (ER) stress & diabetes. *Indian J Med Res* **125**, 411-24.

Swindle, M. M. i. C., P. M., ed. (2008). "Sourcebook of models for biomedical research." Humana Press Inc., Totowa, , NJ 233-239.

Szegezdi, E., Logue, S. E., Gorman, A. M., and Samali, A. (2006). Mediators of endoplasmic reticulum stress-induced apoptosis. *EMBO Rep* **7**, 880-5.

Tager, H., Given, B., Baldwin, D., Mako, M., Markese, J., Rubenstein, A., Olefsky, J., Kobayashi, M., Kolterman, O., and Poucher, R. (1979). A structurally abnormal insulin causing human diabetes. *Nature* **281**, 122-5.

Tao, B., Pietropaolo, M., Atkinson, M., Schatz, D., and Taylor, D. (2010). Estimating the cost of type 1 diabetes in the U.S.: a propensity score matching method. *PLoS One* **5**, e11501.

Tattersall, R. B., and Pyke, D. A. (1973). Growth in diabetic children. Studies in identical twins. *Lancet* **2**, 1105-9.

Taylor, D. R., Lee, S. B., Romano, P. R., Marshak, D. R., Hinnebusch, A. G., Esteban, M., and Mathews, M. B. (1996). Autophosphorylation sites participate in the activation of the double-stranded-RNA-activated protein kinase PKR. *Mol Cell Biol* **16**, 6295-302.

Temple, I. K., Gardner, R. J., Robinson, D. O., Kibirige, M. S., Ferguson, A. W., Baum, J. D., Barber, J. C., James, R. S., and Shield, J. P. (1996). Further evidence for an imprinted gene for neonatal diabetes localised to chromosome 6q22-q23. *Hum Mol Genet* **5**, 1117-21.

Tesfaye, S., Chaturvedi, N., Eaton, S. E., Ward, J. D., Manes, C., Ionescu-Tirgoviste, C., Witte, D. R., Fuller, J. H., and Group, E. P. C. S. (2005). Vascular risk factors and diabetic neuropathy. *N Engl J Med* **352**, 341-50.

Tiedge, M., Richter, T., and Lenzen, S. (2000). Importance of cysteine residues for the stability and catalytic activity of human pancreatic beta cell glucokinase. *Arch Biochem Biophys* **375**, 251-60.

Tirasophon, W., Lee, K., Callaghan, B., Welihinda, A., and Kaufman, R. J. (2000). The endoribonuclease activity of mammalian IRE1 autoregulates its mRNA and is required for the unfolded protein response. *Genes Dev* **14**, 2725-36.

Tirasophon, W., Welihinda, A. A., and Kaufman, R. J. (1998). A stress response pathway from the endoplasmic reticulum to the nucleus requires a novel bifunctional protein kinase/endoribonuclease (Ire1p) in mammalian cells. *Genes Dev* **12**, 1812-24.

Tjalve, H., Wilander, E., and Johansson, E. B. (1976). Distribution of labeled streptozotocin in mice: uptake and retention in pancreatic islets. *J Endocrinol* **69**, 455-6.

Toledo, F. G., Sniderman, A. D., and Kelley, D. E. (2006). Influence of hepatic steatosis (fatty liver) on severity and composition of dyslipidemia in type 2 diabetes. *Diabetes Care* **29**, 1845-50.

Torbenson, M., Chen, Y. Y., Brunt, E., Cummings, O. W., Gottfried, M., Jakate, S., Liu, Y. C., Yeh, M. M., and Ferrell, L. (2006). Glycogenic hepatopathy: an underrecognized hepatic complication of diabetes mellitus. *Am J Surg Pathol* **30**, 508-13.

Torres, M., and Lopez, D. (2001). Liver glycogen storage associated with uncontrolled type 1 diabetes mellitus. *J Hepatol* **35**, 538.

Tournier, C., Hess, P., Yang, D. D., Xu, J., Turner, T. K., Nimnual, A., Bar-Sagi, D., Jones, S. N., Flavell, R. A., and Davis, R. J. (2000). Requirement of JNK for stress-induced activation of the cytochrome c-mediated death pathway. *Science* **288**, 870-4.

Turner, R. C., Holman, R. R., Matthews, D., Hockaday, T. D., and Peto, J. (1979). Insulin deficiency and insulin resistance interaction in diabetes: estimation of their relative contribution by feedback analysis from basal plasma insulin and glucose concentrations. *Metabolism* **28**, 1086-96.

Turner, R. C., Mathews, D. R., Holman, R. R., and Peto, J. (1982). Relative contributions of insulin deficiency and insulin resistance in maturity-onset diabetes. *Lancet* **1**, 596-8.

Turner, R. C., Matthews, D. R., Clark, A., O'Rahilly, S., Rudenski, A. S., and Levy, J. (1988). Pathogenesis of NIDDM--a disease of deficient insulin secretion. *Baillieres Clin Endocrinol Metab* **2**, 327-42.

Tyrberg, B., Ustinov, J., Otonkoski, T., and Andersson, A. (2001). Stimulated endocrine cell proliferation and differentiation in transplanted human pancreatic islets: effects of the ob gene and compensatory growth of the implantation organ. *Diabetes* **50**, 301-7.

Uchigata, Y., Yamamoto, H., Kawamura, A., and Okamoto, H. (1982). Protection by superoxide dismutase, catalase, and poly(ADP-ribose) synthetase inhibitors against alloxan- and streptozotocin-induced islet DNA strand breaks and against the inhibition of proinsulin synthesis. *J Biol Chem* **257**, 6084-8.

Umeyama, K., Watanabe, M., Saito, H., Kurome, M., Tohi, S., Matsunari, H., Miki, K., and Nagashima, H. (2009). Dominant-negative mutant hepatocyte nuclear factor 1alpha induces diabetes in transgenic-cloned pigs. *Transgenic Res* **18**, 697-706.

Unger, R. H., Aguilar-Parada, E., Muller, W. A., and Eisentraut, A. M. (1970). Studies of pancreatic alpha cell function in normal and diabetic subjects. *J Clin Invest* **49**, 837-48.

Urano, F., Wang, X., Bertolotti, A., Zhang, Y., Chung, P., Harding, H. P., and Ron, D. (2000). Coupling of stress in the ER to activation of JNK protein kinases by transmembrane protein kinase IRE1. *Science* **287**, 664-6.

Vachon, G., Laalami, S., Grunberg-Manago, M., Julien, R., and Cenatiempo, Y. (1990). Purified internal G-domain of translational initiation factor IF-2 displays guanine nucleotide binding properties. *Biochemistry* **29**, 9728-33.

Vajta, G., Zhang, Y., and Machaty, Z. (2007). Somatic cell nuclear transfer in pigs: recent achievements and future possibilities. *Reprod Fertil Dev* **19**, 403-23.

van Deijnen, J. H., Hulstaert, C. E., Wolters, G. H., and van Schilfgaarde, R. (1992). Significance of the peri-insular extracellular matrix for islet isolation from the pancreas of rat, dog, pig, and man. *Cell Tissue Res* **267**, 139-46.

van der Kallen, C. J., van Greevenbroek, M. M., Stehouwer, C. D., and Schalkwijk, C. G. (2009). Endoplasmic reticulum stress-induced apoptosis in the development of diabetes: is there a role for adipose tissue and liver? *Apoptosis* **14**, 1424-34.

Van Lommel, L., Janssens, K., Quintens, R., Tsukamoto, K., Vander Mierde, D., Lemaire, K., Denef, C., Jonas, J. C., Martens, G., Pipeleers, D., and Schuit, F. C. (2006). Probe-independent and direct quantification of insulin mRNA and growth hormone mRNA in enriched cell preparations. *Diabetes* **55**, 3214-20.

Vanelli, M., De Fanti, A., Cantoni, S., and Chiari, G. (1994). Transient neonatal diabetes mellitus: a relapse after 10 years of complete remission. *Acta Diabetol* **31**, 116-8.

Varma, S. D., and Kinoshita, J. H. (1974). The absence of cataracts in mice with congenital hyperglycemia. *Exp Eye Res* **19**, 577-82.

Vattem, K. M., and Wek, R. C. (2004). Reinitiation involving upstream ORFs regulates ATF4 mRNA translation in mammalian cells. *Proc Natl Acad Sci U S A* **101**, 11269-74.

Vaxillaire, M., Boccio, V., Philippi, A., Vigouroux, C., Terwilliger, J., Passa, P., Beckmann, J. S., Velho, G., Lathrop, G. M., and Froguel, P. (1995). A gene for maturity onset diabetes of the young (MODY) maps to chromosome 12q. *Nat Genet* **9**, 418-23.

Vaxillaire, M., and Froguel, P. (2006). Genetic basis of maturity-onset diabetes of the young. *Endocrinol Metab Clin North Am* **35**, 371-84, x.

Vaxillaire, M., Rouard, M., Yamagata, K., Oda, N., Kaisaki, P. J., Boriraj, V. V., Chevre, J. C., Boccio, V., Cox, R. D., Lathrop, G. M., Dussoix, P., Philippe, J., Timsit, J., Charpentier, G., Velho, G., Bell, G. I., and Froguel, P. (1997). Identification of nine novel mutations in the hepatocyte nuclear factor 1 alpha gene associated with maturity-onset diabetes of the young (MODY3). *Hum Mol Genet* **6**, 583-6.

Velho, G., and Froguel, P. (1998). Genetic, metabolic and clinical characteristics of maturity onset diabetes of the young. *Eur J Endocrinol* **138**, 233-9.

Velho, G., Petersen, K. F., Perseghin, G., Hwang, J. H., Rothman, D. L., Pueyo, M. E., Cline, G. W., Froguel, P., and Shulman, G. I. (1996). Impaired hepatic glycogen synthesis in glucokinase-deficient (MODY-2) subjects. *J Clin Invest* **98**, 1755-61.

Veriter, S., Aouassar, N., Beaurin, G., Goebbels, R. M., Gianello, P., and Dufrane, D. (2012). Improvement of Pig Islet Function by In Vivo Pancreatic Tissue Remodeling: A "Human-Like" Pig Islet Structure With Streptozotocin Treatment. *Cell Transplant*.

Verspohl, E. J., and Ammon, H. P. (1980). Evidence for presence of insulin receptors in rat islets of Langerhans. *J Clin Invest* **65**, 1230-7.

von Heijne, G. (1988). Transcending the impenetrable: how proteins come to terms with membranes. *Biochim Biophys Acta* **947**, 307-33.

von Muhlendahl, K. E., and Herkenhoff, H. (1995). Long-term course of neonatal diabetes. *N Engl J Med* **333**, 704-8.

Vuorinen-Markkola, H., Koivisto, V. A., and Yki-Jarvinen, H. (1992). Mechanisms of hyperglycemia-induced insulin resistance in whole body and skeletal muscle of type I diabetic patients. *Diabetes* **41**, 571-80.

Wallace, T. M., Levy, J. C., and Matthews, D. R. (2004). Use and abuse of HOMA modeling. *Diabetes Care* **27**, 1487-95.

Walsh, G., and Jefferis, R. (2006). Post-translational modifications in the context of therapeutic proteins. *Nat Biotechnol* **24**, 1241-52.

Walter, P., and Johnson, A. E. (1994). Signal sequence recognition and protein targeting to the endoplasmic reticulum membrane. *Annu Rev Cell Biol* **10**, 87-119.

Wang, C. C. (1998). Isomerase and chaperone activities of protein disulfide isomerase are both required for its function as a foldase. *Biochemistry (Mosc)* **63**, 407-12.

Wang, H., Maechler, P., Ritz-Laser, B., Hagenfeldt, K. A., Ishihara, H., Philippe, J., and Wollheim, C. B. (2001). Pdx1 level defines pancreatic gene expression pattern and cell lineage differentiation. *J Biol Chem* **276**, 25279-86.

Wang, J., Takeuchi, T., Tanaka, S., Kubo, S. K., Kayo, T., Lu, D., Takata, K., Koizumi, A., and Izumi, T. (1999). A mutation in the insulin 2 gene induces diabetes with severe pancreatic beta-cell dysfunction in the Mody mouse. *J Clin Invest* **103**, 27-37.

Wang, Y., Shen, J., Arenzana, N., Tirasophon, W., Kaufman, R. J., and Prywes, R. (2000). Activation of ATF6 and an ATF6 DNA binding site by the endoplasmic reticulum stress response. *J Biol Chem* **275**, 27013-20.

Wanke, R. (1996). zur Morpho- und Pathogenese der progressiven Glomerulosklerose. pp. 1-257. Ludwig-Maximilians-Universität München.

Wanke, R., Weis, S., Kluge, D., Kahnt, E., Schenck, E., Brem, G. and Hermanns, W. (1994). Morphometric evaluation of the pancreas of growth hormone-transgenic mice. *Acta Stereologica* **13**, 3-3.

Warren-Perry, M. G., Manley, S. E., Ostrega, D., Polonsky, K., Mussett, S., Brown, P., and Turner, R. C. (1997). A novel point mutation in the insulin gene giving rise to hyperproinsulinemia. *J Clin Endocrinol Metab* **82**, 1629-31.

Watanabe, M., Umeyama, K., Kawano, H. O., Izuno, N., Nagashima, H., and Miki, K. (2007). The production of a diabetic mouse using constructs encoding porcine insulin promoter-driven mutant human hepatocyte nuclear factor-1alpha. *J Reprod Dev* **53**, 189-200.

Wedemeyer, W. J., Welker, E., Narayan, M., and Scheraga, H. A. (2000). Disulfide bonds and protein folding. *Biochemistry* **39**, 4207-16.

Wehling, M. (2008). Translational medicine: science or wishful thinking? *J Transl Med* **6**, 31.

Weibel, E. R., and Gomez, D. M. (1962). A principle for counting tissue structures on random sections. *J Appl Physiol* **17**, 343-8.

Weiss, M. A. (2009). Proinsulin and the genetics of diabetes mellitus. *J Biol Chem* **284**, 19159-63.

Welsh, M., Scherberg, N., Gilmore, R., and Steiner, D. F. (1986). Translational control of insulin biosynthesis. Evidence for regulation of elongation, initiation and signal-recognition-particle-mediated translational arrest by glucose. *Biochem J* **235**, 459-67.

Westermark, P., Andersson, A., and Westermark, G. T. (2011). Islet amyloid polypeptide, islet amyloid, and diabetes mellitus. *Physiol Rev* **91**, 795-826.

Weyer, C., Bogardus, C., and Pratley, R. E. (1999). Metabolic characteristics of individuals with impaired fasting glucose and/or impaired glucose tolerance. *Diabetes* **48**, 2197-203.

Wicksteed, B., Uchizono, Y., Alarcon, C., McCuaig, J. F., Shalev, A., and Rhodes, C. J. (2007). A cis-element in the 5' untranslated region of the preproinsulin mRNA (ppIGE) is required for glucose regulation of proinsulin translation. *Cell Metab* **5**, 221-7.

Wieczorek, G., Pospischil, A., and Perentes, E. (1998). A comparative immunohistochemical study of pancreatic islets in laboratory animals (rats, dogs, minipigs, nonhuman primates). *Exp Toxicol Pathol* **50**, 151-72.

Wieczorek, L. A. (2002). Nervenzupfpräparation (nerve fibre teasing) in der Diagnostik peripherer Neuropathien beim Tier: Methodik und Interpretation, Ludwig-Maximilians University, Munich.

Wild, S., Roglic, G., Green, A., Sicree, R., and King, H. (2004). Global prevalence of diabetes: estimates for the year 2000 and projections for 2030. *Diabetes Care* **27**, 1047-53.

Wildin, R. S., Smyk-Pearson, S., and Filipovich, A. H. (2002). Clinical and molecular features of the immunodysregulation, polyendocrinopathy, enteropathy, X linked (IPEX) syndrome. *J Med Genet* **39**, 537-45.

Wilkinson, B. M., Regnacq, M., and Stirling, C. J. (1997). Protein translocation across the membrane of the endoplasmic reticulum. *J Membr Biol* **155**, 189-97.

Wilson, J. D., Dhall, D. P., Simeonovic, C. J., and Lafferty, K. J. (1986). Induction and management of diabetes mellitus in the pig. *Aust J Exp Biol Med Sci* **64 (Pt 6)**, 489-500.

Wiske, P. S., Wentworth, S. M., Norton, J. A., Jr., Epstein, S., and Johnston, C. C., Jr. (1982). Evaluation of bone mass and growth in young diabetics. *Metabolism* **31**, 848-54.

Wolcott, C. D., and Rallison, M. L. (1972). Infancy-onset diabetes mellitus and multiple epiphyseal dysplasia. *J Pediatr* **80**, 292-7.

Wolf, E., Schernthaner, W., Zakhartchenko, V., Prelle, K., Stojkovic, M., and Brem, G. (2000). Transgenic technology in farm animals--progress and perspectives. *Exp Physiol* **85**, 615-25.

Wolf, G. (2004). New insights into the pathophysiology of diabetic nephropathy: from haemodynamics to molecular pathology. *Eur J Clin Invest* **34**, 785-96.

Wu, J., Rutkowski, D. T., Dubois, M., Swathirajan, J., Saunders, T., Wang, J., Song, B., Yau, G. D., and Kaufman, R. J. (2007). ATF6alpha optimizes long-term endoplasmic reticulum function to protect cells from chronic stress. *Dev Cell* **13**, 351-64.

Xu, G., Marshall, C. A., Lin, T. A., Kwon, G., Munivenkatappa, R. B., Hill, J. R., Lawrence, J. C., Jr., and McDaniel, M. L. (1998). Insulin mediates glucose-stimulated phosphorylation of PHAS-I by pancreatic beta cells. An insulin-receptor mechanism for autoregulation of protein synthesis by translation. *J Biol Chem* **273**, 4485-91.

Yaguchi, M., Nagashima, K., Izumi, T., and Okamoto, K. (2003). Neuropathological study of C57BL/6Akita mouse, type 2 diabetic model: enhanced expression of alphaB-crystallin in oligodendrocytes. *Neuropathology* **23**, 44-50.

Yamagata, K., Furuta, H., Oda, N., Kaisaki, P. J., Menzel, S., Cox, N. J., Fajans, S. S., Signorini, S., Stoffel, M., and Bell, G. I. (1996a). Mutations in the hepatocyte nuclear factor-4alpha gene in maturity-onset diabetes of the young (MODY1). *Nature* **384**, 458-60.

Yamagata, K., Oda, N., Kaisaki, P. J., Menzel, S., Furuta, H., Vaxillaire, M., Southam, L., Cox, R. D., Lathrop, G. M., Boriraj, V. V., Chen, X., Cox, N. J., Oda, Y., Yano, H., Le Beau, M. M., Yamada, S., Nishigori, H., Takeda, J., Fajans, S. S., Hattersley, A. T., Iwasaki, N., Hansen, T., Pedersen, O., Polonsky, K. S., Bell, G. I., and et al. (1996b). Mutations in the hepatocyte nuclear factor-1alpha gene in maturity-onset diabetes of the young (MODY3). *Nature* **384**, 455-8.

Yamamoto, H., Uchigata, Y., and Okamoto, H. (1981a). DNA strand breaks in pancreatic islets by in vivo administration of alloxan or streptozotocin. *Biochem Biophys Res Commun* **103**, 1014-20.

Yamamoto, H., Uchigata, Y., and Okamoto, H. (1981b). Streptozotocin and alloxan induce DNA strand breaks and poly(ADP-ribose) synthetase in pancreatic islets. *Nature* **294**, 284-6.

Yamamoto, K., Ichijo, H., and Korsmeyer, S. J. (1999). BCL-2 is phosphorylated and inactivated by an ASK1/Jun N-terminal protein kinase pathway normally activated at G(2)/M. *Mol Cell Biol* **19**, 8469-78.

Yamamoto, K., Sato, T., Matsui, T., Sato, M., Okada, T., Yoshida, H., Harada, A., and Mori, K. (2007). Transcriptional induction of mammalian ER quality control proteins is mediated by single or combined action of ATF6alpha and XBP1. *Dev Cell* **13**, 365-76.

Yamamoto, K., Yoshida, H., Kokame, K., Kaufman, R. J., and Mori, K. (2004). Differential contributions of ATF6 and XBP1 to the activation of endoplasmic reticulum stress-responsive cis-acting elements ERSE, UPRE and ERSE-II. *J Biochem* **136**, 343-50.

Yang, X. O., Panopoulos, A. D., Nurieva, R., Chang, S. H., Wang, D., Watowich, S. S., and Dong, C. (2007). STAT3 regulates cytokine-mediated generation of inflammatory helper T cells. *J Biol Chem* **282**, 9358-63.

Yano, H., Kitano, N., Morimoto, M., Polonsky, K. S., Imura, H., and Seino, Y. (1992). A novel point mutation in the human insulin gene giving rise to hyperproinsulinemia (proinsulin Kyoto). *J Clin Invest* **89**, 1902-7.

Yared, Z., and Chiasson, J. L. (2003). Ketoacidosis and the hyperosmolar hyperglycemic state in adult diabetic patients. Diagnosis and treatment. *Minerva Med* **94**, 409-18.

Ye, J., Rawson, R. B., Komuro, R., Chen, X., Dave, U. P., Prywes, R., Brown, M. S., and Goldstein, J. L. (2000). ER stress induces cleavage of membrane-bound ATF6 by the same proteases that process SREBPs. *Mol Cell* **6**, 1355-64.

Yki-Jarvinen, H., Helve, E., and Koivisto, V. A. (1987). Hyperglycemia decreases glucose uptake in type I diabetes. *Diabetes* **36**, 892-6.

Yoneda, T., Imaizumi, K., Oono, K., Yui, D., Gomi, F., Katayama, T., and Tohyama, M. (2001). Activation of caspase-12, an endoplastic reticulum (ER) resident caspase, through tumor necrosis factor receptor-associated factor 2-dependent mechanism in response to the ER stress. *J Biol Chem* **276**, 13935-40.

Yoon, K. H., Ko, S. H., Cho, J. H., Lee, J. M., Ahn, Y. B., Song, K. H., Yoo, S. J., Kang, M. I., Cha, B. Y., Lee, K. W., Son, H. Y., Kang, S. K., Kim, H. S., Lee, I. K., and Bonner-Weir, S. (2003). Selective beta-cell loss and alpha-cell expansion in patients with type 2 diabetes mellitus in Korea. *J Clin Endocrinol Metab* **88**, 2300-8.

Yoshida, H., Haze, K., Yanagi, H., Yura, T., and Mori, K. (1998). Identification of the cis-acting endoplasmic reticulum stress response element responsible for transcriptional induction of mammalian glucose-regulated proteins. Involvement of basic leucine zipper transcription factors. *J Biol Chem* **273**, 33741-9.

Yoshida, H., Matsui, T., Hosokawa, N., Kaufman, R. J., Nagata, K., and Mori, K. (2003). A time-dependent phase shift in the mammalian unfolded protein response. *Dev Cell* **4**, 265-71.

Yoshida, H., Matsui, T., Yamamoto, A., Okada, T., and Mori, K. (2001a). XBP1 mRNA is induced by ATF6 and spliced by IRE1 in response to ER stress to produce a highly active transcription factor. *Cell* **107**, 881-91.

Yoshida, H., Okada, T., Haze, K., Yanagi, H., Yura, T., Negishi, M., and Mori, K. (2000). ATF6 activated by proteolysis binds in the presence of NF-Y (CBF) directly to the cis-acting element responsible for the mammalian unfolded protein response. *Mol Cell Biol* **20**, 6755-67.

Yoshida, H., Okada, T., Haze, K., Yanagi, H., Yura, T., Negishi, M., and Mori, K. (2001b). Endoplasmic reticulum stress-induced formation of transcription factor complex ERSF including NF-Y (CBF) and activating transcription factors 6alpha and 6beta that activates the mammalian unfolded protein response. *Mol Cell Biol* **21**, 1239-48.

Yoshinaga, T., Nakatome, K., Nozaki, J., Naitoh, M., Hoseki, J., Kubota, H., Nagata, K., and Koizumi, A. (2005). Proinsulin lacking the A7-B7 disulfide bond, Ins2Akita, tends to aggregate due to the exposed hydrophobic surface. *Biol Chem* **386**, 1077-85.

Yoshioka, M., Kayo, T., Ikeda, T., and Koizumi, A. (1997). A novel locus, Mody4, distal to D7Mit189 on chromosome 7 determines early-onset NIDDM in nonobese C57BL/6 (Akita) mutant mice. *Diabetes* **46**, 887-94.

Zatz, R., Meyer, T. W., Rennke, H. G., and Brenner, B. M. (1985). Predominance of hemodynamic rather than metabolic factors in the pathogenesis of diabetic glomerulopathy. *Proc Natl Acad Sci U S A* **82**, 5963-7.

Zhang, L., and Zhao, Y. (2007). The regulation of Foxp3 expression in regulatory CD4(+)CD25(+)T cells: multiple pathways on the road. *J Cell Physiol* **211**, 590-7.

Zimmet, P., Alberti, K. G., and Shaw, J. (2001). Global and societal implications of the diabetes epidemic. *Nature* **414**, 782-7.

Zinszner, H., Kuroda, M., Wang, X., Batchvarova, N., Lightfoot, R. T., Remotti, H., Stevens, J. L., and Ron, D. (1998). CHOP is implicated in programmed cell death in response to impaired function of the endoplasmic reticulum. *Genes Dev* **12**, 982-95.

Zoete, V., and Meuwly, M. (2006). Importance of individual side chains for the stability of a protein fold: computational alanine scanning of the insulin monomer. *J Comput Chem* **27**, 1843-57.

Zou, H., Li, Y., Liu, X., and Wang, X. (1999). An APAF-1.cytochrome c multimeric complex is a functional apoptosome that activates procaspase-9. *J Biol Chem* **274**, 11549-56.

Zuber, C., Fan, J. Y., Guhl, B., and Roth, J. (2004). Misfolded proinsulin accumulates in expanded pre-Golgi intermediates and endoplasmic reticulum subdomains in pancreatic beta cells of Akita mice. *FASEB J* **18**, 917-9.

XII. ACKNOWLEDGEMENT

First of all I would like to express my gratitude to Prof. Dr. Eckhard Wolf for providing me the opportunity to work on this doctorate at the Chair for Molecular Animal Breeding and Biotechnology (LMU, Munich). I am particularly thankful for his constant support and encouragement as well as for critical discussions and for reviewing this manuscript.

I am thankful to Dr. Simone Renner for mentoring and supporting this work as well as for reviewing this manuscript.

I would like to thank Prof. Dr. Rüdiger Wanke for allowing me to work in his laboratory, for his scientific support and for the critical review of this manuscript

Furthermore, I would like to thank Priv.-Doz. Dr. Nadja Herbach, Dr. Andreas Blutke and Dr. Daniela Emrich for great collaboration, for all the data they shared with me, for their helpful advice concerning all pathological questions as well as for reviewing parts of this manuscript.

I would like to acknowledge Dr. Stefan Krebs for performing next generation sequencing, Dr. Oliver Puk for his collaboration concerning lens preparation and Dr. Lelia Wolf-van Bürck for isolating neonatal pancreatic islets.

Many thanks to all my colleagues at the Moorversuchsgut for creating a memorable time. I am especially grateful to Dr. Andrea Bähr, Dr. Barbara Keßler and Michaela Dmochewitz for their expert assistance with the veterinary care for the diabetic pigs during all the weekends and their veterinary expertise. This applies likewise for Siegfried Elsner for his excellent animal care. Special thanks also to Angela Siebert, Miwako Kösters, Lisa Pichl and Elfi Holupirek for their great technical assistance.

This doctorate was supported by a research scholarship from the Elite Network of Bavaria and the financial and scientific support is therefore deeply acknowledged. Furthermore I would like to thank Prof. Dr. Stefan Endres for providing me the opportunity to join in the research training group “Oligonucleotides in Cell Biology and Therapy” (DFG Graduiertenkolleg 1202) and all my fellow graduate students for their input and for sharing a nice time.

Special thanks to Dr. Pauline Fezert, Dr. Stefanie Sklenak and Dr. Laura Klingseisen for their encouragement and friendship.

My deepest gratitude goes to Lisa Streckel, for her priceless loyalty, encouragement as well as for her friendship. Thank you so much for everything.

I am particularly thankful to my best friend Susanne Röll for sharing all the ups and downs, for her unlimited understanding and loyal friendship no matter what happened.

To my daddy and my grandparents Centa and Albert Braun - in loving memory - their endless support and encouragement remain unforgotten. To my grandfather Erich Fischer, who certainly would have been very proud.

The last and most important acknowledgement is dedicated to my parents, my sister, my grandmother, as well as Heidi and Pepp Hauner with their family for their love, unrestricted support and encouragement during all the years. Without you, all this would not have been possible. Thank you so much for everything.